frontiers | Research Topics

Insights in
Parkinson's disease and aging-related movement disorders
2022

Edited by
Robert Petersen, Muthuraman Muthuraman, Jee-Young Lee and Huaibin Cai

Published in
Frontiers in Aging Neuroscience

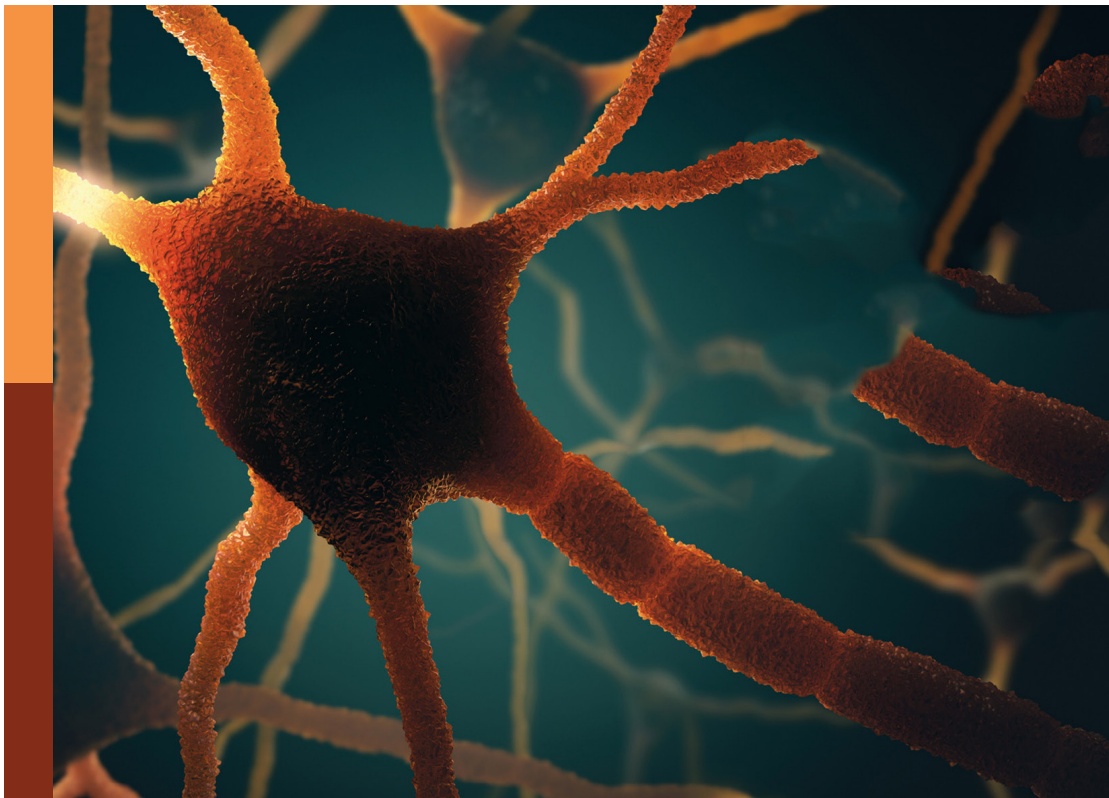

ISSN 1664-8714
ISBN 978-2-8325-3836-4
DOI 10.3389/978-2-8325-3836-4

About Frontiers

Frontiers is more than just an open access publisher of scholarly articles: it is a pioneering approach to the world of academia, radically improving the way scholarly research is managed. The grand vision of Frontiers is a world where all people have an equal opportunity to seek, share and generate knowledge. Frontiers provides immediate and permanent online open access to all its publications, but this alone is not enough to realize our grand goals.

Frontiers journal series

The Frontiers journal series is a multi-tier and interdisciplinary set of open-access, online journals, promising a paradigm shift from the current review, selection and dissemination processes in academic publishing. All Frontiers journals are driven by researchers for researchers; therefore, they constitute a service to the scholarly community. At the same time, the *Frontiers journal series* operates on a revolutionary invention, the tiered publishing system, initially addressing specific communities of scholars, and gradually climbing up to broader public understanding, thus serving the interests of the lay society, too.

Dedication to quality

Each Frontiers article is a landmark of the highest quality, thanks to genuinely collaborative interactions between authors and review editors, who include some of the world's best academicians. Research must be certified by peers before entering a stream of knowledge that may eventually reach the public - and shape society; therefore, Frontiers only applies the most rigorous and unbiased reviews. Frontiers revolutionizes research publishing by freely delivering the most outstanding research, evaluated with no bias from both the academic and social point of view. By applying the most advanced information technologies, Frontiers is catapulting scholarly publishing into a new generation.

What are Frontiers Research Topics?

Frontiers Research Topics are very popular trademarks of the *Frontiers journals series*: they are collections of at least ten articles, all centered on a particular subject. With their unique mix of varied contributions from Original Research to Review Articles, Frontiers Research Topics unify the most influential researchers, the latest key findings and historical advances in a hot research area.

Find out more on how to host your own Frontiers Research Topic or contribute to one as an author by contacting the Frontiers editorial office: frontiersin.org/about/contact

Insights in Parkinson's disease and aging-related movement disorders: 2022

Topic editors

Robert Petersen — Central Michigan University, United States
Muthuraman Muthuraman — University Hospital Würzburg, Germany
Jee-Young Lee — Seoul Metropolitan Government - Seoul National University Boramae Medical Center, Republic of Korea
Huaibin Cai — National Institute on Aging (NIH), United States

Citation

Petersen, R., Muthuraman, M., Lee, J.-Y., Cai, H., eds. (2023). *Insights in Parkinson's disease and aging-related movement disorders: 2022*. Lausanne: Frontiers Media SA. doi: 10.3389/978-2-8325-3836-4

Table of contents

frontiers | Frontiers in Aging Neuroscience

TYPE Perspective
PUBLISHED 27 October 2022
DOI 10.3389/fnagi.2022.1029824

OPEN ACCESS

EDITED BY
Muthuraman Muthuraman,
Johannes Gutenberg University Mainz, Germany

REVIEWED BY
Svetlana Tomic,
Osijek Clinical Hospital Center, Croatia

*CORRESPONDENCE
Tanya Gurevich
tanyag@tlvmc.gov.il

SPECIALTY SECTION
This article was submitted to Parkinson's Disease and Aging-related Movement Disorders, a section of the journal Frontiers in Aging Neuroscience

RECEIVED 27 August 2022
ACCEPTED 12 September 2022
PUBLISHED 27 October 2022

CITATION
Gurevich T, Arkadir D, Badarny S, Benizri S, Cohen O, Djaldetti R, Hassin-Baer S, Kestenbaum M, Nitsan Z, Zlotnik Y and Yahalom G (2022) Management of advanced Parkinson's disease in Israel: Clinicians viewpoint and action items. *Front. Aging Neurosci.* 14:1029824. doi: 10.3389/fnagi.2022.1029824

Management of advanced Parkinson's disease in Israel: Clinicians viewpoint and action items

Tanya Gurevich[1,2]*, David Arkadir[3], Samih Badarny[4,5], Sandra Benizri[6], Oren Cohen[2,7], Ruth Djaldetti[2,8], Sharon Hassin-Baer[2,9], Meir Kestenbaum[2,10], Zeev Nitsan[11], Yair Zlotnik[12] and Gilad Yahalom[13]

[1]Movement Disorders Unit, Tel Aviv Medical Center, Sagol School of Neuroscience, Tel Aviv University, Tel Aviv, Israel, [2]Sackler School of Medicine, Tel Aviv University, Tel Aviv, Israel, [3]Department of Neurology, Faculty of Medicine, Hadassah Medical Organization, Hebrew University, Jerusalem, Israel, [4]Galilee Medical Center, Naharyia, Israel, [5]Azrieli Faculty of Medicine, Bar Ilan University, Safed, Israel, [6]Movement Disorders Unit, Assuta Ramat HaHayal Hospital, Tel Aviv, Israel, [7]Department of Neurology, Shamir (Assaf Harofeh) Medical Center, Zerifin, Israel, [8]Department of Neurology, Movement Disorders Clinic, Rabin Medical Center—Beilinson Hospital, Petach Tikva, Israel, [9]Department of Neurology, Movement Disorders Institute, Chaim Sheba Medical Center, Ramat-Gan, Israel, [10]Department of Neurology, Meir Medical Center, Kfar-Saba, Israel, [11]Movement Disorder Clinic, Barzilai Medical Center, Ashkelon, Israel, [12]Department of Neurology, Movement Disorders Clinic, Soroka University Medical Center, Beersheba, Israel, [13]Department of Neurology, Movement Disorders Clinic, Shaare Zedek Medical Center, School of Medicine, Hebrew University, Jerusalem, Israel

Parkinson's disease (PD) is taking a staggering toll on healthcare systems worldwide, with the bulk of the expenditures invested in the late stages of the disease. Considering the rising life expectancy and the increasing prevalence of PD across the globe, a clear understanding of the early signs and treatment options available for advanced PD (APD), will facilitate tailoring management programs and support services. This task is complicated by the lack of both global consensus in defining APD and standardized care guidelines. This perspective prepared by a panel of movement disorder specialists, proposes to extend and optimize currently accepted PD coding to better reflect the diverse disease manifestations, with emphasis on non-motor features. The panel seeks to promote timely diagnosis by adjustment of evaluation tools for use by community neurologists and suggests modification of eligibility criteria for advanced therapy. Moreover, it advocates multidisciplinary assessments of APD patients to drive personalized, patient-centered and holistic management. Overall, earlier and more targeted intervention is expected to markedly improve patient quality of life.

KEYWORDS

Parkinson's disease stage-appropriate healthcare facilities, Delphi criteria, burden on public health care systems, clinical challenges, tailored management programs, patient-centered holistic management, intensified device aided therapies, advanced Parkinson's disease

Introduction

Parkinson's disease (PD) currently affects 41 in 100,000 individuals between the ages of 40 and 49 and 1,607 in 100,000 individuals over the age of 80 (Pringsheim et al., 2014; Elbaz et al., 2016; Dorsey and Bloem, 2018). In Israel, the prevalence in 2007 was estimated at 256:100,000 (Chillag-Talmor et al., 2011). By 2040, PD is expected to affect approximately 14.2 million individuals worldwide (Dorsey and Bloem, 2018). Its onset is influenced by a host of genetic and environmental factors, with age serving as a central determinant, as well as the most critical risk factor of disease progression and responsiveness to treatment (Levy, 2007; Collier et al., 2011). The disease takes a marked toll on healthcare resources, incurring an estimated $51.9 billion in direct and indirect costs in 2017 in the United States alone (Yang et al., 2020). The largest proportion of expenditures is invested in patients in late stages of the disease, as unidirectional phenotype shifts result in progressive disability and severely compromised patient quality of life (Lim et al., 2009). Given the rising life expectancy across the globe, and increased PD prevalence in the world (GBD 2016 Parkinson's Disease Collaborators, 2018), PD burden on public healthcare systems is expected to grow, and will require reconsideration of health policies and programs to adequately address the growing needs of the PD population. In this viewpoint, special attention is given to advanced PD (APD), also referred to as complex PD, estimated to impact 10% of the PD patient population (Worth, 2013; Giugni and Okun, 2014).

Evolution of the clinical picture of Parkinson's disease

Historically, motor syndrome was the main recognized clinical manifestation of PD and the prevalence of severe disability and mortality within 5 and 10 years of onset was 25 and 65%, respectively (Maier Hoehn, 1992). Yet, since the introduction of levodopa, the mainstay of modern PD treatment, PD-associated motor syndrome has proven responsive to the pharmaceutical treatments and mortality rates have declined, albeit remaining higher than in age-matched controls (Chen et al., 2006). Owing to the remarkable progress in the treatment of motor manifestations, PD is now considered a relatively slowly-progressing, chronic disease with distinctly different manifestations at its various stages, with the APD stage being the most challenging for patients and healthcare providers.

Advanced Parkinson's disease: A multisystem disease

This stage is characterized by moderate to severe motor deficits (Hoehn & Yahr stage III-V during off periods), generally accompanied by troublesome motor and non-motor symptoms: fluctuations, dyskinesias, frequent off-periods, postural instability leading to frequent falls with increased risk of fractures, sleep disturbances, hallucinations, and cognitive decline, among others. However, with close support, patients are not entirely dependent at this stage and are still capable of independent activity, and may be effectively managed by timely adjustment of the treatment. As PD patients progress to the advanced stage, they typically require intensive and individualized multidisciplinary pharmacological and non-pharmacological care to manage disease and treatment-related complications (**Figure 1**). Furthermore, as PD symptoms become less controlled with conventional therapies, targeted treatment options, including device-assisted therapies (DAT), such as deep brain stimulation or continuous levodopa-carbidopa infusions *via* pumps, are needed to improve response fluctuations.

Clinical challenges of advanced Parkinson's disease

Despite the wealth of knowledge of PD pathology and its natural course, there is a lack of global consensus regarding the precise definition of APD. This is largely due to its heterogenic origins, the vast variety of subphenotypes, variable trajectories and prognostics, as well as the absence of robust biomarkers for disease progression. In turn, it has challenged development of standardized care guidelines, and has brought to a lag in appropriate alignment of diagnostic instruments and grading scales for classification of disease severity and evaluation of treatment and management strategies. Furthermore, it has stymied early APD identification, and tailoring of interventional programs and appropriate allocation of funds. The most popular assessment tools use PD duration as an anchor and primarily focus on cardinal overt motor features. They have been proven to lack universality due to different phenotypes and rates of disease progression and generally fail to recognize the true weight of non-motor features on patient performance and quality of life (Braak et al., 2003; Wolters, 2008). Recent initiatives to develop comprehensive toolkits for evaluating PD status have been steered by the increasing understanding that motor disability, non-motor manifestations, treatment-related complications, and comorbidities are central contributors to APD and its associated limited activities of daily living (ADL), disability and greatly impaired quality of life (Korczyn, 1999; Martinez-Martin et al., 2011; Ray Chaudhuri et al., 2013). All these aspects are well-represented in the recently defined Delphi criteria for APD, which integrate degree of control achieved with oral anti-PD medications, assessment of an array of motor and non-motor symptoms, as well as patient functioning and independence (Antonini et al., 2018).

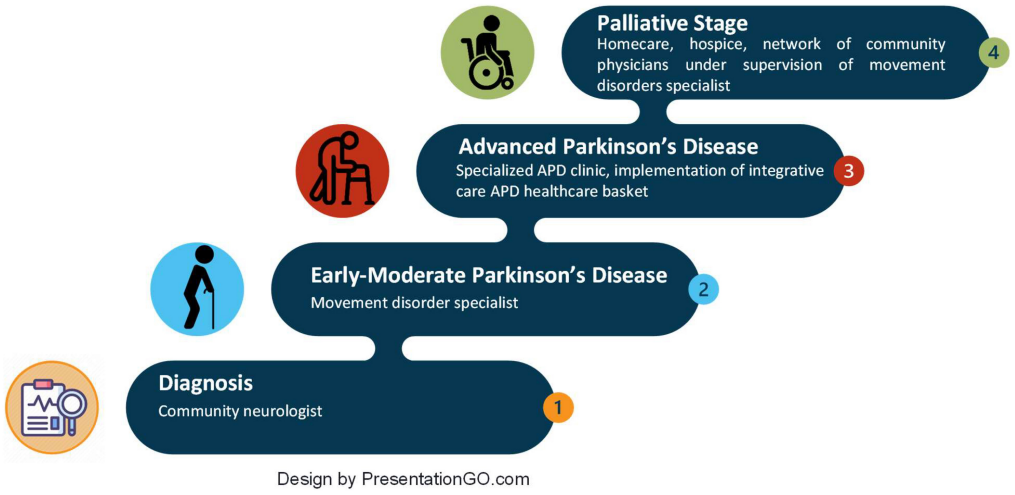

FIGURE 1
Parkinson's disease stages and stage-appropriate healthcare facilities.

The cross-sectional, multinational, observational OBSERVE-PD review of 2,615 PD patient charts (Fasano et al., 2019) found most significant agreement between physician global assessment and APD diagnosis based on the Delphi criteria, with regards to current treatment programs, limited ADL, motor fluctuations and time from diagnosis. In a subanalysis of the Israeli cohort of 120 patients, physician judgment in classifying APD correlated with select Delphi criteria (Djaldetti et al., 2018). Recently, the intensified therapy component of the "5-2-1" criteria proposed by the Delphi expert consensus panel for identifying APD, has been shown to correlate with established disease burden predictors, including extended disease duration, increased motor and non-motor burden, and compromised quality of life (Fasano et al., 2019; Aldred et al., 2020; Santos-Garcia et al., 2020; Barer et al., 2022) and is included in the recently published MANAGE-PD comprehensive screening tool (Antonini et al., 2019). Integration of wearable sensors into clinical practice are projected to provide objective, quantitative digital patient function-related markers, and thereby improve the sensitivity, accuracy and feasibility of the assessment of motor and non-motor symptoms of PD and diagnosis of APD (Mirelman et al., 2021).

Discussion

Definition and diagnosis of advanced Parkinson's disease

In line with the global efforts to moderate PD impact on quality of life, the authors, representing a panel of Israeli movement disorders specialists, propose to define APD in the International Classification of Disease 11th revision (ICD-11) as a unique health entity that demands adjusted healthcare provider attitudes and relevant social services. Modification of the ICD-11 PD coding should include severity- and fluctuation-based subcodes that accurately capture APD and distinguish it from early-stage PD. While very few diseases have been assigned severity-based subcodes in ICD-10 (diabetes, alcoholic liver disease, renal insufficiency, residual schizophrenia), the growing evidence of the distinct clinical manifestations and medical needs of this patient subpopulation, justifies reconsideration of its coding status.

In addition, we call for optimization of the Delphi criteria by extending them to include a more extensive list of non-motor features, such as autonomic disturbances (e.g., orthostatic hypotension, urinary incontinence), pain, daytime somnolence, and apathy. Furthermore, in the opinion of the Israeli panel, the Delphi criteria for APD from motor fluctuations, regardless of their duration and severity, should be the main eligibility criteria for advanced therapy. Evaluation of PD patients should be based on a structured questionnaire applied as a preliminary tool geared to be implemented by community neurologists or case managers (e.g., nurse practitioners). Patients with suspected APD should undergo multidisciplinary evaluation, ideally in specialized APD centers, to define the extent of disability, outline an individualized treatment program, and weigh the need for rehabilitation and social support services. Routine evaluations should be adequately sensitive to allow for timely diagnosis of palliative-stage PD, which should be addressed by end-of-life palliative/hospice referral (Akbar et al., 2021).

Comprehensive management of advanced Parkinson's disease

Management protocols should implement personalized patient-centered and holistic approaches to target the

heterogenic manifestations and course of PD. These should include tools for timely diagnosis and treatment of osteoporosis. Furthermore, patients should be informed of opportunities to participate in relevant clinical trials. In addition to the clinical benefits of integrated and coordinated care (Nijkrake et al., 2009; van der Eijk et al., 2011; Loewenbrück et al., 2020; Tenison et al., 2020), such programs have been associated with improved psychological health indicators and self-management capacities (Coulter et al., 2015; Minkman, 2016). Rehabilitation facilities should be staffed by multidisciplinary teams of physiotherapists, speech and swallowing therapists, occupation therapists and social workers. Such programs should be coordinated by specialized nurses (or nurse practitioners) under the supervision of a movement disorders specialist (Cohen et al., 2021).

The panel also suggests standardization of DAT eligibility and prioritization of its use to early-stage APD patients, while minimizing its use in palliative-stage patients. Furthermore, integration of telemedicine and nurse practitioners can tighten surveillance and improve treatment optimization efforts.

These can be further supported by establishment of a network of community physicians, led by movement disorder specialists, to promote case-sharing, research dissemination and exchange of professional know-how.

Social assistance to patients with advanced Parkinson's disease

Expanded APD-geared health baskets clearly outline eligibility for reimbursement for a part/full time paid attendant, mobility allowance, and rehabilitation services. In parallel, attention should be paid to informal and non-specialized caregivers by providing them PD-specific education and support (Rosqvist et al., 2021). Patients and caregivers should be made aware of PD-oriented organizations and social networking groups.

Summary

In summary, the globally rising life expectancy has increased the prevalence of PD in general, and of APD, in particular. Appreciation of the heterogeneity of PD etiology and manifestations has underscored the need for updated PD coding. Precise and standardized definition and evaluation of APD will promote earlier APD identification and timely referral to adequate therapies and specialists. Moreover, it will enhance holistic management, which is expected to markedly improve APD patient quality of life. Future works should focus on validating the proposed extension of the Delphi APD criteria, and on tailoring treatment to APD phenotypes.

Author contributions

TG: draft preparation and literature search. All authors conceptualized, critically revised, and approved the submitted version.

Funding

Medical writing assistance and APD advisory board were funded by AbbVie. Medical writing assistance was provided by Ebiodata, Israel.

Conflict of interest

Author TG was member of the advisory board on Advanced Parkinson's disease 23.07.2020 supported by Abbvie, consultant and/or scientific advisor/lecturer for Neuroderm, AbbVie, Cytora, Allergan, Teva, and Medison, and received research support from Parkinson's Foundation and Israel Innovation Authority. Author SH-B had received funding for research from Abbvie and speaker honoraria from Abbvie, Medison, and Allergan, consultancy fees from Neuroderm, Abbvie, and Takeda and Teva, and advisory fees from Teva and Abbvie. Author MK was consultant and lecturer for Teva, Medison, and Abbvie. Author ZN participated in advisory boards, received speaker fees from Abbvie and Teva, and had received educational travel bursaries from Abbvie and Teva. Author YZ participated in advisory boards, received speaker fees from Abbvie, Medison, and Teva, and had received educational travel bursaries from Abbvie and Teva. Author GY was consultant for Abbvie and Takeda.

The remaining authors declare that the research was conducted in the absence of any commercial or financial relationships that could be construed as a potential conflict of interest.

Publisher's note

References

Akbar, U., McQueen, R. B., Bemski, J., Carter, J., Goy, E. R., Kutner, J., et al. (2021). Prognostic predictors relevant to end-of-life palliative care in Parkinson's disease and related disorders: a systematic review. *J. Neurol. Neurosurg. Psychiatry* 92, 629–636. doi: 10.1136/jnnp-2020-323939

Aldred, J., Anca-Herschkovitsch, M., Antonini, A., Bajenaru, O., Bergmann, L., Bourgeois, P., et al. (2020). Application of the '5-2-1' screening criteria in advanced Parkinson's disease: interim analysis of duoglobe. *Neurodegener. Dis. Manag.* 10, 309–323. doi: 10.2217/nmt-2020-0021

Antonini, A., Odin, P., Jalundhwala, Y. J., Schmidt, P. N., Skalicky, A. M., Kleinman, L., et al. (2019). Manage-pd: a clinician-reported tool to identify patients with Parkinson's disease inadequately controlled on oral medications – results from vignette-based validation. *Neurology* 92(15 Suppl.), 239–240. doi: 10.1016/j.jns.2019.10.1252

Antonini, A., Stoessl, A. J., Kleinman, L. S., Skalicky, A. M., Marshall, T. S., Sail, K. R., et al. (2018). Developing consensus among movement disorder specialists on clinical indicators for identification and management of advanced Parkinson's disease: a multi-country delphi-panel approach. *Curr. Med. Res. Opin.* 34, 2063–2073. doi: 10.1080/03007995.2018.1502165

Barer, Y., Gurevich, T., Chodick, G., Giladi, N., Gross, R., COhen, R., et al. (2022). Advanced-stage Parkinson's disease: from identification to characterization using a nationwide database. *Mov. Disord. Clin. Pract.* 9, 458–467. doi: 10.1002/mdc3.13458

Braak, H., Del Tredici, K., Rub, U., de Vos, R. A., Jansen Steur, E. N., and Braak, E. (2003). Staging of brain pathology related to sporadic Parkinson's disease. *Neurobiol. Aging* 24, 197–211. doi: 10.1016/S0197-4580(02)00065-9

Chen, H., Zhang, S. M., Schwarzschild, M. A., Hernán, M. A., and Ascherio, A. (2006). Survival of Parkinson's disease patients in a large prospective cohort of male health professionals. *Mov. Disord.* 21, 1002–1007. doi: 10.1002/mds.20881

Chillag-Talmor, O., Giladi, N., Linn, S., Gurevich, T., El-Ad, B., Silverman, B., et al. (2011). Use of a refined drug tracer algorithm to estimate prevalence and incidence of Parkinson's disease in a large israeli population. *J. Parkinsons Dis.* 1, 35–47. doi: 10.3233/JPD-2011-11024

Cohen, N., Manor, Y., Green, Y., Tahel, G., Badichi, I., Ben-Or, G., et al. (2021). Multidisciplinary intensive outpatient rehabilitation program for patients with moderate-to-advanced Parkinson's disease. *NeuroRehabilitation* 49, 47–55. doi: 10.3233/NRE-210031

Collier, T. J., Kanaan, N. M., and Kordower, J. H. (2011). Ageing as a primary risk factor for Parkinson's disease: evidence from studies of non-human primates. *Nat. Rev. Neurosci.* 12, 359–366. doi: 10.1038/nrn3039

Coulter, A., Entwistle, V. A., Eccles, A., Ryan, S., Shepperd, S., and Perera, R. (2015). Personalised care planning for adults with chronic or long-term health conditions. *Cochrane Database Syst. Rev.* 2015:CD010523. doi: 10.1002/14651858.CD010523.pub2

Djaldetti, R., Hassin-Baer, S., Anca-Herschkovitsch, M., Gross, R., Cohen, R., Banayan, H., et al. (2018). Advanced Parkinson's disease diagnosis and treatment trends in israel-sub-analysis of the observe-pd multi-country, cross-sectional study. *Mov. Disord.* 33, 14–17.

Dorsey, E. R., and Bloem, B. R. (2018). The parkinson pandemic-a call to action. *JAMA Neurol.* 75, 9–10. doi: 10.1001/jamaneurol.2017.3299

Elbaz, A., Carcaillon, L., Kab, S., and Moisan, F. (2016). Epidemiology of Parkinson's disease. *Rev. Neurol.* 172, 14–26. doi: 10.1016/j.neurol.2015.09.012

Fasano, A., Fung, V. S. C., Lopiano, L., Elibol, B., Smolentseva, I. G., Seppi, K., et al. (2019). Characterizing advanced Parkinson's disease: observe-pd observational study results of 2615 patients. *BMC Neurol.* 19:50. doi: 10.1186/s12883-019-1276-8

GBD 2016 Parkinson's Disease Collaborators (2018). Global, regional, and national burden of Parkinson's disease, 1990-2016: a systematic analysis for the global burden of disease study 2016. *Lancet Neurol.* 17, 939–953.

Giugni, J. C., and Okun, M. S. (2014). Treatment of advanced Parkinson's disease. *Curr. Opin. Neurol.* 27, 450–460. doi: 10.1097/WCO.0000000000000118

Korczyn, A. D. (1999). Parkinson's disease: one disease entity or many? *J. Neural Transm. Suppl.* 56, 107–111. doi: 10.1007/978-3-7091-6360-3_5

Levy, G. (2007). The relationship of parkinson disease with aging. *Arch. Neurol.* 64, 1242–1246. doi: 10.1001/archneur.64.9.1242

Lim, S.-Y., Fox, S. H., and Lang, A. E. (2009). Overview of the extranigral aspects of parkinson disease. *Arch. Neurol.* 66, 167–172. doi: 10.1001/archneurol.2008.561

Loewenbrück, K. F., Stein, D. B., Amelung, V. E., Bitterlich, R., Brumme, M., Falkenburger, B., et al. (2020). Parkinson network eastern saxony (panos): reaching consensus for a regional intersectoral integrated care concept for patients with Parkinson's disease in the region of eastern saxony, germany. *J. Clin. Med.* 9:2906. doi: 10.3390/jcm9092906

Maier Hoehn, M. M. (1992). The natural history of Parkinson's disease in the pre-levodopa and post-levodopa eras. *Neurol. Clin.* 10, 331–339. doi: 10.1016/S0733-8619(18)30213-5

Martinez-Martin, P., Rodriguez-Blazquez, C., Kurtis, M. M., and Chaudhuri, K. R. (2011). The impact of non-motor symptoms on health-related quality of life of patients with Parkinson's disease. *Mov. Disord.* 26, 399–406. doi: 10.1002/mds.23462

Minkman, M. (2016). The development model for integrated care: a validated tool for evaluation and development. *J. Integr. Care* 24, 38–52. doi: 10.1108/JICA-01-2016-0005

Mirelman, A., Ben Or Frank, M., Melamed, M., Granovsky, L., Nieuwboer, A., Rochester, L., et al. (2021). Detecting sensitive mobility features for Parkinson's disease stages via machine learning. *Mov. Disord.* 36, 2144–2155. doi: 10.1002/mds.28631

Nijkrake, M. J., Keus, S. H., Oostendorp, R. A., Overeem, S., Mulleners, W., Bloem, B. R., et al. (2009). Allied health care in Parkinson's disease: referral, consultation, and professional expertise. *Mov. Disord.* 24, 282–286. doi: 10.1002/mds.22377

Pringsheim, T., Jette, N., Frolkis, A., and Steeves, T. D. (2014). The prevalence of Parkinson's disease: a systematic review and meta-analysis. *Mov. Disord.* 29, 1583–1590. doi: 10.1002/mds.25945

Ray Chaudhuri, K., Rojo, J. M., Schapira, A. H., Brooks, D. J., Stocchi, F., Odin, P., et al. (2013). A proposal for a comprehensive grading of Parkinson's disease severity combining motor and non-motor assessments: meeting an unmet need. *PLoS One* 8:e57221. doi: 10.1371/journal.pone.0057221

Rosqvist, K., Kylberg, M., Lofqvist, C., Schrag, A., Odin, P., and Iwarsson, S. (2021). Perspectives on care for late-stage Parkinson's disease. *Parkinsons Dis.* 2021:9475026. doi: 10.1155/2021/9475026

Santos-Garcia, D., de Deus Fonticoba, T., Suarez Castro, E., Aneiros Diaz, A., and McAfee, D. (2020). 5-2-1 criteria: a simple screening tool for identifying advanced pd patients who need an optimization of Parkinson's treatment. *Parkinsons Dis.* 2020:7537924. doi: 10.1155/2020/7537924

Tenison, E., Smink, A., Redwood, S., Darweesh, S., Cottle, H., van Halteren, A., et al. (2020). Proactive and integrated management and empowerment in Parkinson's disease: designing a new model of care. *Parkinson Dis.* 2020:8673087. doi: 10.1155/2020/8673087

van der Eijk, M., Faber, M. J., Al Shamma, S., Munneke, M., and Bloem, B. R. (2011). Moving towards patient-centered healthcare for patients with Parkinson's disease. *Parkinson. Relat. Disord.* 17, 360–364. doi: 10.1016/j.parkreldis.2011.02.012

Wolters, E. C. (2008). Variability in the clinical expression of Parkinson's disease. *J. Neurol. Sci.* 266, 197–203. doi: 10.1016/j.jns.2007.08.016

Worth, P. F. (2013). When the going gets tough: how to select patients with Parkinson's disease for advanced therapies. *Pract. Neurol.* 13:140. doi: 10.1136/practneurol-2012-000463

Yang, W., Hamilton, J. L., Kopil, C., Beck, J. C., Tanner, C. M., Albin, R. L., et al. (2020). Current and projected future economic burden of Parkinson's disease in the U.S. *NPJ Parkinsons Dis.* 6:15. doi: 10.1038/s41531-020-0117-1

frontiers | Frontiers in Aging Neuroscience

TYPE Original Research
PUBLISHED 26 January 2023
DOI 10.3389/fnagi.2023.1019239

OPEN ACCESS

EDITED BY
Jee-Young Lee,
Seoul Metropolitan Government,
Seoul National University,
Republic of Korea

REVIEWED BY
Mario Stampanoni Bassi,
Mediterranean Neurological Institute
Neuromed (IRCCS), Italy
Jung Hwan Shin,
Seoul National University Hospital,
Republic of Korea
Yasuo Terao,
Kyorin University,
Japan

*CORRESPONDENCE
Asha Kishore
✉ asha.kishore@asterdmhealthcare.com

SPECIALTY SECTION
This article was submitted to
Parkinson's Disease and Aging-related
Movement Disorders,
a section of the journal
Frontiers in Aging Neuroscience

RECEIVED 14 August 2022
ACCEPTED 06 January 2023
PUBLISHED 26 January 2023

CITATION
Radhakrishnan V, Gallea C, Valabregue R, Krishnan S, Kesavadas C, Thomas B, James P, Menon R and Kishore A (2023) Cerebellar and basal ganglia structural connections in humans: Effect of aging and relation with memory and learning.
Front. Aging Neurosci. 15:1019239.
doi: 10.3389/fnagi.2023.1019239

Cerebellar and basal ganglia structural connections in humans: Effect of aging and relation with memory and learning

Vineeth Radhakrishnan[1], Cecile Gallea[2], Romain Valabregue[2], Syam Krishnan[1], Chandrasekharan Kesavadas[3], Bejoy Thomas[3], Praveen James[1], Ramshekhar Menon[4] and Asha Kishore[1,5]*

[1]Comprehensive Care Centre for Movement Disorders, Department of Neurology, Sree Chitra Tirunal Institute of Medical Sciences and Technology, Thiruvananthapuram, India, [2]INSERM, CNRS, Paris Brain Institute, Sorbonne Université, Paris, France, [3]Department of Imaging Sciences and Interventional Radiology, Sree Chitra Tirunal Institute of Medical Sciences and Technology, Thiruvananthapuram, India, [4]Department of Neurology, Sree Chitra Tirunal Institute for Medical Sciences and Technology, Thiruvananthapuram, India, [5]Parkinson and Movement Disorder Centre, Department of Neurology, Aster Medcity, Kochi, India

Introduction: The cerebellum and basal ganglia were initially considered anatomically distinct regions, each connected *via* thalamic relays which project to the same cerebral cortical targets, such as the motor cortex. In the last two decades, transneuronal viral transport studies in non-human primates showed bidirectional connections between the cerebellum and basal ganglia at the subcortical level, without involving the cerebral cortical motor areas. These findings have significant implications for our understanding of neurodevelopmental and neurodegenerative diseases. While these subcortical connections were established in smaller studies on humans, their evolution with natural aging is less understood.

Methods: In this study, we validated and expanded the previous findings of the structural connectivity within the cerebellum-basal ganglia subcortical network, in a larger dataset of 64 subjects, across different age ranges. Tractography and fixel-based analysis were performed on the 3T diffusion-weighted dataset using Mrtrix3 software, considering fiber density and cross-section as indicators of axonal integrity. Tractography of the well-established cerebello-thalamo-cortical tract was conducted as a control. We tested the relationship between the structural white matter integrity of these connections with aging and with the performance in different domains of Addenbrooke's Cognitive Examination.

Results: Tractography analysis isolated connections from the dentate nucleus to the contralateral putamen *via* the thalamus, and reciprocal tracts from the subthalamic nucleus to the contralateral cerebellar cortex *via* the pontine nuclei. Control tracts of cerebello-thalamo-cortical tracts were also isolated, including associative cerebello-prefrontal tracts. A negative linear relationship was found between the fiber density of both the ascending and descending cerebellum-basal ganglia tracts and age. Considering the cognitive assessments, the fiber density values of cerebello-thalamo-putaminal tracts correlated with the registration/learning domain scores. In addition, the fiber density values of cerebello-frontal and subthalamo-cerebellar (Crus II) tracts correlated with the cognitive assessment scores from the memory domain.

Conclusion: We validated the structural connectivity within the cerebellum-basal ganglia reciprocal network, in a larger dataset of human subjects, across wider age range. The structural features of the subcortical cerebello-basal ganglia tracts in human subjects display age-related neurodegeneration. Individual morphological variability of cerebellar tracts to the striatum and prefrontal cortex was associated with different cognitive functions, suggesting a functional contribution of cerebellar tracts to cognitive decline with aging. This study offers new perspectives to consider the functional role of these pathways in motor learning and the pathophysiology of movement disorders involving the cerebellum and striatum.

KEYWORDS
aging, memory, learning, cerebellum, basal ganglia, tractography, connectivity, diffusion

1. Introduction

For a long time, basal ganglia (BG) and cerebellum (CB) were considered anatomically and functionally distinct subcortical structures, each involved in specific types of learning (Doya, 2000), namely reinforcement and supervised learning (Kawato and Gomi, 1992; Schultz et al., 1997; Doya, 2000; O'Doherty et al., 2003). The two structures project to cortical areas *via* separate thalamic nuclei forming the striato-thalamo-cortical (STC) and cerebello-thalamocortical (CTC) loops (Kemp and Powell, 1971; Allen et al., 1978; Asanuma et al., 1983; Sakai et al., 1996). Abnormal engagement of these loops in diseases involving BG and/or CB results in different behavioral impairments. For instance, Parkinson's disease (PD) with dysregulation of the striatal dopaminergic pathway shows impaired reinforcement learning (Voon et al., 2010), while ataxic patients with structural abnormalities of the CB show decreased error-based (supervised) learning during sensorimotor adaptation (Panouillères et al., 2017). These traditional perspectives were challenged by neuroanatomical studies in primates that demonstrated reciprocal connections between BG and CB through thalamic and pontine structures without involving cortical cerebral areas, raising doubts about such clear functional dissociation. Dense disynaptic projections were demonstrated between the dentate nucleus (DN) of the CB and the putamen *via* the central-lateral nucleus of the thalamus and between the subthalamic nucleus (STN) and the cerebellar cortex *via* the pontine nucleus (Hoshi et al., 2005; Bostan et al., 2010; Bostan and Strick, 2018). A pathological interaction between the two structures is also suspected in movement disorders such as PD (Wu and Hallett, 2013; Kishore et al., 2014; Kishore and Popa, 2014), dystonia (Sadnicka et al., 2012; Kaji et al., 2018), Tourette's syndrome and psychiatric disorders such as attention-defcit/hyperactivity disorder, and schizophrenia (Strick et al., 2009; Maia and Frank, 2011; O'Halloran et al., 2012). However, whether the morphology and the functional contribution of CB-BG reciprocal connections are affected by normal aging is not well-delineated.

Investigating anatomical connections within the CB-BG network in the human brain is possible *in-vivo* with non-invasive diffusion-weighted imaging (DWI) and tractography. These techniques can measure connectivity strength, i.e., the probability of connection based on the density of streamlines from a seed to a target region. In 12 participants, an exploratory study quantified the connectivity strength of the cerebellar output pathways involving the DN, respectively, to the caudate (12%), the putamen (9%), and the pallidum (11%; Pelzer et al., 2013). In 15 participants, another study used constrained spherical deconvolution (CSD) capable of resolving the crossing, kissing, or branching white matter bundles (Milardi et al., 2016). This study established contralateral tracts from the DN to the thalamus as in the primate studies and also proposed the presence of contralateral and ipsilateral tracts from DN to the thalamus, and from STN to the CB cortex (Hoshi et al., 2005). Given the inter-individual variability of human anatomy, studies involving a larger number of participants are needed to validate these exploratory findings.

While the cognitive functions of the BG are well-recognized (Haber, 2003), CB is more recently considered as a hub that regulates various non-motor functions (Hoche et al., 2018; Schmahmann, 2019). Descending and ascending connections between the CB and the cerebral cortical areas involving the prefrontal cortex have been described and corroborate the role of the CB in modulating cognitive behavior (Parker et al., 2014; Jobson et al., 2021). Lobules I–VI and VIII are involved in sensorimotor tasks, whereas the Crus II lobule is primarily associated with non-motor functions (Stoodley et al., 2012, 2020), especially social mentalizing, and emotional self-experiences (Van Overwalle et al., 2020a, b) language, emotions, and working memory (Habas et al., 2009; Stoodley and Schmahmann, 2009). The functional contribution of the CB-BG connections is often inferred and not directly assessed. Recent studies showed that both CB and BG contribute to associative and reward-based learning, suggesting a physiological interaction between them (Wu and Hallett, 2013; Kishore et al., 2014; Kishore and Popa, 2014).

Age-related degeneration of white matter tracts such as CB-BG interconnections could result in the decline of functions, including movement and cognition. Age-related degeneration of white matter tracts affects cortical brain areas and subcortical structures including BG (Raz et al., 2003; Koikkalainen et al., 2007; Zwirner et al., 2016). Age-related changes in water diffusivity in the white matter of the middle cerebellar peduncles were observed in several studies (Cox et al., 2016; Coelho et al., 2021). Recent technical advances of DTI provide an opportunity to investigate the evolution of the integrity of white matter connections with age. For instance, the "disconnection hypothesis" suggests that age-related cognitive decline is linked to brain structural changes, i.e., the alteration of white matter tracts between cortical regions can lead to a decline in cognitive performance (Bennett and Madden, 2014; Fjell et al., 2016). However, the specific contribution of cerebellar connections to this process is unclear. As healthy aging itself influences the morphological characteristics of white matter tracts, including cerebellar tracts, its impact on CB-BG connections should be known to better understand the changes in pathological conditions. Since aging affects cognitive functions (Bendlin et al., 2010; Coelho et al., 2021), we hypothesized that aging will affect cerebellar pathways (including the CB-BG connections) proportionally to cognitive abilities.

In the present study, we aimed to (i) validate and expand the imaging evidence of the presence of the anatomical tracks linking CB and BG as reported in non-human primates (Hoshi et al., 2005; Bostan et al., 2010) and (ii) evaluate age-related changes in the morphology of CB-BG reciprocal connections and its relation to specific cognitive domains. We enrolled 64 human healthy subjects across a wide age range (30–80 yrs.). We applied DWI with CSD.

We evaluated the age-related neurodegeneration on the CB-BG reciprocal white matter tracts using the fixel-based analysis (FBA) technique. This novel model for diffusion MRI analysis is optimized to isolate crossing or kissing fibers and allows evaluating axonal parameters along a tract, namely fiber density (FD, reflecting intra-axonal volume), fiber cross-section (FC, reflecting the area occupied by the axons), and a combination of FD and FC, namely FDC (Raffelt et al., 2015). In addition, we tested the association between the individual characteristics of FBA metrics and the measures of specific cognitive performance. Since the cerebellum and prefrontal cortices are involved in learning and

retention (Elhalal et al., 2014), cognitive assessments in these domains were used to explore their relationship with the FBA metrics.

2. Materials and methods

2.1. Subjects and neuropsychological testing

Sixty-four healthy volunteers (HV; mean age:55.69 ± 9.96 years, M/F:34/30, age range:30–80 years) with no history of neurological or psychiatric illness and formal education > 6 years were recruited for the study over 3 years from a single center (Sree Chitra Tirunal Institute for Medical Sciences and Technology, India). The MRI scans were screened by a radiologist for any structural non-symptomatic lesions. The subjects were recruited *via* notification exhibited at the hospital campus. Among these 64 participants, 20 subjects (mean age:56.8 ± 8.7 years, age range: 41–66 years) with a Clinical Dementia Rating (CDR) score of 0, underwent neuropsychological battery tests assessing global cognitive score *via* vernacular (Malayalam, a south Indian language) adaptation of Addenbrooke's Cognitive Examination battery (ACE-M) along with Rey Auditory Verbal Learning Test (RAVLT; Mathuranath et al., 2004; Menon et al., 2014). Learning and retention were assessed *via* distinct domains of ACE neuropsychological analysis: ACE-M-Reg-24 (Registration/learning: 24 point scale; registration of 3 words = 3 points; 3-trial learning of an address = 21 points), ACE-M-Recall [10 point scale (recall of 3 words, each after a delay of 5 min = 3 points; recall of address = 7 points)], along with the total score of ACE-M. Other retention scores included the delayed recall and total scores of RAVLT.

2.2. Ethics statement

All subjects provided written informed consent according to the declaration of Helsinki and the study was approved by the Institutional Ethics Committee (SCT/IEC/816/OCTOBER-2015).

2.3. MRI data acquisition

Structural and diffusion MRI data were acquired in a 3-tesla scanner (GE MEDICAL SYSTEMS, Discovery MR750w, Chicago, Illinois, United States) using a 32-channel, phased-array head coil designed for parallel imaging. A high-resolution 3D, T1-weighted, fast spoiled, gradient-echo sequence (TR = 7.924 ms, TE = 2.984 ms, Flip angle = 12, matrix = 256 × 256, 172 sections of 1 mm each) and diffusion-weighted MRI (dMRI) of single-shot echo-planar spin-echo sequence with 64 directions (TR = 9,000 ms, TE = 99.8 ms, matrix = 256 × 256, b = 0 and 1,000 s/mm^2, 57 slices of 2 mm thick) were acquired for each subject.

2.4. Tractography

The tractography analysis was performed using the Mrtrix3 toolbox (Tournier et al., 2019) and the functions in the FSL toolkit as shown in Figure 1. Standard pre-processing was performed including denoising using the Marchenko-Pastur Principal Component Analysis (MP-PCA; Veraart et al., 2016; Cordero-Grande et al., 2019) followed by Gibbs ringing removal (Kellner et al., 2015), and Eddy current correction (Smith et al., 2004). The non-brain tissues were removed using Brain Extraction Tool (BET; Smith, 2002; Smith et al., 2004). We estimated the response function from the brain using the *dwi2response* function with the "dhollander" algorithm (Tournier et al., 2004). We then estimated the fiber orientation distribution (FOD) based on eighth-order CSD using the *dwi2fod* function (Jenkinson et al., 2002; Tournier et al., 2004). Fiber tracking was performed for each subject using the *tckgen* function with the "iFOD2" option which performs improved second-order integration over fiber orientation distribution. This option enhances anatomical plausibility by facilitating more accurate fiber reconstruction in heavily curved regions (Tournier et al., 2004). During the tracking process, the probability of a particular direction is set to be proportional to the amplitude of the FOD along that direction. The following additional *tckgen* settings were used: max angle between successive steps = 22.5°, max length = 250 mm, min length = 10 mm, cut-off FA value = 0.4, and the maximum number of fibers = 1 million. The cut-off value for FA and max angle between successive steps are kept at a conservative level to ensure minimal false positives in the streamline estimation. The Region of Interests (ROIs) to extract the targeted interconnecting tracts were manually segmented by two independent observers and intersection of the two ROIs with overlap greater than 80% was considered as the final ROI. To extract the tract parameters, a fixel mask for the tracts was created using the *tck2fixel* function and applied over the whole brain FD (measure of density of intra-axonal space), FC (measure of cross-sectional size of the bundle in each voxel), FDC (the total capacity of the fiber bundle to carry information), and logFC fixel images of individual subjects after transforming them into a common template space.

2.5. Definition of regions of interest

ROIs were defined based on the automated anatomical labeling atlas 3 (AAL3; Rolls et al., 2020) and included the motor (region indexes: 1–2, 15–16, 61–62, 73–74) and prefrontal cortices (region indexes 19–20, 151–156). Masks of these regions were denormalized from MNI to individual native space using the inverse transform. For deep and small nuclei for which the inverse transform lacked spatial precision, we used a manual segmentation protocol. Two independent observers (V.R. and S.K.) draw the ROIs using FSLeyes (McCarthy, 2019), on the T1w MRI images (Thalamus and Putamen) and FOD images (STN and Dentate Nucleus). To control for inter-observer variability for each manual ROI, voxels that overlapped between the observers were considered for the analysis. We computed (i) the intersection volume of the ROIs by multiplying the binary mask of the ROI from two observers using *fslmaths and fslstats;* (ii) the total volume of their combination was calculated by adding them using *fslmaths and fslstats*. The ratio between the volume of intersection and combination of ROIs was computed. The overlap between each given ROI drawn by the two observers had to be greater than at least 80% to consider the ROI for the analysis.

2.5.1. Thalamus

The thalamus was segmented on the T1-weighted image of each subject in the coronal plane (Figure 2A). The anterior boundary was the stria terminalis; the lateral and ventromedial boundaries were formed by the internal capsule; the genu and the caudate nucleus formed the dorsolateral boundary. Corrections were made in the sagittal and axial planes.

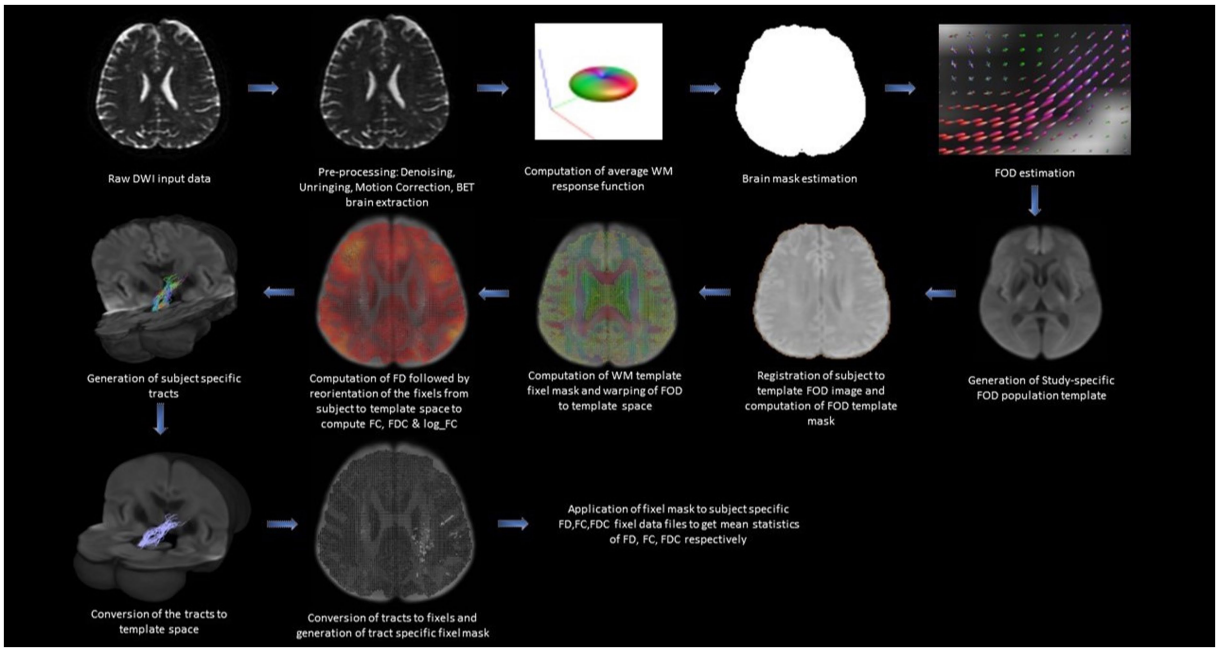

FIGURE 1
Figure showing the steps involved in the generation of tract-specific FBA metrics.

2.5.2. Putamen

The putamen was segmented on the T1-weighted image of each subject in the axial plane (Figure 2B). The lateral border was the external capsule. The ventromedial boundary was the anterior limb of the internal capsule, whereas the posterior limb formed the posteromedial boundary. The mask was corrected for in the sagittal and coronal planes.

2.5.3. Subthalamic nucleus

The STN (subthalamic nucleus) was segmented on the FOD image obtained from the diffusion-weighted image. It was located relative to the red nucleus, observable as the hypointense region at the brain stem as seen in the axial slice (Figure 2C). The STN was drawn 3 mm from the red nucleus in the anterolateral direction below the thalamus. The overlap between the manually drawn STN and standard atlas STN ROI denormalized to subject space is shown in Appendix Figure A1(B).

2.5.4. Dentate

The DN (dentate nucleus) was drawn on the fiber orientation density image obtained from the diffusion-weighted image of individual subjects (Figure 2D) and defined by the hypointense semi-circular region in the CB with the opening facing the midline.

2.5.5. Ventral tegmental area

VTA was segmented on the axial section of the FOD image obtained from the diffusion image as previously outlined by Ballard et al. (2011) as shown in Figure 2E. The overlap between the manually drawn VTA and standard atlas VTA ROI denormalized to subject space is shown in Appendix Figure A1(A).

2.6. Total intracranial volume

The total intracranial volume (TIV) was computed from the acquired T1-weighted images using Computational Anatomy Toolbox (CAT12) in the Statistical Parametric Mapping (SPM12) software running in MATLAB (R2019a: The MathWorks, Inc., Natick, Massachusetts, United States). The TIV value was calculated as the sum of volumes for White Matter (WM), Gray Matter (GM), and Cerebrospinal Fluid (CSF) obtained by segmenting the T1-weighted images into respective components.

2.7. Tract reconstruction

For all the ascending tracts described below, we considered the thalamus as an inclusion mask to build a reliable trajectory based on the anatomy of human and non-human primates (Hoshi et al., 2005; Bostan et al., 2010; Bostan and Strick, 2018). To identify the contralateral tracts, exclusion masks of the opposite cerebellar hemisphere and an interhemispheric mask covering the corpus callosum were considered.

2.7.1. Cerebello-thalamocortical ascending tracts

Cerebello-thalamocortical (CTC) tracts projecting to cortical motor areas with known trajectories (Yamada et al., 2010) were studied as controls. We defined the cerebellar dentate nucleus as the seed region and the contralateral cortical motor areas as target regions (inclusion mask = contralateral thalamus).

2.7.2. Cerebello-thalamo-striatal (CB-BG) ascending tract

We defined the dentate nucleus as the seed and the contralateral putamen as a target region (inclusion mask = contralateral thalamus).

2.7.3. Subthalamo-cerebellar (a) crus II (b) VIIb descending tract

We defined the STN as the seed and the contralateral CrusII and VIIb as the target.

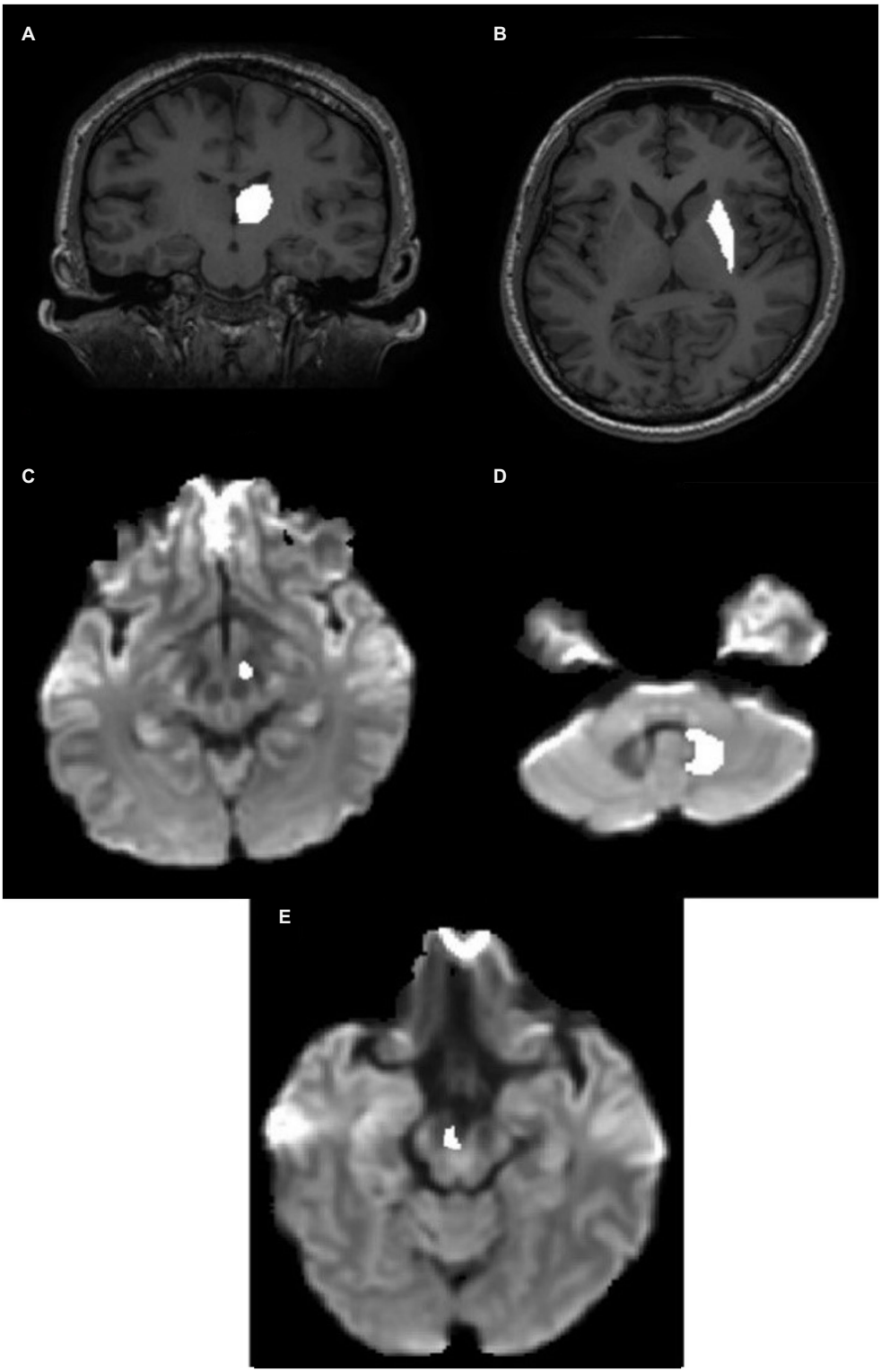

FIGURE 2
ROI definition in the individual native space. **(A)** Thalamic ROI mask superimposed on the T1 image. **(B)** Putamen ROI mask superimposed on the T1 image. **(C)** STN ROI superimposed on the Fiber Orientation Distribution (FOD) image. **(D)** Hypointense regions in the FOD image around the DN in the CB. **(E)** VTA ROI superimposed on the FOD image. CB, cerebellum; DN, dentate nucleus; STN, subthalamic nucleus; VTA, ventral tegmental area.

2.7.4. Cerebello-prefrontal tracts *via* (a) VTA and (b) thalamus

Tractography was performed on tracts from the dentate nucleus to the contralateral prefrontal cortex (ACC/mPFC) with VTA (Carta et al., 2019) or thalamus as inclusion regions.

2.8. Statistical analysis

After verification of the normal distribution of data, to study the effect of age on morphological features of cerebellar tracts, a linear regression model was used to identify the association between

individual mean parameters of FD, FC, and FDC across fixels of each tract (cerebello-thalamo-striatal and STN-Crus7b;) considering age as a covariable of interest, using the sex, education, and total intracranial volume (TIV) of the subjects as regressors of nuisance. The statistics and machine learning toolbox in MATLAB (R2019a: The MathWorks, Inc., Natick, Massachusetts, United States) was used for the analysis. Statistical significance was corrected for multiple comparisons using Bonferroni correction at $p < 0.05$. To study the relationship between the neuropsychological scores determined from ACE-M/RAVLT and FBA tract parameters, partial Pearson's correlation analysis was performed after controlling for variables age, sex and education. Statistical significance was corrected for multiple comparisons using Bonferroni correction at $p < 0.05$.

2.9. Data availability statement

All the subject MRI data were collected at the Imaging Sciences and Interventional Radiology (IS/IR) Department and is the property of the Neurology Department at SCTIMST. These data will be made available to the academic researchers upon reasonable request to the corresponding author and the approval of the Institute Ethics Committee (IEC) at SCTIMST.

2.10. Declaration of competing interest

The authors declare that they have no known competing financial interests or personal ties that could have influenced the research presented in this study.

3. Results

Table 1 shows the demographics and the neuropsychological measures for the cognitive subject group.

3.1. Tractography of CB-BG interconnecting networks

The tractography analysis revealed the bilateral and reciprocal tracts between the CB and BG. The ascending tract between the dentate nucleus to the contralateral thalamus traversed the superior cerebellar peduncles and decussated at the level of the midbrain to the contralateral side, terminating in the Putamen (Figure 3A). The descending tract between STN to the contralateral cerebellar cortex, C7b and Crus II, traversed the basilar part of the pons, decussated along regions associated with the pontine nuclei, and passed through the middle cerebellar peduncle (Figure 3B).

We generated a specific fixel mask for each of the ascending and descending tracts (in the study template space) using the individual white matter FOD image that was spatially normalized in the study template space. The fixel mask generated from the tracts was intersected with the whole brain white matter FD, FC, and FDC fixel data image to obtain the tract-specific metric for individual subjects.

TABLE 1 Table showing the demographics and the neuropsychological measures for the cognitive subject group.

Characteristic	Mean (*n=20*)	Std. deviation
Age (years)	56.8	8.7
Sex (M/F)	11\09	
Education (years)	12.58	2.53
MMSE	29.1	0.95
ACE-M (Reg-24)*	21.86	1.58
ACE-M (Recall-10)*	7.52	1.53
ACE-M (total)	92.9	3
ACE-orientation	9.95	0.22
ACE-attention	7.95	0.22
ACE-memory	28.22	2.53
ACE-verbal fluency	13.6	0.66
ACE-visuospatial	4.6	0.74
ACE-language	27.85	0.65
RAVLT (total)*	47.24	8.08
RAVLT delayed recall	9.62	2.85

*ACE-M (Reg-24): Subdomain of ACE-Malayalam, registration/learning with 24-point scale (3 points for registration of 3 words and 21 points for learning of 3-trial learning of an address); ACE-M (Recall-10): subdomain of ACE-Malayalam with 10-point scale (3 points for recall of 3 words and 7 points for recall of address, each after a delay of 5 min); RAVLT, Rey Auditory Verbal Learning Test.

3.2. Tractography on the control tracts

We successfully reconstructed the CTC tracts (Figure 3C). For the sensorimotor tracts, the DN exited the CB *via* the superior cerebellar peduncle, decussated at the level of the midbrain, traversed the contralateral thalamus *via* the ventral intermediary nucleus (VIM), and reached the contralateral primary motor and sensory cortices (Figure 3C). For the associative tracts, the dentate exited the CB *via* the superior cerebellar peduncle, traversed the contralateral thalamus *via* the mediodorsal nuclei, and reached the contralateral frontal cortex (ACC/mPFC; Figure 3C). In addition, we reconstructed the tracts between the dentate nucleus to the contralateral frontal cortex (ACC/mPFC) passing through the VTA (Figure 3C). The reconstruction of the cerebellar tract was performed using an inclusion mask comprising the whole thalamus. However, looking at the tract trajectories through their thalamic relays, (i) the CB-BG tract passed through the central-medial nucleus; (ii) the CTC connecting the sensorimotor areas passed through the ventral intermediary nucleus; (iii) the CTC connecting the prefrontal areas passed through the medial-dorsal nucleus. These thalamic relays (Figure 4A) are in correspondence with what is known of the neuroanatomy of these pathways.

The linear regression analysis showed a significant negative linear relationship between FD and age for the ascending and descending CB-BG tracts (Figures 4B, C; Table 2). In all the tracts, the mean FC and logFC values were unaffected by age. FDC values were found to be negatively correlated with age in the ascending tract between the right Dentate to left Putamen.

Mean values of FDC across fixels within all the tracts showed a significant positive linear relationship with TIV (Table 2). TIV was also found to have a significant positive linear relationship with the mean parameter, log_FC of the bilateral tract from STN to the Cerebellar cortex. TIV was significantly higher in males compared to females, most

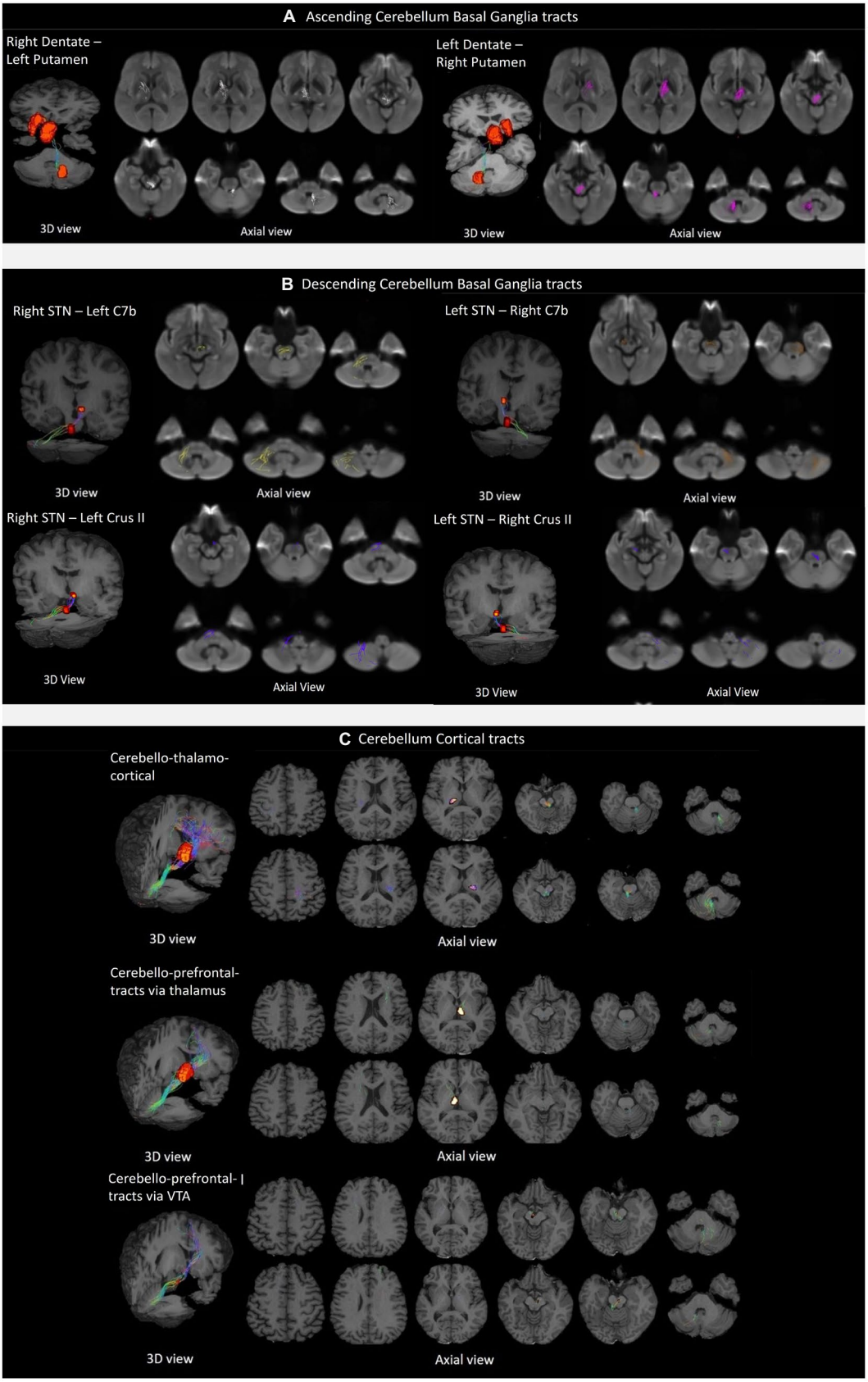

FIGURE 3
Tractography of crossed reciprocal tracts between the CB-BG and cortical targets in a representative subject. Tracts are superimposed on the study template (3D view, and axial views for a display of the tract trajectory). **(A)** Ascending cerebellum basal ganglia tracts; From left to right, Tracts between Right DN and Left Putamen, traversing Left Thalamus; Tracts between Left DN and Right Putamen, traversing Right Thalamus. **(B)** Descending cerebellum

(Continued)

FIGURE 3 (Continued)
basal ganglia tracts; In the clockwise direction, Tracts between Right STN and contralateral Cerebellar cortex, C7b Left; Tracts between Left STN and contralateral Cerebellar cortex, C7b Right; Tracts between Right STN and contralateral Cerebellar cortex, C7b Left; Tracts between Left STN and contralateral CB cortex, Crus II Right; Tracts between Right STN and contralateral Cerebellar cortex, Crus II Left; **(C)** Cerebellar cortical tracts; From top to bottom, the first row shows the tracts between the DN and the sensorimotor cortex traversing the ventral intermediary nucleus of the thalamus. The top and bottom rows display axial views of the right CB-left thalamus/Cortex and left CB-right Thalamus/Cortex respectively; The second row shows the tracts between the DN to the contralateral mPFC/ACC *via* the medial dorsal nuclei of the thalamus. The top and bottom rows display axial views of the left CB-right Thalamus/Cortex and right CB-left thalamus/Cortex, respectively. The third row shows the tracts from the dentate to the contralateral mPFC/ACC *via* the ventral tegmental area.

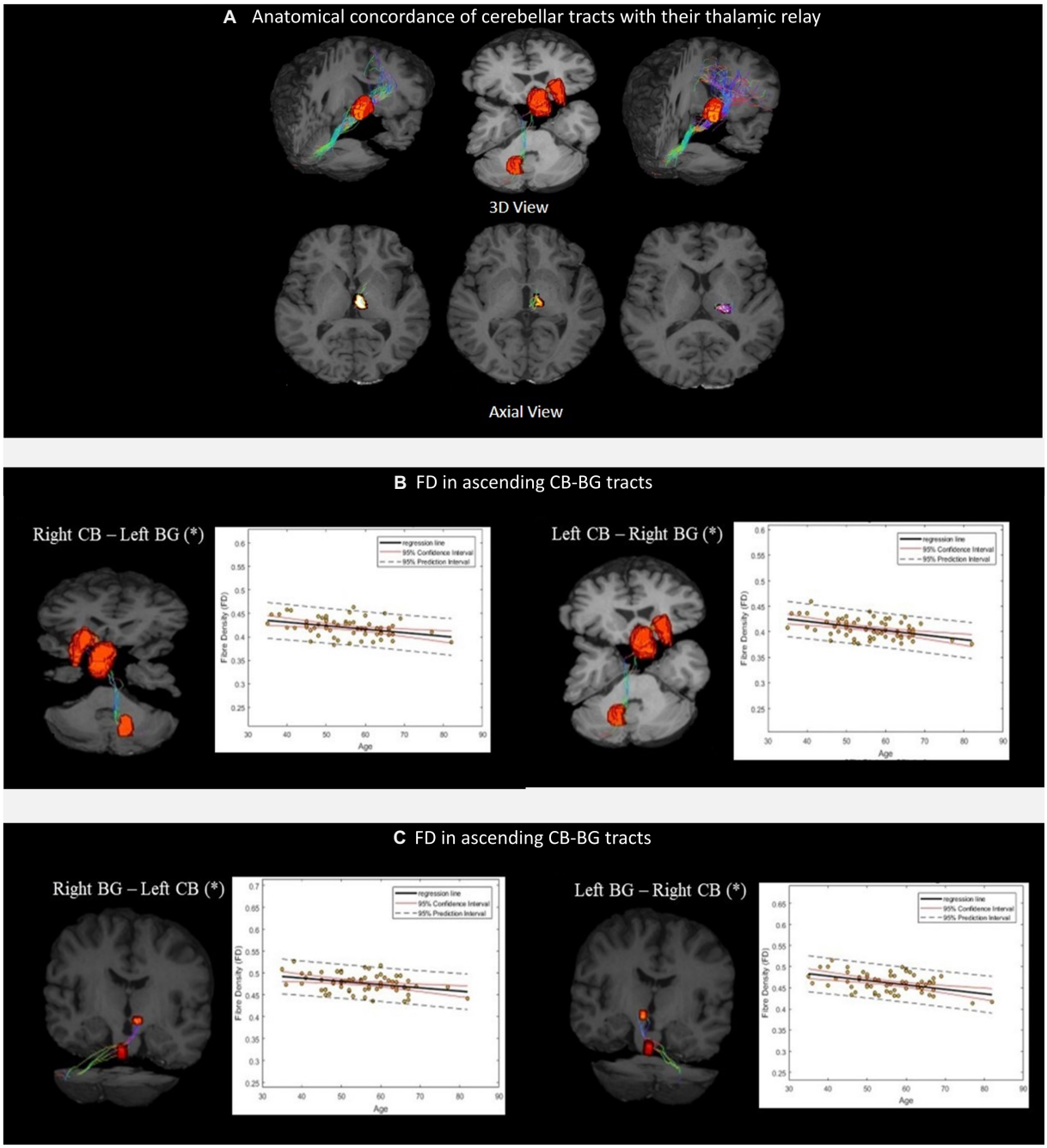

FIGURE 4
(A) Thalamic nuclei as specific relays of the cerebellar tracts. From left to right, Medial Dorsal (MD) nuclei with cerebello-frontal tracts; Central median (CM) nuclei with cerebello-thalamo-striatal (CTS) tracts; Ventral Intermediary (VIM) nuclei with cerebello-thalamocortical (CTC) tracts. Scatterplots **(B,C)** show the mean FD values of the corresponding CB-BG tracts included in the analysis. The black solid lines represent the regression line, whereas the dashed red lines represent the 95% confidence interval and the black dashed lines represent the 95% prediction interval. (*) indicates the significant linear relationship with age.

TABLE 2 Table showing the estimated value of the standardized regression coefficients for the tract-level analysis metrics along with their *p*-values.

FBA metric	Tracts	Age		Sex		TIV		Education	
		β	p	β	p	β	p	β	p
FD	Dn_L → Put_R	**−0.40994**	**0.00087457**	−0.03281	0.82751	−0.18287	0.2317	0.190501	0.10523
	Dn_R → Put_L	**−0.49802**	**5.26E-05**	0.01276	0.93086	−0.1371	0.35745	0.097072	0.39419
	STN_R → C7b_L	**−0.35857**	**0.00024516**	0.324362	0.59763	−0.23155	0.83761	0.184973	0.5422
	STN_L → C7b_R	**−0.4552**	**0.0031548**	0.079334	0.053923	−0.03106	0.12995	0.070781	0.11418
FDC	Dn_L → Put_R	−0.25413	0.0624673	−0.11796	0.40737	**0.502846**	**0.00083**	0.075748	0.4905
	Dn_R → Put_L	**−0.29739**	**0.0054045**	−0.09823	0.45983	**0.563221**	**8.36E-05**	−0.01399	0.89133
	STN_R → C7b_L	−0.10082	0.078241	0.124569	0.65756	**0.394158**	**0.00022**	0.114996	0.69805
	STN_L → C7b_R	−0.22577	0.37206	−0.06085	0.38969	**0.542427**	**0.00865**	0.041124	0.30452
log_FC	Dn_L → Put_R	−0.20606	0.1115	−0.11263	0.49373	−0.09478	0.56809	0.060059	0.6362
	Dn_R → Put_L	−0.13495	0.29755	−0.1608	0.33275	−0.06666	0.68981	0.050139	0.69481
	STN_R → C7b_L	0.128051	0.58676	−0.12466	0.26621	**0.507762**	**0.00575**	0.019757	0.74253
	STN_L → C7b_R	0.067096	0.28536	−0.17672	0.4164	**0.455513**	**0.00163**	0.040131	0.86719

The values of regression coefficients in bold are significant at Bonferroni corrected *p*-value of $p < 0.05$.

likely reflecting a gender effect. Multiple regression analysis of gray matter volume with age considering education, TIV, and sex as covariates yielded no significant relation at FWE corrected *p*-value of 0.05.

3.3. Neuropsychological analysis

3.3.1. Ascending tracts

FD in the cerebello-thalamo-striatal tracts was positively correlated with the ACE-M (Reg-24) score (DN_L to Putamen_R, $p_{corrected} = 0.0117$; DN_R to Putamen_R, $p_{corrected} = 0.0386$ as in Figures 5A, B). For the DN-mPFC tracts passing through thalamic or VTA relays, FD was positively correlated with the ACE-M (Recall-10) score (DN_L-VTA-ACC_R, $p_{corrected} = 0.0070$; DN_R-VTA-ACC_L, $p_{corrected} = 0.0201$ as in Figures 5C, D; DN L-Thal-ACC_R, $p_{corrected} = 0.0014$; DN_R-Thal-ACC_L $p_{corrected} = 0.0061$ as in Figures 5E, F). The RAVLT, ACE-M (total), and ACE-M (Reg-24) scores did not correlate with FD in any of these tracts. In the case of CTC tracts, none of the tract parameters correlated with the neuropsychological parameters. Other subdomains of ACE-M were not found to be significant with any of the FBA metric of the ascending tracts.

3.3.2. Descending tracts

The FBA metrics for the tracts from STN to the contralateral cerebellar cortex were extracted for STN-C7b tracts as well as STN-CrusII tracts. Pearson's correlation between the FBA metrics of the C7b tract and neuropsychological scores of ACE-M and RAVLT did not yield any significant relationship. FD in the STN-R_CrusII_L was positively correlated with ACE-M(Recall-10) score ($p_{corrected} = 0.0431$) as in Figures 5G, H. The ACE-M, ACE-M (Reg-24), ACE-M (total), RAVLT, and RAVLT Delayed Recall scores did not correlate with FD in this tract. Other subdomains of ACE-M were not found to be significant with any of the FBA metric of the descending tracts.

4. Discussion

We validated the subcortical CB-BG connection in a large database of 64 healthy volunteers and expanded the findings reported earlier in primates and small samples of healthy subjects. In addition, we showed for the first time, that the microstructure of subcortical reciprocal connections between the CB and BG in human subjects was affected by aging. We further explored the cognitive functional roles of these tracts and found that inter-individual variability of descending and ascending CB-BG reciprocal tracts was associated with cognitive scores. These findings bring important consideration for the understanding of neurodevelopmental and neurodegenerative diseases.

4.1. White matter tracts constituting the CB-BG direct subcortical network

The tractography using constrained spherical deconvolution that addresses the issue of crossing fibers present in the majority of the white matter voxels (Raffelt et al., 2015), validated the presence of ascending tracts from the output nuclei of the CB, the dentate nucleus, to the contralateral putamen, *via* the thalamus. The tracts traversed primarily through the centromedian nucleus of the thalamus before reaching the putamen (Figure 4A). This is an important validation since the connections from the dentate to the striatum in mice pass through the anatomical equivalent thalamic nucleus (Coutant et al., 2022). A similar trajectory of the dentato-thalamo-striatal pathway through the thalamus was reported in the transneuronal viral transport study in macaques (Hoshi et al., 2005).

The descending tracts from the STN were found to innervate the contralateral cerebellar cortex *via* the middle cerebellar peduncles with decussations along the regions that include the pontine nuclei (Figure 3B). We showed that the CB-BG subcortical tracts in healthy human subjects have similar trajectories as reported in non-human primate studies and is congruent with the findings of Milardi et al. which established the dentato-thalamic pathways (Milardi et al., 2016).

We performed tractography on the cerebello-thalamo-cortical tract as a control tract with a known trajectory (Yamada et al., 2010) from the dentate nucleus to the primary motor and sensory cortical areas. We confirmed that this tract passes *via* the VIM nucleus of the thalamus,

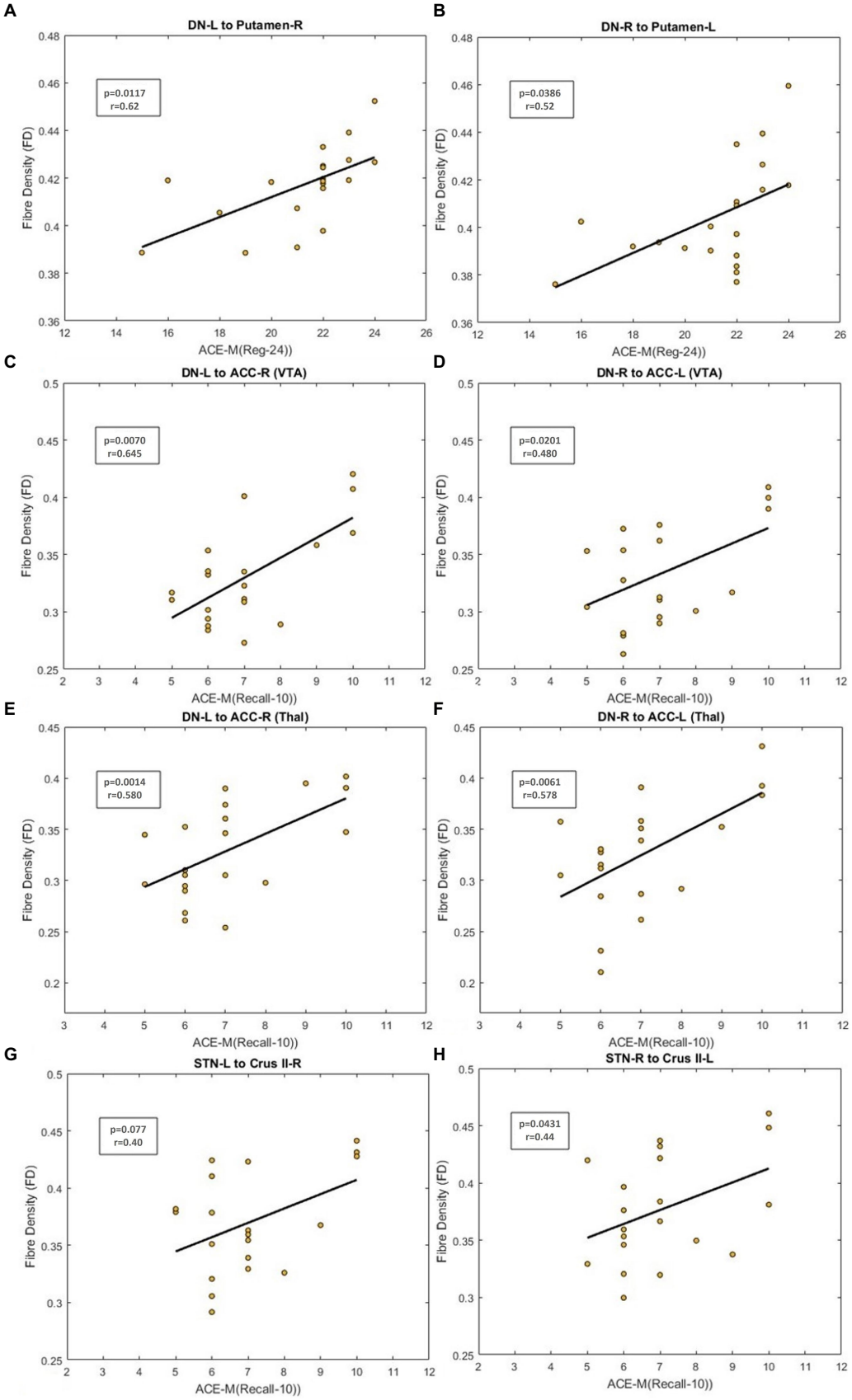

FIGURE 5
Figure showing the scatterplot between Fiber Density (FD) and neuropsychological scores. **(A,B)** Scatterplot for ACE-M (Reg-24) against FD for the dentate nucleus to contralateral Putamen tract. **(C,D)** Scatter plot for ACE-M (Recall-10) against FD for the dentate nucleus to prefrontal cortex tract *via* VTA **(E,F)** Scatter plot for ACE-M (Recall-10) against FD for the dentate nucleus to prefrontal cortex tract *via* thalamus **(G,H)** Scatter plot for ACE-M (Recall-10) against FD for tracts from STN to contralateral Crus II tract.

thus establishing that the tractography algorithms used in the study have anatomical validity. In addition, we showed that CB tracts also reach ACC, and mPFC, passing through the VTA and medial-dorsal nucleus of the thalamus.

The projections from VTA to the prefrontal cortex (Björklund and Dunnett, 2007) mediate higher-order cognitive functions, and the recent work of Carta et al. (2019) proves the role of cerebellum-VTA connection in social behavior and reward circuitry. We, therefore, tested for a direct connection from cerebellar output nuclei to the prefrontal cortex *via* VTA. The tractography results in Figure 3C demonstrate the anatomical connections from the dentate nucleus to the prefrontal cortex *via* VTA.

4.2. Age-related changes in the morphometry of the CB-BG connections

Going further than the anatomical description of the tracts, we demonstrated for the first time, a negative linear relationship between age and FD in the ascending and descending tracts between CB-BG. Fiber morphometric measures are an indicator of the ability of the axonal bundle to relay information, depending on the number of axons and the volume of the axonal cross-section. In the FBA analysis technique used in this study, the FD metric, calculated as an integral of the fiber orientation distribution in a fixel, is proportional to the intra-axonal volume of the fiber bundles in that fixel and is a measure of the number of axons in a fiber bundle (Raffelt et al., 2012). The relationship between FD and age in CB-BG reciprocal tracts could arise from reduced free water volume in the fixel associated with aging and possibly axonal loss.

Age-related changes to whole-brain white matter morphology have been widely reported both in human and animal studies using the diffusion scalar metrics such as Fractional Anisotropy (FA), Radial Diffusivity (RD), and Axial Diffusivity (AD) as well as postmortem studies (Tang et al., 1997; Salat et al., 2005; Bowley et al., 2010; Sala et al., 2012; Bennett and Madden, 2014; Cox et al., 2016). However, very few studies have investigated precise cerebellar tracts. The age-related decline in FD indicates a reduction in the number of fibers in the white matter bundle connecting the CB-BG with advancing age. Postmortem studies on age-related WM atrophy in human subjects at the corpus callosum have identified a reduction in the number of fibers and density as the primary factor contributing to WM atrophy (Hou and Pakkenberg, 2012). FD and FC provide a macrostructural and microstructural measure of change in the fiber tracts, respectively, and their combined measure of FDC obtained as a product of FD and FC provides an overall measure of the ability of the fiber bundle to relay information (Raffelt et al., 2017). One of the arguments proposed to explain the relative preservation of FC with age is the presence of different caliber axons in the bundle. The larger axons are better preserved during aging, thus maintaining FC (Choy et al., 2020). and this could explain preserved FC in the CB-BG connections in this study. Greater axonal caliber is associated with a higher information rate (Perge et al., 2012). The preservation of FC in the CB-BG with aging could indicate these tracts may be involved in the rapid information exchanges that are necessary to efficiently update the comparison between expectations with the current state of the cognitive and motor system, a function that is dear to the cerebellum. Future studies including more of older subjects are required to quantify the relation between age-related deterioration in motor function and FC of the CB-BG network.

To fully comprehend the functional changes associated with the age-related degeneration of the CB-BG tracts, it is imperative to understand the changes in BG as well as thalamic regions. The striatal regions of the putamen and caudate undergo bilateral shrinkage with age and their volumes display a negative trend with age (Gunning-Dixon et al., 1998; Raz et al., 2003; Koikkalainen et al., 2007). Similarly, STN volumes and cell count also decrease in an age-dependent fashion (Zwirner et al., 2016). In the case of the thalamus which forms the relay between the CB and BG regions, the volume also has a downward trend with aging (Pfefferbaum et al., 2013). The regions of the brain that age first and result in changes in the FD of CB-BG tracts are yet to be identified.

4.3. Psychometric and behavioral correlations with CB-BG tract microstructure

We found a positive association between FD of subthalamo-cerebellar and cerebello-frontal tracts and the learning/retention domain of ACE-M scoring. Descending tracts between STN to CrusII have been primarily associated with non-motor processes (Guell and Schmahmann, 2020). Viral tracing studies on non-human primates demonstrated the presence of second-order neurons projecting from CrusIIp to STN (Bostan et al., 2010). In addition, the basic framework for a resting-state executive control network consists of regions from BG such as the associative territory of the striatum, the caudate, and regions of CB such as Crus I and II along with the prefrontal cortical region and is associated with non-motor functions such as verbal fluency and working as well as episodic memory (Habas et al., 2009). The relationship we show between the tract FBA metrics and cognitive scores involves the cerebello-frontal network and reciprocal CB-BG network. Subthalamo-cerebellar tract from STN to pontine nuclei to Crus II showed a positive linear relationship with the FD metric while the FBA metrics of the subthalamo-cerebellar tract to C7b showed no significant linear relationship with any of the neuropsychological scores. This is congruent with the fact that the CB C7b region is primarily associated with motor tasks and CrusII is primarily involved in non-motor functions (Van Overwalle et al., 2020a,b).

We found that individual neuropsychological scores were correlated with individual FD values in tracts from the CB to ACC/mPFC region traversing (a) VTA and (b) mediodorsal nuclei of the thalamus. FD for these tracts had a positive linear relationship with the 10-point score of 10 min recall of 3 words and address, ACE-M (Recall-10). Lower FD values could be associated with a reduction in the information-carrying capability of the white matter bundle leading to a reduction in the ability to recall the word list and address from memory and *vice-versa*. In the case of the cerebello-thalamo-striatal tract (putamen), FD had a positive linear relationship with the ACE-M (Reg-24) scores, implying that this tract could be primarily associated with the initial learning capability of the words/address. Neuroimaging studies on instrumental learning have demonstrated the role of putamen in the acquisition of cue-response association during the exploration phase (Brovelli et al., 2011). This could imply the cerebello-thalamo-putamen tract properties can affect learning and memory registration.

4.4. Implication for movement disorders where BG and CB are affected

Connections between CB and BG are particularly relevant to BG disorders such as PD and dystonia (Wu and Hallett, 2013; Bologna and Berardelli, 2017). Supporting findings for the presence of the dentato-thalamo-striatal pathway in human subjects come from deep brain stimulation (DBS) studies on dystonia and tremor patients (Paraguay et al., 2021). Despite being conventionally classified as a BG disorder, in PD patients with tremor symptoms, DBS of the thalamic nuclei, ventral intermediary nuclei (VIM), which receive input from the CB, provides greater beneficial effects rather than the nuclei receiving inputs from BG (Narabayashi et al., 1987). Preliminary finding on DBS of the dentate nucleus has shown positive outcomes for dystonia and tremor patients (Diniz et al., 2021). The STN is an excitatory nucleus that drives the output of the BG. Thus, age-dependent structural changes of CB-BG tracts might influence the efficacy of STN-DBS.

In the reciprocal connections of the CB-BG tract, little is known about the functional involvement of feedback loops connecting the cerebrum to the cerebellum through the STN.

Basal ganglia hyperactivity in PD patients was supposedly transferred to the cerebellum *via* subthalamo-cerebellar connections (Asanuma et al., 2005) and STN-DBS ameliorates the hyperactivity in the CB thereby improving motor function in PD patients (Payoux et al., 2004; Asanuma et al., 2006). Age-related progressive loss in nigrostriatal dopamine neurons has been recorded to result in age-related functional deficits (Gibb and Lees, 1991). A multi-fold acceleration of this phenomenon leads to PD. Similarly, it can be hypothesized that over time, an accelerated loss of CB-BG subcortical tracts as demonstrated in aging could substantially weaken the cerebellar control over BG and contribute to the pathophysiology of PD. In the case of spinocerebellar ataxias (SCA), which are clinically and genetically heterogeneous, the mean age at onset of symptoms differs for SCA1, SCA2, SCA3, SCA6, SCA7, and could vary from third to fourth and even sixth decade of life (Warrenburg et al., 2005). The knowledge of the age effects of CB-BG circuits could help better understand the clinically diverse manifestation of the disease including the occurrence of parkinsonism and dystonia in some of the SCA (Meira et al., 2019).

4.5. Limitations

One of the limitations of this study is the use of a single shell and relatively low b-value ($b = 1000 S/mm^2$) for the acquisition of diffusion data. Estimation of FOD and apparent FD (AFD) could be made more robust with higher and multiple b-value acquisitions. Another limitation of the study is the medium range of the effect size (Cohen's f^2: 0.15–0.35) for the multiple linear regression analysis for age vs. FD. Even though the negative linear relation is statistically significant, the change in FD with unit change in age is smaller. Another limitation is the small sample size of cognitive data. Although the results provide a new perspective on the functional role of these tracts in memory registration and recall, a longitudinal study with a larger sample size is required to further validate the results of the association between CB-BG tract parameters and cognitive scores. Even though the correlation values between the neuropsychological scores and FD values provide information on the involvement of these tracts on the task, the exact role played by these tracts in the memory and learning network needs to be further explored.

5. Conclusion

In this study, we confirmed the existence and trajectories of subcortical connections between the CB and BG in a large group of human subjects, as reported in non-human primates. We observed that FD in reciprocal CB-BG tracts was negatively correlated with age and positively correlated with specific cognitive psychometric scores. The recall memory assessment domain of ACE-M was associated with FD for both the subthalamic-cerebello (Crus II) tract and the cerebello-frontal tracts to the prefrontal cortex. The FD metric in the cerebello-thalamo-putamen tracts was positively correlated with the learning/registration domain of the ACE-M score. Further investigation is required to study the functional roles of these tracts in movement disorders particularly PD and dystonia and its therapeutic implications. Deepening our knowledge of the functional neuroanatomy of the CB-BG connections in humans has much value in understanding their interactions in health and disease. This warrants more studies, including post-mortem studies, for confirmation of these interconnections.

Data availability statement

The datasets presented in this article are not readily available because of ethical and privacy restrictions. Requests to access the datasets should be directed to asha.kishore@asterdmhealthcare.com.

Ethics statement

The studies involving human participants were reviewed and approved by Institutional Ethics Committee, Sree Chitra Tirunal Institute for Medical Sciences and Technology, Kerala, India. The patients/participants provided their written informed consent to participate in this study.

Author contributions

AK, SK, CG, and VR formulated the research goals. AK acquired funding and supervised the project. VR, PJ, and RM acquired the data. VR, CG, and RV analyzed the data. VR, AK, and CG wrote the manuscript. SK, CK, and BT read and revised the manuscript. All authors contributed to the article and approved the submitted version.

Funding

This work received intramural funding (Project No: 5170) from the Sree Chitra Tirunal Institute for Medical Sciences and Technology, Kerala, India.

Conflict of interest

The authors declare that the research was conducted in the absence of any commercial or financial relationships that could be construed as a potential conflict of interest.

Publisher's note

All claims expressed in this article are solely those of the authors and do not necessarily represent those of their affiliated organizations, or those of the publisher, the editors and the reviewers. Any product that may be evaluated in this article, or claim that may be made by its manufacturer, is not guaranteed or endorsed by the publisher.

Supplementary material

The Supplementary material for this article can be found online at: https://www.frontiersin.org/articles/10.3389/fnagi.2023.1019239/full#supplementary-material

References

Allen, G. I., Gilbert, P. F., and Yin, T. C. (1978). Convergence of cerebral inputs onto dentate neurons in monkey. *Exp. Brain Res.* 32, 151–170. doi: 10.1007/BF00239724

Asanuma, K., Ma, Y., Huang, C., Carbon-Correll, M., Edwards, C., Raymond, D., et al. (2005). The metabolic pathology of Dopa-responsive dystonia. *Ann. Neurol.* 57, 596–600. doi: 10.1002/ana.20442

Asanuma, K., Tang, C., Ma, Y., Dhawan, V., Mattis, P., Edwards, C., et al. (2006). Network modulation in the treatment of Parkinson's disease. *Brain J. Neurol.* 129, 2667–2678. doi: 10.1093/brain/awl162

Asanuma, C., Thach, W. T., and Jones, E. G. (1983). Distribution of cerebellar terminations and their relation to other afferent terminations in the ventral lateral thalamic region of the monkey. *Brain Res. Rev.* 5, 237–265. doi: 10.1016/0165-0173(83)90015-2

Ballard, I. C., Murty, V. P., McKell Carter, R., MacInnes, J. J., Huettel, S. A., and Alison Adcock, R. (2011). Dorsolateral prefrontal cortex drives mesolimbic dopaminergic regions to initiate motivated behavior. *J. Neurosci.* 31, 10340–10346. doi: 10.1523/JNEUROSCI.0895-11.2011

Bendlin, B. B., Fitzgerald, M. E., Ries, M. L., Guofan, X., Kastman, E. K., Thiel, B. W., et al. (2010). White matter in aging and cognition: a cross-sectional study of microstructure in adults aged eighteen to eighty-three. *Dev. Neuropsychol.* 35, 257–277. doi: 10.1080/87565641003696775

Bennett, I. J., and Madden, D. J. (2014). Disconnected aging: cerebral white matter integrity and age-related differences in cognition. *Neuroscience* 276, 187–205. doi: 10.1016/j.neuroscience.2013.11.026

Björklund, A., and Dunnett, S. B. (2007). Dopamine neuron Systems in the Brain: an update. *Trends Neurosci.* 30, 194–202. doi: 10.1016/j.tins.2007.03.006

Bologna, M., and Berardelli, A. (2017). Cerebellum: an explanation for dystonia? *Cerebell. Ataxias* 4:6. doi: 10.1186/s40673-017-0064-8

Bostan, A. C., Dum, R. P., and Strick, P. L. (2010). The basal ganglia communicate with the cerebellum. *Proc. Natl. Acad. Sci.* 107, 8452–8456. doi: 10.1073/pnas.1000496107

Bostan, A. C., and Strick, P. L. (2018). The basal ganglia and the cerebellum: nodes in an integrated network. *Nat. Rev. Neurosci.* 19, 338–350. doi: 10.1038/s41583-018-0002-7

Bowley, M. P., Cabral, H., Rosene, D. L., and Peters, A. (2010). Age changes in Myelinated nerve fibers of the cingulate bundle and corpus callosum in the rhesus monkey. *J. Comp. Neurol.* 518, 3046–3064. doi: 10.1002/cne.22379

Brovelli, A., Nazarian, B., Meunier, M., and Boussaoud, D. (2011). Differential roles of caudate nucleus and putamen during instrumental learning. *Neuroimage* 57, 1580–1590. doi: 10.1016/j.neuroimage.2011.05.059

Carta, I., Chen, C. H., Schott, A., Dorizan, S., and Khodakhah, K. (2019). Cerebellar modulation of the reward circuitry and social behavior. *Science* 363:eaav0581. doi: 10.1126/science.aav0581

Choy, S. W., Bagarinao, E., Watanabe, H., Ho, E. T. W., Maesawa, S., Mori, D., et al. (2020). Changes in white matter fiber density and morphology across the adult lifespan: a cross-sectional Fixel-based analysis. *Hum. Brain Mapp.* 41, 3198–3211. doi: 10.1002/hbm.25008

Coelho, A., Fernandes, H. M., Magalhães, R., Moreira, P. S., Marques, P., Soares, J. M., et al. (2021). Signatures of white-matter microstructure degradation during aging and its association with cognitive status. *Sci. Rep.* 11:4517. doi: 10.1038/s41598-021-83983-7

Cordero-Grande, L., Christiaens, D., Hutter, J., Price, A. N., and Hajnal, J. V. (2019). Complex diffusion-weighted image estimation via matrix recovery under general noise models. *Neuroimage* 200, 391–404. doi: 10.1016/j.neuroimage.2019.06.039

Coutant, B., Frontera, J. L., Perrin, E., Combes, A., Tarpin, T., Menardy, F., et al. (2022). Cerebellar stimulation prevents levodopa-induced dyskinesia in mice and normalizes activity in a motor network. *Nat. Commun.* 13:3211. doi: 10.1038/s41467-022-30844-0

Cox, S. R., Ritchie, S. J., Tucker-Drob, E. M., Liewald, D. C., Hagenaars, S. P., Davies, G., et al. (2016). Ageing and brain white matter structure in 3,513 UK biobank participants. *Nat. Commun.* 7:13629. doi: 10.1038/ncomms13629

Diniz, J. M., Cury, R. G., Iglesio, R. F., Lepski, G. A., França, C. C., Barbosa, E. R., et al. (2021). Dentate nucleus deep brain stimulation: technical note of a novel methodology assisted by Tractography. *Surg. Neurol. Int.* 12:400. doi: 10.25259/SNI_338_2021

Doya, K. (2000). Complementary roles of basal ganglia and cerebellum in learning and motor control. *Curr. Opin. Neurobiol.* 10, 732–739. doi: 10.1016/S0959-4388(00)00153-7

Elhalal, A., Davelaar, E. J., and Usher, M. (2014). The role of the frontal cortex in memory: an investigation of the Von Restorff effect. *Front. Hum. Neurosci.* 8:410. doi: 10.3389/fnhum.2014.00410

Fjell, A. M., Sneve, M. H., Storsve, A. B., Grydeland, H., Yendiki, A., and Walhovd, K. B. (2016). Brain events underlying episodic memory changes in aging: a longitudinal investigation of structural and functional connectivity. *Cereb. Cortex* 26, 1272–1286. doi: 10.1093/cercor/bhv102

Gibb, W. R., and Lees, A. J. (1991). Anatomy, pigmentation, ventral and dorsal subpopulations of the Substantia Nigra, and differential cell death in Parkinson's disease. *J. Neurol. Neurosurg. Psychiatry* 54, 388–396. doi: 10.1136/jnnp.54.5.388

Guell, X., and Schmahmann, J. (2020). Cerebellar functional anatomy: a didactic summary based on human FMRI evidence. *Cerebellum* 19, 1–5. doi: 10.1007/s12311-019-01083-9

Gunning-Dixon, F. M., Head, D., McQuain, J., Acker, J. D., and Raz, N. (1998). Differential aging of the human striatum: a prospective MR imaging study. *Am. J. Neuroradiol.* 19, 1501–1507.

Habas, C., Kamdar, N., Nguyen, D., Prater, K., Beckmann, C. F., Menon, V., et al. (2009). Distinct cerebellar contributions to intrinsic connectivity networks. *J. Neurosci.* 29, 8586–8594. doi: 10.1523/JNEUROSCI.1868-09.2009

Haber, S. N. (2003). The primate basal ganglia: parallel and integrative networks. *J. Chem. Neuroanat.* 26, 317–330. doi: 10.1016/j.jchemneu.2003.10.003

Hoche, F., Guell, X., Vangel, M. G., Sherman, J. C., and Schmahmann, J. D. (2018). The cerebellar cognitive affective/Schmahmann syndrome scale. *Brain J. Neurol.* 141, 248–270. doi: 10.1093/brain/awx317

Hoshi, E., Tremblay, L., Féger, J., Carras, P. L., and Strick, P. L. (2005). The cerebellum communicates with the basal ganglia. *Nat. Neurosci.* 8, 1491–1493. doi: 10.1038/nn1544

Hou, J., and Pakkenberg, B. (2012). Age-related degeneration of corpus callosum in the 90+ years measured with stereology. *Neurobiol. Aging* 33, 1009.e1–1009.e9. doi: 10.1016/j.neurobiolaging.2011.10.017

Jenkinson, M., Bannister, P., Brady, M., and Smith, S. (2002). Improved optimization for the robust and accurate linear registration and motion correction of brain images. *Neuroimage* 17, 825–841. doi: 10.1016/s1053-8119(02)91132-8

Jobson, D. D., Hase, Y., Clarkson, A. N., and Kalaria, R. N. (2021). The role of the medial prefrontal cortex in cognition, ageing and dementia. *Brain Commun.* 3:fcab125. doi: 10.1093/braincomms/fcab125

Kaji, R., Bhatia, K., and Graybiel, A. M. (2018). Pathogenesis of dystonia: is it of cerebellar or basal ganglia origin? *J. Neurol. Neurosurg. Psychiatry* 89, 488–492. doi: 10.1136/jnnp-2017-316250

Kawato, M., and Gomi, H. (1992). A computational model of four regions of the cerebellum based on feedback-error learning. *Biol. Cybern.* 68, 95–103. doi: 10.1007/BF00201431

Kellner, E., Dhital, B., and Reisert, M.. (2015). "Gibbs-ringing artifact removal based on local subvoxel-shifts." ArXiv:1501.07758 [Preprint].

Kemp, J. M., and Powell, T. P. (1971). The Connexions of the striatum and Globus Pallidus: synthesis and speculation. *Philos. Trans. R. Soc. Lond. B Biol. Sci.* 262, 441–457. doi: 10.1098/rstb.1971.0106

Kishore, A., Meunier, S., and Popa, T. (2014). Cerebellar influence on motor cortex plasticity: behavioral implications for Parkinson's disease. *Front. Neurol.* 5:68. doi: 10.3389/fneur.2014.00068

Kishore, A., and Popa, T. (2014). Cerebellum in levodopa-induced Dyskinesias: the unusual suspect in the motor network. *Front. Neurol.* 5:157. doi: 10.3389/fneur.2014.00157

Koikkalainen, J., Hirvonen, J., Nyman, M., Lötjönen, J., Hietala, J., and Ruotsalainen, U. (2007). Shape variability of the human striatum--effects of age and gender. *Neuroimage* 34, 85–93. doi: 10.1016/j.neuroimage.2006.08.039

Maia, T. V., and Frank, M. J. (2011). From reinforcement learning models to psychiatric and neurological disorders. *Nat. Neurosci.* 14, 154–162. doi: 10.1038/nn.2723

Mathuranath, P. S., Hodges, J. R., Robert Mathew, P., Cherian, J., George, A., and Bak, T. H. (2004). Adaptation of the ACE for a Malayalam speaking population in southern India. *Int. J. Geriatr. Psychiatry* 19, 1188–1194. doi: 10.1002/gps.1239

McCarthy, P. (2019). FSLeyes. *Zenodo*, doi: 10.5281/zenodo.3530921

Meira, A. T., Arruda, W. O., Ono, S. E., Neto, A. D. C., Raskin, S., Camargo, C. H. F., et al. (2019). Neuroradiological findings in the Spinocerebellar ataxias. *Tremor Other Hyperkin. Movements* 9, 1–8. doi: 10.7916/tohm.v0.682

Menon, R., Lekha, V., Sunitha Justus, P., Sarma, S., and Mathuranath, P. (2014). A pilot study on utility of Malayalam version of Addenbrooke's cognitive examination in detection of amnestic mild cognitive impairment: a critical insight into utility of learning and recall measures. *Ann. Indian Acad. Neurol.* 17, 420–425. doi: 10.4103/0972-2327.144018

Milardi, D., Arrigo, A., Anastasi, G., Cacciola, A., Marino, S., Mormina, E., et al. (2016). Extensive direct subcortical cerebellum-basal ganglia connections in human brain as revealed by constrained spherical Deconvolution Tractography. *Front. Neuroanat.* 10, 1–10. doi: 10.3389/fnana.2016.00029

Narabayashi, H., Maeda, T., and Yokochi, F. (1987). Long-term follow-up study of nucleus Ventralis Intermedius and Ventrolateralis Thalamotomy using a microelectrode technique in parkinsonism. *Appl. Neurophysiol.* 50, 330–337. doi: 10.1159/000100736

O'Doherty, J. P., Dayan, P., Friston, K., Critchley, H., and Dolan, R. J. (2003). Temporal difference models and reward-related learning in the human brain. *Neuron* 38, 329–337. doi: 10.1016/s0896-6273(03)00169-7

O'Halloran, C. J., Kinsella, G. J., and Storey, E. (2012). The cerebellum and neuropsychological functioning: a critical review. *J. Clin. Exp. Neuropsychol.* 34, 35–56. doi: 10.1080/13803395.2011.614599

Panouillères, M. T. N., Joundi, R. A., Benitez-Rivero, S., Cheeran, B., Butler, C. R., Németh, A. H., et al. (2017). Sensorimotor adaptation as a Behavioural biomarker of early Spinocerebellar ataxia type 6. *Sci. Rep.* 7, 1–12. doi: 10.1038/s41598-017-02469-7

Paraguay, I. B., França, C., Duarte, K. P., Diniz, J. M., Galhardoni, R., Silva, V., et al. (2021). Dentate nucleus stimulation for essential tremor. *Parkinsonism Relat. Disord.* 82, 121–122. doi: 10.1016/j.parkreldis.2020.12.001

Parker, K. L., Narayanan, N. S., and Andreasen, N. C. (2014). The therapeutic potential of the cerebellum in schizophrenia. *Front. Syst. Neurosci.* 8, 1–11. doi: 10.3389/fnsys.2014.00163

Payoux, P., Remy, P., Damier, P., Miloudi, M., Loubinoux, I., Pidoux, B., et al. (2004). Subthalamic nucleus stimulation reduces abnormal motor cortical Overactivity in Parkinson disease. *Arch. Neurol.* 61, 1307–1313. doi: 10.1001/archneur.61.8.1307

Pelzer, E. A., Hintzen, A., Goldau, M., Yves, D., von Cramon, L., Timmermann, A., et al. (2013). Cerebellar networks with basal ganglia: feasibility for tracking Cerebello-Pallidal and Subthalamo-cerebellar projections in the human brain. *Eur. J. Neurosci.* 38, 3106–3114. doi: 10.1111/ejn.12314

Perge, J. A., Niven, J. E., Mugnaini, E., Balasubramanian, V., and Sterling, P. (2012). Why do axons differ in caliber? *J. Neurosci.* 32, 626–638. doi: 10.1523/JNEUROSCI.4254-11.2012

Pfefferbaum, A., Rohlfing, T., Rosenbloom, M. J., Chu, W., Colrain, I. M., and Sullivan, E. V. (2013). Variation in longitudinal trajectories of regional brain volumes of healthy men and women (ages 10 to 85 years) measured with atlas-based Parcellation of MRI. *Neuroimage* 65, 176–193. doi: 10.1016/j.neuroimage.2012.10.008

Raffelt, D., Tournier, J. D., Rose, S., Gerard, R., Ridgway, R., Henderson, S., et al. (2012). Apparent fibre density: a novel measure for the analysis of diffusion-weighted magnetic resonance images. *Neuroimage* 59, 3976–3994. doi: 10.1016/j.neuroimage.2011.10.045

Raffelt, D. A., Tournier, J. D., Smith, R. E., Vaughan, D. N., Jackson, G., Ridgway, G. R., et al. (2017). Investigating white matter fibre density and morphology using Fixel-based analysis. *Neuroimage* 144, 58–73. doi: 10.1016/j.neuroimage.2016.09.029

Raffelt, D. A., Smith, R., Ridgway, G., Tournier, J., Vaughan, D., Rose, S., et al. (2015). Connectivity-based Fixel enhancement: whole-brain statistical analysis of diffusion MRI measures in the presence of crossing Fibres. *Neuroimage* 117, 40–55. doi: 10.1016/j.neuroimage.2015.05.039

Raz, N., Rodrigue, K. M., Kennedy, K. M., Head, D., Gunning-Dixon, F., and Acker, J. D. (2003). Differential aging of the human striatum: longitudinal evidence. *Am. J. Neuroradiol.* 24, 1849–1856.

Rolls, E. T., Huang, C.-C., Lin, C.-P., Feng, J., and Joliot, M. (2020). Automated anatomical Labelling atlas 3. *Neuroimage* 206:116189. doi: 10.1016/j.neuroimage.2019.116189

Sadnicka, A., Hoffland, B. S., Bhatia, K. P., van de Warrenburg, B. P., and Edwards, M. J. (2012). The cerebellum in dystonia–help or hindrance? *Clin. Neurophysiol.* 123, 65–70. doi: 10.1016/j.clinph.2011.04.027

Sakai, S. T., Inase, M., and Tanji, J. (1996). Comparison of Cerebellothalamic and Pallidothalamic projections in the monkey (Macaca Fuscata): a double anterograde labeling study. *J. Comp. Neurol.* 368, 215–228. doi: 10.1002/(SICI)1096-9861(19960429)368:2<215::AID-CNE4>3.0.CO;2-6

Sala, S., Agosta, F., Pagani, E., Copetti, M., Comi, G., and Filippi, M. (2012). Microstructural changes and atrophy in brain white matter tracts with aging. *Neurobiol. Aging* 33, 488–498.e2. doi: 10.1016/j.neurobiolaging.2010.04.027

Salat, D. H., Tuch, D. S., Greve, D. N., van der Kouwe, A. J. W., Hevelone, N. D., Zaleta, A. K., et al. (2005). Age-related alterations in white matter microstructure measured by diffusion tensor imaging. *Neurobiol. Aging* 26, 1215–1227. doi: 10.1016/j.neurobiolaging.2004.09.017

Schmahmann, J. D. (2019). The cerebellum and cognition. *Neurosci. Lett.* 688, 62–75. doi: 10.1016/j.neulet.2018.07.005

Schultz, W., Dayan, P., and Montague, P. R. (1997). A neural substrate of prediction and reward. *Science* 275, 1593–1599. doi: 10.1126/science.275.5306.1593

Smith, S. M. (2002). Fast robust automated brain extraction. *Hum. Brain Mapp.* 17, 143–155. doi: 10.1002/hbm.10062

Smith, S. M., Jenkinson, M., Woolrich, M. W., Beckmann, C. F., Behrens, T. E. J., Johansen-Berg, H., et al. (2004). Advances in functional and structural MR image analysis and implementation as FSL. *Neuroimage* 23, S208–S219. doi: 10.1016/j.neuroimage.2004.07.051

Stoodley, C. J., Desmond, J. E., Guell, X., and Schmahmann, J. D. (2020). "Functional topography of the human cerebellum revealed by functional neuroimaging studies" in *Handbook of the cerebellum and cerebellar disorders*. eds. M. Manto, D. Gruol, J. Schmahmann, N. Koibuchi and R. Sillitoe (Cham: Springer International Publishing), 1–37.

Stoodley, C. J., and Schmahmann, J. D. (2009). Functional topography in the human cerebellum: a meta-analysis of neuroimaging studies. *Neuroimage* 44, 489–501. doi: 10.1016/j.neuroimage.2008.08.039

Stoodley, C. J., Valera, E. M., and Schmahmann, J. D. (2012). Functional topography of the cerebellum for motor and cognitive tasks: an FMRI study. *Neuroimage* 59, 1560–1570. doi: 10.1016/j.neuroimage.2011.08.065

Strick, P. L., Dum, R. P., and Fiez, J. A. (2009). Cerebellum and nonmotor function. *Annu. Rev. Neurosci.* 32, 413–434. doi: 10.1146/annurev.neuro.31.060407.125606

Tang, Y., Nyengaard, J. R., Pakkenberg, B., and Gundersen, H. J. (1997). Age-induced white matter changes in the human brain: a stereological investigation. *Neurobiol. Aging* 18, 609–615. doi: 10.1016/s0197-4580(97)00155-3

Tournier, J. D., Smith, R., Raffelt, D., Tabbara, R., Dhollander, T., Pietsch, M., et al. (2019). MRtrix3: a fast, flexible and open software framework for Medical image processing and visualisation. *Neuroimage* 202:116137. doi: 10.1016/j.neuroimage.2019.116137

Tournier, J. D., Calamante, F., Gadian, D. G., and Connelly, A. (2004). Direct estimation of the fiber orientation density function from diffusion-weighted MRI data using spherical Deconvolution. *Neuroimage* 23, 1176–1185. doi: 10.1016/j.neuroimage.2004.07.037

Van Overwalle, F., Ma, Q., and Heleven, E. (2020a). The posterior crus II cerebellum is specialized for social Mentalizing and emotional self-experiences: a meta-analysis. *Soc. Cogn. Affect. Neurosci.* 15, 905–928. doi: 10.1093/scan/nsaa124

Van Overwalle, F., Manto, M., Cattaneo, Z., Clausi, S., Ferrari, C., Gabrieli, J. D. E., et al. (2020b). Consensus paper: cerebellum and social cognition. *Cerebellum* 19, 833–868. doi: 10.1007/s12311-020-01155-1

Veraart, J., Novikov, D. S., Christiaens, D., Ades-aron, B., Sijbers, J., and Fieremans, E. (2016). Denoising of diffusion MRI using random matrix theory. *Neuroimage* 142, 394–406. doi: 10.1016/j.neuroimage.2016.08.016

Voon, V., Pessiglione, M., Brezing, C., Gallea, C., Fernandez, H. H., Dolan, R. J., et al. (2010). Mechanisms underlying dopamine-mediated reward bias in compulsive behaviors. *Neuron* 65, 135–142. doi: 10.1016/j.neuron.2009.12.027

Warrenburg, B. P. C. V. D., Hendriks, H., Dürr, A., van Zuijlen, M. C. A., Stevanin, G., Camuzat, A., et al. (2005). Age at onset variance analysis in Spinocerebellar ataxias: a study in a Dutch-French cohort. *Ann. Neurol.* 57, 505–512. doi: 10.1002/ana.20424

Wu, T., and Hallett, M. (2013). The cerebellum in Parkinson's disease. *Brain* 136, 696–709. doi: 10.1093/brain/aws360

Yamada, K., Akazawa, K., Yuen, S., Goto, M., Matsushima, S., Takahata, A., et al. (2010). MR imaging of ventral thalamic nuclei. *Am. J. Neuroradiol.* 31, 732–735. doi: 10.3174/ajnr.A1870

Zwirner, J., Möbius, D., Bechmann, I., Arendt, T., Hoffmann, K.-T., Jäger, C., et al. (2016). Subthalamic nucleus volumes are highly consistent but decrease age-dependently-a combined magnetic resonance imaging and stereology approach in humans. *Hum. Brain Mapp.* 38, 909–922. doi: 10.1002/hbm.23427

frontiers | Frontiers in Aging Neuroscience

TYPE Original Research
PUBLISHED 09 February 2023
DOI 10.3389/fnagi.2023.1114022

OPEN ACCESS

EDITED BY
Huaibin Cai,
National Institute on Aging (NIH),
United States

REVIEWED BY
Haigang Ren,
Soochow University,
China
Zhangyu Zou,
Fujian Medical University Union Hospital,
China

*CORRESPONDENCE
Junling Wang
junling.wang@csu.edu.cn

SPECIALTY SECTION
This article was submitted to Parkinson's Disease and Aging-related Movement Disorders, a section of the journal Frontiers in Aging Neuroscience

RECEIVED 02 December 2022
ACCEPTED 23 January 2023
PUBLISHED 09 February 2023

CITATION
Tang X, Yuan Y, Liu Z, Bu Y, Tang L, Zhao Q, Jiao B, Guo J, Shen L, Jiang H, Tang B and Wang J (2023) Genetic and clinical analysis of *TP73* gene in amyotrophic lateral sclerosis patients from Chinese mainland. *Front. Aging Neurosci.* 15:1114022. doi: 10.3389/fnagi.2023.1114022

Genetic and clinical analysis of *TP73* gene in amyotrophic lateral sclerosis patients from Chinese mainland

Xuxiong Tang[1], Yanchun Yuan[1], Zhen Liu[1], Yue Bu[1], Linxin Tang[1], Qianqian Zhao[1], Bin Jiao[1,2,3,4,5], Jifeng Guo[1,2,3,4,5], Lu Shen[1,2,3,4,5], Hong Jiang[1,2,3,4,6], Beisha Tang[1,2,3,4,5] and Junling Wang[1,2,3,4,5]*

[1]Department of Neurology, Xiangya Hospital, Central South University, Changsha, Hunan, China, [2]National Clinical Research Center for Geriatric Diseases, Xiangya Hospital, Central South University, Changsha, Hunan, China, [3]Key Laboratory of Hunan Province in Neurodegenerative Disorders, Central South University, Changsha, Hunan, China, [4]Hunan International Scientific and Technological Cooperation Base of Neurodegenerative and Neurogenetic Diseases, Changsha, China, [5]Engineering Research Center of Hunan Province in Cognitive Impairment Disorders, Central South University, Changsha, China, [6]School of Basic Medical Science, Central South University, Changsha, Hunan, China

Introduction: *TP73* was recently identified as a novel causative gene for amyotrophic lateral sclerosis (ALS). We aimed to determine the contribution of variations in *TP73* in the Chinese ALS population and to further explore the genotype-phenotype correlations.

Methods: We screened rare, putative pathogenic *TP73* mutations in a large Chinese ALS cohort and performed association analysis of both rare and common *TP73* variations between cases and controls.

Results: Of the 985 ALS patients studied, six rare, heterozygous putative pathogenic variants in *TP73* were identified among six unrelated sALS patients. Exon 14 of *TP73* might be a mutant hotspot in our cohort. Patients with ALS with only rare, putative pathogenic *TP73* mutations exhibited a characteristic clinical profile. Patients harboring multiple mutations in *TP73* and other ALS-related genes displayed a significantly earlier onset of ALS. Association analysis revealed that rare *TP73* variants in the untranslated regions (UTRs) were enriched among ALS patients; meanwhile, two common variants in the exon-intron boundary were discovered to be associated with ALS.

Discussion: We demonstrate that *TP73* variations also have contributed to ALS in the Asian population and broaden the genotypic and phenotypic spectrum of *TP73* variants in the ALS-frontotemporal dementia (FTD) spectrum. Furthermore, our findings first suggest that *TP73* is not only a causative gene, but also exerts a disease-modifying effect. These results may contribute to a better understanding of the molecular mechanism of ALS.

KEYWORDS

amyotrophic lateral sclerosis, TP73, gene mutation, phenotype–genotype association, neurodegenerative disease, clinical characteristic

1. Introduction

Amyotrophic lateral sclerosis (ALS) is a fatal neurodegenerative disorder characterized by the rapidly progressive loss of motor neurons in the brain and spinal cord, resulting in relentlessly worsening weakness and wasting of voluntary muscle until death from respiratory failure occurs, typically within 2–4 years of symptom onset (Al-Chalabi and Hardiman, 2013; Feldman et al., 2022; Goutman et al., 2022). ALS has generally been considered a relatively rare disease, nonetheless, the number of ALS patients

worldwide is projected to reach 376,674 by 2040, predominantly due to aging (Al-Chalabi and Hardiman, 2013; Arthur et al., 2016). This rise is expected to put a huge socioeconomic strain on global healthcare systems. As with most neurodegenerative diseases, only 10% of ALS cases are hereditary, referred to as familial ALS (fALS), with the remaining 90% of cases classified as sporadic ALS (sALS) (Renton et al., 2014). ALS shows a significant degree of clinical and genetic heterogeneity, and still, much remains unclear about the etiology and pathophysiological mechanisms underlying this disease (Swinnen and Robberecht, 2014). Genetic variation contributed to ALS (Renton et al., 2014; Taylor et al., 2016). To date, over 40 genes have been identified as being implicated in the pathogenesis of ALS (Ghasemi and Brown, 2018).

Recently, a published study identified the gene of tumor protein P73 (*TP73*) as a novel causative gene for ALS (Russell et al., 2021). By screening the whole-exome sequencing (WES) data from a discovery cohort of 87 European patients with sALS and two replication cohorts comprising 2,853 individuals with sALS, the researchers discovered 24 rare protein-coding variants in *TP73*. To further validate the pathogenic role of *TP73* variants in ALS, they then performed functional experiments including C2C12 myoblast differentiation assays *in vitro* and spinal motor neuron (SMN) axonal branching assay *in vivo*. Furthermore, they first proposed that apoptosis in motor neurons may be involved in the pathology of ALS. Following that, Pereira and colleagues linked rare mutations in *TP73* with frontotemporal dementia (FTD), particularly primary progressive aphasia, which further corroborated the contribution of *TP73* variations in the ALS-FTD spectrum (Tabuas-Pereira et al., 2022).

However, mutation analysis of the *TP73* gene conducted on other countries and Asian populations is insufficient. A plethora of studies has highlighted that the genetic epidemiology of ALS varies among different racial groups (Zou et al., 2017). Therefore, we performed a thorough genetic analysis using whole-exome sequencing to investigate the contributions of *TP73* variations in the Chinese ALS population and further characterized the clinical features of these patients to explore the genotype–phenotype correlations in this work.

2. Materials and methods

2.1. Participants

In this study, a large cohort of 1,004 patients with ALS was enrolled from Xiangya Hospital, Central South University, in either an inpatient or outpatient setting. Each patient got a thorough examination and was diagnosed with ALS by at least two experienced neurologists based on the current Gold Coast criteria (Shefner et al., 2020). Detailed demographic data and clinical information were collected when enrolled and updated at follow-up visits. Participants having known pathogenic mutations in the established ALS causative genes were excluded first. In total, 1,258 neurological disease-free individuals of Chinese ancestry matched by geography were recruited as healthy controls (HCs). This study was approved by the Ethics Committee and the Expert Committee of Xiangya Hospital, Central South University. All participants completed written informed consent in compliance with the Helsinki Declaration.

2.2. WES analysis

Genomic DNA was prepared from peripheral blood leukocytes of each subject *via* standard extraction procedures. The purity and quantity of extracted DNA were detected with a NanoDrop spectrophotometer 1,000 (Thermo Scientific). WES was performed on all participants using a previously published method (Zeng et al., 2019). The resulting data were mapped to the reference genome (GRCh37/hg19). Variants with a depth of coverage <10, allele balance <0.25, or Phred quality score <20 were removed. Proceed to annotate variations with the ANNOVAR software (Wang et al., 2010). After the quality control, totaling 985 patients and 1,224 healthy controls were included for further analysis. The data generation processes have already been described in detail (Liu et al., 2021).

We screened for rare, putative pathogenic variants of *TP73* in the Chinese ALS population. Inclusion criteria for the rare, putative pathogenic variants were: (1). the frequency was lower than 0.001 in our in-house and the following public database: the 1,000 Genome Project-East Asian (1000G_EAS), the NHLBI Exome Sequencing Project-East Asian (ESP6500s_EAS), the Exome Aggregation Consortium-East Asian (ExAC_EAS), and the Genome Aggregation Database-East Asian (GnomAD_EAS); (2). absent from HCs (3). located in the protein-coding regions; (4). present in a heterozygous state; (5). annotated as missense, stop gain/loss, frameshift, or splice-site variants; and (6). rare missense variants predicted to be pathogenic by at least five of 11 *in silico* (Quadri et al., 2018). It's worth emphasizing that, considering the relatively small number of our control group, we only judged the pathogenicity of a rare variant to be robust if it was absent from HCs.

2.3. The single common variant association test

The common and rare variants were defined according to the minor allele frequency (MAF) in all participants in our cohort (common variants: MAF $\geq$ 0.01; rare variants: MAF < 0.01).

To evaluate the association of *TP73* variants with ALS risk in the Chinese population, we conducted the single common variant association test between the ALS and control groups using the Mixed Linear Model (MLM). The extracted top three principal components of population stratification in the principal component analysis (PCA) were included as covariates in our cohort. The possible effect of common variants inside exon-intron boundaries on the *TP73* gene expression was assessed by Expression Quantitative Trait Locus (eQTL) analysis (Zhu et al., 2016), which was widely utilized to compare the gene expression levels among individuals with different genotypes. All data were available from the Genotype-Tissue Expression (GTEx) database.

2.4. The gene-based rare variants association test

For the gene-based rare variants association test, the cumulative burden of rare variants across defined genomic regions of *TP73* between cases and controls was evaluated using the optimal sequence kernel association test (SKAT-O) implemented in the R package SKAT (Lee et al., 2012). The SKAT-O test maximized the test power of detecting the target gene by unifying the advantages of both the burden test and SKAT (Lee et al., 2012). Gender, age, and WES coverage were considered as possible covariates for adjustment before computing the *p* value.

2.5. Statistical analysis

Descriptive statistics are reported as mean ± SD or median ± SD (standard deviation, SD) for continuous variables and percentages for categorical variables. The comparison of continuous variables was assessed by Student's t-test. For categorical variables, the Fisher's exact test or Chi-square test was used to verify the significant differences between the two compared groups. Statistical analyses were carried out in SPSS (version 26.0) software. All tests were two-tailed, and significance was set at $p < 0.05$.

3. Results

3.1. Demographics

In all, 985 patients with ALS and 1,224 healthy controls were analyzed in our study. The 985 ALS patients were on average 54.2 years old at the time of onset, and 56.2 years old at the time of sampling; the geographically matched controls were older (mean age 68.47 years). 75.3% (740/985) of our ALS cohort had limb onset, while 19.39% (191/985) had bulbar onset. Detailed demographic information for all individuals is shown in Supplementary Table S1.

3.2. Rare, putative pathogenic mutation analysis

We screened all *TP73* exon regions and their surrounding sequences in each ALS patient. A total of six rare, heterozygous putative pathogenic mutations that fulfilled pathogenicity criteria were discovered among six unrelated sALS patients but not in HCs. The overall frequency of patients with rare pathogenic *TP73* mutations was 0.6%. All these six variations were protein-altering missense mutations. And the majority of them substituted amino acids that were highly conserved across species. The six variants were c.187G > A (p.A63T), c.1226C > T (p.P409L), c.1613G > A (p.R538H), c.1628G > A (p.R543Q), c.1679 T > C (p.L560P), and c.1736G > A (p.R579H). The variant, c.187G > A (p.A63T), was novel and absent from all databases. Three of these six variations (50%), namely c.187G > A (p.A63T), c.1226C > T (p.P409L), and c.1613G > A (p.R538H) have never been reported in association with the ALS-FTD spectrum. Interestingly, when investigating the distribution of these six potential pathogenic loci present in *TP73*, we discovered that a significant portion of them (4/6, 66.7%) were located inside exon 14, which differed from earlier studies. Consequently, we hypothesize that exon 14 of *TP73* might be a mutant hotspot in our ALS series. The location and pathogenicity information of these six variants identified in this study were summarized in Figure 1 and Supplementary Tables S2, S3 (Liu et al., 2015).

3.3. Clinical features of ALS patients with rare, putative pathogenic *TP73* mutations

For the six patients carrying potential pathogenic *TP73* variants described above, the age at disease onset ranged from 32 to 69 years old. We observed a completely masculine involvement since all six patients were men. In addition, we screened for other pathogenic mutations in the known ALS genes in these patients (Supplementary Table S4). There were no reported pathogenic mutations in the causative genes for ALS in each of these six individuals. Notably, two of the six patients (patient A0048 and patient S7918) had multiple variants in ALS-related genes with uncertain pathogenicity (patient A0048: *KIF5A* c.A86G: p.K29R and *TP73* c.1613G > A: p.R538H; patient S7918: *CCNF* c.2199delC: p.D733fs and *TP73* c.187G > A: p.A63T), and the remaining four patients only had *TP73* mutations. Considering the burden of multiple variants in ALS-causing genes on the disease expression, including the age at onset, progression rate, and survival, we separated these six patients into two subgroups for further clinical phenotype analysis (one subgroup with only *TP73* mutations, the other with multiple mutations in both *TP73* and other ALS-related genes) (Cady et al., 2015; Pang et al., 2017; Naruse et al., 2019). When the clinical phenotype analysis was restricted to patients with ALS with only *TP73* mutations, a distinct clinical profile emerges, with a considerably higher mean age at onset (61.5 ± 7.72 years), a shorter survival time (19.25 ± 10.01 months), and invariably limb onset. In the other subgroup, in contrast to patients carrying only *TP73* mutations, the age at onset in patients with ALS with multiple mutations is accelerated (patient A0048: 32-year-old, patient S7918:38-year-old). Furthermore, one of the six patients, S0423, suffered from cognitive impairment and behavioral problems and was eventually diagnosed with ALS-FTD. Most of these affected individuals exhibited typical symptoms and signs of the simultaneous impairment of upper and lower motor neurons. The clinical features of the six sALS patients were listed in Table 1.

The variant, c.1226C > T (p.P409L), was identified in patient S0423, diagnosed with ALS-FTD. He was a farmer without specific environmental exposure. At the age of 65, he presented with muscle weakness in his upper limbs initiated from bilateral hands, which quickly extended to all four extremities in only 1 month. He then developed dysarthria and dysphagia 2 months later. Concurrently, his primary care providers complained of his language difficulties, behavioral changes, and cognitive impairment, which included trouble retrieving words, effortful speech restricted to short, simple sentences, hyperphagia, irritability, attacks on others, decreased memory, dropped comprehension, inability to find out things, and failure to understand some instructions. At the time of the first observation after 8 months of onset (at 66 years old), he was unable to walk or talk, and was reliant on family members for his daily requirements. On comprehensive neurological evaluation, he showed signs of upper motor neuron (UMN) damage and lower motor neuron (LMN) depletion features, such as positive palmomental reflex, hyperreflexia, and muscle atrophy of all four extremities. Electromyogram (EMG) revealed abundant and diffuse ongoing denervation (spontaneous potentials) and chronic reinnervation changes in all four segments (bulbar, cervical, thoracic, and lumbar). Brain magnetic resonance imaging (MRI) scan indicated mild age-related brain atrophy (Supplementary Figure S1). A battery of neuropsychological tests, including the Edinburgh Cognitive and Behavior ALS Screen (ECAS), the Mini-Mental State Examination (MMSE), the Montreal Cognitive Assessment (MoCA), and the Frontal Assessment Battery (FAB) was not completed due to his inability to communicate. He eventually died of respiratory failure 13 months after disease onset.

Another two male patients, S3513 and S4096, carrying variants c.1736G > A (p.R579H) and c.1628G > A (p.R543Q) separately, had similar clinical manifestations. They all began with muscle weakness in the right hand, at the ages of 61 and 69, respectively. They both developed muscle weakness and atrophy in all four limbs over the next year, along with extensive fasciculation, and dysarthria. Patient S3513 subsequently reported simultaneous involvement of the contralateral arm, and bilateral legs, accompanied by fasciculation, 5 months after disease onset. He developed dysarthria in the seventh month of onset, at which point the weakness of four limbs aggravated: he was unable to lift heavy objects with his upper limbs and had difficulty walking independently. For patient S4096 with a right-hand onset, his left upper

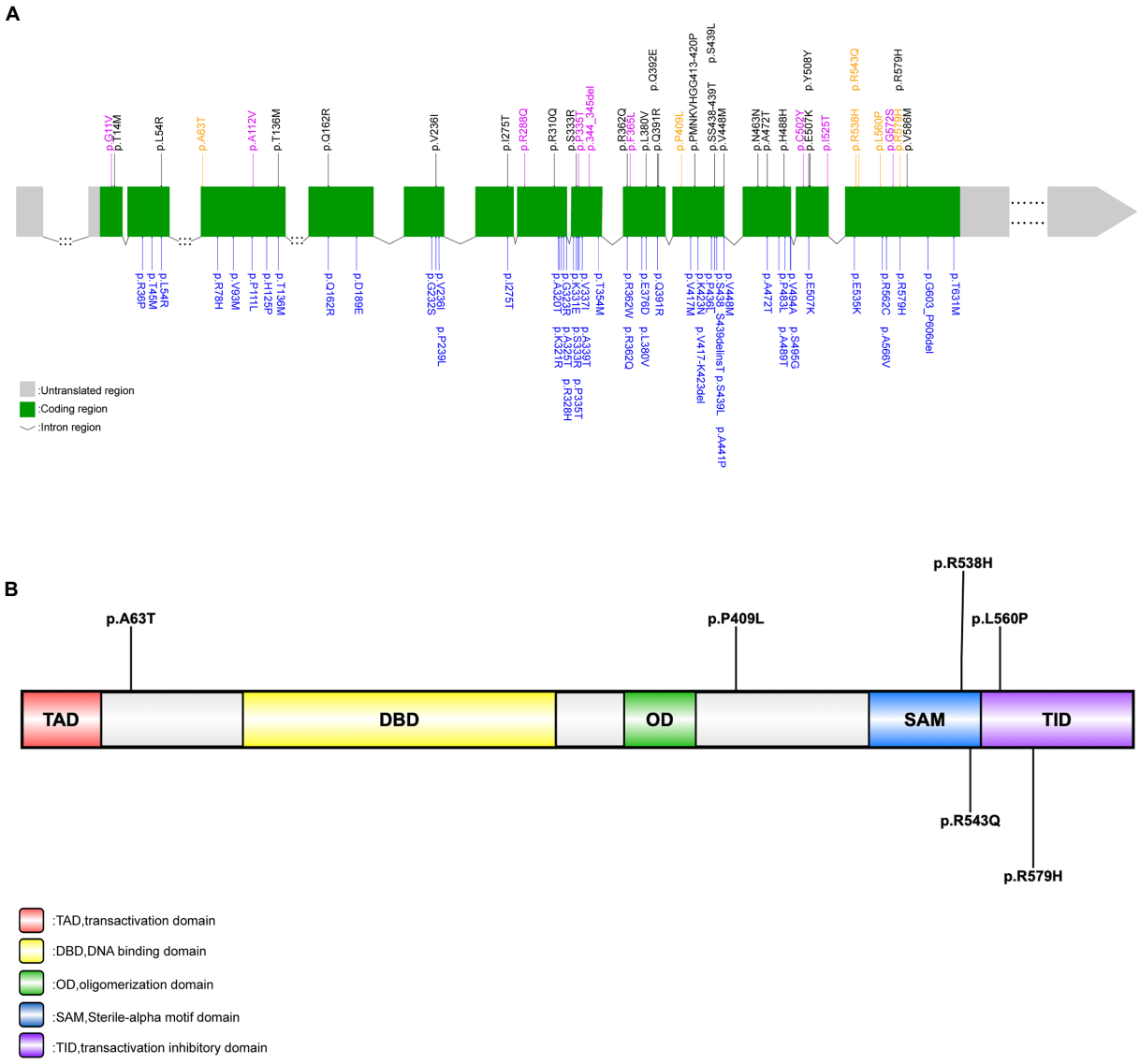

FIGURE 1
Rare *TP73* variants identified in Russell et al.'s (2021), Dilliott et al.'s (2022), and this study. **(A)** Schematic representation of the *TP73* transcript NM_005427. Rare, putative pathogenic missense variants identified in this study's ALS cohort (yellow font); rare variants identified in this study's control group (purple font); rare, protein-coding variants in *TP73* identified by Russell et al. (2021) (black font); rare, non-synonymous variants in *TP73* identified by Dilliott et al. (2022) (blue font). **(B)** Schematic representation of the TAp73 protein. Rare, putative pathogenic missense variants identified in this study (black font).

limb and bulbar (choking) were reported as the second symptomatic sites. Following that, at the fifth month of the disease course, the weakness continuously progressed to both lower limbs, and dysarthria appeared. Their bilateral deep tendon reflexes were brisk, the Hoffman sign and palmomental reflex were present. EMGs both showed abundant and diffuse ongoing denervation as well as chronic reinnervation alterations at four segments. However, brain MRI revealed that patient S4096 with the c.1628G > A (p.R543Q) variant had mild brain atrophy (Supplementary Figure S1), whereas patient S3513 with the c.1736G > A (p.R579H) had no obvious abnormalities. ECAS score of patient S4096 was 56/136, and each subgroup score of this scale suggested that the decline was driven from executive dysfunction and memory impairments, rather than behavioral dysfunction. In the end, patient S3513 died at 13 months after onset and 17 months for patient S4096.

Another patient (S5941), carrying c.1679 T > C (p.L560P) variants, was a male, who complained of progressive muscle weakness and atrophy in his right arm at the 51-year-old. The weakness gradually extended to his bilateral lower limbs, making stair climbing difficult. Besides, he developed autonomic dysfunction, manifesting as sometimes excessive sweating during the day and heat intolerance, with no nocturnal sweating or cold intolerance, as revealed by the Scale for Outcomes in Parkinson's disease (PD) for Autonomic Symptoms (SCOPA-AUT), a self-reported questionnaire widely used for the assessment of autonomic function in neurodegenerative disease (Visser et al., 2004; Damon-Perriere et al., 2012; Del et al., 2020; Assante et al., 2022). Neurological examination revealed no evidence of upper motor neuron damage, and EMG demonstrated abundant and diffuse ongoing denervation and chronic reinnervation changes in three segments (cervical, thoracic, and lumbar). No symptoms of dysphagia or dysarthria were found at the most recent follow-up visit after 34 months of onset. Based on all the available information thus far, he was clinically diagnosed with progressive muscular atrophy (PMA).

The remaining two patients, both harbored multiple variants in *TP73* and other ALS-related genes. Patient A0048 who carried the c.1613G > A

TABLE 1 Clinical features of patients with ALS with rare, putative pathogenic variants in the *TP73* gene.

Patients no.	S0423	S3513	S4096	S5941	A0048	S7918
Variants	c.1226C > T (p.P409L)	c.1736G > A (p.R579H)	c.1628G > A (p.R543Q)	c.1679 T > C (p.L560P)	c.1613G > A (p.R538H)	c.187G > A (p.A63T)
Family history	S	S	S	S	S	S
Sex	M	M	M	M	M	M
Age at onset, y	65	61	69	51	32	38
Disease duration, m	13[a]	13[a]	17[a]	34	49	42
Site of onset	Spinal	Spinal	Spinal	Spinal	Spinal	Bulbar
Muscle weakness and atrophy	Generalized	Generalized	Generalized	lower limbs, right upper limb	Generalized	Lower limbs, right upper limb
Muscle fasciculation	NA	Extensive	Extensive	NA	Extensive	Right upper limb
Dysarthria	+	+	+	–	+	+
Dysphagia	+	+	+	–	+	+
Dyspnea	+	+	+	–	–	–
Autonomic dysfunction	–	–	–	+	–	–
Reflexes	Hyperreflexia	Hyperreflexia	Hyperreflexia	Normal	Hyperreflexia	Hyporeflexia in upper limbs; hyperreflexia in lower limbs
Cognition	FTD	Normal	Executive dysfunction and memory impairments	Normal	Executive dysfunction and memory impairments	Normal
Brain MRI	Brain atrophy	No obvious abnormalities	Brain atrophy	No obvious abnormalities	No obvious abnormalities	No obvious abnormalities
Education level, y	NA	0	9	8	9	15
MMSE score	#	20/30	NA	NA	NA	NA
ECAS score	#	NA	56/136	104/136	63/136	101/136
ALS-FRS score	32/48	31/48	41/48	43/48	26/48	35/48
EMG	Ongoing denervation and chronic reinnervation in all four segments	Ongoing denervation and chronic reinnervation in all four segments	Ongoing denervation and chronic reinnervation in all four segments	Ongoing denervation and chronic reinnervation in three segments	Ongoing denervation and chronic reinnervation in all four segments	Ongoing denervation and chronic reinnervation in all four segments

ALS, Amyotrophic lateral sclerosis; MMSE, Mini-Mental State Examination; ECAS, Edinburgh Cognitive and Behavioral ALS Screen; ALSFRS-R, ALS Functional Rating Scale–Revised; MRI, Magnetic resonance imaging; EMG, Electromyogram; NA, Data not available; +, Affected; –, Unaffected.

[a]The patient was dead at the time of the study.

#: Unable to complete the scale.

10.3389/fnagi.2023.1114022

(p.R538H) variant, and patient S7918 who had the c.187G > A (p.A63T) variant, were both young men with no family history of the condition, starting with ALS phenotype at 32 and 38-year-old, respectively. Patient A0048 first displayed weakness in his left lower extremity, and then spread fast in the early disease course. By the fourth month from symptom onward, he had weakness in all four limbs; he then gradually experienced bulbar muscle weakness, presenting with dysarthria, dysphagia, and bucking during the next 2 years. Patient S7918 showed bulbar onset, initially with dysarthria and dysphagia, then developed asymmetric weakness and atrophy in bilateral lower limbs and the right arm within 3 years, accompanied by extensive fasciculation. Neurological evaluation and EMGs on them both indicated evident signs of involvement of both upper and lower motor neurons. According to ECAS, patient A0048 had executive function deficits and memory impairments (total score: 63/136, subscore of executive function:14/60; subscore of memory: 3/24), whereas patient S7918 had no cognitive changes.

3.4. Association analysis and eQTL analysis of single common variants in *TP73*

We performed the single-variant analysis of each common variant discovered in the exon and near exon-intron boundary regions to ascertain the association between common variations of *TP73* and ALS. As shown in Figure 2, 36 common *TP73* variants were identified in our cohort (Figure 2, Supplementary Table S5). Then, utilizing PLINK 1.90, we obtained linkage disequilibrium (LD) statistics for these 36 common variants to plot linkage blocks (Supplementary Table S6). As 24 of the 36 common variants were mapped to 6 separate blocks, the estimated number of independent tests was 18, and the corresponding assumed Bonferroni-corrected significance threshold of p was 0.0028 (0.05/18). The resulting data revealed that none of the common variants inside the exon regions displayed significant univariate association with ALS. While two common variants rs2181486 and rs2146657 in the same block at exon-intron boundary, attained Bonferroni-corrected statistical significance (Table 2). Taking into consideration these two common variants in nearly perfect LD (the R^2 of these two variants is 0.9850), we next chose the rs2181486 mutant locus to search the publicly accessible GTEx database to find if these two common variations impact the expression of TP73. Of note, based on the calculation of the eQTL algorithm, the rs2181486 variants might give rise to a decreased TP73 protein level in the cerebral cortex, spinal cord, as well as skeletal muscles (Table 3). These results provided suggestive evidence for association of ALS and common *TP73* variants in the near-exon intron boundaries.

3.5. Burden analysis of rare *TP73* variants at the gene level

We applied the SKAT-O test to compare the aggregate burden of rare variants residing in the coding regions, untranslated regions, and intron-exon boundaries of *TP73* between ALS cases and HCs, separately. Compared with HCs, the frequency of carriers of rare *TP73* variants in the coding regions and intron-exon boundaries was not significantly higher in the ALS group. We observed an enrichment of rare *TP73* variations in the UTRs among ALS cases, with a p value of 0.046 for the cumulative burden of rare *TP73* variations in the UTRs between the two compared groups, indicating that rare *TP73* UTRs variants were significantly associated with ALS (Supplementary Table S7).

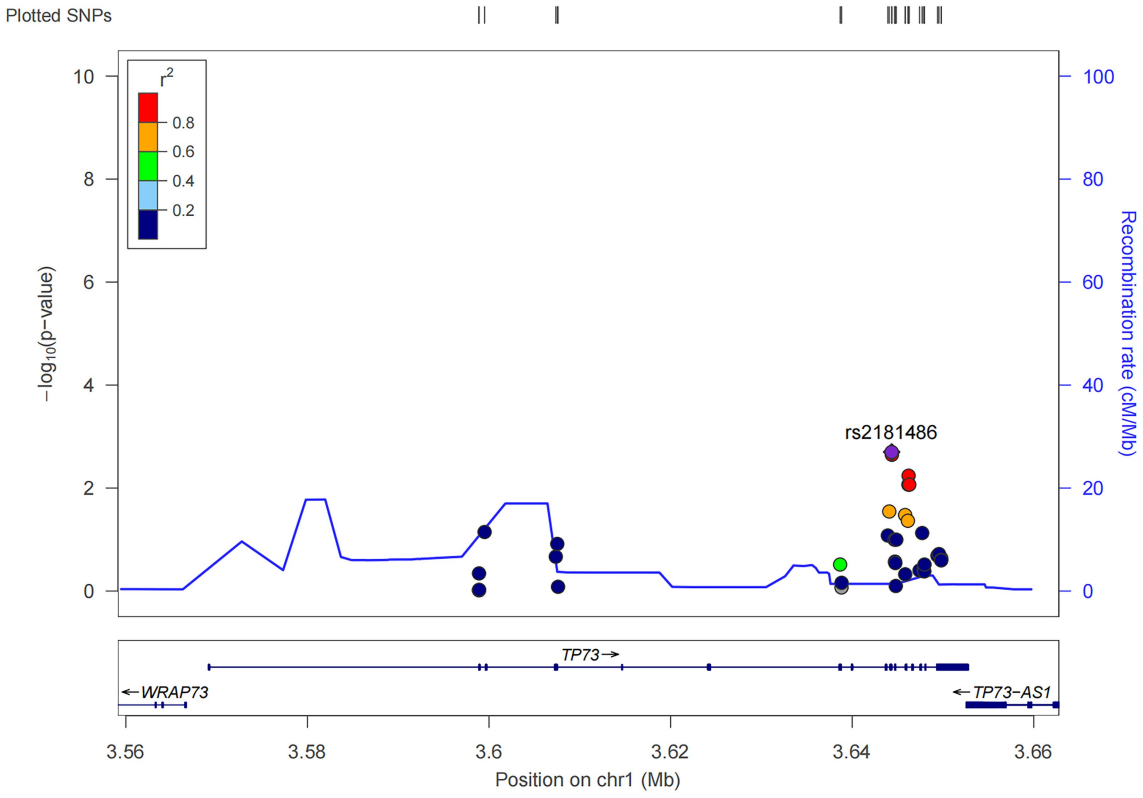

FIGURE 2
Locuszoom of the 36 common *TP73* variants identified in this study (http://locuszoom.org/).

TABLE 2 Association analysis for the two common variants achieving statistical significance in the *TP73* gene.

Position	Ref	Alt	dbSNP	Frequency	*N*	MAF_ case	MAF_ control	*p*-value	*p**-value	SE
Chr1:3644349	A	G	rs2181486	0.3014	2,209	0.2766	0.3215	0.002	0.0359	0.0168
Chr1:3644374	A	G	rs2146657	0.2997	2,209	0.2751	0.3194	0.002	0.0406	0.0169

Chr: chromosome; Ref: reference allele; Alt: alternate allele; dbSNP: dbSNP137 (https://www.ncbi.nlm.nih.gov/snp/); *N*: number of subjects in this study; *p**-value: *p*-value after the Bonferroni correction; SE: standard error.

TABLE 3 Effect of the common variant rs2181486 on TP73 protein expression in different regions of normal human brain and skeletal muscles.

rsID	Chr:position	Alt	Frequency of the Alt_cases	Frequency of the Alt_controls	Ensebl Gencode ID	Tissue	NES
rs2181486	chr1_3,644,349_A_G	G	0.2732	0.3213	ENSG00000078900.14	Brain - Cortex	0.24
rs2181486	chr1_3,644,349_A_G	G	0.2732	0.3213	ENSG00000078900.14	Brain - Spinal cord (cervical c-1)	0.13
rs2181486	chr1_3,644,349_A_G	G	0.2732	0.3213	ENSG00000078900.14	Muscle - Skeletal	0.24

Chr: chromosome; Alt: alternate allele; NES: normalized effect size.

4. Discussion

The p73 protein belonging to the p53 family, encoded by the *TP73* gene, has five functional domains: a transactivation domain (TAD), a DNA binding domain (DBD), an oligomerization domain (OD), a Sterile-alpha motif domain (SAM), and a transactivation inhibitory domain (TID) (Figure 1B; Jost et al., 1997; Dotsch et al., 2010; Osterburg and Dotsch, 2022). The p73 is a multifunctional protein in neurobiology and P73-deficient mice were found to develop neurological defects (Pozniak et al., 2000; Yang et al., 2000; Lee et al., 2004). Wetzel et al. (2008) demonstrated that p73 haploinsufficiency can cause age-related neuronal degeneration, indicating that p73 is implicated in neurodegeneration diseases. Recently, a large case–control research demonstrated *TP73* as a new ALS risk gene, although a replication study yielded conflicting results (Dilliott et al., 2022). Of note, neither of these two studies included the Asian population. Considering the distinct genetic architecture among different ethnicities, we screened *TP73* variants in a large Chinese ALS cohort to evaluate the contribution of *TP73* variants to Chinese ALS patients.

We identified six rare, heterozygous putative pathogenic variants among six unrelated sALS patients. Overall, *TP73* mutation accounted for 0.60% of Chinese sALS patients, which was similar with previously reported in Russell's research (0.60% & 0.82%), both implying that it is an uncommon genetic determination in ALS population worldwide. Interestingly, we discovered that exon 14 of the *TP73* gene appeared to be a mutant hotspot in the Chinese ALS cohort, unlike the earlier studies where the mutated sites were relatively clustered in exons eight, nine, ten, eleven and twelve (Figure 1A; Russell et al., 2021; Dilliott et al., 2022). To clarify whether exon 14 was simply more prone to variation and under less selection pressure in the Asian population, we examined the distribution of rare *TP73* variants found in HCs that met similar criteria (except for the (2) in the inclusion criteria). The nine rare variants detected in the control group were dispersed across whole coding regions of *TP73*, with just one mutant site situated in exon 14, which did not exhibit any mutant site clustering (Supplementary Table S8; Figure 1A). These data provided support to the hypothesis that exon 14 may be a hotspot mutation in the Chinese ALS population. However, there was no significant difference in the frequency of rare *TP73* variants within exon 14 between cases and controls ($p = 0.1789$). In the current study, we found four of the six (66.7%) variants at exon 14 (Figure 1A), which were all located in the C-terminal functional domains of p73 protein. Variants p.R538H and p.R543Q are in the SAM region, which is involved in hetero-oligomerization; variants p.L560P and R579H vitiations are in the TIA region, which is critical for suppressing its own transcriptional activity. This distribution of mutant sites may be unique to Chinese ALS patients, due to the combined effect of different ethnic origins and environmental circumstances. More multicenter research with larger sample sizes is needed to validate it further. Moreover, the functional impact of these six rare, putative pathogenic variants should be studied to clarify the molecular etiology of ALS, too.

In terms of the genotype–phenotype correlations, we systematically described the clinical manifestations of these six patients with rare, putative pathogenic *TP73* variations to establish the existence of any commonalities between these individuals. Among the six carriers of *TP73* mutations, there were both pure ALS patients and ALS patient with concomitant frontotemporal dementia. Compared with the common features of Chinese ALS population, the patients only carrying rare, putative pathogenic *TP73* mutations showed a later age at onset (61.5 vs. 54.3 years), the lower disease duration (19.25 months vs. 71 months), and the higher spinal onset rate (100% vs. 76.6%) (Chen et al., 2015; Liu et al., 2021). These findings suggest that ALS patients with only rare, putative pathogenic *TP73* mutations tend to have a late onset, a rapidly progressive course, and a poorer prognosis. Next, we further analyzed the clinical characteristics of patients with ALS with multiple variants in *TP73* and other ALS-related genes. We observed an obviously earlier disease onset in these two patients when compared to ALS patients with only *KIF5A*, or *CCNF* mutations (Nicolas et al., 2018; Tian et al., 2018). Based on these data, we deduced that *TP73* also exerts disease-modifying effects in the presence of a combination with other rare variants in the known causative genes for ALS, mainly in accelerating the age at onset, rather than shortening survival time. Our current findings corroborate the previously published research that the burden of multiple rare variants advances the age at onset of ALS (Cady et al., 2015). Nevertheless, there is no clear relationship between mutation sites and clinical phenotypes.

A most recent publication by Li et al. (2022) identified 24 rare *TP73* variants among 34 sALS patients in a large Chinese ALS cohort and briefly described the clinical presentation of these patients having rare *TP73* mutation: the average age at onset was 54.32 (11.76) years, with a sex ratio of 1.45:1. There was no data on disease progression or survival available. Our findings suggest that patients with ALS with only rare, putative

pathogenic *TP73* mutations tend to have a late onset, faster progression, and worse prognosis. The following might be the causes of these clinical phenotypic contradictions: Patients and controls in Li, Chunyu et al's and our studies came from different Chinese areas; The criteria for rare, pathogenic variants in Li, Chunyu et al's study were inconsistent with those in our study; Two studies varied in the exclusion of patients with ALS with known pathogenic mutations in established ALS genes, making Li, Chunyu et al' patients' clinical presentation more complex and variable; However, in the present study, we tightly restricted the rarity and pathogenicity of *TP73* variations, and separated these ALS patients with *TP73* mutation into two subgroups for further clinical phenotype analysis (one subgroup with only *TP73* mutations, the other with multiple mutations).

Herein, we also found two common *TP73* variants in the exon-intron boundaries associated with ALS, and both can lead to a reduced P73 protein expression in the human brain based on the eQTL analysis. In addition, we noted an enrichment of rare variants in the UTRs of *TP73* among our ALS patients. Increasing evidence has shown that variations in the UTRs are strongly linked to human diseases by impacting the transcription of nearby genes and protein expression level by changing the poly(A) motifs, RNA secondary structure, and RNA binding protein-binding sites (Li et al., 2021). From these findings, we suggest that these ALS-related *TP73* variants in the UTRs and exon-intron boundaries may have a haploinsufficiency effect that confers a loss-of-function phenotype, and hence impart a risk of ALS. Of course, further biological research is warranted to validate this concept.

In summary, we screened *TP73* variants in a large Chinese ALS cohort and identified six rare, candidate pathogenic mutations in six unrelated sALS patients. We provide the systematical characterization of the clinical manifestations of ALS patients carrying *TP73* mutations and investigate the phenotype–genotype associations. Our research expands the genotypic and phenotypic spectrum of *TP73* mutations in the ALS-FTD spectrum, adding to our current understanding of the characteristic clinical phenotype of ALS patients carrying rare pathogenic *TP73* variants. These results may contribute to a better grasp of the molecular mechanism of ALS. More research with larger sample size and robust functional studies are warranted to elucidate the contribution and potential molecular mechanisms of *TP73* mutations in the ALS-FTD spectrum.

Data availability statement

The original contributions presented in the study are included in the article/Supplementary material, further inquiries can be directed to the corresponding author.

Ethics statement

The studies involving human participants were reviewed and approved by the Ethics Committee of Xiangya Hospital of Central South University in China. The patients/participants provided their written informed consent to participate in this study.

Author contributions

XT performed the majority of the analyses and wrote the manuscript. YY and ZL contributed to the bioinformatic analyses. YB, LT, and QZ contribute to the collection of detailed clinical data. BJ, JG, LS, and HJ contributed to the clinical part of the project. BT contributed to the supervision of the analyses. JW designed the study and wrote the manuscript. All authors contributed to the article and approved the submitted version.

Funding

This work was supported by the Science and Technology Innovation 2030 (STI2030-Major Projects:2021ZD0201803); National Key R&D Program of China (No. 2021YFA0805202 and 2018YFC1312003); the Program of the National Natural Science Foundation of China (#82171431, 81671120 and 81300981); the National Key Research and Development Program of China (#2018YFC1312003); the Natural Science Fund for Distinguished Young Scholars of Hunan Province, China (#2020JJ2057); the Project Program of National Clinical Research Center for Geriatric Disorders at Xiangya Hospital (#2020LNJJ13).

Acknowledgments

We are grateful to the participating patients for their involvement. We are grateful for resources from the Bioinformatics Center, Xiangya Hospital, Central South University.

Conflict of interest

The authors declare that the research was conducted in the absence of any commercial or financial relationships that could be construed as a potential conflict of interest.

Publisher's note

Supplementary material

The Supplementary material for this article can be found online at: https://www.frontiersin.org/articles/10.3389/fnagi.2023.1114022/full#supplementary-material

References

Al-Chalabi, A., and Hardiman, O. (2013). The epidemiology of ALS: a conspiracy of genes, environment and time. *Nat. Rev. Neurol.* 9, 617–628. doi: 10.1038/nrneurol.2013.203

Arthur, K. C., Calvo, A., Price, T. R., Geiger, J. T., Chio, A., and Traynor, B. J. (2016). Projected increase in amyotrophic lateral sclerosis from 2015 to 2040. *Nat. Commun.* 7:12408. doi: 10.1038/ncomms12408

Assante, R., Salvatore, E., Nappi, C., Peluso, S., De Simini, G., Di Maio, L., et al. (2022). Autonomic disorders and myocardial 123i-metaiodobenzylguanidine scintigraphy in huntington's disease. *J. Nucl. Cardiol.* 29, 642–648. doi: 10.1007/s12350-020-02299-7

Cady, J., Allred, P., Bali, T., Pestronk, A., Goate, A., Miller, T. M., et al. (2015). Amyotrophic lateral sclerosis onset is influenced by the burden of rare variants in known amyotrophic lateral sclerosis genes. *Ann. Neurol.* 77, 100–113. doi: 10.1002/ana.24306

Chen, L., Zhang, B., Chen, R., Tang, L., Liu, R., Yang, Y., et al. (2015). Natural history and clinical features of sporadic amyotrophic lateral sclerosis in China. *J. Neurol. Neurosurg. Psychiatry* 86, 1075–1081. doi: 10.1136/jnnp-2015-310471

Damon-Perriere, N., Foubert-Samier, A., De Cock, V. C., Gerdelat-Mas, A., Debs, R., Pavy-Le, T. A., et al. (2012). Assessment of the scopa-aut questionnaire in multiple system atrophy: relation to umsars scores and progression over time. *Parkinsonism Relat. Disord.* 18, 612–615. doi: 10.1016/j.parkreldis.2011.12.009

Del, P. R., Murueta-Goyena, A., Acera, M., Carmona-Abellan, M., Tijero, B., Lucas-Jimenez, O., et al. (2020). Autonomic dysfunction is associated with neuropsychological impairment in Lewy body disease. *J. Neurol.* 267, 1941–1951. doi: 10.1007/s00415-020-09783-7

Dilliott, A. A., Rouleau, G. A., and Farhan, S. M. K. (2022). Lack of association of TP73 with amyotrophic lateral sclerosis in a large cohort of cases. *Neurobiol. Aging* 115, 109–111. doi: 10.1016/j.neurobiolaging.2022.04.004

Dotsch, V., Bernassola, F., Coutandin, D., Candi, E., and Melino, G. (2010). p63 and p73, the ancestors of p53. *Cold Spring Harb. Perspect. Biol.* 2:a004887 doi: 10.1101/cshperspect.a004887

Feldman, E. L., Goutman, S. A., Petri, S., Mazzini, L., Savelieff, M. G., Shaw, P. J., et al. (2022). Amyotrophic lateral sclerosis. *Lancet* 400, 1363–1380. doi: 10.1016/S0140-6736(22)01272-7

Ghasemi, M., and Brown, R. H. (2018). Genetics of amyotrophic lateral sclerosis. *Cold Spring Harb. Perspect. Med.* 8. doi: 10.1101/cshperspect.a024125

Goutman, S. A., Hardiman, O., Al-Chalabi, A., Chio, A., Savelieff, M. G., Kiernan, M. C., et al. (2022). Recent advances in the diagnosis and prognosis of amyotrophic lateral sclerosis. *Lancet Neurol.* 21, 480–493. doi: 10.1016/S1474-4422(21)00465-8

Jost, C. A., Marin, M. C., and Kaelin, W. G. Jr. (1997). p73 is a simian [correction of human] p53-related protein that can induce apoptosis. *Nature* 389, 191–194. doi: 10.1038/38298

Lee, A. F., Ho, D. K., Zanassi, P., Walsh, G. S., Kaplan, D. R., and Miller, F. D. (2004). Evidence that DeltaNp73 promotes neuronal survival by p53-dependent and p53-independent mechanisms. *J. Neurosci.* 24, 9174–9184. doi: 10.1523/JNEUROSCI.1588-04.2004

Lee, S., Emond, M. J., Bamshad, M. J., Barnes, K. C., Rieder, M. J., Nickerson, D. A., et al. (2012). Optimal unified approach for rare-variant association testing with application to small-sample case-control whole-exome sequencing studies. *Am. J. Hum. Genet.* 91, 224–237. doi: 10.1016/j.ajhg.2012.06.007

Li, C., Hou, Y., Wei, Q., Lin, J., Jiang, Q., Yang, T., et al. (2022). Lack of association of tp73 rare variants with amyotrophic lateral sclerosis in a chinese cohort. *Hum. Genomics* 16:63. doi: 10.1186/s40246-022-00437-5

Li, L., Huang, K. L., Gao, Y., Cui, Y., Wang, G., Elrod, N. D., et al. (2021). An atlas of alternative polyadenylation quantitative trait loci contributing to complex trait and disease heritability. *Nat. Genet.* 53, 994–1005. doi: 10.1038/s41588-021-00864-5

Liu, W., Xie, Y., Ma, J., Luo, X., Nie, P., Zuo, Z., et al. (2015). Ibs: an illustrator for the presentation and visualization of biological sequences. *Bioinform.* 31, 3359–3361. doi: 10.1093/bioinformatics/btv362

Liu, Z., Yuan, Y., Wang, M., Ni, J., Li, W., Huang, L., et al. (2021). Mutation spectrum of amyotrophic lateral sclerosis in central South China. *Neurobiol. Aging* 107, 181–188. doi: 10.1016/j.neurobiolaging.2021.06.008

Naruse, H., Ishiura, H., Mitsui, J., Takahashi, Y., Matsukawa, T., Tanaka, M., et al. (2019). Burden of rare variants in causative genes for amyotrophic lateral sclerosis (ALS) accelerates age at onset of ALS. *J. Neurol. Neurosurg. Psychiatry* 90, 537–542. doi: 10.1136/jnnp-2018-318568

Nicolas, A., Kenna, K. P., Renton, A. E., Ticozzi, N., Faghri, F., Chia, R., et al. (2018). Genome-wide analyses identify KIF5A as a novel ALS gene. *Neuron* 21:e1266, 1268–1283. doi: 10.1016/j.neuron.2018.02.027

Osterburg, C., and Dotsch, V. (2022). Structural diversity of p63 and p73 isoforms. *Cell Death Differ.* 29, 921–937. doi: 10.1038/s41418-022-00975-4

Pang, S. Y., Hsu, J. S., Teo, K. C., Li, Y., Kung, M. H. W., Cheah, K. S. E., et al. (2017). Burden of rare variants in ALS genes influences survival in familial and sporadic ALS. *Neurobiol. Aging* 58, 238.e9–238.e15. doi: 10.1016/j.neurobiolaging.2017.06.007

Pozniak, C. D., Radinovic, S., Yang, A., McKeon, F., Kaplan, D. R., and Miller, F. D. (2000). An anti-apoptotic role for the p53 family member, p73, during developmental neuron death. *Science* 289, 304–306. doi: 10.1126/science.289.5477.304

Quadri, M., Mandemakers, W., Grochowska, M. M., Masius, R., Geut, H., Fabrizio, E., et al. (2018). LRP10 genetic variants in familial Parkinson's disease and dementia with Lewy bodies: a genome-wide linkage and sequencing study. *Lancet Neurol.* 17, 597–608. doi: 10.1016/S1474-4422(18)30179-0

Renton, A. E., Chio, A., and Traynor, B. J. (2014). State of play in amyotrophic lateral sclerosis genetics. *Nat. Neurosci.* 17, 17–23. doi: 10.1038/nn.3584

Russell, K. L., Downie, J. M., Gibson, S. B., Tsetsou, S., Keefe, M. D., Duran, J. A., et al. (2021). Pathogenic effect of TP73 gene variants in people with amyotrophic lateral sclerosis. *Neurology* 16:E225-E235. doi: 10.1212 WNL.0000000000012285

Shefner, J. M., Al-Chalabi, A., Baker, M. R., Cui, L. Y., de Carvalho, M., Eisen, A., et al. (2020). A proposal for new diagnostic criteria for ALS. *Clin. Neurophysiol.* 131, 1975–1978. doi: 10.1016/j.clinph.2020.04.005

Swinnen, B., and Robberecht, W. (2014). The phenotypic variability of amyotrophic lateral sclerosis. *Nat. Rev. Neurol.* 10, 661–670. doi: 10.1038/nrneurol.2014.184

Tabuas-Pereira, M., Santana, I., Almeida, M. R., Duraes, J., Lima, M., Duro, D., et al. (2022). Rare variants in TP73 in a frontotemporal dementia cohort link this gene with primary progressive aphasia phenotypes. *Eur. J. Neurol.* 29, 1524–1528. doi: 10.1111/ene.15248

Taylor, J. P., Brown, R. H. Jr., and Cleveland, D. W. (2016). Decoding ALS: from genes to mechanism. *Nature* 539, 197–206. doi: 10.1038/nature20413

Tian, D., Li, J., Tang, L., Zhang, N., and Fan, D. (2018). Screening for CCNF mutations in a Chinese amyotrophic lateral sclerosis cohort. *Front. Aging Neurosci.* 10:185. doi: 10.3389/fnagi.2018.00185

Visser, M., Marinus, J., Stiggelbout, A. M., and Van Hilten, J. J. (2004). Assessment of autonomic dysfunction in parkinson's disease: the scopa-aut. *Mov. Disord.* 19, 1306–1312. doi: 10.1002/mds.20153

Wang, K., Li, M., and Hakonarson, H. (2010). ANNOVAR: functional annotation of genetic variants from high-throughput sequencing data. *Nucleic Acids Res.* 38:e164. doi: 10.1093/nar/gkq603

Wetzel, M. K., Naska, S., Laliberte, C. L., Rymar, V. V., Fujitani, M., Biernaskie, J. A., et al. (2008). p73 regulates neurodegeneration and phospho-tau accumulation during aging and Alzheimer's disease. *Neuron* 59, 708–721. doi: 10.1016/j.neuron.2008.07.021

Yang, A., Walker, N., Bronson, R., Kaghad, M., Oosterwegel, M., Bonnin, J., et al. (2000). p73-deficient mice have neurological, pheromonal and inflammatory defects but lack spontaneous tumours. *Nature* 404, 99–103. doi: 10.1038/35003607

Zeng, S., Zhang, M. Y., Wang, X. J., Hu, Z. M., Li, J. C., Li, N., et al. (2019). Long-read sequencing identified intronic repeat expansions in SAMD12 from Chinese pedigrees affected with familial cortical myoclonic tremor with epilepsy. *J. Med. Genet.* 56, 265–270. doi: 10.1136/jmedgenet-2018-105484

Zhu, Z., Zhang, F., Hu, H., Bakshi, A., Robinson, M. R., Powell, J. E., et al. (2016). Integration of summary data from GWAS and eQTL studies predicts complex trait gene targets. *Nat. Genet.* 48, 481–487. doi: 10.1038/ng.3538

Zou, Z. Y., Zhou, Z. R., Che, C. H., Liu, C. Y., He, R. L., and Huang, H. P. (2017). Genetic epidemiology of amyotrophic lateral sclerosis: a systematic review and meta-analysis. *J. Neurol. Neurosurg. Psychiatry* 88, 540–549. doi: 10.1136/jnnp-2016-315018

frontiers | Frontiers in Aging Neuroscience

TYPE Original Research
PUBLISHED 16 February 2023
DOI 10.3389/fnagi.2023.1114466

OPEN ACCESS

EDITED BY
Robert Petersen,
Central Michigan University,
United States

REVIEWED BY
M. Gustavo Murer,
University of Buenos Aires,
Argentina
Maria Sheila Guimarães Rocha,
Hospital Santa Marcelina,
Brazil

*CORRESPONDENCE
Jianguo Zhang
✉ zjguo73@126.com
Anchao Yang
✉ yang.anchao@163.com

SPECIALTY SECTION
This article was submitted to Parkinson's Disease and Aging-related Movement Disorders, a section of the journal Frontiers in Aging Neuroscience

RECEIVED 02 December 2022
ACCEPTED 30 January 2023
PUBLISHED 16 February 2023

CITATION
Wu D, Zhao B, Xie H, Xu Y, Yin Z, Bai Y, Fan H, Zhang Q, Liu D, Hu T, Jiang Y, An Q, Zhang X, Yang A and Zhang J (2023) Profiling the low-beta characteristics of the subthalamic nucleus in early- and late-onset Parkinson's disease.
Front. Aging Neurosci. 15:1114466.
doi: 10.3389/fnagi.2023.1114466

Profiling the low-beta characteristics of the subthalamic nucleus in early- and late-onset Parkinson's disease

Delong Wu[1], Baotian Zhao[1], Hutao Xie[1], Yichen Xu[1], Zixiao Yin[1], Yutong Bai[1,2,3], Houyou Fan[1], Quan Zhang[1], Defeng Liu[1], Tianqi Hu[1], Yin Jiang[2,3], Qi An[1], Xin Zhang[2,3], Anchao Yang[1,2,3]* and Jianguo Zhang[1,2,3]*

[1]Department of Neurosurgery, Beijing Tiantan Hospital, Capital Medical University, Beijing, China, [2]Beijing Key Laboratory of Neurostimulation, Beijing, China, [3]Department of Functional Neurosurgery, Beijing Neurosurgical Institute, Capital Medical University, Beijing, China

Objectives: Low-beta oscillation (13–20Hz) has rarely been studied in patients with early-onset Parkinson's disease (EOPD, age of onset ≤50years). We aimed to explore the characteristics of low-beta oscillation in the subthalamic nucleus (STN) of patients with EOPD and investigate the differences between EOPD and late-onset Parkinson's disease (LOPD).

Methods: We enrolled 31 EOPD and 31 LOPD patients, who were matched using propensity score matching. Patients underwent bilateral STN deep brain stimulation (DBS). Local field potentials were recorded using intraoperative microelectrode recording. We analyzed the low-beta band parameters, including aperiodic/periodic components, beta burst, and phase-amplitude coupling. We compared low-beta band activity between EOPD and LOPD. Correlation analyses were performed between the low-beta parameters and clinical assessment results for each group.

Results: We found that the EOPD group had lower aperiodic parameters, including offset (p=0.010) and exponent (p=0.047). Low-beta burst analysis showed that EOPD patients had significantly higher average burst amplitude (p=0.016) and longer average burst duration (p=0.011). Furthermore, EOPD had higher proportion of long burst (500–650ms, p=0.008), while LOPD had higher proportion of short burst (200–350ms, p=0.007). There was a significant difference in phase-amplitude coupling values between low-beta phase and fast high frequency oscillation (300–460Hz) amplitude (p=0.019).

Conclusion: We found that low-beta activity in the STN of patients with EOPD had characteristics that varied when compared with LOPD, and provided electrophysiological evidence for different pathological mechanisms between the two types of PD. These differences need to be considered when applying adaptive DBS on patients of different ages.

KEYWORDS

Parkinson's disease, aging, subthalamic nucleus, microelectrode recording, local field potential

1. Introduction

Parkinson's disease (PD) is a movement disorder characterized by bradykinesia and at least one of resting tremor and rigidity, as well as a variety of non-motor symptoms (Postuma et al., 2015). PD can be classified into two subtypes according to age of onset: early-onset PD [EOPD, age of onset ≤50 years (Butterfield et al., 1993; Schrag and Schott, 2006; Mehanna and Jankovic, 2019; Niemann and Jankovic, 2019), although some studies define the upper age limit as 40 years (Quinn et al., 1987; Schrag et al., 2000)] and late-onset PD (LOPD). Patients with EOPD typically have poorer social adjustment, higher rates of depression, and inferior quality of life compared to LOPD patients, as it affects those who are in the prime of their productivity (Mehanna and Jankovic, 2019). EOPD patients may experience more severe physical, financial, and psychological problems by the time they reach the age of LOPD patients, because of their longer disease duration. Therefore, maintaining daily social and occupational functioning is the treatment focus in EOPD, while postponing or ameliorating motor complications of treatment, offering psychological support, and, if possible, preventing psychiatric problems such as anxiety and depression (Schrag and Schott, 2006; Niemann and Jankovic, 2019).

Although current medication can provide good symptomatic remission, patients will still develop motor complications and fluctuations as the disease progresses. Deep brain stimulation (DBS) is a well-established treatment for PD, and provides a unique opportunity to gain insights into local field potentials (LFPs), which are recorded from the neuron population surrounding the target area by the depth electrodes (Okun, 2012; Fox et al., 2018). Aiming to save energy and reduce side effects, adaptive DBS (aDBS) automatically trims stimulation depending on neurophysiological feedback, in which sensitive and specific electrophysiological biomarkers play a vital role (Rosin et al., 2011; Swann et al., 2018).

In recent years, aperiodic components of spectra have been noticed in electrophysiological signal analyze, which was considered as 1/*f*-like instructed noise before. In oscillatory analysis, reliance on *a priori* frequency bands may lead to the inclusion of aperiodic activity from outside the real physiological oscillation range (Donoghue et al., 2020). Studies have proved that there is correlation between age and this 1/*f*-like component (Voytek et al., 2015). Many researchers have found that beta activity could potentially be a feedback signal for aDBS, owing to its correlation with parkinsonian symptom severity and because it can be regulated by medical treatment and DBS. Evidence has shown that low-beta activity is more dominant within the subthalamic nucleus (STN) and is regarded as a pathological oscillation (Tsiokos et al., 2017). In addition, low beta has been proved to be more sensitive to dopaminergic or STN DBS (Litvak et al., 2011; Neumann et al., 2016a). Furthermore, beta burst has been proved to have a closer relationship with motor impairment and etiology of PD (Tinkhauser et al., 2017a; Torrecillos et al., 2018; Lofredi et al., 2019a,b). Moreover, a recent study with a large cohort of 106 PD patients shows similar results that both band power and burst duration of frequency-specific low beta (13–20 Hz) have significant correlations with motor symptom severity, and the dopamine-related reduction of band power and burst duration are paralleled by dopamine-related symptom alleviation (Lofredi et al., 2023). Phase-amplitude coupling (PAC) may be interpreted considerably differently between STN PAC and cortical PAC, as cortical PAC involves the amplitude of broadband activity (50–200 Hz), not an oscillatory rhythm, whereas STN PAC involves the amplitude of high frequency oscillation (HFO, 200–500 Hz). Beta/HFO PAC in the basal ganglia has been found to be correlated to motor impairment severity (Lopez-Azcarate et al., 2010). Another study has similar findings, and furthermore, this effect was more pronounced within the low-beta range, while coherence between subthalamic nucleus and motor cortex was dominant in the high-beta range (van Wijk et al., 2016). However, most previous studies on PD electrophysiology have obtained signals from elderly patients. It is noted that most EOPD cases result from Lewy body like LOPD, or less commonly, gene mutation (Schrag and Schott, 2006). Nevertheless, EOPD has the characteristics such as increased genetic predisposition, slower progression, and increased risk of levodopa-related complications, when compared to LOPD (Niemann and Jankovic, 2019). So we hypothesized that electrophysiological features of low beta in the STN of patients with EOPD would be different from those of patients with LOPD. This study aimed to explore the low-beta oscillation characteristics of the STN in patients with EOPD, to promote the development of aDBS in PD. In particular, we separated the aperiodic and periodic components, and addressed the differences in low-beta burst and beta/HFO PAC in the STN between patients with EOPD and those with LOPD.

2. Materials and methods

2.1. Patient inclusion

A total of 202 consecutive patients diagnosed with PD who underwent STN-DBS surgery between December 2019 and January 2021 at Tiantan Hospital were sampled. In our center, patients who showed dyskinesia or other L-dopa related complications were recommended to STN DBS, while patients with cognitive decline or mental disorder were prone to globus pallidus internus (GPi) DBS (Rughani et al., 2018). The inclusion criteria were (1) diagnosis of idiopathic PD, according to the United Kingdom Parkinson's Disease Society Brain Bank Clinical Diagnostic Criteria, (2) bilateral STN-DBS surgery was performed, and (3) preoperative clinical assessments were completed, including minimum demographic information; age of disease onset; disease duration; levodopa equivalent daily dose (LEDD); Movement Disorders Society Unified Parkinson's Disease Rating Scale (MDS-UPDRS) including medication (Med) ON and OFF; Hamilton Anxiety Scale (HAMA), Hamilton Depression Scale (HAMD); Beijing version of Mini-Mental State Examination (MMSE; Li et al., 2016); and Chinese version of Montreal Cognitive Assessment (MoCA; Huang et al., 2018; permission was obtained at https://www.mocatest.org/). Excluded were (1) patients who had received any other intracranial surgery previously and (2) patients who had severe surgery-related complications such as cerebral hemorrhage and hemiplegia. Patients were matched in terms of clinical baseline by propensity score matching (PSM; details in Statistical Analysis section). Patients gave informed written consent, and the study was approved by the institutional review board of Beijing Tiantan Hospital.

2.2. Surgical procedures and signal recording

Patients were operated by the same team and a standard surgical procedure was conducted as previously reported (Fan et al., 2020; Xie et al., 2022). Briefly, the STN target coordinates and trajectory were determined using a surgical planning system (Surgiplan, Elekta

Instrument AB, Stockholm, Sweden) with which we combined the CT scan with a stereotactic frame and 3-D high resolution magnetic resonance (MR) images, preoperatively. The STN target coordinates for the lower contact were 2–3 mm posterior to the mid commissural point (MCP), 12–14 mm lateral to the anterior commissure–posterior commissure (AC-PC), and 4–6 mm below the inter-commissural line. We performed intraoperative microelectrode recording (MER) using a tungsten microelectrode (10–20 μm at the tip with impedance 0.4–1 MΩ, Alpha Omega Engineering, Nazareth, Israel) and the Neuro-Omega system (Alpha Omega Engineering, Nazareth, Israel), sampled at 44 kHz. MER was started at 10 mm above the target and advanced in small discrete steps (stepwise ranging from 0.1 to 0.5 mm), controlled by the neurophysiologist to achieve optimal recording and identification of the borders of the STN. The STN was identified visually as characterized by a prominent increase in background activity with typical multiple neuronal discharges of high frequency. During MER, patients were awake and not under sedation. Data were obtained in the resting state and at least 12 h since last dopaminergic medication. Macro-stimulation was then performed to confirm the target position, testing the effect on motor symptom control and observing for any side effects. The programmable pulse generator (IPG) was then implanted in the subclavicular area under general anesthesia. Postoperative CT was performed to exclude intracranial hemorrhage and the exact locations of the DBS leads verified by merging with preoperative MR images.

2.3. Electrophysiological data processing

Data preprocessing was performed in MATLAB (Version 2020b, MathWorks, United States) with customized scripts and the Fieldtrip toolbox (Oostenveld et al., 2011).[1] All electrophysiological data were manually visualized offline and recordings with obvious artifacts were discarded. Artifact-free LFP data from all the recording depths inside STN were accumulated for further analysis. The electrophysiology data were downsampled to 2000 Hz and a notch filter was applied to the data to remove the 50 Hz line noise and harmonics. Data were z-score normalized for subsequent process and analysis.

2.3.1. Aperiodic and periodic component

The data were filtered between 2 and 500 Hz using a zero-phase third-order Butterworth bandpass filter. The power spectral density (PSD) was calculated in each trace using Welch's method with a 1 s Hanning window (50% overlap). We separated the aperiodic and periodic component of the LFP signal using the FOOOF algorithm (Donoghue et al., 2020). We set the FOOOF parameters as follows: peak width limits: 2–12; maximum number of peaks: infinite; minimum peak height: 0; peak threshold: 2; and aperiodic model: fixed. The Welch's PSD was fitted into the FOOOF model and parameterized across the frequency range of 2–45 Hz, which separated the aperiodic components (offset and exponent) from the periodic components, which included peak frequency (arrow in Figure 1A) for further analysis of beta burst. After the parameterization of the power spectra, the fitted spectra were used to subtract the aperiodic power (area under the aperiodic fit curve) to obtain periodic PSD (blue shadow in Figure 1B).

2.3.2. Low-beta burst

The criteria for burst determination generally followed a previous study (Tinkhauser et al., 2017b). The low-beta band power was represented as the averaged power across the corresponding frequency band (13–20 Hz). The beta peak frequency with the highest power of each recording trace, which was acquired from FOOOF peak identification, was selected. The envelope of the beta peak band filtered LFP was calculated using the Hilbert transform with a 6 Hz bandwidth centered around the selected peak frequency (beta peak band; Figure 2A). Threshold was defined in terms of the 75th percentiles of the Hilbert envelope amplitude (red dash line in Figures 2B,C). Beta burst was identified as wavelet amplitude exceeding the applied amplitude threshold. Bursts with durations shorter than 100 ms were excluded to limit the contribution of spontaneous fluctuations in amplitude due to noise (Deffains et al., 2018). The burst amplitude was defined as the area between the signal curve and threshold line (yellow shadow in Figure 2C). The distribution of burst durations was considered by categorizing them into five time windows of 150 ms, starting from 200 ms to >800 ms in duration (Lofredi et al., 2019a). Considering that the absolute number of bursts may have varied across traces, we calculated the percentage distribution of bursts in each time window, which served as a normalization step. The averaged amplitude and duration of all identified bursts were also calculated (Figure 3).

2.3.3. Phase-amplitude coupling

PAC was calculated as we previously reported (Yin et al., 2022). We investigated 2–45 Hz as phase frequencies and 50–500 Hz range as amplitude frequencies. LFP data were bandpass filtered with a third-order Butterworth filter from 2 to 50 Hz with a 2 Hz bandwidth and 1 Hz shift, while the same LFP data were filtered from 50 to 500 Hz with a 4 Hz bandwidth and 2 Hz shift. Then, the instantaneous phase of the low frequency bandpass filtered signal and the instantaneous amplitude of the high frequency filtered signal were extracted using the Hilbert transform. We used the Kullback–Leibler distance, which measures the divergence between the probability distribution of high frequency amplitudes and uniform distribution, to calculate the modulation index (MI; Tort et al., 2010). The obtained MI was normalized by calculating the z-score of 200 surrogates generated by randomly swapping amplitude time blocks. Z-scored PAC computed for multiple frequencies of phase and amplitude were demonstrated as a comodulogram. The PAC calculations were conducted in Python 3 using the Tensorpac toolbox (Combrisson et al., 2020).[2]

2.4. Statistical analysis

We performed PSM to minimize the effects of potential confounding factors. Patients in this study were divided into two groups, EOPD group and LOPD group. Patients in the EOPD group were matched with a similar cohort of patients with LOPD (age of onset >50 years) in our dataset with a 1:1 ratio for disease duration, LEDD, MDS-UPDRS III scores (Med OFF), HAMA, HAMD, MMSE, and MoCA. PSM was performed using the nearest neighbor method within a caliper of 0.01 in SPSS (Version 27.0, IBM, United States).

1 https://www.fieldtriptoolbox.org/

2 https://etiennecmb.github.io/tensorpac/

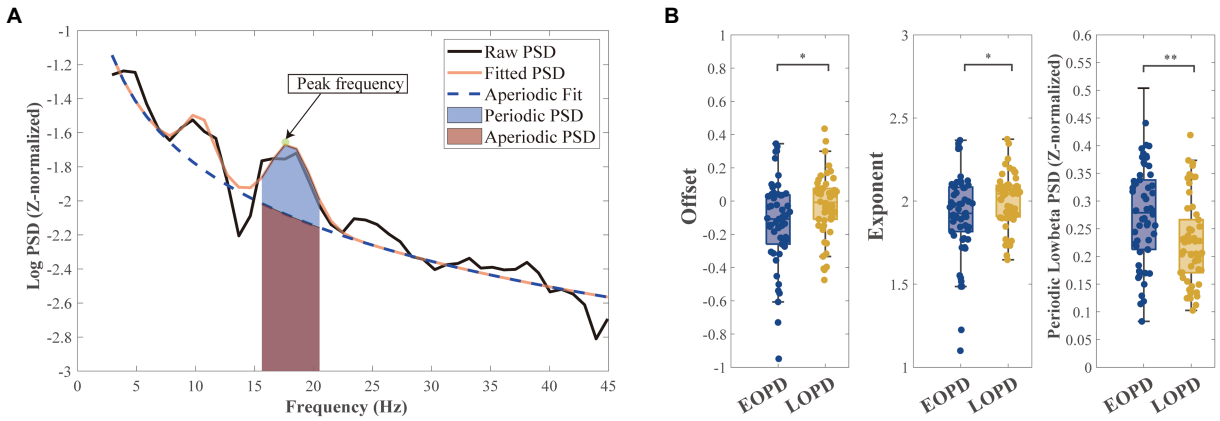

FIGURE 1
Schematic diagram of parameterization of power spectra. **(A)** An example of parameterizing the power spectra: the aperiodic component (blue dashed line) and the fitted spectra (orange full line). Mixed power is equal to the sum of periodic power (light blue shadow) and aperiodic power (light purple shadow). Peak frequency (green point and arrowed) in low-beta band with highest power was selected for subsequent burst analysis. **(B Left)** Early-onset Parkinson disease (EOPD) patients demonstrated lower offset than late-onset Parkinson disease (LOPD) patients (EOPD: −0.14±0.28, LOPD: −0.02±0.19, p=0.010), meaning EOPD patients had a lower spectrum curve. **(B Middle)** EOPD patients demonstrated lower exponent than LOPD patients (EOPD: 1.92±0.25, LOPD: 2.00±0.16, p=0.047), meaning LOPD patients had a steeper spectrum curve. **(B Right)** After separating the aperiodic components from the periodic components, we observed periodic low-beta power that was significantly higher in EOPD patients than LOPD patients (EOPD: 0.26±0.09, LOPD: 0.22±0.08, p=0.002).

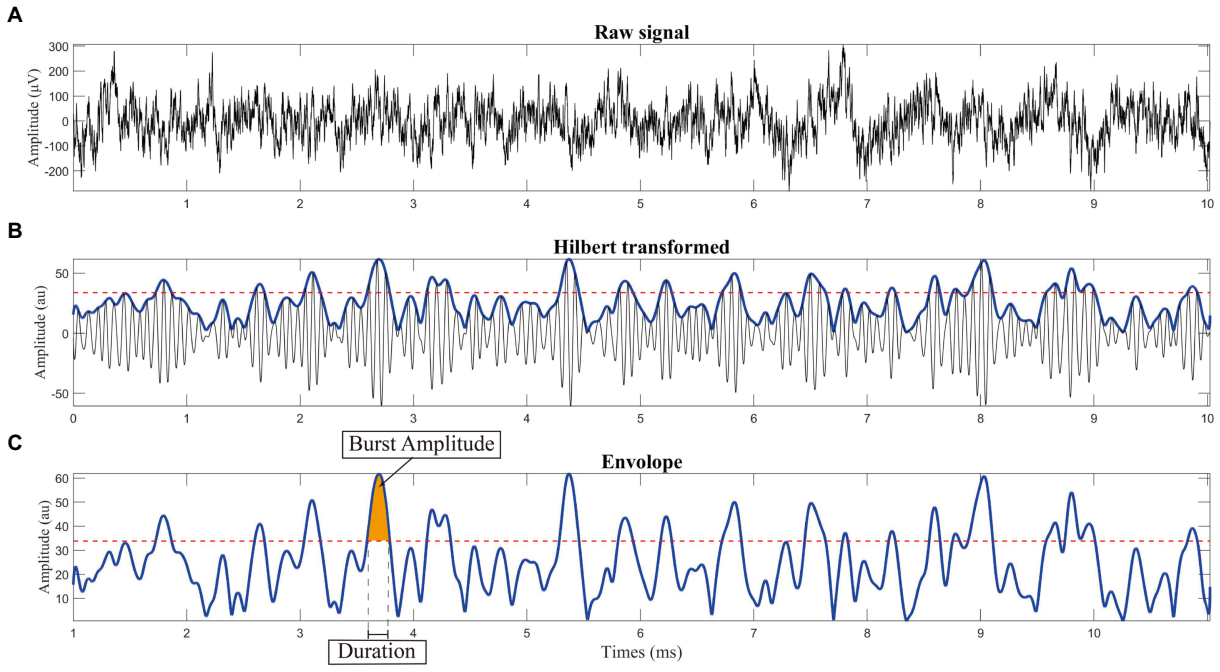

FIGURE 2
Schematic diagram of burst analysis. **(A)** Raw signal recorded from the subthalamic nucleus using microelectrode recoding. **(B)** Calculating the envelope: we used the Hilbert transform with a 6Hz bandwidth centered around the selected peak frequency (peak frequency is shown in Figure 1A). **(C)** Threshold was defined in terms of the 75th percentile of the Hilbert envelope amplitude, as shown by the red dashed line. Burst was identified as wavelet amplitude exceeding the applied amplitude threshold. Burst duration was defined by the time points at which the selected time evolution of the wavelet amplitude exceeded a given amplitude threshold. To reduce the contribution of other noise, bursts with durations shorter than 100ms were excluded before further analysis.

Independent non-parametric tests (Wilcoxon rank-sum test) and Spearman's correlation were used when the data were not normally distributed, which was tested by the Kolmogorov–Smirnov test; otherwise, independent Student's t-tests and Person's correlation were used. Correlation analysis was performed between age of onset and LFP characteristics in whole population. Correlation analysis was also performed between LFP characteristics and MDS-UPDRS III total and subdivided scores, including Med ON/OFF and improvement rate in whole population and within each groups, respectively. False Discovery Rate (FDR) correction was used for multiple comparison. A value of p

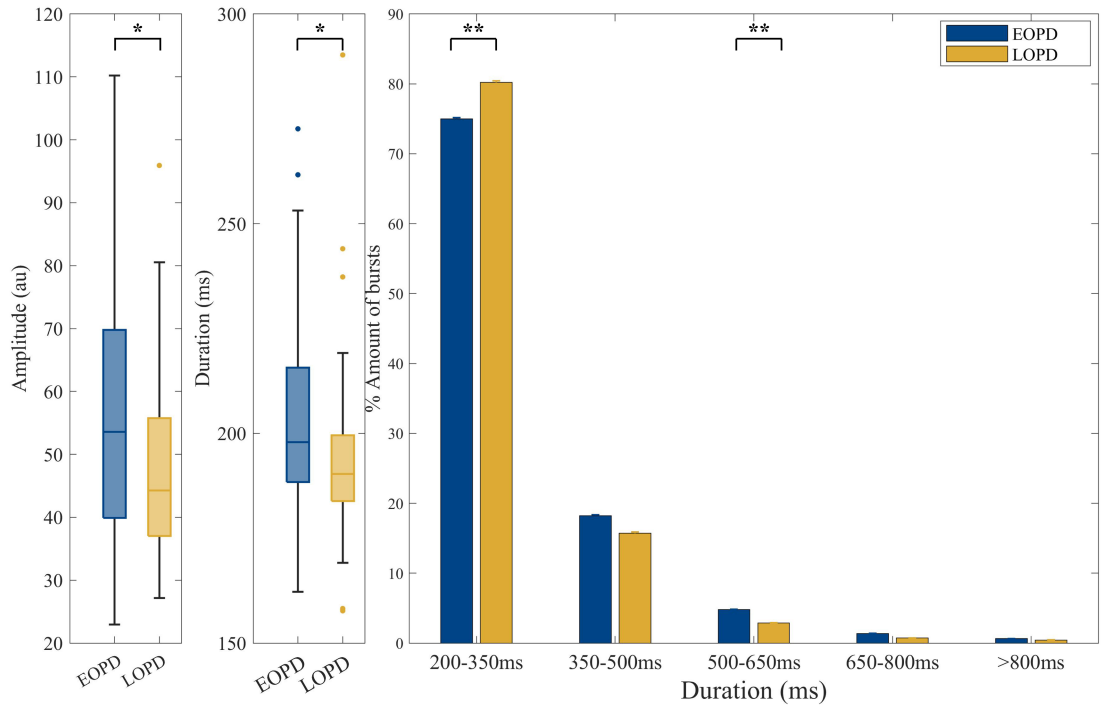

FIGURE 3
Comparison of low-beta burst between EOPD and LOPD. **(A)** The average low-beta burst power was significantly higher in EOPD (EOPD: 56.70±20.10 au. LOPD: 47.27±14.73 au, p=0.016). **(B)** The average low-beta burst duration of EOPD was significantly longer than that of LOPD (EOPD: 203.74±22.55ms, LOPD: 193.79±20.80ms, p=0.011). **(C)** Illustration of beta burst duration categorized into five time windows. The proportion of long burst (burst duration 500–650ms) was significantly increased in EOPD when compared to LOPD (EOPD: 4.79%±3.86%, LOPD, 2.88%±2.87%, p=0.008). In contrast, the proportion of short low-beta bursts (burst duration 200–350ms) was significantly higher in LOPD when compared to EOPD (EOPD: 75.00%±10.52%, LOPD, 80.22%±10.79%, p=0.007).

<0.05 was considered significant. Statistical analyses were performed in MATLAB and R Studio (Version 1.4.17, PBC, United States).

$$\text{improvement rate} = \left(\frac{\text{Med OFF} - \text{Med ON}}{\text{Med OFF}} \right) \times 100\%$$

3. Results

3.1. Patients

A total of 62 patients were enrolled including 31 with EOPD (11 female, 20 male) and 31 with LOPD (16 female, 15 male), matched through PSM. There were no significant differences between the two groups in preoperative clinical assessments such as disease duration ($p = 0.963$), LEDD ($p = 0.086$), MDS-UPDRS III scores (Med OFF, $p = 0.832$), HAMA ($p = 0.216$), HAMD ($p = 0.061$), MMSE ($p = 0.140$), and MoCA ($p = 0.154$). EOPD patients had a significantly higher improvement rate ($p = 0.005$) in MDS-UPDRS III scores, including total and some subdivided (bradykinesia and rigidity) scores, than the LOPD patients. The detailed patient demographics and clinical characteristics are summarized in Table 1. There was no significance difference in average signal duration between groups (EOPD: 229.39 ± 106.10 s, LOPD: 188.04 ± 125.29 s, $p = 0.16$).

3.2. Aperiodic components and periodic power spectral density

After parameterizing the LFP, we found significant differences in offset (EOPD: −0.14 ± 0.28, LOPD: −0.02 ± 0.19, $p = 0.010$) and exponent (EOPD: 1.92 ± 0.25, LOPD: 2.00 ± 0.16, $p = 0.047$) parameters between the two groups. Offset parameters represent broadband up/down shift of the whole spectrum, and our results showed that EOPD patients had a lower spectrum curve than LOPD patients. However, exponent represents the slope of the spectrum, which means in our study LOPD patients had a steeper spectrum curve than EOPD patients. By subtracting the aperiodic power with the fitted power, low-beta periodic PSD was found to be higher in EOPD patients (EOPD: 0.26 ± 0.09, LOPD: 0.22 ± 0.08, $p = 0.002$). The results are shown in Figure 1B.

3.3. Comparison of low-beta burst

The average amplitude of low-beta burst was significantly higher in EOPD (EOPD: 56.70 ± 20.10 au, LOPD: 47.27 ± 14.73 au, $p = 0.016$). The average low-beta burst duration of EOPD was significantly longer than that of LOPD (EOPD: 203.74 ± 22.55 ms, LOPD: 193.79 ± 20.80 ms, $p = 0.011$). Also, the ratio of long bursts (burst duration 500–650 ms) was significantly increased in EOPD when compared to LOPD (EOPD: 4.79% ± 3.86%, LOPD, 2.88% ± 2.87%, $p = 0.008$). In contrast, the proportion of short

10.3389/fnagi.2023.1114466

low-beta bursts (burst duration 200–350 ms) was significantly higher in LOPD when compared to EOPD (EOPD: 75.00% ± 10.52%, LOPD, 80.22% ± 10.79%, $p = 0.007$).

TABLE 1 Demographic and clinical characteristics.

	EOPD	LOPD	*p* value
Age*	43.6 ± 6.3	60.0 ± 6.0	<0.001*
Gender(F/M)	11/20	16/15	
LEDD (mg/day)	936.26 ± 372.89	788.13 ± 289.25	0.086
Disease duration (years)	8.13 ± 2.60	8.16 ± 2.89	0.963
MDS-UPDRS	49.94 ± 16.36	49.03 ± 16.97	0.832
Part III (Med off)			
Axial	10.42 ± 4.65	10.26 ± 4.95	0.896
Bradykinesia	21.32 ± 7.46	20.71 ± 9.36	0.776
Rigidity	8.55 ± 3.01	7.81 ± 3.64	0.385
Tremor	9.65 ± 7.85	10.26 ± 6.64	0.741
MDS-UPDRS	*17.97 ± 8.86*	*25.00 ± 13.44*	*0.018**
Part III (Med on)			
Axial	3.94 ± 3.04	5.39 ± 3.73	0.098
Bradykinesia	*7.90 ± 4.85*	*11.29 ± 7.26*	*0.035**
Rigidity	3.03 ± 1.663	3.94 ± 2.41	0.091
Tremor	3.10 ± 2.95	4.39 ± 4.90	0.214
Improve rate (%)	*63.06 ± 17.77*	*51.07 ± 14.70*	0.005*
Axial	60.79 ± 25.01	49.28 ± 26.64	0.085
Bradykinesia	*62.37 ± 20.00*	*47.28 ± 17.17*	*0.002**
Rigidity	*64.53 ± 18.35*	*50.19 ± 20.21*	*0.005**
Tremor	70.73 ± 25.65	64.05 ± 28.22	0.356
HAMA	19.97 ± 8.94	16.90 ± 10.31	0.216
HAMD	20.03 ± 8.67	15.58 ± 9.64	0.061
MMSE	26.61 ± 5.36	24.77 ± 4.24	0.140
MoCA	22.35 ± 6.67	20.03 ± 5.99	0.154

Values are presented as mean ± standard deviation (SD). LEDD, Levodopa equivalent daily doses; MDS-UPDRS, Movement Disorders Society Unified Parkinson's Disease Rating Scale; HAMA, Hamilton Anxiety scale; HAMD, Hamilton Depression scale; MMSE, Mini-mental State Examination; MoCA, Montreal Cognitive Assessment. MDS-UPDRS III off-medication evaluations were performed after the withdrawal of anti-parkinsonism medications for 8–12 h, and on-medication evaluations were performed when the patient had maximum clinical benefit following the patient's regular dose of anti-parkinsonism medication.
*A significant difference.

3.4. Beta/fHFO phase-amplitude coupling

The comodulograms of group-level PAC for EOPD and LOPD and their subtraction are shown in Figure 4. There was a significant difference between EOPD and LOPD groups in MI of low-beta phase (13–20 Hz) and fast HFO (fHFO, 300–460 Hz) amplitude coupling ($p = 0.019$), as shown in the right image of Figure 4.

3.5. Correlation analysis

After calculating the results above, we tried to establish their relationship with clinical data. As show in Figure 5, age had significant correlation with offset ($r = 0.305$, FDR corrected $p = 0.047$, Figure 5A) and periodic low-beta PSD ($r = -0.315$, FDR corrected $p = 0.047$, Figure 5C) in whole population. Moreover, exponent ($r = 0.271$, FDR corrected $p = 0.050$, Figure 5B) and PAC value of low beta/fHFO ($r = -0.284$, FDR corrected $p = 0.050$, Figure 5F) were marginal significantly correlated with age. In Figure 6, circles with uncorrected p value greater than 0.05 were crossed. However, after FDR correction, there were no significant correlations between LFP parameters and the motor scores (including total scores and subdivided scores), neither within whole population nor each groups, respectively.

4. Discussion

To date, there has been no specific research on LFP in EOPD. Here, we demonstrated for the first time several characteristics of the electrophysiological signals recorded from the STN of patients with EOPD.

In the past few decades, the vast majority of electrophysiological investigations have examined the combined periodic oscillatory component and the aperiodic component rather than separating them. Because apparent changes in narrowband power may represent a variety of physiological processes, using narrowband filtering (for example, 13–30 Hz for the beta band) without parameterization can lead to a misrepresentation and incorrect interpretation of physiological phenomena (Donoghue et al., 2020). The aperiodic offset parameter represents total up/down shift of the whole spectrum, and it was proved to be correlated with both the blood-oxygen-level-dependent (BOLD) signal from functional MR

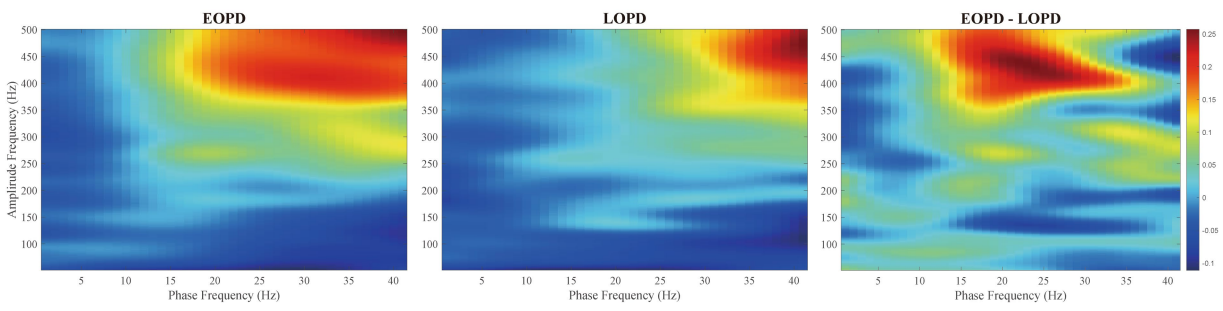

FIGURE 4
Comodulograms of phase-amplitude coupling. Modulation index (MI) was averaged across all EOPD **(Left)** and LOPD patients **(Middle)**, with phase frequency (range from 2 to 45Hz) and amplitude frequency (range from 50 to 500Hz) shown. **(Right)** Inter-group comparison showed a significant difference in MI of low beta phase (13–20 Hz) and fast HFO (fHFO, 300–460 Hz) amplitude coupling (p = 0.019).

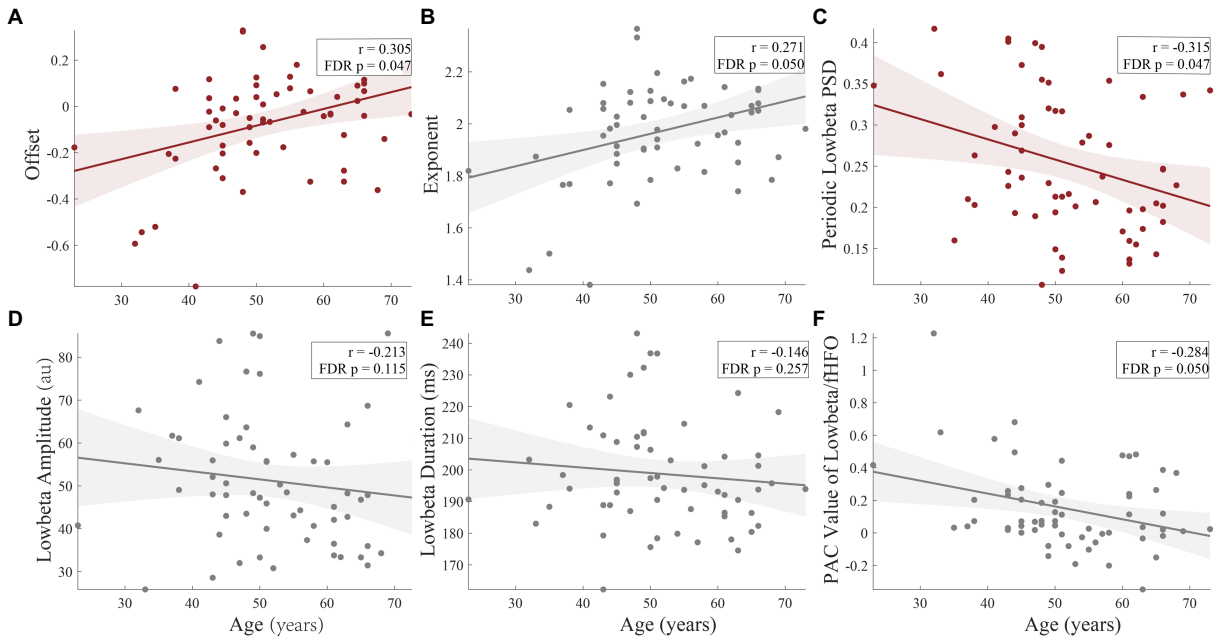

FIGURE 5
The correlations of age and the LFP parameters. There were significant correlations between age and offset (r=0.305, FDR corrected p=0.047), **(A)** and periodic low-beta PSD (r=−0.315, FDR corrected p=0.047), **(C)** in whole population. Moreover, exponent (r=0.271, FDR corrected p=0.050), **(B)** and PAC value of low-beta/fHFO (r=−0.284, FDR corrected p=0.050), **(E)** were marginal significantly correlated with age. The amplitude (FDR corrected p=0.115) **(D)** and duration (FDR corrected p=0.257) **(F)** had no significant correlations with age.

imaging (Winawer et al., 2013) and neuronal spiking (Manning et al., 2009). The aperiodic exponent has been related to the integration of the synaptic currents (Buzsáki et al., 2012). Recent studies have found the 1/f-like aperiodic components, which had been considered as noise before, have a unique function and are associated with brain activity (Adelhöfer et al., 2021; Zhang et al., 2021) and age (Voytek et al., 2015; Schaworonkow and Voytek, 2021). Here, our study found the results analogous to previous research, in which offset ($r = 0.305$, corrected $p = 0.047$, Figure 5A) and exponent ($r = 0.271$, corrected $p = 0.050$, Figure 5B) were positively correlated with age.

By investigating the relationship between resting-state EEG activity and the efficiency of cognitive functioning, Ouyang et al. (2020) found that 1/*f* brain activity plays an essential role in cognitive function, and pointed out the necessity of isolating the 1/*f* component from oscillatory activities. Synaptic excitation (E) and inhibition (I), typically represented by quick glutamate and slower GABA inputs, are balanced in neural circuits (Xue et al., 2014). The balance of E:I interaction is essential for the formation of neural oscillations (Atallah and Scanziani, 2009). One study found that reduced E/I ratio resulted in steeper power spectra, reflecting conscious state over time (Gao et al., 2017). In other words, exponent will be lower when E/I ratio increases, and larger when E/I ratio decreases. As in our study, the positive correlation between the aperiodic parameters and age provided evidence that neurons located in the STN of patients with EOPD showed higher excitability than in LOPD. It is noted that symptoms of most PD patients with older onset age result from neurodegeneration, whereas some patients with younger onset age suffer from motor impairment owing to selective dysregulation of dopaminergic production and transfer caused by variable factors such as genetic mutation (Angeli et al., 2013; Pal et al., 2016; Mehanna and Jankovic, 2019; Leuzzi et al., 2021).

The beta pathological oscillatory band has become the most studied band in PD, as it is strongly correlated with movement impairment and can be suppressed by medication (Brown et al., 2001) and DBS (Neumann et al., 2016b). Evidence shows that low-beta activity (13–20 Hz) is more sensitive to levodopa or DBS than high beta (Litvak et al., 2011), and a sub-band (10–14 Hz) partially within the low-beta range is most robustly correlated with UPDRS III total score (Neumann et al., 2016a). Weinberger et al. found positive correlation between the incidence of beta oscillatory neurons and the patient's response to dopaminergic medications, but not with baseline motor deficits off medication (Weinberger et al., 2006). Similarly in our study, EOPD patients, with higher periodic low-beta power, had better response to anti-parkinsonism medication when compared to LOPD patients, under similar clinical baseline measurements such as LEDD and disease severity (UPDRS III total scores under Med OFF condition) for the PSM we used.

The amount of low-beta burst activity in STN correlates with the progressive decline in movement velocity in a spectrally specific manner, which can better explain motor impairment when compared to average beta power (Lofredi et al., 2019b). The presence, amplitude, and duration of beta bursts in the STN of PD patients were modulated by context and may be crucial for the transformation of physiological information (Torrecillos et al., 2018; Kehnemouyi et al., 2021). The presence of abnormal beta bursts was significantly correlated with the severity of motor impairment in PD, and the distribution of beta burst duration could be changed from long to short by medication and DBS, which represented a more physiological state (Tinkhauser et al., 2017b). They also proved that beta bursts of longer duration were positively correlated and bursts of shorter duration were negatively correlated with motor impairment (Tinkhauser et al., 2017a). Furthermore, Lofredi et al. discovered that frequency-specific low-beta (13–20 Hz) band power and

10.3389/fnagi.2023.1114466

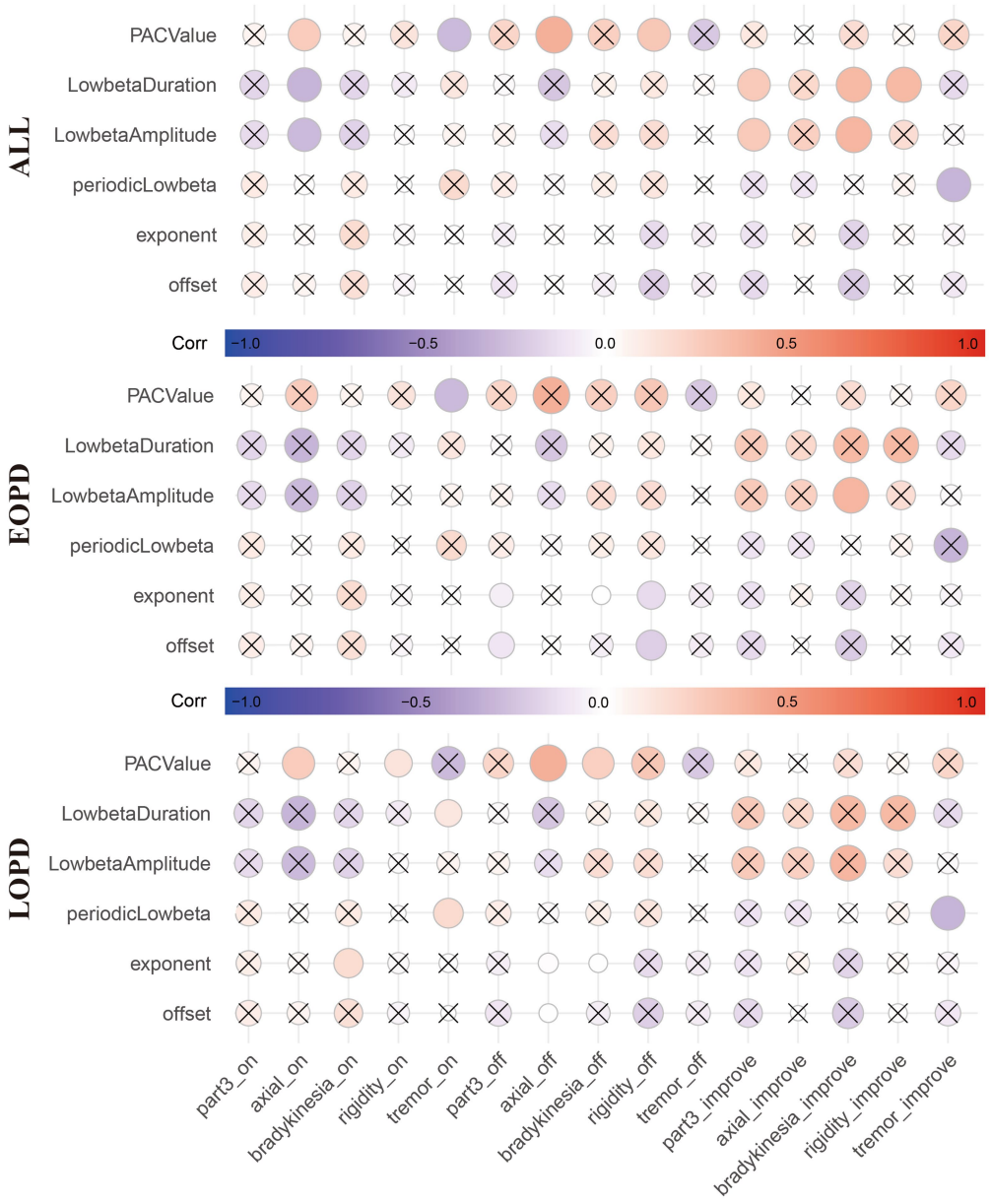

FIGURE 6
The correlation matrix shows the correlation between the local field potential (LFP) parameter and motor symptom scores (total scores and subdivided scores) and improvement rates in all patients **(Top)**, EOPD **(Middle)** and LOPD **(Bottom)**, respectively. Red represents positive correlation and blue represents negative correlation. Circles with uncorrected *p* values greater than 0.05 were crossed. However, after FDR correction, there were no significant correlations between LFP parameters and the motor scores (including total scores and subdivided scores), neither within whole population nor each group, respectively. *_on indicates Med ON. *_off indicates Med OFF. *_improve indicates improvement rate.

burst duration exhibited substantial relationships with the severity of motor impairments, and that dopamine-related symptom relief occurred simultaneously with reduction of both band power and burst duration (Lofredi et al., 2023). These features indicated low-beta burst duration as a better potential biomarker for aDBS. Our study showed that the average low-beta burst duration of EOPD was significantly longer than that of LOPD. Additionally, EOPD had more longer durations whereas LOPD had more shorter durations. These findings showed that neurons in the STN of patients with EOPD showed more over-synchronization, which was thought to be responsible for pathological beta bursts. Because synchronized neurons are prone to firing simultaneously, they are less likely to fire separately, which means the chances for them to transfer different information individually decrease, leading to restriction of the overall information coding capacity of the circuit (Brittain and Brown, 2014). Our study about burst provided electrophysiological evidence that neurons in the STN of patients with EOPD had higher excitability as we mentioned above. This may be because EOPD involves dysregulation of dopaminergic production and transfer rather than neurodegeneration.

Another potential biomarker for adaptive stimulation is PAC, modulation of the amplitude of high frequency oscillations by the phase of low frequency oscillations (Hwang et al., 2020). By

coordinating the activity time of neurons in connected networks, PAC plays an important role in the mechanism for communication within and between neurons in different brain regions (Canolty and Knight, 2010). PAC from different brain regions in PD has been found to be associated with motor impairment (Yin et al., 2022) and cognitive decline (Sacks et al., 2021), and can be affected by medication (Ozturk et al., 2020) and DBS (de Hemptinne et al., 2015; Steiner et al., 2017). Evidence has shown that exaggerated STN PAC between beta band and HFO is correlated with severity of motor impairments (bradykinesia/rigidity), and sub-band low beta is more closely linked to pathology in PD (Lopez-Azcarate et al., 2010; Connolly et al., 2015; van Wijk et al., 2016). Beta/HFO PAC was also found predictive of response to DBS therapy as the PAC with the greatest strength was found to be located in the dorsal STN, where stimulation was most clinically effective (Yang et al., 2014). In our study, with EOPD patients having stronger beta/HFO PAC in the STN, suggesting that neurons in the STN of younger patients may maintain their capacity for information processing and communications.

In our study, the age limit (50 years) was defined based on past experience, habits, epidemiology and clinical characteristics. There were still doubts that this age limit may not truly separate the groups so that the results should be interpreted cautiously. Continuous recordings from DBS device with sensing technology (i.e., Percept™ PC Neurostimulator, Medtronic) may provide a chance to get insight of the electrophysiological changes as age grows. More researches are needed to deepen our understanding of the relationship between age and disease.

5. Limitations

There were several limitations in our study. First, the data were recorded under the resting state, and the electrophysiological properties of the STN may vary in different movement states, which was not fully evaluated. Second, postoperative data were not complete and the follow-up period was short, so we were unable to identify the relationship between symptom improvement and electrophysiological signals of the STN. Third, we lacked patient genetic information, so we were unable to explore the genetic mechanism underlying the electrophysiological phenotype, which is worth exploring in the future.

In addition, the fact that the different median ages of the groups differed raised another important concern that some of the observed differences may be caused by age differences, when the patients underwent DBS and the signals were recorded, rather than disease factors. Further research of recordings from patients with other diseases or EOPD patients after aging may help ease this issue.

6. Conclusion

Our study revealed the electrophysiological features of the STN in EOPD for the first time. It is widely acknowledged that aDBS will play an inevitable role in the management of functional disease of the central nervous system, and sensitive and specific electrophysiological biomarkers in cohorts of different ages are required. We found that low-beta activity in the STN of patients with EOPD had different characteristics to LOPD, which may be because the different pathological processes in EOPD cause neurons to exhibit higher excitability. This should be considered when applying aDBS on patients of different ages.

Data availability statement

The original contributions presented in the study are included in the article/Supplementary material, further inquiries can be directed to the corresponding authors.

Ethics statement

The studies involving human participants were reviewed and approved by institutional review board of Beijing Tiantan Hospital. The patients/participants provided their written informed consent to participate in this study.

Author contributions

JZ performed conceptual design of experiments and experiment's integration, co-wrote the manuscript, and performed all the DBS surgery. AY checked the MER and postoperative CT scan. DW designed, performed, and analyzed electrophysiology recordings, and co-wrote the manuscript. BZ wrote the custumed code in MATLAB and R studio. HX co-wrote the manuscript. YX plotted the first three figures in MATLAB. ZY wrote the code in Python to calculate the PAC value. YB performed the PSM in SPSS. HF, QZ, and DL re-checked the data and analyzed results. TH, XZ, YJ, and QA did the clinical assessments and data collection. All authors contributed to the article and approved the submitted version.

Funding

This work was funded by the National Natural Science Foundation of China (81830033 and 81870888).

Conflict of interest

The authors declare that the research was conducted in the absence of any commercial or financial relationships that could be construed as a potential conflict of interest.

Publisher's note

References

Adelhöfer, N., Paulus, T., Mückschel, M., Bäumer, T., Bluschke, A., Takacs, A., et al. (2021). Increased scale-free and aperiodic neural activity during sensorimotor integration-a novel facet in Tourette syndrome. *Brain Commun.* 3:fcab250. doi: 10.1093/braincomms/fcab250

Angeli, A., Mencacci, N. E., Duran, R., Aviles-Olmos, I., Kefalopoulou, Z., Candelario, J., et al. (2013). Genotype and phenotype in Parkinson's disease: lessons in heterogeneity from deep brain stimulation. *Mov. Disord.* 28, 1370–1375. doi: 10.1002/mds.25535

Atallah, B. V., and Scanziani, M. (2009). Instantaneous modulation of gamma oscillation frequency by balancing excitation with inhibition. *Neuron* 62, 566–577. doi: 10.1016/j.neuron.2009.04.027

Brittain, J. S., and Brown, P. (2014). Oscillations and the basal ganglia: motor control and beyond. *NeuroImage* 85, 637–647. doi: 10.1016/j.neuroimage.2013.05.084

Brown, P., Oliviero, A., Mazzone, P., Insola, A., Tonali, P., and Di Lazzaro, V. (2001). Dopamine dependency of oscillations between subthalamic nucleus and pallidum in Parkinson's disease. *J. Neurosci.* 21, 1033–1038. doi: 10.1523/Jneurosci.21-03-01033.2001

Butterfield, P. G., Valanis, B. G., Spencer, P. S., Lindeman, C. A., and Nutt, J. G. (1993). Environmental antecedents of young-onset Parkinson's disease. *Neurology* 43, 1150–1158. doi: 10.1212/wnl.43.6.1150

Buzsáki, G., Anastassiou, C. A., and Koch, C. (2012). The origin of extracellular fields and currents – EEG, ECoG, LFP and spikes. *Nat. Rev. Neurosci.* 13, 407–420. doi: 10.1038/nrn3241

Canolty, R. T., and Knight, R. T. (2010). The functional role of cross-frequency coupling. *Trends Cogn. Sci.* 14, 506–515. doi: 10.1016/j.tics.2010.09.001

Combrisson, E., Nest, T., Brovelli, A., Ince, R. A. A., Soto, J. L. P., Guillot, A., et al. (2020). Tensorpac: an open-source python toolbox for tensor-based phase-amplitude coupling measurement in electrophysiological brain signals. *PLoS Comput. Biol.* 16:e1008302. doi: 10.1371/journal.pcbi.1008302

Connolly, A. T., Jensen, A. L., Bello, E. M., Netoff, T. I., Baker, K. B., Johnson, M. D., et al. (2015). Modulations in oscillatory frequency and coupling in globus pallidus with increasing parkinsonian severity. *J. Neurosci.* 35, 6231–6240. doi: 10.1523/JNEUROSCI.4137-14.2015

de Hemptinne, C., Swann, N. C., Ostrem, J. L., Ryapolova-Webb, E. S., San Luciano, M., Galifianakis, N. B., et al. (2015). Therapeutic deep brain stimulation reduces cortical phase-amplitude coupling in Parkinson's disease. *Nat. Neurosci.* 18, 779–786. doi: 10.1038/nn.3997

Deffains, M., Iskhakova, L., Katabi, S., Israel, Z., and Bergman, H. (2018). Longer β oscillatory episodes reliably identify pathological subthalamic activity in parkinsonism. *Mov. Disord.* 33, 1609–1618. doi: 10.1002/mds.27418

Donoghue, T., Haller, M., Peterson, E. J., Varma, P., Sebastian, P., Gao, R., et al. (2020). Parameterizing neural power spectra into periodic and aperiodic components. *Nat. Neurosci.* 23, 1655–1665. doi: 10.1038/s41593-020-00744-x

Fan, S. Y., Wang, K. L., Hu, W., Eisinger, R. S., Han, A., Han, C. L., et al. (2020). Pallidal versus subthalamic nucleus deep brain stimulation for levodopa-induced dyskinesia. *Ann. Clin. Transl. Neurol.* 7, 59–68. doi: 10.1002/acn3.50961

Fox, S. H., Katzenschlager, R., Lim, S. Y., Barton, B., de Bie, R. M. A., Seppi, K., et al. (2018). International Parkinson and movement disorder society evidence-based medicine review: update on treatments for the motor symptoms of Parkinson's disease. *Mov. Disord.* 33, 1248–1266. doi: 10.1002/mds.27372

Gao, R., Peterson, E. J., and Voytek, B. (2017). Inferring synaptic excitation/inhibition balance from field potentials. *NeuroImage* 158, 70–78. doi: 10.1016/j.neuroimage.2017.06.078

Huang, L., Chen, K. L., Lin, B. Y., Tang, L., Zhao, Q. H., Lv, Y. R., et al. (2018). Chinese version of Montreal cognitive assessment basic for discrimination among different severities of Alzheimer's disease. *Neuropsychiatr. Dis. Treat.* 14, 2133–2140. doi: 10.2147/Ndt.S174293

Hwang, B. Y., Salimpour, Y., Tsehay, Y. K., Anderson, W. S., and Mills, K. A. (2020). Perspective: phase amplitude coupling–based phase–dependent neuromodulation in Parkinson's disease. *Front. Neurosci.* 14:558967. doi: 10.3389/fnins.2020.558967

Kehnemouyi, Y. M., Wilkins, K. B., Anidi, C. M., Anderson, R. W., Afzal, M. F., and Bronte-Stewart, H. M. (2021). Modulation of beta bursts in subthalamic sensorimotor circuits predicts improvement in bradykinesia. *Brain* 144, 473–486. doi: 10.1093/brain/awaa394

Leuzzi, V., Nardecchia, F., Pons, R., and Galosi, S. (2021). Parkinsonism in children: clinical classification and etiological spectrum. *Parkinsonism Relat. Disord.* 82, 150–157. doi: 10.1016/j.parkreldis.2020.10.002

Li, H., Jia, J., and Yang, Z. (2016). Mini-mental state examination in elderly Chinese: a population-based normative study. *J. Alzheimers Dis.* 53, 487–496. doi: 10.3233/JAD-160119

Litvak, V., Jha, A., Eusebio, A., Oostenveld, R., Foltynie, T., Limousin, P., et al. (2011). Resting oscillatory cortico-subthalamic connectivity in patients with Parkinson's disease. *Brain* 134, 359–374. doi: 10.1093/brain/awq332

Lofredi, R., Neumann, W. J., Brucke, C., Huebl, J., Krauss, J. K., Schneider, G. H., et al. (2019a). Pallidal beta bursts in Parkinson's disease and dystonia. *Mov. Disord.* 34, 420–424. doi: 10.1002/mds.27524

Lofredi, R., Okudzhava, L., Irmen, F., Brücke, C., Huebl, J., Krauss, J. K., et al. (2023). Subthalamic beta bursts correlate with dopamine-dependent motor symptoms in 106 Parkinson's patients. *NPJ Parkinsons Dis.* 9:2. doi: 10.1038/s41531-022-00443-3

Lofredi, R., Tan, H., Neumann, W. J., Yeh, C. H., Schneider, G. H., Kuhn, A. A., et al. (2019b). Beta bursts during continuous movements accompany the velocity decrement in Parkinson's disease patients. *Neurobiol. Dis.* 127, 462–471. doi: 10.1016/j.nbd.2019.03.013

Lopez-Azcarate, J., Tainta, M., Rodriguez-Oroz, M. C., Valencia, M., Gonzalez, R., Guridi, J., et al. (2010). Coupling between Beta and High-frequency activity in the human subthalamic nucleus may be a pathophysiological mechanism in Parkinson's disease. *J. Neurosci.* 30, 6667–6677. doi: 10.1523/Jneurosci.5459-09.2010

Manning, J. R., Jacobs, J., Fried, I., and Kahana, M. J. (2009). Broadband shifts in local field potential power spectra are correlated with single-neuron spiking in humans. *J. Neurosci.* 29, 13613–13620. doi: 10.1523/JNEUROSCI.2041-09.2009

Mehanna, R., and Jankovic, J. (2019). Young-onset Parkinson's disease: its unique features and their impact on quality of life. *Parkinsonism Relat. Disord.* 65, 39–48. doi: 10.1016/j.parkreldis.2019.06.001

Neumann, W. J., Degen, K., Schneider, G. H., Brucke, C., Huebl, J., Brown, P., et al. (2016a). Subthalamic synchronized oscillatory activity correlates with motor impairment in patients with Parkinson's disease. *Mov. Disord.* 31, 1748–1751. doi: 10.1002/mds.26759

Neumann, W. J., Staub, F., Horn, A., Schanda, J., Mueller, J., Schneider, G. H., et al. (2016b). Deep brain recordings using an implanted pulse generator in Parkinson's disease. *Neuromodulation* 19, 20–24. doi: 10.1111/ner.12348

Niemann, N., and Jankovic, J. (2019). Juvenile parkinsonism: differential diagnosis, genetics, and treatment. *Parkinsonism Relat. Disord.* 67, 74–89. doi: 10.1016/j.parkreldis.2019.06.025

Okun, M. S. (2012). Deep-brain stimulation for Parkinson's disease. *N. Engl. J. Med.* 367, 1529–1538. doi: 10.1056/NEJMct1208070

Oostenveld, R., Fries, P., Maris, E., and Schoffelen, J. M. (2011). Field trip: open source software for advanced analysis of MEG, EEG, and invasive electrophysiological data. *Comput. Intell. Neurosci.* 2011:156869. doi: 10.1155/2011/156869

Ouyang, G., Hildebrandt, A., Schmitz, F., and Herrmann, C. S. (2020). Decomposing alpha and 1/f brain activities reveals their differential associations with cognitive processing speed. *NeuroImage* 205:116304. doi: 10.1016/j.neuroimage.2019.116304

Ozturk, M., Abosch, A., Francis, D., Wu, J., Jimenez-Shahed, J., and Ince, N. F. (2020). Distinct subthalamic coupling in the ON state describes motor performance in Parkinson's disease. *Mov. Disord.* 35, 91–100. doi: 10.1002/mds.27800

Pal, G. D., Hall, D., Ouyang, B., Phelps, J., Alcalay, R., Pauciulo, M. W., et al. (2016). Genetic and clinical predictors of deep brain stimulation in young-onset Parkinson's disease. *Mov. Disord. Clin. Pract.* 3, 465–471. doi: 10.1002/mdc3.12309

Postuma, R. B., Berg, D., Stern, M., Poewe, W., Olanow, C. W., Oertel, W., et al. (2015). MDS clinical diagnostic criteria for Parkinson's disease. *Mov. Disord.* 30, 1591–1601. doi: 10.1002/mds.26424

Quinn, N., Critchley, P., and Marsden, C. D. (1987). Young onset Parkinson's disease. *Mov. Disord.* 2, 73–91. doi: 10.1002/mds.870020201

Rosin, B., Slovik, M., Mitelman, R., Rivlin-Etzion, M., Haber, S. N., Israel, Z., et al. (2011). Closed-loop deep brain stimulation is superior in ameliorating parkinsonism. *Neuron* 72, 370–384. doi: 10.1016/j.neuron.2011.08.023

Rughani, A., Schwalb, J. M., Sidiropoulos, C., Pilitsis, J., Ramirez-Zamora, A., Sweet, J. A., et al. (2018). Congress of Neurological Surgeons systematic review and evidence-based guideline on subthalamic nucleus and Globus pallidus internus deep brain stimulation for the treatment of patients with Parkinson's disease: executive summary. *Neurosurgery* 82, 753–756. doi: 10.1093/neuros/nyy037

Sacks, D. D., Schwenn, P. E., McLoughlin, L. T., Lagopoulos, J., and Hermens, D. F. (2021). Phase-amplitude coupling, mental health and cognition: implications for adolescence. *Front. Hum. Neurosci.* 15:622313. doi: 10.3389/fnhum.2021.622313

Schaworonkow, N., and Voytek, B. (2021). Longitudinal changes in aperiodic and periodic activity in electrophysiological recordings in the first seven months of life. *Dev. Cogn. Neurosci.* 47:100895. doi: 10.1016/j.dcn.2020.100895

Schrag, A., Ben-Shlomo, Y., and Quinn, N. P. (2000). Cross sectional prevalence survey of idiopathic Parkinson's disease and parkinsonism in London. *BMJ* 321, 21–22. doi: 10.1136/bmj.321.7252.21

Schrag, A., and Schott, J. M. (2006). Epidemiological, clinical, and genetic characteristics of early-onset parkinsonism. *Lancet Neurol.* 5, 355–363. doi: 10.1016/S1474-4422(06)70411-2

Steiner, L. A., Neumann, W. J., Staub-Bartelt, F., Herz, D. M., Tan, H., Pogosyan, A., et al. (2017). Subthalamic beta dynamics mirror parkinsonian bradykinesia months after neurostimulator implantation. *Mov. Disord.* 32, 1183–1190. doi: 10.1002/mds.27068

Swann, N. C., de Hemptinne, C., Thompson, M. C., Miocinovic, S., Miller, A. M., Gilron, R., et al. (2018). Adaptive deep brain stimulation for Parkinson's disease using motor cortex sensing. *J. Neural Eng.* 15:046006. doi: 10.1088/1741-2552/aabc9b

Tinkhauser, G., Pogosyan, A., Little, S., Beudel, M., Herz, D. M., Tan, H., et al. (2017a). The modulatory effect of adaptive deep brain stimulation on beta bursts in Parkinson's disease. *Brain* 140, 1053–1067. doi: 10.1093/brain/awx010

Tinkhauser, G., Pogosyan, A., Tan, H., Herz, D. M., Kuhn, A. A., and Brown, P. (2017b). Beta burst dynamics in Parkinson's disease OFF and ON dopaminergic medication. *Brain* 140, 2968–2981. doi: 10.1093/brain/awx252

Torrecillos, F., Tinkhauser, G., Fischer, P., Green, A. L., Aziz, T. Z., Foltynie, T., et al. (2018). Modulation of Beta bursts in the subthalamic nucleus predicts motor performance. *J. Neurosci.* 38, 8905–8917. doi: 10.1523/JNEUROSCI.1314-18.2018

Tort, A. B. L., Komorowski, R., Eichenbaum, H., and Kopell, N. (2010). Measuring phase-amplitude coupling between neuronal oscillations of different frequencies. *J. Neurophysiol.* 104, 1195–1210. doi: 10.1152/jn.00106.2010

Tsiokos, C., Malekmohammadi, M., AuYong, N., and Pouratian, N. (2017). Pallidal low β-low γ phase-amplitude coupling inversely correlates with Parkinson disease symptoms. *Clin. Neurophysiol.* 128, 2165–2178. doi: 10.1016/j.clinph.2017.08.001

van Wijk, B. C., Beudel, M., Jha, A., Oswal, A., Foltynie, T., Hariz, M. I., et al. (2016). Subthalamic nucleus phase-amplitude coupling correlates with motor impairment in Parkinson's disease. *Clin. Neurophysiol.* 127, 2010–2019. doi: 10.1016/j.clinph.2016.01.015

Voytek, B., Kramer, M. A., Case, J., Lepage, K. Q., Tempesta, Z. R., Knight, R. T., et al. (2015). Age-related changes in 1/f neural electrophysiological noise. *J. Neurosci.* 35, 13257–13265. doi: 10.1523/JNEUROSCI.2332-14.2015

Weinberger, M., Mahant, N., Hutchison, W. D., Lozano, A. M., Moro, E., Hodaie, M., et al. (2006). Beta oscillatory activity in the subthalamic nucleus and its relation to dopaminergic response in Parkinson's disease. *J. Neurophysiol.* 96, 3248–3256. doi: 10.1152/jn.00697.2006

Winawer, J., Kay, K. N., Foster, B. L., Rauschecker, A. M., Parvizi, J., and Wandell, B. A. (2013). Asynchronous broadband signals are the principal source of the BOLD response in human visual cortex. *Curr. Biol.* 23, 1145–1153. doi: 10.1016/j.cub.2013.05.001

Xie, H. T., Zhang, Q., Jiang, Y., Bai, Y. T., and Zhang, J. G. (2022). Parkinson's disease with mild cognitive impairment may has a lower risk of cognitive decline after subthalamic nucleus deep brain stimulation: a retrospective cohort study. *Front. Hum. Neurosci.* 16:943472. doi: 10.3389/fnhum.2022.943472

Xue, M., Atallah, B. V., and Scanziani, M. (2014). Equalizing excitation-inhibition ratios across visual cortical neurons. *Nature* 511, 596–600. doi: 10.1038/nature13321

Yang, A. I., Vanegas, N., Lungu, C., and Zaghloul, K. A. (2014). Beta-coupled high-frequency activity and beta-locked neuronal spiking in the subthalamic nucleus of Parkinson's disease. *J. Neurosci.* 34, 12816–12827. doi: 10.1523/JNEUROSCI.1895-14.2014

Yin, Z. X., Zhu, G. Y., Liu, Y. Y., Zhao, B. T., Liu, D. F., Bai, Y. T., et al. (2022). Cortical phase-amplitude coupling is key to the occurrence and treatment of freezing of gait. *Brain* 145, 2407–2421. doi: 10.1093/brain/awac121

Zhang, Q., Gheres, K. W., and Drew, P. J. (2021). Origins of 1/f–like tissue oxygenation fluctuations in the murine cortex. *PLoS Biol.* 19:e3001298. doi: 10.1371/journal.pbio.3001298

frontiers | Frontiers in Aging Neuroscience

TYPE Original Research
PUBLISHED 23 February 2023
DOI 10.3389/fnagi.2023.1117802

OPEN ACCESS

EDITED BY
Muthuraman Muthuraman,
Johannes Gutenberg University Mainz,
Germany

REVIEWED BY
Abdulrahman Aloyayri,
University of Birmingham,
United Kingdom
Jianqiao Mao,
University of Birmingham,
United Kingdom

*CORRESPONDENCE
Robert A. McGovern
✉ rmcgover@umn.edu

SPECIALTY SECTION
This article was submitted to Parkinson's Disease and Aging-related Movement Disorders, a section of the journal Frontiers in Aging Neuroscience

RECEIVED 06 December 2022
ACCEPTED 31 January 2023
PUBLISHED 23 February 2023

CITATION
Nouriani A, Jonason A, Sabal LT, Hanson JT, Jean JN, Lisko T, Reid E, Moua Y, Rozeboom S, Neverman K, Stowe C, Rajamani R and McGovern RA (2023) Real world validation of activity recognition algorithm and development of novel behavioral biomarkers of falls in aged control and movement disorder patients. *Front. Aging Neurosci.* 15:1117802. doi: 10.3389/fnagi.2023.1117802

Real world validation of activity recognition algorithm and development of novel behavioral biomarkers of falls in aged control and movement disorder patients

Ali Nouriani[1], Alec Jonason[2], Luke T. Sabal[2], Jacob T. Hanson[3], James N. Jean[2], Thomas Lisko[2], Emma Reid[2], Yeng Moua[2], Shane Rozeboom[2], Kaiser Neverman[2], Casey Stowe[2], Rajesh Rajamani[1] and Robert A. McGovern[2,4]*

[1]Laboratory for Innovations in Sensing, Estimation and Control, Department of Mechanical Engineering, University of Minnesota, Minneapolis, MN, United States, [2]Department of Neurosurgery, University of Minnesota Medical School, Minneapolis, MN, United States, [3]Rocky Vista University College of Osteopathic Medicine, Parker, CO, United States, [4]Division of Neurosurgery, Minneapolis Veterans Affairs Health Care System, Minneapolis, MN, United States

The use of wearable sensors in movement disorder patients such as Parkinson's disease (PD) and normal pressure hydrocephalus (NPH) is becoming more widespread, but most studies are limited to characterizing general aspects of mobility using smartphones. There is a need to accurately identify specific activities at home in order to properly evaluate gait and balance at home, where most falls occur. We developed an activity recognition algorithm to classify multiple daily living activities including high fall risk activities such as sit to stand transfers, turns and near-falls using data from 5 inertial sensors placed on the chest, upper-legs and lower-legs of the subjects. The algorithm is then verified with ground truth by collecting video footage of our patients wearing the sensors at home. Our activity recognition algorithm showed >95% sensitivity in detection of activities. Extracted features from our home monitoring system showed significantly better correlation (~69%) with prospectively measured fall frequency of our subjects compared to the standard clinical tests (~30%) or other quantitative gait metrics used in past studies when attempting to predict future falls over 1year of prospective follow-up. Although detecting near-falls at home is difficult, our proposed model suggests that near-fall frequency is the most predictive criterion in fall detection through correlation analysis and fitting regression models.

KEYWORDS

Parkinson's disease, postural instability, gait, wearable sensors, falls, near-falls

1. Introduction

Postural instability is both a cardinal symptom of movement disorders like Parkinson's disease (PD) and a major cause of falls in these patients (Palakurthi and Burugupally, 2019). Injurious falls and hip fractures occur at higher rates in PD patients, with approximately 75% of international hospitalizations in patients with PD occurring due to fractures or falls (Chou et al., 2011). Therefore, if subtle balance dysfunction could be properly identified and characterized,

this information could be used to initiate falls preventions and physical therapy programs, improve fall prediction algorithms, and monitor or evaluate new treatments.

The Movement Disorder Society-Unified Parkinson's Disease rating scale (MDS-UPDRS) (Goetz et al., 2008) analyzes all motor symptoms using a semi-quantitative scale. Its validity and reliability are well recognized and it is the clinical gold-standard in terms of monitoring symptoms related to PD (Ramaker et al., 2002). However, these assessments are subject to inter-rater variability, and the unavailability of continuous monitoring limits these methods. The score of the evaluation depends on the patient's current status, which may fluctuate day-to-day and depending on the time since the last dose of medication was taken. On the other hand, traditional lab-based assessments using infrared cameras or quantitative analysis to characterize postural instability in patients with movement disorders are costly, not portable, and are unable to track long-term movement data from these patients in their day-to-day lives when most falls occur. Therefore, there is a serious need for long-term, real-time, and objective characterization of movement as a complement to clinical and lab-based assessments (Ramaker et al., 2002).

A few methods of characterizing mobility in patients with movement disorders have been proposed, including home movement diaries (Hauser et al., 2006) and characterizing mobility using smartphone applications (Lorenzi et al., 2016; Zhan et al., 2018). Patient diaries and questionnaires at home are frequently used in clinical routine to study motor stages and fluctuations in late-stage PD (Papapetropoulos, 2012). However, diaries are subject to fatigue, errors, and bias which impacts the quality and credibility of the data, particularly in patients with cognitive dysfunction (Papapetropoulos, 2012). Some methods of tracking participants at home may involve using mobile phone-based systems that gather data using inertial sensors that are built into smartphones (Motolese et al., 2020). This yields data that allows for general tracking of activities such as walking, sitting and sleeping, but does not provide quantitative insights into participants' postural responses when experiencing a fall or near-fall. Additionally, relying on data from a device that is not fixed to the patient's body may introduce error or leave long gaps in data. More elaborate systems using multiple cameras throughout a person's home in order to track their movements may also be used, but this may not be feasible on a wide scale due to its cost, complexity, and privacy concerns (Rougier et al., 2011). In past studies, IMUs have shown to be both accurate and repeatable for measuring gait parameters in healthy young adults (Washabaugh et al., 2017). Additionally, publicly available datasets collected from patients with movement disorders using IMUs have been utilized to analyze gait parameters and freezing of gait episodes (O'Day et al., 2022).

To address some of the problems with characterizing mobility in patients with movement disorders, we have developed an algorithm that can both accurately measure gait parameters and enable real-time detection of high-risk activities in the patient's home environment using inexpensive and widely available wearable technology. The merging of cost-effective technology with deep learning techniques yields significant promise in the field of wearable sensor technology (Ramanujam et al., 2021). The goal of this study was to create a video-validated dataset of movement disorder patients and healthy controls engaged in daily living activities in their homes, develop an algorithm for automatic recognition of near-falls/high fall risk activities and subsequently quantitatively characterize the patient's response to these events in order to predict future fall risk. Our collected dataset includes 29 participants in total, comprised of 11 participants with Parkinson's disease (PD), eight participants with Normal Pressure Hydrocephalus (NPH) and 10 Healthy Controls (C). Finally, we developed novel behavioral biomarkers based on this data to assess their relationship to patients' prospective fall risk over 1 year of follow-up.

2. Methods

2.1. Participant population characteristics

Nineteen movement disorder patients who were being clinically evaluated and/or treated for either normal pressure hydrocephalus or Parkinson's disease and 10 age-matched healthy control participants were enrolled over a period of 2 years from the Minneapolis VA Health Care System (MVAHCS) and University of Minnesota (UMN). Enrollment was designed to enroll a variety of types of movement disorder patients with varying gait dysfunction and postural instability ranging from normal gait and balance (MDS-UPDRS gait and pull test item scores of 0) to moderate dysfunction (MDS-UPDRS scores of 3). Patient participants were excluded if they were non-ambulatory or if they were unable to give consent. Control participants were excluded if they had any movement, gait, or balance disorders. Demographic information was collected (Table 1). This study was approved by the MVAHCS and UMN Institutional Review Boards, and all participants provided informed consent for participation according to the Declaration of Helsinki.

2.2. Measurement setup

The measurement sensors were customized and reprogrammed inertial measurement units (IMU; SparkFun, Inc. Boulder, CO, United States). The board was equipped with a high-performance ARM Cortex-M4 processor powered by 500 mAh high-capacity Lithium battery (InvenSense. ICM-20948 - SparkFun Electronics, 2017). The

TABLE 1 Demography of participants.

Condition*	Age (year)	Female	Height (cm)	Weight (kg)	UPDRS pull test	UPDRS gait	Duration of disease (year)
	Mean (SD)	*N*, %	Mean (SD)	Mean (SD)	Mean (SD)	Mean (SD)	Mean (SD)
PD ($n = 11$)	65 (4.76)	2, 20%	181.54 (8.97)	92.94 (23.63)	0.56 (0.96)	0.90 (0.74)	10.50 (5.41)
NPH ($n = 8$)	69.8 (8.21)	1, 11%	180.72 (3.50)	102.57 (20.71)	1.04 (0.56)	1.85 (0.89)	N/A
C ($n = 10$)	61.1 (9.97)	8, 80%	172.20 (6.83)	79.75 (27.69)	0 (0)	0 (0)	N/A

*PD, Parkinson's disease; NPH, normal pressure hydrocephalus; C, control.

measurement Integrated circuit (IC) was an ICM-20948 (InvenSense, San Jose, CA, United States) which can log nine degrees of freedom (accelerometer, gyroscope, magnetometer) at nearly 250 Hz (ICM-20948 Datasheet|TDK, 2021). The data from the IMU was sampled with a 100 Hz frequency and stored on a flash memory though it can be streamed wirelessly through Bluetooth connectivity to a smartphone or computer (Figure 1).

The sensor configuration is one IMU sensor on each shank (just above the ankle), one IMU on each thigh, and one IMU sensor on the chest. This five sensor configuration uses an angle-based method taking advantage of the geometry of human in-plane walking. Each IMU sensor measures the acceleration and angular rate of movement of different body segments. An LMI-based non-linear sensor fusion algorithm is designed to estimate the limb segment orientations by taking advantage of the acceleration for lower frequencies and gyro in higher frequencies. The details of our estimation algorithm and the accuracy of a variety of kinematic variables which can be calculated using this configuration compared to a gold standard infrared camera measurements has been previously described (Nouriani et al., 2021).

2.3. Home wearable sensor usage

Each participant was shown how to properly place the IMUs (Figure 1) in the clinic at their baseline visit. They were then sent home for 1 week and were instructed to wear the IMUs during all waking hours. The IMUs were charged overnight. The entirety of the dataset was able to be stored on the available flash memory on the sensor board and therefore participants did not need to upload data or stream any data to an app. They simply wore the sensors during the day and charged them at night. Each patient is provided with a custom charger connected to a Raspberry Pi Zero board (Raspberry Pi Foundation, Cambridge, England) which is programmed to synchronize the sensors together using threading with an extremely accurate real-time clock module (DS3231 RTC, Adafruit, New York, NY, United States) every time the sensors are connected to the charger (Extremely Accurate I2C-Integrated DS3231 RTC Datasheet, 2015). During the week of wearable sensor use, a research coordinator contacted the participants daily to troubleshoot any technical problems and check in. Participants were then prospectively followed for 1 year and asked to complete fall diaries according to accepted fall data formatting. To supplement the fall diaries, a research coordinator called the participants weekly for the follow-up year to inquire about any falls occurring during the past week.

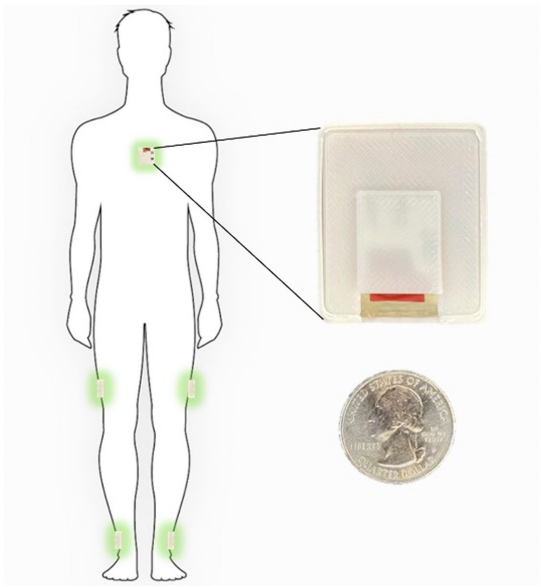

FIGURE 1
Inertial sensors placement on the body in 5-sensor configuration, one on the chest and one on each lower leg and on each upper leg.

2.4. Home wearable sensor activity definitions and video validation

In order to properly identify home activities, we first defined a variety of activities using the IMU data (Supplementary Table S1). The algorithm used to identify each home activity is a deep learning-based activity recognition architecture using a convolutional neural network with long short term memory cells (CNN-LSTM). The CNN-LSTM network implements a nonlinear observer for the estimation of the tilt angles of the human body limb segments as the input of the CNN layers followed by LSTM layers and finally fully connected layers with Softmax activation which we have detailed previously (Nouriani et al., 2022). We also used three other commonly used classifiers (logistic regression, support vector machine, decision tree) to compare their performance to our CNN-LSTM. The details of these algorithms can be found in the Supplementary methods. In order to validate the algorithm-defined activities, we asked a subset of participants ($n = 10$) to wear a small video camera (Runcam, Aberdeen, Hong Kong Island, Hong Kong; Runcam 5 Datasheet, 2020) with a necklace to wear at home. Each patient was asked to record for 45–60 min each day, ideally while ambulating or performing some type of algorithm-detectable activity. The videos were then manually annotated using a video-defined equivalent of each IMU-defined home activity (Supplementary Table S1) and synchronized with the sensors using the camera timestamps. Examples of the video footage captured by the patients are provided in Supplementary materials.

2.5. Fall prediction modeling

We prospectively followed all patient participants for 1 year with fall diaries and weekly individual participant contact to document the presence of any falls and the total number of falls over the entire year. From this data, we calculated the fall frequency as #falls/week. Using fall frequency as our outcome, we then examined the correlation between multiple computed features and fall frequency. These features ranged from standard demographic characteristics such as age, height, and weight, to clinical measurements such as the MDS-UPDRS pull test score, and also included a number of quantitative features from home measurements (denoted with an "_h") that have been used in prior studies such as the total ambulatory time each day and number of ambulatory bouts each day (Supplementary Table S2). We also computed several novel features based on our previously video-validated activities described above. These include the frequency of near falls, turns and bends among others (events defined in

Supplementary Table S1, all features used for correlation analysis are seen in Supplementary Table S2). We then created correlation confusion matrices to examine correlation of the previously mentioned data features with fall frequency. Using the fall diary data above, we also examined the time to first fall within the first year.

From the 29 participants, we have collected fall diaries and have survival data for 17 subjects. We did not collect the fall diaries from the control subjects and hence excluded them for the fall prediction model. From the remaining subjects, nine are censored since they are either new patients, or their home data is missing, or stopped sending their fall diaries to us before week 52.

3. Results

3.1. Population characteristics

Eight patients with NPH and 11 with PD were enrolled for a total of 19 patient participants. Ten healthy, age-matched control participants were also enrolled. Demographic characteristics are demonstrated in Table 1. There were no significant differences in age, sex, height or weight between controls and patient participants. As expected, patient participants had significantly worse gait and postural stability MDS-UPDRS scores as compared to healthy, age-matched control participants.

3.2. Activity recognition algorithm validation

Ten of our patients generated more than 40 h of video footage which was manually annotated (see Supplementary Table S1 for definitions). Figure 2 demonstrates an example of 1 day of recorded data using our sensors compared to the video footage obtained from a patient at home. This patient generated approximately 90 min of video footage during which he was ambulatory for approximately 45 min punctuated in the middle by 45 min where he was sitting at rest. The algorithm-predicted activity (blue) overlies the actual video-annotated activity (orange) for the vast majority of the time, with an example of one misclassified activity (~8:58 am, standing misclassified as walking, seen in the Figure 2 inset).

The sum total of video footage in the entire subset of patients resulted in more than 14,000 total events which were used for algorithm predictions. Figure 3 demonstrates the home activities predicted by our activity recognition algorithm in comparison to the video-annotated data collected on the subset of patients with video recorded events. Events which were common and straightforward to both define and detect such as walking, standing and turning demonstrated the highest accuracy (>99%). Because these three events were the most common overall, they also represented most of the false positive and false negative errors for all events. Bending, sitting and transitions from sit to stand or stand to sit were significantly less common and slightly less accurately predicted (91–94%). Near falls in any direction were among the least common events and were less accurately predicted (~80%).

Table 2 shows the number of true positive (TP), false positive (FP), true negative (TN), and false negative (FN) samples from our activity recognition algorithm compared to the ground truth from video annotations. We can use these values to calculate the sensitivity (true positive rate or TPR), specificity (true negative rate or TNR), positive predictive value (PPV), negative predictive value (NPV), and accuracy (ACC). Because the number of total events is quite high, the specificity and overall accuracy of all the events are high, particularly for the low likelihood events such as sit to stand transitions, near-falls and falls. Nonetheless, even the low likelihood events had sensitivities >95% with the exception of near-falls which was 80%.

To compare our LSTM algorithm to other standard classifiers commonly used to make predictions on large datasets, we have created receiver operating characteristic (ROC) curves for 6 activities of standing, walking, sit-stand transitions, turning, bending and near-falls. Figure 4 shows the ROC curves for four binary classifiers of Logistic Regression (LOG), Support Vector Machines (SVM), Decision Tree (DT), and our Long-Short-Term-Memory cells (LSTM) for each activity (Nouriani et al., 2022). The area under the curve for each plot is summarized in Table 3. The performance of the LSTM classifier is superior in all activities with AUCs ranging from 0.982 to 0.999 for all activities while DT performs next best with slightly worse results. The SVM and LOG methods are significantly less accurate

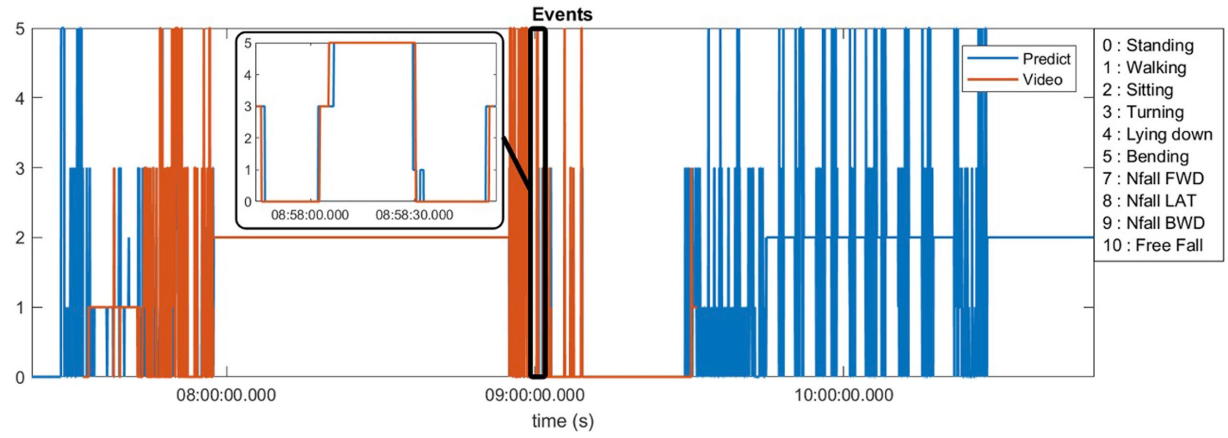

FIGURE 2
Predicted activities compared to the video annotations obtained from a patient at home environment.

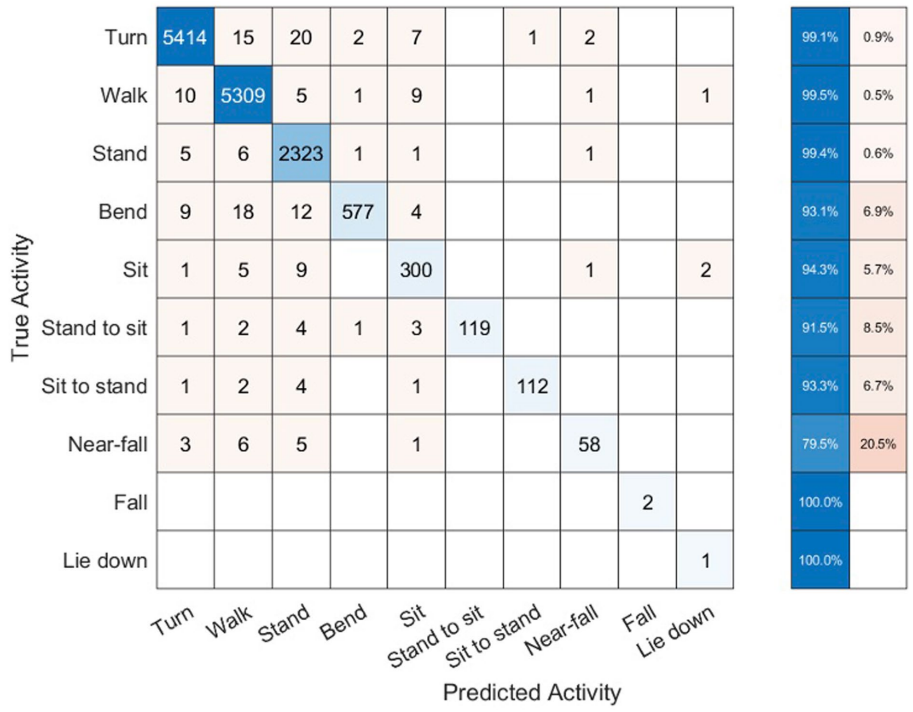

FIGURE 3
Confusion matrix of activity recognition algorithm result compared to the annotated videos for six subjects.

TABLE 2 Statistics of each activity in our activity recognition algorithm.

Activity	TP	FP	TN	FN	TPR	TNR	PPV	NPV	ACC
Stand	2,323	54	11,998	14	0.994009	0.995519	0.977282	0.998834	0.995274
Walk	5,309	47	9,006	27	0.99494	0.994808	0.991225	0.997011	0.994857
Stand to sit	119	0	14,259	11	0.915385	1	1	0.999229	0.999236
Sit	300	26	14,045	18	0.943396	0.998152	0.920245	0.99872	0.996942
Sit to stand	112	1	14,268	8	0.933333	0.99993	0.99115	0.99944	0.999375
Turn	5,414	30	8,898	47	0.991394	0.99664	0.994489	0.994746	0.994649
Lie down	1	3	14,385	0	1	0.999791	0.25	1	0.999792
Bend	577	5	13,779	28	0.953719	0.999637	0.991409	0.997972	0.997707
Near-fall	58	5	14,311	15	0.794521	0.999651	0.920635	0.998953	0.99861
Fall	2	0	14,387	0	1	1	1	1	1

than LSTM or DT but still show acceptable results for a diagnostic classifier with AUCs ranging from 0.65 to 0.97. All classifiers worked well for relatively easily classified activities such as standing, walking or bending, but more difficult activities to classify such as near falls required the more sophisticated CNN-LSTM algorithm. There were no differences in activity classification between groups such that the CNN-LSTM algorithm was able to accurately classify activities in controls, NPH and PD patients equally well (Supplementary Figure S2). The overall performance (in terms of area under the curve) of each classifier is very similar across different patient groups.

Figure 5 demonstrates a correlation matrix examining the top 10 features correlated with prospectively observed fall frequency over the subsequent year of follow-up. Two of our novel metrics: the total number and frequency of near falls detected by the home monitoring setup showed the highest correlation with patient fall frequency (0.69 and 0.67, respectively). Supplementary Figure S1 shows the median of number of near-falls per week (Nfalls_h) for the three groups of our subjects. As expected, control subjects had significantly lower number of near-falls than our PD and NPH patients. PD patients showed a slightly higher median compared to NPH patients.

Eight of the most correlated features with fall frequency come from values calculated solely using the IMUs while the patient moves around their home and surrounding environment. For example, time spent lying down per day (lie down frequency, i.e., lying duration/total time), the total number of ambulatory bouts at home (totNumABs), the frequency of sitting at home (sit_freq_h, i.e., sitting duration/total time), walking frequency at home (walk_freq_h), the peak acceleration of the chest at home (peak_acc_h,

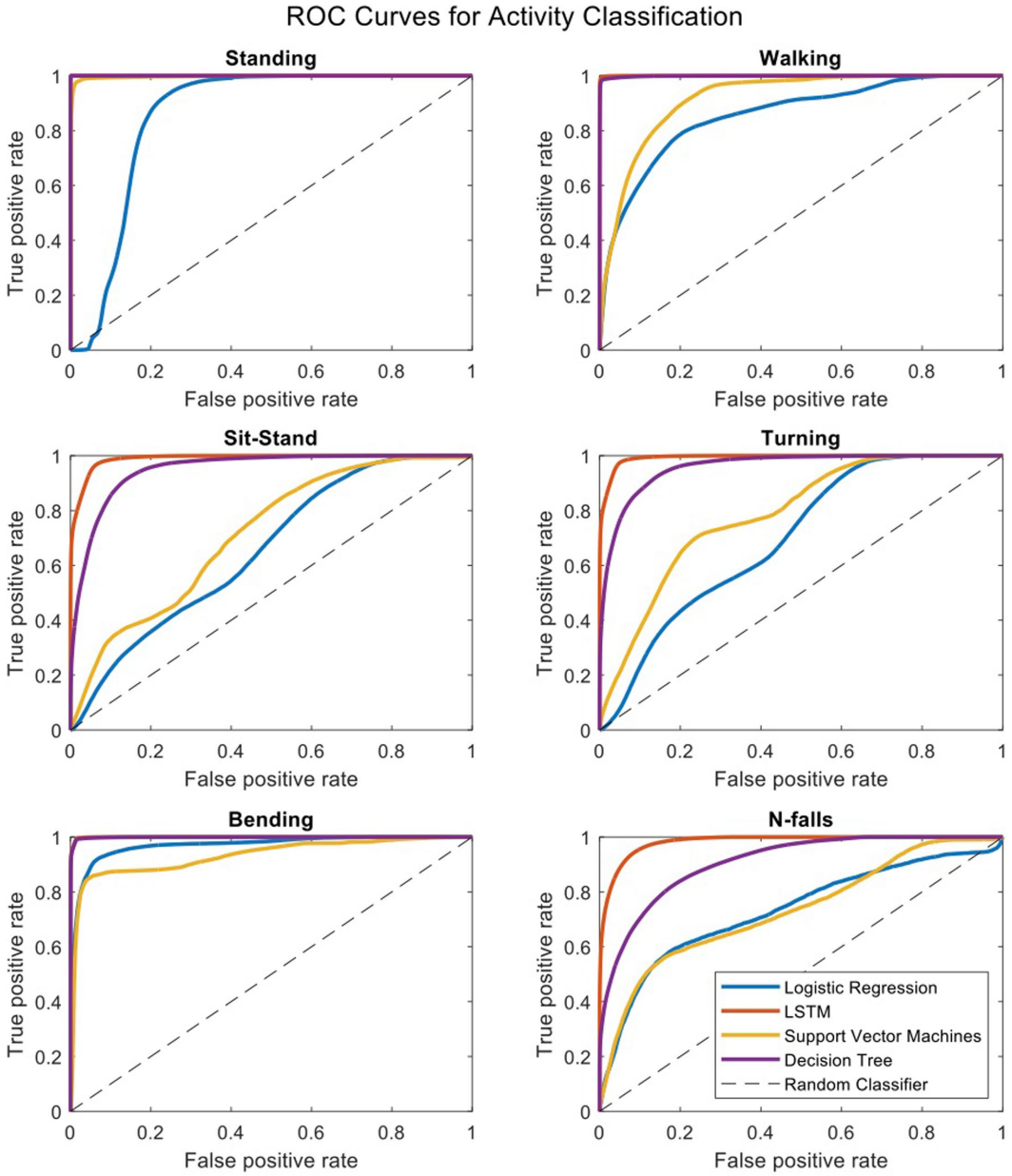

FIGURE 4
Receiver operating characteristic curves for four binary classifiers plotted separately for each activity.

TABLE 3 Area under the ROC curves for each activity.

Classifier	Standing	Walking	Sit-stands	Turning	Bending	Near-falls
LOG	0.85759	0.85745	0.65548	0.69863	0.96702	0.73180
SVM	0.99691	0.91850	0.71383	0.78733	0.95410	0.73401
DT	0.99999	0.99881	0.95043	0.95940	0.98589	0.90834
LSTM	0.99999	0.99985	0.98920	0.99288	0.99774	0.98253

which represents the strongest perturbation the subject experiences at home as measured by the chest accelerometer in each day) and the distribution of ambulatory bouts in time [alpha parameter for ABs of more than 8 s (alpha_8) (Nouriani et al., 2022)] at home are all within the 10 features with the highest correlation with fall frequency. It should be noted that some features were inversely correlated with fall frequency such that increased number of ambulatory bouts and increased walking frequency at home were associated with fewer falls (−0.40 and −0.36, respectively). Furthermore, Figure 5 also shows how correlated some of these features are with each other. For example, the total number of ABs are highly correlated with walking frequency (0.81), and the total number and frequency of near falls are

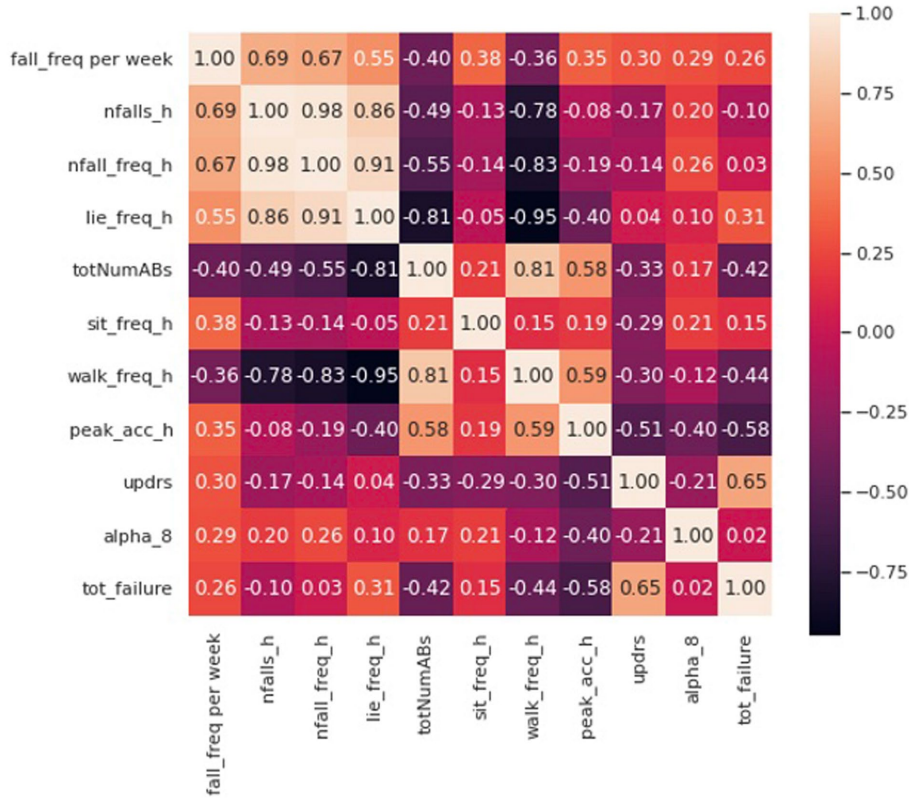

FIGURE 5
Correlation matrix including the first 10 features with the most correlation with the fall frequency of patients at home.

almost perfectly correlated (0.98). We constructed a linear regression model on 5 features which are not highly correlated with each other. The details of the regression model are presented in Tables 4, 5. The model shows that near-fall frequency (nfall_freq), alpha parameter for ABs of more than 8 s (alpha_8) and UPDRS score (updrs) were the most significant predictors, respectively. The regression model parameters are summarized in Table 5. The only non-quantitative features included in the 10 most correlated features were the MDS-UPDRS pull test item score measured in clinic, and the total number of failures (needing to be caught by examiner) in clinical pull tests (tot_failures). These were among the most weakly correlated features (0.30 and 0.26, respectively) overall and were not significantly associated with fall frequency in the multivariable linear regression model.

TABLE 4 Linear regression coefficients for fall frequency prediction.

Feature	Estimate	Standard error	*t*-stat	*p*-value
Intercept	0.047251	0.020211	2.337934	0.041485
Nfall_Freq_h	0.696391	0.188534	3.69372	0.004151
Tot_Num_Abs	6.82E-08	1.62E-06	0.042112	0.967239
Sit_Freq_h	−0.00035	0.000178	−1.99592	0.073889
UPDRS	−0.01573	0.006449	−2.43948	0.03488
Alpha_8	−0.00391	0.001185	−3.30116	0.007998

TABLE 5 Linear regression model summary for fall frequency prediction.

Feature	SumSq	MeanSq	*F*	*p*-value
Total	0.014705	0.0009803		
Model	0.012228	0.0024457	9.8737	0.001268
Residual	0.002477	0.0002477		

4. Discussion

Using a combination of domain specific knowledge and machine learning techniques, we developed an automatic algorithm for detection and characterization of near-falls and high fall risk activities of the patients. We created a validated, video annotated and quantitative dataset of movement disorder subjects wearing inertial sensors at their home environment. The statistical analysis of our algorithm shows >95% sensitivity in detection of activities apart from near-falls, which showed 80% sensitivity. The correlation analysis of the computed features in our dataset showed that our novel metrics based on near-falls are superior in terms of the highest correlation with patient fall frequency over an entire year of follow-up while clinic-based features were either not correlated or were among the most weakly correlated features.

4.1. Video validation of CNN-LSTM algorithm in the home setting

Using video to validate algorithm predictions based on IMU data is a necessary component to reliably interpret any wearable dataset,

but is frequently lacking in studies employing wearable sensors (Del Din et al., 2019). Studies that do employ some measure of validation typically do so in the clinic or laboratory setting, rather than "in the wild" as we have done in this study (Nouredanesh et al., 2021). There are essentially no studies that have attempted to capture and validate near falls or "stumbles" in the wild. Nor are there any widely accepted definitions or datasets that contain or even attempt to define these events. For example, one study asked participants in a survey whether they had near falls which they defined as "a fall initiated but arrested by support from the wall, railing or another person." This study used purely clinical data to predict falls and near falls. No quantitative data was included (Lindholm et al., 2015). Another study artificially induced "missteps" in the laboratory and then developed an algorithm to detect such "missteps" during 3 days of home wearable use. There were no video recordings to validate these missteps and as such, they acknowledge there is no way to know if any of their detected missteps was in fact a misstep. Additionally, anything that did not look like a misstep in the lab would, by definition, be missing from their dataset (Iluz et al., 2014).

As such, our video-validated home data represents an ecologically valid quantitative dataset that can then be leveraged to understand the factors relevant in producing falls with far more detail compared to the current standard solution which involves qualitative clinical examination or laboratory-based task assessments that may or not be related to real world balance perturbations. Since most falls occur at home and surrounding environment, a wearable dataset that is "validated" in the clinic or lab may not be ecologically valid for fall prediction or other uses. On the other hand, some activities such as walking, standing and bending may be able to be easily validated in the clinic setting and so datasets validated with video "in the wild" should be compared to datasets using clinic-based assessments in order to better understand what can accurately assessed in the clinic vs. which assessments need to occur at home.

Our activity recognition algorithm uses a nonlinear switched-gain observer based on measurements from IMUs worn on leg segments and the chest in order to estimate body segment orientation. The observer estimates the tilt angles and measurement bias is estimated and removed. This has been measured in prior studies using infrared-based motion capture systems to ensure its accuracy (Nouriani et al., 2021). These estimates are then used to train the LSTM deep learning algorithm on all of the activities. Since many of the activity definitions are based on the tilt angles (Supplementary Table S1), this may be one reason that our LSTM activity recognition method showed superior accuracy. In addition, our deep learning network demonstrated lower computation cost compared to the other methods as it reduces the number of raw IMU signals necessary for activity recognition. Future studies should investigate how to reduce both the number of worn IMUs and number of recorded events without affecting diagnostic accuracy in order to minimize the burden on patients wearing the IMUs.

4.2. Development of novel behavioral biomarkers of falls

We have developed prospective, predictive falls risk metrics that integrate the patient's postural response along with data that reflects the patient's home environment based on near-falls detection. We have included all known gait parameters used in prior studies and current clinical standards in the study, however our proposed metrics showed superior performance in predicting falls in these patients. While there are simple measures which may be more easily measured with a smartphone or smartwatch (e.g., frequency of lying down, number of ambulatory bouts), our study suggests these are inferior to the number or frequency of near-falls. Similarly, clinical tests are typically inadequate in describing the likelihood of the subject falling and in characterizing the extent of their postural instability (Ramaker et al., 2002). Inter-and intra-rater variability in the execution and interpretation of clinical testing likely is responsible for some of their poor predictive power. Furthermore, incidents that trigger stumbles and falls at home are almost certainly different from testing conducted by clinicians or researchers in an artificial environment. Unfortunately, there are few studies on postural instability in home environments and these studies typically do not provide enough validation for their results in real-life situations at home or at least the demonstration of generalizability to the home environment (Silva de Lima et al., 2020). While there may be overlap in the postural response to balance testing in the clinic or lab and that at home, datasets such as the one described in our study should be used to investigate similarities and differences between these two settings in the future. This could lead to better fall prediction algorithms and improved diagnostic monitoring and treatment evaluations in the clinic, lab and at home in the future.

Despite being the most relevant feature of the dataset for fall prediction, near-falls were the most difficult activity to accurately detect with a sensitivity of 80%. This was for several reasons. First, near-falls look similar to other activities (like sit-stand transitions and bending) when examining inertial sensor data. Second, some of the near-falls were so subtle that they could not even be detected in videos. Finally, the natural occurrence of near-falls is relatively rare and obtaining video-validated samples is difficult since most of the patients who are at risk of falling are usually less active or use a walking aid to avoid falling. As such, they were also among the least common events and our algorithm, like all machine learning algorithms, performs better with more samples. Continued data collection with more validated events will likely help increase the accuracy of the algorithm over time.

4.3. Future dataset usage

We have collected our dataset using an inexpensive wearable system based on inertial sensors to provide kinematic data of PD and NPH patients at home. Typical uses of IMUs worn by movement disorder patients at home are detailed gait analysis and metrics on mobility/ambulation which can be used for a wide variety of purposes such as disease stage assessment, fall prediction, and treatment evaluation, among others (Lee et al., 2014; Mohammadian Rad et al., 2018; Pang et al., 2019; Pardoel et al., 2019). An advantage of our system is that it contains data from sensors on the chest and both feet that can be used to give detailed information on the postural response to near falls that occur in a natural setting in addition to all of those typical uses described above. Given the contribution of postural instability to falls in these patients, characterizing postural instability at home could potentially be very useful in their monitoring and treatment evaluation, particularly as their disease progresses and their likelihood of falling increases. Most studies of postural instability are

still based on questionnaires or short-term simulations of near-falls in a clinical or lab setup (Ramaker et al., 2002). In addition, while wearable studies are becoming more common, clinical fall risk assessment is usually performed using diaries and questionnaires or one-time evaluations of gait and balance factors of the patients in a clinical trial (Ramaker et al., 2002; Hauser et al., 2006; Papapetropoulos, 2012). These methods are questionable in their quality and credibility due to their short-term and subjective assessment of the patients' response (Ramaker et al., 2002). Thus, there is a crucial need for a long-term, easily obtained, and objective characterization of gait and postural instability in the home setting as a complement to clinical assessments. We would argue that a dataset such as the one described in this manuscript would represent the first step toward that goal.

One limitation of this dataset is its practicality as the current setup with five sensors might not be practical for everyday patient use. Future research should develop algorithms to use as few sensors as possible in optimal locations on the body. Because we were interested mainly in postural instability and falls, we did not include IMUs on the upper limbs and so our dataset does not include hand or arm movements. Given the frequent presence of upper extremity tremor in PD, this is particularly relevant for these patients in their diagnosis, monitoring and treatment evaluation. In addition, many activities of daily living can likely be classified with an upper extremity IMU. Further research should plan to integrate IMU/smartwatch-based data to obtain the widest variety of activities with the best diagnostic accuracy. Wearable usage should also be tailored to the specific usage desired by the clinician and patient. Finally, we plan to further develop activity recognition algorithms using unsupervised and semi-supervised learning methods to increase their accuracy or discover new activities which might have been missed by the current methods.

Even though near-fall detection is difficult to recognize and our algorithm shows 80% sensitivity, near-fall frequency at home was still the most predictive criterion in the linear regression model compared to any other metric. Our results showed that the detection of near-falls is a far more powerful way to examine home monitoring data compared to current methods and should be incorporated into fall prediction algorithms. This validated dataset of movement disorder patients engaged in daily living activities in their homes can serve as a valuable resource for researchers to provide a ground truth for IMU algorithm comparison that include the natural responses of patients at home.

Data availability statement

The raw data supporting the conclusions of this article will be made available by the authors, without undue reservation upon request.

Ethics statement

The studies involving human participants were reviewed and approved by University of Minnesota IRB. The patients/participants provided their written informed consent to participate in this study.

Author contributions

RM conceived the original idea. AN developed the algorithms, designed the sensors and measurement setup with the help and supervision of RR. AN, AJ, JH, LS, JJ, TL, ER, YM, SR, KN, and CS helped with the data collection and annotations. AN analyzed and interpreted the results with the help and supervision of RM. AN and RM wrote the manuscript with the help of AJ and LS. RM and RR supervised the project. All authors contributed to the article and approved the submitted version.

Funding

This work was funded in part by a grant from the University of Minnesota MnDRIVE Neuromodulation Program and Institute for Engineering in Medicine (IEM) doctoral fellowship.

Conflict of interest

The authors declare that the research was conducted in the absence of any commercial or financial relationships that could be construed as a potential conflict of interest.

Publisher's note

Supplementary material

The Supplementary material for this article can be found online at: https://www.frontiersin.org/articles/10.3389/fnagi.2023.1117802/full#supplementary-material

References

Chou, K. L., Zamudio, J., Schmidt, P., Price, C. C., Parashos, S. A., Bloem, B. R., et al. (2011). Hospitalization in Parkinson disease: a survey of national Parkinson foundation centers. *Parkinsonism Relat. Disord.* 17, 440–445. doi: 10.1016/j.parkreldis.2011.03.002

Del Din, S., Galna, B., Godfrey, A., Bekkers, E. M., Pelosin, E., Nieuwhof, F., et al. (2019). Analysis of free-living gait in older adults with and without Parkinson's disease and with and without a history of falls: identifying generic and disease-specific characteristics. *J. Gerontol. Series A* 74, 500–506. doi: 10.1093/gerona/glx254

Extremely Accurate I2C-Integrated DS3231 RTC Datasheet (2015). Extremely Accurate I2C-Integrated DS3231 RTC Datasheet. Available at: https://datasheets.maximintegrated.com/en/ds/DS3231.pdf ().

Goetz, C. G., Tilley, B. C., Shaftman, S. R., Stebbins, G. T., Fahn, S., Martinez-Martin, P., et al. (2008). Movement Disorder Society-sponsored revision of the unified Parkinson's disease rating scale (MDS-UPDRS): scale presentation and clinimetric testing results. *Movement Disord.* 23, 2129–2170. doi: 10.1002/mds.22340

Hauser, R. A., Russ, H., Haeger, D. A., Bruguiere-Fontenille, M., Müller, T., and Wenning, G. K. (2006). Patient evaluation of a home diary to assess duration and severity of dyskinesia in Parkinson disease. *Clin. Neuropharmacol.* 29, 322–330. doi: 10.1097/01.WNF.0000229546.81245.7F

ICM-20948 Datasheet|TDK (2021). ICM-20948 Datasheet|TDK. Available at: https://invensense.tdk.com/download-pdf/icm-20948-datasheet/ (Accessed December 19, 2021).

Iluz, T., Gazit, E., Herman, T., Sprecher, E., Brozgol, M., Giladi, N., et al. (2014). Automated detection of missteps during community ambulation in patients with Parkinson's disease: a new approach for quantifying fall risk in the community setting. *J. Neuroeng. Rehabil.* 11, 1–9. doi: 10.1186/1743-0003-11-48

InvenSense. ICM-20948 - SparkFun Electronics. (2017) Available at: https://cdn.sparkfun.com/assets/7/f/e/c/d/DS-000189-ICM-20948-v1.3.pdf (Accessed December 19, 2021).

Lee, J. K., Robinovitch, S. N., and Park, E. J. (2014). Inertial sensing-based pre-impact detection of falls involving near-fall scenarios. *IEEE Trans. Neural Syst. Rehabil. Eng.* 23, 258–266. doi: 10.1109/TNSRE.2014.2357806

Lindholm, B., Hagell, P., Hansson, O., and Nilsson, M. H. (2015). Prediction of falls and/or near falls in people with mild Parkinson's disease. *PLoS One* 10:e0117018. doi: 10.1371/journal.pone.0117018

Lorenzi, P., Rao, R., Romano, G., Kita, A., and Irrera, F. (2016). Mobile devices for the real-time detection of specific human motion disorders. *IEEE Sensors J.* 16, 1–7. doi: 10.1109/JSEN.2016.2530944

Mohammadian Rad, N., Van Laarhoven, T., Furlanello, C., and Marchiori, E. (2018). Novelty detection using deep normative modeling for IMU-based abnormal movement monitoring in Parkinson's disease and autism spectrum disorders. *Sensors* 18:3533. doi: 10.3390/s18103533

Motolese, F., Magliozzi, A., Puttini, F., Rossi, M., Capone, F., Karlinski, K., et al. (2020). Parkinson's disease remote patient monitoring during the COVID-19 lockdown. *Front. Neurol.* 11:567413. doi: 10.3389/fneur.2020.567413

Nouredanesh, M., Godfrey, A., Howcroft, J., Lemaire, E. D., and Tung, J. (2021). Fall risk assessment in the wild: a critical examination of wearable sensor use in free-living conditions. *Gait Posture* 85, 178–190. doi: 10.1016/j.gaitpost.2020.04.010

Nouriani, A., McGovern, R. A., and Rajamani, R. (2021). Step length estimation with wearable sensors using a switched-gain nonlinear observer. *Biomed. Signal Process. Control* 69:102822. doi: 10.1016/j.bspc.2021.102822

Nouriani, A., McGovern, R. A., and Rajamani, R. (2022). Deep-learning-based human activity recognition using wearable sensors. *IFAC-PapersOnLine* 55, 1–6. doi: 10.1016/j.ifacol.2022.11.152

O'Day, J., Lee, M., Seagers, K., Hoffman, S., Jih-Schiff, A., Kidziński, Ł., et al. (2022). Assessing inertial measurement unit locations for freezing of gait detection and patient preference. *J. Neuroeng. Rehabil.* 19:20. doi: 10.1186/s12984-022-00992-x

Palakurthi, B., and Burugupally, S. P. (2019). Postural instability in Parkinson's disease: a review. *Brain Sci.* 9:239. Published 2019 Sep 18. doi: 10.3390/brainsci9090239

Pang, I., Okubo, Y., Sturnieks, D., Lord, S. R., and Brodie, M. A. (2019). Detection of near falls using wearable devices: a systematic review. *J. Geriatr. Phys. Ther.* 42, 48–56. doi: 10.1519/JPT.0000000000000181

Papapetropoulos, S. (2012). Patient diaries as a clinical endpoint in Parkinson's disease clinical trials. *CNS Neurosci. Ther.* 18, 380–387. doi: 10.1111/J.1755-5949.2011.00253.X

Pardoel, S., Kofman, J., Nantel, J., and Lemaire, E. D. (2019). Wearable-sensor-based detection and prediction of freezing of gait in Parkinson's disease: a review. *Sensors* 19:5141. doi: 10.3390/s19235141

Ramaker, C., Marinus, J., Stiggelbout, A. M., and Van Hilten, B. J. (2002). Systematic evaluation of rating scales for impairment and disability in Parkinson's disease. *Mov. Disord.* 17, 867–876. doi: 10.1002/mds.10248

Ramanujam, E., Perumal, T., and Padmavathi, S. (2021). Human activity recognition with smartphone and wearable sensors using deep learning techniques: a review. *IEEE Sensors J.* 21, 13029–13040. doi: 10.1109/JSEN.2021.3069927

Rougier, C., Meunier, J., St-Arnaud, A., and Rousseau, J. (2011). Robust video surveillance for fall detection based on human shape deformation. *IEEE Trans. Circuits Syst. Video Technol.* 21, 611–622. doi: 10.1109/TCSVT.2011.2129370

Runcam 5 Datasheet (2020). Runcam 5 Datasheet. Available at: https://www.runcam.com/download/runcam5/RunCam5-Manual-EN.pdf (Accessed December 19, 2021).

Silva de Lima, A. L., Smits, T., Darweesh, S. K., Valenti, G., Milosevic, M., Pijl, M., et al. (2020). Home-based monitoring of falls using wearable sensors in Parkinson's disease. *Mov. Disord.* 35, 109–115. doi: 10.1002/mds.27830

Washabaugh, E. P., Kalyanaraman, T., Adamczyk, P. G., Claflin, E. S., and Krishnan, C. (2017). Validity and repeatability of inertial measurement units for measuring gait parameters. *Gait Posture* 55, 87–93. doi: 10.1016/j.gaitpost.2017.04.013

Zhan, A., Mohan, S., Tarolli, C., Schneider, R. B., Adams, J. L., Sharma, S., et al. (2018). Using smartphones and machine learning to quantify Parkinson disease severity: the mobile Parkinson disease score. *JAMA Neurol.* 75, 876–880. doi: 10.1001/jamaneurol.2018.0809

frontiers | Frontiers in Aging Neuroscience

TYPE Original Research
PUBLISHED 14 March 2023
DOI 10.3389/fnagi.2023.1120615

OPEN ACCESS

EDITED BY
Huaibin Cai,
National Institute on Aging (NIH),
United States

REVIEWED BY
Zhonghua Hu,
Central South University,
China
Ling Long,
Third Affiliated Hospital of Sun Yat-sen University,
China
Johann Faouzi,
National School of Statistics and Information Analysis,
France

*CORRESPONDENCE
Jifeng Guo
guojifeng2003@163.com

†These authors have contributed equally to this work

SPECIALTY SECTION
This article was submitted to Parkinson's Disease and Aging-related Movement Disorders, a section of the journal Frontiers in Aging Neuroscience

RECEIVED 10 December 2022
ACCEPTED 21 February 2023
PUBLISHED 14 March 2023

CITATION
Wu Q, Liu S, Huang X, Liu J, Wang Y, Xiang Y, Tang X, Xu Q, Yan X, Tang B and Guo J (2023) Bidirectional Mendelian randomization study of psychiatric disorders and Parkinson's disease. *Front. Aging Neurosci.* 15:1120615. doi: 10.3389/fnagi.2023.1120615

Bidirectional Mendelian randomization study of psychiatric disorders and Parkinson's disease

Qi Wu[1,2†], Shulin Liu[1†], Xiurong Huang[1], Jiabin Liu[1], Yige Wang[1], Yaqing Xiang[1], Xuxiong Tang[1,2], Qian Xu[1,2,3,4,5,6], Xinxiang Yan[1,2,3,5,6], Beisha Tang[1,2,3,5,6] and Jifeng Guo[1,2,3,4,5,6*]

[1]Department of Neurology, Xiangya Hospital, Central South University, Changsha, Hunan, China, [2]Key Laboratory of Hunan Province in Neurodegenerative Disorders, Central South University, Changsha, Hunan, China, [3]Hunan International Scientific and Technological Cooperation Base of Neurodegenerative and Neurogenetic Diseases, Changsha, China, [4]Center for Medical Genetics and Hunan Key Laboratory of Medical Genetics, School of Life Sciences, Central South University, Changsha, Hunan, China, [5]Engineering Research Center of Hunan Province in Cognitive Impairment Disorders, Central South University, Changsha, China, [6]National Clinical Research Center for Geriatric Disorders, Xiangya Hospital, Central South University, Changsha, Hunan, China

Introduction: Although the relationship between psychiatric disorders and Parkinson's disease (PD) has attracted continuous research attention, the causal linkage between them has not reached a definite conclusion.

Methods: To identify the causal relationship between psychiatric disorders and PD, we used public summary-level data from the most recent and largest genome-wide association studies (GWASs) on psychiatric disorders and PD to conduct a bidirectional two-sample Mendelian randomization (MR). We applied stringent control steps in instrumental variable selection using the Mendelian randomization pleiotropy residual sum and outlier (MR-PRESSO) method to rule out pleiotropy. The inverse-variance weighted (IVW) method was used to identify the causal relationship between psychiatric disorders and PD. Multiple MR analysis methods, including MR-Egger, weighted-median, and leave-one-out analyses, were used for sensitivity analysis, followed by heterogeneity tests. Further validation and reverse MR analyses were conducted to strengthen the results of the forward MR analysis.

Results: The lack of sufficient estimation results could suggest a causal relationship between psychiatric disorders and PD in the forward MR analysis. However, the subsequent reverse MR analysis detected a causal relationship between PD and bipolar disorder (IVW: odds ratios [OR]=1.053, 95% confidence interval [CI]=1.02–1.09, p=0.001). Further analysis demonstrated a causal relationship between genetically predicted PD and the risk of bipolar disorder subtype. No pleiotropy or heterogeneity was detected in the analyses.

Discussion: Our study suggested that while psychiatric disorders and traits might play various roles in the risk of developing PD, PD might also be involved in the risk of developing psychiatric disorders.

KEYWORDS

Parkinson's disease, psychiatric disorders, Mendelian randomization, genome-wide association studies, causal relationship

Introduction

Parkinson's disease (PD), the most common movement disorder and the second most common neurodegenerative disease, is characterised by a wide range of motor and non-motor symptoms (NMS) (Lees et al., 2009). PD affects 1% of the population over 60 years of age, and its prevalence generally ranges from 100 to 200 per 100,000 persons in unselected populations (von Campenhausen et al., 2005). Owing to PD aetiology, particularly in sporadic cases, distinguishing causal risk factors could be meaningful for treatment and prevention of this disease. PD diagnosis is mainly based on typical motor symptoms, including tremors, rigidity, bradykinesia, and motor impairment, which have also been increasingly considered an important component of PD (Armstrong and Okun, 2020). NMS, including sleep disorders, autonomic dysfunction, cognitive/neurobehavioural abnormalities, and sensory abnormalities (such as anosmia, pain, and paraesthesia) have an even higher negative impact on the quality of life than motor symptoms (Karlsen et al., 2000). In general, NMS are highly prevalent in PD patients; NMS can also develop at any phases of the disease and frequently precedes the onset of motor symptoms (Krishnan et al., 2011; Kim et al., 2013). Psychiatric disorders, including anxiety, depression, psychosis, sleep disturbances, and behavioural and cognitive changes, are widely recognised as common NMS in PD and are more frequent in PD patients than in the general population (Aarsland et al., 2009). Furthermore, numerous studies have shown that the morbidity of psychotic illnesses is higher in PD patients (Djamshidian and Friedman, 2014; Ghaddar et al., 2016; Ffytche et al., 2017).

Increasing evidence points to the multifactorial aetiology of PD, which involves ageing, genetic predisposition, environmental agents, trauma, and psychosocial impact (Perry et al., 2016). Additionally, psychiatric disorders have a significant influence on the quality of life of PD patients and may play a critical role in the rapid deterioration of clinical manifestations (Alvarado-Bolanos et al., 2015; Ng et al., 2015; Elefante et al., 2021). Therefore, further understanding of the association between psychiatric disorders and PD is valuable for research and clinical practice.

Psychiatric disorders have been proposed to precede PD development and be a possible PD risk factor, which has been proven in observational studies (Ishihara-Paul et al., 2008; Jacob et al., 2010; Sanyal et al., 2010; Lin et al., 2014; Gustafsson et al., 2015; Schrag et al., 2015). A meta-analysis of prospective studies using a large United Kingdom biobank indicated that neuroticism was consistently associated with a higher risk of PD (Terracciano et al., 2021). Another analysis of four cohort studies and three cross-sectional studies, consisting of 4,374,211 individuals, also reported that patients with bipolar disorder (BD) might be at risk of having a subsequent idiopathic PD diagnosis (Dols and Lemstra, 2020). Additionally, sleep disturbances, including insomnia and rapid eye movement sleep behaviour disorder (RBD), are often considered early markers of PD pathology and an independent PD risk factor (Hsiao et al., 2017). Although specific underlying mechanism of this phenomenon remains unclear, recent studies have indicated that this process could be related to abnormal brainstem α-synucleinopathy, which caused RBD (Bohnen and Hu, 2019). These studies suggested that psychiatric disorders might potentially trigger the onset of PD. With the global escalation of the ageing process, the rapidly increasing incidence of PD is impacting the quality of life of more people. Therefore, clarifying the causality of these associations could be of practical value for improving the health of the elderly.

Mendelian randomization (MR) is an epidemiological technique that investigates the causal relationship between risk factors and outcomes. MR tends to avoid confounding issues and reverse causality by using genetic variants as instrumental variables (IVs). This technique has been extensively used to validate causal relationships discovered in observational studies (Plotnikov and Guggenheim, 2019). Owing to the development of genomic techniques and methodologies, an increasing number of disease-associated variants have been detected by genome-wide association studies (GWAS), which provide sufficient IV resources that could be used to increase the power of MR. Therefore, we used publicly available GWAS summary-level data of psychiatric disorders and PD for a bidirectional two-sample MR analysis to validate and explore the relationships among these traits.

Methods

Data source

In this two-sample MR analysis, we included publicly available GWAS results of eight psychiatric disorders/traits and PD conducted in European populations. The basic characteristics of GWASs, including exposures and outcomes, are listed in Table 1. Exposure to interest included anorexia nervosa (AN) (Watson et al., 2019), anxiety disorder (Purves et al., 2020), BD (Mullins et al., 2021), insomnia (Watanabe et al., 2022), major depressive disorder (MDD) (Howard et al., 2019), neuroticism (Nagel et al., 2018), obsessive–compulsive disorder (OCD) [International Obsessive Compulsive Disorder Foundation Genetics Collaborative (IOCDF-GC) and OCD Collaborative Genetics Association Studies (OCGAS), 2018], and schizophrenia (Trubetskoy et al., 2022). For PD, we used the largest GWAS conducted in the European population (Nalls et al., 2019) as a discovery study and a GWAS conducted in the Finnish population (Kurki et al., 2023) as a validation study. Detailed information regarding genotype platforms, statistical analysis protocols, and participants for each study is available in the corresponding papers (Data presentation).

IV selection

Valid IVs need to meet the following three assumptions: (1) association with the risk exposure of interest (relevance); (2) no shared common cause with the outcome (independence); and (3) they affect the outcome only through the risk factor (exclusion restriction assumption) (Davies et al., 2018). To ensure that all included IVs were valid, we employed a series of stringent control steps (Figure 1). First, we extracted genome-wide significant ($p < 5 \times 10^{-8}$) single-nucleotide polymorphisms (SNPs) from exposure GWASs. Since no genome-wide significant SNPs were detected in the GWAS of OCD, we chose to use suggestive significant SNPs ($p < 1 \times 10^{-5}$) as IVs. We then performed linkage disequilibrium (LD) clumping ($R^2 < 0.001$, window size = 10,000 kb) based on the European 1,000 Genomes Project reference panel to select independent significant SNPs. Those with

TABLE 1 Characteristics of GWASs used for each disorder.

Traits	Sample size (cases/controls)	Population	Consortium	PMID
Exposure				
Anorexia nervosa	72,517 (16,992/55,525)	Europeans	PGC*	31,308,545
Anxiety	83,565 (25,453/58,113)	Europeans	UKBB*	31,748,690
Bipolar disorder	413,466 (41,917/371,549)	Europeans	PGC	34,002,096
Insomnia	2,365,010 (593,724/1,771,286)	Europeans	CNCR*	30,804,565
MDD*	500,199 (170,756/329,443)	Europeans	PGC	30,718,901
Neuroticism	390,278[#]	Europeans	CNCR	29,942,085
OCD*	9,725 (2,688/7,037)	Europeans	PGC	28,761,083
Schizophrenia	130,644 (53,386/77,258)	Europeans	PGC	35,396,580
Outcome				
Parkinson's disease	482,730 (33,674/449,056)	Europeans	IPDGC*	31,701,892
Parkinson's disease	260,405 (2,496/257,909)	Finnish	FinnGen	www.finngen.fi

*MDD, major depressive disorder; OCD, obsessive–compulsive disorder; PGC, Psychiatric Genomics Consortium; UKB, UK Biobank; CNCR, Center for Neurogenomics and Cognitive Research; IPDGC, International Parkinson Disease Genomics Consortium. [#]Weighted neuroticism sum-score.

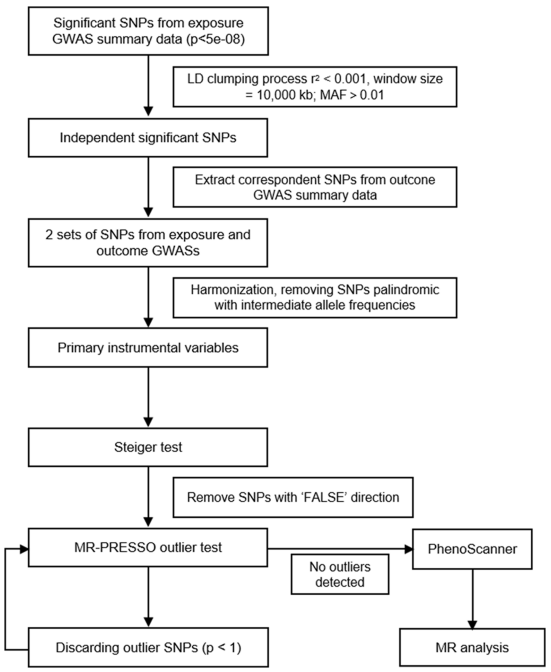

FIGURE 1
Flowchart of IVs selection strategy.

minor allele frequency (MAF) >0.01 and the lowest value of p were retained. F and weak instrumental variables.

Using the selected SNPs, we extracted SNPs from the outcome/PD GWASs. For those absent in the outcome GWASs, a proxy SNP in LD ($R^2 > 0.8$) with the requested SNP was searched according to 1,000 genomes of European samples. After harmonisation of the two aforementioned sets of SNPs, palindromic SNPs with intermediate allele frequencies were removed, and the remaining SNPs were kept as primary IVs. Next, we performed the Steiger test for each SNP to determine whether the R^2 (variance of disease/trait explained by selected SNPs) of the exposure was larger than the R^2 of the outcome. SNPs tested as "FALSE" direction (R^2 of the outcome $>R^2$ of the exposure) would be excluded.

The horizontal pleiotropy, which occurs when an IV affects the outcome outside of its effect on the exposure, is the main factor that violates the assumptions (Hemani et al., 2018). The MR pleiotropy residual sum and outlier (MR-PRESSO) test was developed to identify horizontal pleiotropy in multi-instrument summary-level MR testing (Verbanck et al., 2018). It is a sequential method comprising three components: a global test for horizontal pleiotropy, an outlier test for each genetic variant, and a distortion test of the difference in the causal estimates before and after outlier removal. At the stage of IV selection, we adopted a stringent filtering step by discarding SNPs with a value of $p < 1$ in the outlier test and repeated this step until no outliers were detected. Finally, the remaining SNPs were uploaded to PhenoScanner to examine whether any of them was previously associated with PD ($p < 5 \times 10^{-8}$ in published PD GWASs) and remove possible confounding SNPs (Kamat et al., 2019).

Utilizing R^2 (variance of exposure explained by the selected IVs) generated from the Steiger test, we calculated the overall F statistics ($F = R^2\ [n - k - 1]/k[1 - R^2]$, n: sample size, k: number of IVs) to quantify the strength of the IVs, and $F > 10$ was considered sufficient to overcome the weak instrumental variable bias (Burgess et al., 2013).

MR analysis

The inverse variance weighted (IVW) fixed-effect method, which combines the ratio estimated using each variant in a fixed-effect meta-analysis mode, was adopted to estimate the causative effect of each exposure on the outcome (Burgess et al., 2013). Because the IVW method provides an unbiased causal estimation only when all IVs are valid, we adopted other methods of sensitive analysis when a violation of the assumptions inevitably existed. The weighted-median method can provide a consistent estimate when 50% of the IVs are invalid, at the cost of reduced statistical power (Bowden et al., 2016). MR-Egger regression allows all genetic variants to be invalid IVs under the Instrument Strength Independent of Direct Effect (InSIDE)

assumption, which indicates that the pleiotropic effects of genetic variants on the outcome are direct (not through a confounder) (Bowden et al., 2015). The MR-Egger regression method also provides an intercept term for estimating the average pleiotropic effect across genetic variants. Even though we adopted stringent control steps, the MR-PRESSO method might still detect horizontal pleiotropy in the global test in the absence of detected outliers, which may be caused by a violation of the InSIDE assumption (Verbanck et al., 2018). Therefore, if pleiotropy was detected by the MR-PRESSO global test or the value of p of MR-Egger intercept was below 0.05, we used the results from the weighted-median method as the main method. The Cochran's Q statistic was implemented to quantify heterogeneities, and a value of $p < 0.05$ was considered significant heterogeneity. We also performed a leave-one-out sensitivity analysis by sequential exclusion of each SNP at a time to determine whether particular variants were driving the association between the exposure and the outcome, and an IVW method was performed on the remaining SNPs. To ensure the stability of our results, we used another PD GWAS, conducted among the Finnish population, as the outcome as described above. Individual estimates were pooled using a fixed-effect meta-analysis. To adjust for multiple testing, a Bonferroni-corrected value of p was set as 0.05/8, meanwhile value of $p < 0.05$ was regarded as nominally significant.

In addition, we performed reverse MR to examine for reverse causality of PD on psychiatric disorders/traits. Genetic variant selection steps and MR analysis were conducted in a similar manner to that of forward MR. All statistical analyses were conducted using R version 4.2.1, with the use of the 'TwoSampleMR', 'MRPRESSO' and 'META' packages for the MR analysis.

Results

Details of the IVs used for each MR analysis (both primary and validation analyses) are presented in the Supplementary Tables S1–S9. The main results, including causal estimation, the pleiotropy test, and the heterogeneity test, are presented in Tables 2, 3.

Causal effect of psychiatric disorders on PD

For the primary analysis, instrumental variables from GWAS of psychiatric disorders collectively explained 0.18–4.40% of the variance. The F-statistic ranged from 22.40 to 109.40, suggesting no possible weak instrument bias. Under the IVW model, genetic predispositions to psychiatric disorders were not associated with PD (Table 2). Although we performed stringent control steps and no outliers were detected before we conducted MR analysis, the MR-PRESSO global test still indicated the existence of pleiotropy among IVs from schizophrenia GWAS, which indicated that the violation of the InSIDE assumption made causation estimates of IVW and MR-Egger unreliable. However, the estimates calculated using the weighted-median method were not significant. Horizontal pleiotropy in variants generated from MDD was detected by the MR-Egger regression intercept ($p = 0.037$), but not by the MR-PRESSO global test ($p = 0.491$). Therefore, it is more precise to adopt the estimation from MR-Egger calculation that genetically predicted MDD was negatively nominally associated with PD risk (OR = 0.278, 95%CI, 0.09–0.88, $p = 0.035$). However, this association was not confirmed by the weighted-median method. Leave-one-out analysis suggested no potential influence of a particular variant on the estimate (Supplementary Tables S2–S9).

In the validation analysis, no horizontal pleiotropy was detected using the MR-PRESSO global test, and the Cochran's Q statistic value of p suggested no heterogeneity within each set of variants. Under the IVW model, genetically predicted AN was associated with PD risk (OR = 1.381, 95% CI = 1.02–1.87, $p = 0.037$). However, this association was not confirmed in the sensitivity analysis, which also showed a different association direction. Anxiety, insomnia, and MDD were predicted to be inversely associated with PD risk. Similar to AN, the causal estimation of anxiety in PD was not confirmed by other methods, which also showed a different association direction. However, estimation of the causal effect of insomnia and MDD on PD was validated by sensitivity analysis in the same direction, without observance of pleiotropy and heterogeneity. For neuroticism, the MR-Egger regression intercept indicated the presence of pleiotropy ($p = 0.03$), and MR-Egger showed an opposite causal estimate of PD risk (OR = 0.050, 95% CI = 0.00–0.62, $p = 0.022$). The sensitivity analysis also showed the same causal direction. Leave-one-out plots demonstrated that these associations were unlikely to be driven by extreme SNPs (Supplementary Tables S2–S9).

Due to the inconsistent results of the primary and validation analyses, we meta-analysed the results using a fixed-effect model. No significant results were detected, except for anxiety disorders (Pooled OR = 0.84, 95%CI, 0.71–0.99).

Causal effect of PD on psychiatric disorders

To clarify the precise causal relationship between psychiatric disorders and PD, we performed a reverse MR analysis, with PD as the exposure and psychiatric disorders as the outcome. Interestingly, we detected a causal relationship between genetically predicted PD and BD risk (Table 3). No pleiotropy or heterogeneity was detected in these results, and leave-one-out analysis demonstrated no potentially influential SNPs driving the causal link (Figure 2).

Discussion

Based on the potential relevance between psychiatric disorders and PD, our study appears to be the first research using bidirectional two-sample MR analysis to thoroughly investigate the causal relationship between genetically predicted psychiatric disorders/traits and PD. We found some evidence of different effects of psychiatric disorders/traits on the liabilities of PD. For MR detection of certain causal relationships, no reverse causal association was detected in the reverse MR analysis. Notably, we found evidence for the causality of PD on the risk of developing BD.

Although we found no statistical significance to support a causal association between AN and PD in the discovery cohort, the sensitivity analysis showed a consistent trend. Furthermore, a causal relationship was observed in the validation cohort. To our best

TABLE 2 Causal relations of psychiatric disorders with PD (IPDGC).

Exposure	Methods	nSNPs[a]	OR	95%CI	Pval	MR-PRESSO global Pval	Egger intercept Pval	Q_pval
AN versus PD	IVW[b]	6	1.172	(0.98, 1.40)	0.085	0.877		0.842
	MR Egger	6	1.327	(0.68, 2.58)	0.450		0.722	0.753
	Weighted median	6	1.150	(0.91, 1.46)	0.252			
Anxiety versus PD	IVW	3	0.895	(0.73, 1.10)	0.297	-[d]		0.391
	MR Egger	3	1.540	(0.09, 26.29)	0.816		0.771	0.200
	Weighted median	3	0.872	(0.68, 1.12)	0.290			
BD versus PD	IVW	50	1.070	(0.98, 1.17)	0.136	0.443		0.502
	MR Egger	50	0.830	(0.53, 1.29)	0.411		0.254	0.515
	Weighted median	50	1.085	(0.95, 1.23)	0.215			
Insomnia versus PD	IVW	295	0.839	(0.58, 1.21)	0.348	0.081		0.068
	MR Egger	295	0.688	(0.18, 2.66)	0.588		0.857	0.063
	Weighted median	295	0.698	(0.42, 1.17)	0.175			
MDD versus PD	IVW	43	0.960	(0.77, 1.20)	0.723	0.491		0.488
	MR Egger	43	0.278	(0.09, 0.88)	0.035[c]		0.037[c]	0.651
	Weighted median	43	0.834	(0.59, 1.18)	0.305			
Neuroticism versus PD	IVW	79	0.997	(0.72, 1.38)	0.986	0.207		0.218
	MR Egger	79	0.543	(0.08, 3.94)	0.548		0.544	0.204
	Weighted median	79	1.133	(0.71, 1.81)	0.603			
OCD versus PD	IVW	20	0.994	(0.94, 1.05)	0.834	0.422		0.402
	MR Egger	20	1.025	(0.89, 1.19)	0.753		0.677	0.351
	Weighted median	20	0.973	(0.90, 1.05)	0.499			
Schizophrenia versus PD	IVW	141	1.042	(0.98, 1.12)	0.208	0.008[c]		0.008[c]
	MR Egger	141	0.920	(0.72, 1.18)	0.513		0.312	0.008[c]
	Weighted median	141	1.017	(0.93, 1.11)	0.702			

[a]nSNPs: number of SNPs used as instrumental variables; [b]IVW: inverse-variance weighted; [c]$p < 0.05$; [d]Number of SNPs is not enough for MR-PRESSO pleiotropy test.

TABLE 3 Causal relations of psychiatric disorders with PD.

Outcome	Methods	nSNPs	OR	95%CI	Pval	MR-PRESSO global Pval	Egger intercept Pval	Q_pval
BD	IVW	19	1.059	(1.02, 1.09)	0.001[#]	0.741		0.725
	MR Egger	19	1.074	(0.99, 1.17)	0.124		0.586	0.671
	Weighted median	19	1.059	(1.01, 1.11)	0.014[*]			
BDI	IVW	16	1.074	(1.03, 1.12)	0.002[#]	0.946		0.732
	MR Egger	16	1.067	(0.95, 1.20)	0.297		0.568	0.694
	Weighted median	16	1.075	(1.01, 1.14)	0.019[*]			
BDII	IVW	20	1.025	(0.96, 1.10)	0.476	0.841		0.856
	MR Egger	20	1.072	(0.87, 1.32)	0.518		0.658	0.823
	Weighted median	20	1.038	(0.94, 1.14)	0.451			

[#]$p < 6.25 \times 10^{-3}$; [*]$p < 0.05$.

knowledge, few studies have addressed the association between AN and PD. Although both diseases share some common clinical and pathological phenotypes, such as dopamine deficits, hyposmia, micrographia, and hypophonia (Roessner et al., 2005; Schreder et al., 2008; Sekar et al., 2010; Stievenard et al., 2017; Favier et al., 2020), the relationship between these diseases has yet to be firmly verified. Hence, this MR result needs to be interpreted cautiously and requires confirmation through additional relevant studies.

To date, many prospective historical cohorts and observational studies have proven epidemiological links between depression and PD (Wang et al., 2018). Many studies have attempted to demonstrate that depression and PD shared a similar pathophysiological brain

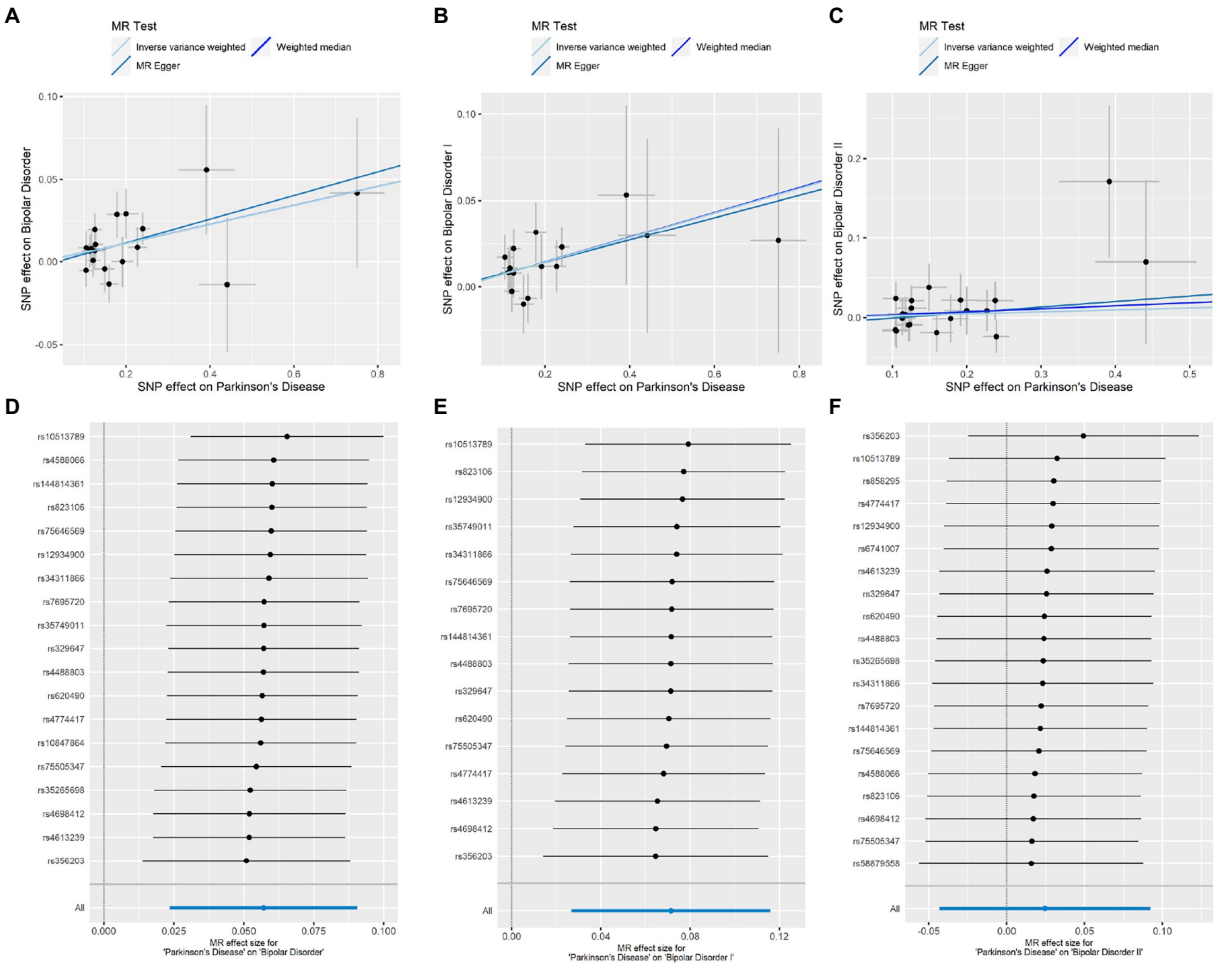

FIGURE 2
Causal effect estimation of PD on BD. **(A–C)** Scatterplots of potential effects of SNPs on BD (BD/BD I/BD II) and PD. Corresponding slope of each represents the estimated MR effect of each method. **(D–F)** Leave-one-out-sensitivity forest plots of PD-BD (BD/BD I/BD II) results.

dysfunction. Specifically, monoamine deficiency (i.e., dopamine, 5-hydroxytryptamine, and noradrenaline), one of the earliest suggested biological mechanisms of MDD, has also been observed in PD patients, particularly in early and prodromal patients with RBD (Hamon and Blier, 2013; Barber et al., 2018). In addition to monoaminergic neurotransmission and chronic inflammation, gamma-aminobutyric acid decline and cerebral atrophy are considered common pathophysiological characteristics underlying depression and PD (Gao and Bao, 2011; Saiki, 2014; Blaszczyk, 2016; Huang et al., 2016; D'Mello and Swain, 2017; Li et al., 2022). On one hand, since approximately 60% of PD patients have experienced psychosis, and many are taking or have taken antipsychotic medications (Weintraub et al., 2017), clinicians are more inclined to misdiagnose drug-induced parkinsonism as PD. On the other hand, as a frequently observed symptom of NMS, depression is more likely to be considered a common complication secondary to PD. First, in the discovery cohort, our analysis revealed a clear causal relationship between MDD and PD. This result was verified by subsequent duplicating assays with different GWAS. However, instead of increasing the risk of PD, genetically predicted MDD had a protective role against PD risk. Such opposing trends have also been observed in the association between insomnia and PD. However, the significant finding in the validation MR (IVW: OR = 0.563, 95%CI: 0.33–0.97, $p = 0.037$) was not supported by the sensitivity analysis. Moreover, these findings also contradicted those from the few current studies in this field, which considered that these diseases could predict an increased risk of PD (Weisskopf et al., 2003; Bower et al., 2010; Lin et al., 2015; Terracciano et al., 2021). This anomalous protective effect may be attributed to the survivor bias, caused by the reduced life expectancy of severe mental illness patients, and the increasing prevalence of PD in the older age group (Lees et al., 2009; Boef et al., 2015; Vansteelandt et al., 2018; Plana-Ripoll et al., 2019).

To clarify the exact causal relationship between psychiatric disorders and PD, we performed a reverse MR analysis, with PD as the exposure and psychiatric disorders as the outcomes. Interestingly, we detected a causal relationship between genetically predicted PD and BD risk. According to the Diagnostic and Statistical Manual Disorders, Fifth Edition (DSM-5), BD I and BD II are the major two clinical subtypes of BD, which are characterized by the classification of mania or hypomania. BD II is sometimes considered a milder form of BD I, because these two subtypes of BD share some phenomenological features (Liu et al., 2022). However, with increasing advances in BD

epidemiology, clinical presentation (Zimmerman et al., 2013), and genetic basis (Charney et al., 2017), the important difference between the two subtypes is gradually being recognised. Further exploration of the specific role of BD subtypes in this association revealed that PD might be a risk factor for BD I rather than BD II. There is growing evidence that PD patients have a high prevalence rate of various psychiatric disorders. BD is generally considered a specific risk factor for PD, rather than an ensuing complication (Huang et al., 2019), which is contrary to our results. However, the diagnosis of PD is currently based on clinical manifestations which became evident when 50% of dopaminergic neurons were lost in the substantia nigra (Marsden, 1990). So it's difficult to find out the exact beginning of the PD pathologic process. Taking the shared molecular mechanism into account, some may think it more appropriate that BD be viewed as an early symptom of PD (Pontone and Koch, 2019). As PD advances psychiatric complications emerge. 17% of patients with PD treated with dopaminergic therapy and 4% undergone DBS develop mania or hypomania, symptomatically similar to that of BD (Temel et al., 2006; Maier et al., 2014). In clinical terms, depression is not only a typical presentation of BD (Vieta et al., 2018), but also an important NMS of PD, which may hint to potential common clinical features between these diseases. However, similar to previous analyses, further related studies are needed to verify this finding.

Regarding other psychiatric disorders/traits, including OCD and schizophrenia, contrary to epidemiologic and other studies, we did not detect the causal association between these psychiatric conditions and PD. However, a close relationship exists between these two conditions. In the most updated nationwide longitudinal study published in 2022, OCD was reportedly an independent risk factor for PD (Liou et al., 2022). Another retrospective record-based case–control study demonstrated that schizophrenia spectrum disorder contributed to the incremental risk of PD in the elderly population (Kuusimaki et al., 2021). Understanding these potential association mechanisms may advance our knowledge of the underlying biology of these diseases and facilitate the early diagnosis of PD.

Our results should be viewed in the context of several limitations. Considering the existence of ethnicity-specific genomic heterogeneity, our findings must be interpreted with caution and may not be applicable to other racial/ethnic backgrounds, since all GWASs were conducted in European populations. Moreover, despite recent advances, existing GWAS methodology may still lack the ability to detect sufficient heritability of diseases, thus limiting the statistical power of the IVs used in this MR analysis. Owing to the lack of explicit measures and knowledge of potential confounders, pleiotropy may not be completely ruled out, and it is difficult to discuss the extent by which the results are influenced by this phenomenon. It is also difficult to determine the degree of sample overlap between the original GWASs of exposures and outcomes, which could cause weak instrument bias and violation of the independence assumption. However, bias from weak instruments in very large consortia may not be substantial and the F statistics was calculated to insure and minimize such bias (Burgess et al., 2016). For the violation of independence assumption, 2-sample MR methods can be safely applied to one-sample MR performed within large bio banks (Minelli et al., 2021). As presented above, many patients with psychiatric disorders have a history of antipsychotic use, which makes them more inclined to be diagnosed with drug-induced parkinsonism rather than PD. This possible misdiagnosis may have increased the effect of confounding factors on our results. Nevertheless, this study has several strengths. First, for each psychiatric exposure trait, we selected the latest and largest GWASs in European populations to ensure a reliable conclusion. Second, we applied a very stringent SNP quality threshold to reduce potential pleiotropic effects as much as possible. Moreover, this bidirectional MR analysis covered a wide variety of psychiatric disorders and traits, filling a gap in the observational literature and broadening our understanding of the relationship between psychosis and PD.

Collectively, in European populations, this 2-sample MR analysis provided evidence that genetically predicted psychiatric disorders may play various roles in the risk of PD. Concurrently, reverse MR analysis suggested that PD should be considered as a risk factor for BD subtype I. This significant result, supported by sensitive MR methods, showed no obvious heterogeneity or pleiotropy. Although these findings could be biased due to horizontal pleiotropy, we did not consider and detect hypotheses between psychiatric disorders and PD. As such, this topic merits further exploration.

Data availability statement

The original contributions presented in the study are included in the article/Supplementary material, further inquiries can be directed to the corresponding author/s.

Ethics statement

The studies involving human participants were reviewed and approved by The Ethics Committee of Xiangya Hospital of Central South University in China, the number of the approval is 202103191. The patients/participants provided their written informed consent to participate in this study.

Author contributions

QW and SL performed the majority of the analyses and wrote the manuscript. SL and YX conducted the systematic review. JG designed the study. All authors contributed to the article and approved the submitted version.

Funding

This study was supported by the national key plan for scientific research and development of China (2021YFC2501204), Technology Major Project of Hunan Provincial Science and Technology Department (grant no. 2021SK1010), the National Natural Science Foundation of China (grant no. 81873785, 82071439, 81974202, and U20A20355), Hunan Province Innovative Construction Project Science (grant no. 2019SK2335), and the Innovation-driven Team Project from Central South University (grant no. 2020CX016), the innovative team program from Department of Science & Technology of Hunan Province (grant no. 2019RS1010).

Acknowledgments

We want to acknowledge the participants and investigators of FinnGen study, Psychiatric Genomics Consortium, UK Biobank, Center for Neurogenomics and Cognitive Research and International Parkinson Disease Genomics Consortium for their generous donation of bio sample and making these data publicly available.

Conflict of interest

The authors declare that the research was conducted in the absence of any commercial or financial relationships that could be construed as a potential conflict of interest.

The reviewer ZH declared a shared affiliation with the authors to the handling editor at the time of review.

Publisher's note

Supplementary material

The Supplementary material for this article can be found online at: https://www.frontiersin.org/articles/10.3389/fnagi.2023.1120615/full#supplementary-material

References

Aarsland, D., Marsh, L., and Schrag, A. (2009). Neuropsychiatric symptoms in Parkinson's disease. *Mov. Disord.* 24, 2175–2186. doi: 10.1002/mds.22589

Alvarado-Bolanos, A., Cervantes-Arriaga, A., Rodriguez-Violante, M., Llorens-Arenas, R., Calderon-Fajardo, H., Millan-Cepeda, R., et al. (2015). Impact of neuropsychiatric symptoms on the quality of life of subjects with Parkinson's disease. *J. Parkinsons Dis.* 5, 541–548. doi: 10.3233/JPD-150597

Armstrong, M. J., and Okun, M. S. (2020). Diagnosis and treatment of Parkinson disease: a review. *JAMA* 323, 548–560. doi: 10.1001/jama.2019.22360

Barber, T. R., Griffanti, L., Muhammed, K., Drew, D. S., Bradley, K. M., McGowan, D. R., et al. (2018). Apathy in rapid eye movement sleep behaviour disorder is associated with serotonin depletion in the dorsal raphe nucleus. *Brain* 141, 2848–2854. doi: 10.1093/brain/awy240

Blaszczyk, J. W. (2016). Parkinson's disease and neurodegeneration: gaba-collapse hypothesis. *Front. Neurosci.* 10:269. doi: 10.3389/fnins.2016.00269

Boef, A. G., le Cessie, S., and Dekkers, O. M. (2015). Mendelian randomization studies in the elderly. *Epidemiology* 26, e15–e16. doi: 10.1097/EDE.0000000000000243

Bohnen, N. I., and Hu, M. (2019). Sleep disturbance as potential risk and progression factor for Parkinson's disease. *J. Parkinsons Dis.* 9, 603–614. doi: 10.3233/JPD-191627

Bowden, J., Davey, S. G., and Burgess, S. (2015). Mendelian randomization with invalid instruments: effect estimation and bias detection through egger regression. *Int. J. Epidemiol.* 44, 512–525. doi: 10.1093/ije/dyv080

Bowden, J., Davey, S. G., Haycock, P. C., and Burgess, S. (2016). Consistent estimation in mendelian randomization with some invalid instruments using a weighted median estimator. *Genet. Epidemiol.* 40, 304–314. doi: 10.1002/gepi.21965

Bower, J. H., Grossardt, B. R., Maraganore, D. M., Ahlskog, J. E., Colligan, R. C., Geda, Y. E., et al. (2010). Anxious personality predicts an increased risk of Parkinson's disease. *Mov. Disord.* 25, 2105–2113. doi: 10.1002/mds.23230

Burgess, S., Butterworth, A., and Thompson, S. G. (2013). Mendelian randomization analysis with multiple genetic variants using summarized data. *Genet. Epidemiol.* 37, 658–665. doi: 10.1002/gepi.21758

Burgess, S., Davies, N. M., and Thompson, S. G. (2016). Bias due to participant overlap in two-sample mendelian randomization. *Genet. Epidemiol.* 40, 597–608. doi: 10.1002/gepi.21998

Charney, A. W., Ruderfer, D. M., Stahl, E. A., Moran, J. L., Chambert, K., Belliveau, R. A., et al. (2017). Evidence for genetic heterogeneity between clinical subtypes of bipolar disorder. *Transl. Psychiatry* 7:e993. doi: 10.1038/tp.2016.242

Davies, N. M., Holmes, M. V., and Davey, S. G. (2018). Reading mendelian randomisation studies: a guide, glossary, and checklist for clinicians. *BMJ* 362:k601. doi: 10.1136/bmj.k601

Djamshidian, A., and Friedman, J. H. (2014). Anxiety and depression in parkinson's disease. *Curr. Treat. Options Neurol.* 16:285. doi: 10.1007/s11940-014-0285-6

D'Mello, C., and Swain, M. G. (2017). Immune-to-brain communication pathways in inflammation-associated sickness and depression. *Curr. Top. Behav. Neurosci.* 31, 73–94. doi: 10.1007/7854_2016_37

Dols, A., and Lemstra, A. W. (2020). Parkinsonism and bipolar disorder. *Bipolar Disord.* 22, 413–415. doi: 10.1111/bdi.12888

Elefante, C., Brancati, G. E., Bacciardi, S., Mazzucchi, S., Del, P. E., Palermo, G., et al. (2021). Prevalence and clinical correlates of comorbid anxiety and panic disorders in patients with Parkinson's disease. *J. Clin. Med.* 10:2302. doi: 10.3390/jcm10112302

Favier, M., Janickova, H., Justo, D., Kljakic, O., Runtz, L., Natsheh, J. Y., et al. (2020). Cholinergic dysfunction in the dorsal striatum promotes habit formation and maladaptive eating. *J. Clin. Invest.* 130, 6616–6630. doi: 10.1172/JCI138532

Ffytche, D. H., Creese, B., Politis, M., Chaudhuri, K. R., Weintraub, D., Ballard, C., et al. (2017). The psychosis spectrum in Parkinson disease. *Nat. Rev. Neurol.* 13, 81–95. doi: 10.1038/nrneurol.2016.200

Gao, S. F., and Bao, A. M. (2011). Corticotropin-releasing hormone, glutamate, and gamma-aminobutyric acid in depression. *Neuroscientist* 17, 124–144. doi: 10.1177/1073858410361780

Ghaddar, A., Fawaz, M., Khazen, G., Abdallah, J., and Milane, A. (2016). Prevalence of depression in Parkinson's disease in a Lebanese tertiary clinic. *J. Clin. Exp. Neuropsychol.* 38, 51–58. doi: 10.1080/13803395.2015.1087466

Gustafsson, H., Nordstrom, A., and Nordstrom, P. (2015). Depression and subsequent risk of Parkinson disease: a nationwide cohort study. *Neurology* 84, 2422–2429. doi: 10.1212/WNL.0000000000001684

Hamon, M., and Blier, P. (2013). Monoamine neurocircuitry in depression and strategies for new treatments. *Prog. Neuro-Psychopharmacol. Biol. Psychiatry* 45, 54–63. doi: 10.1016/j.pnpbp.2013.04.009

Hemani, G., Bowden, J., and Davey, S. G. (2018). Evaluating the potential role of pleiotropy in mendelian randomization studies. *Hum. Mol. Genet.* 27, R195–R208. doi: 10.1093/hmg/ddy163

Howard, D. M., Adams, M. J., Clarke, T. K., Hafferty, J. D., Gibson, J., Shirali, M., et al. (2019). Genome-wide meta-analysis of depression identifies 102 independent variants and highlights the importance of the prefrontal brain regions. *Nat. Neurosci.* 22, 343–352. doi: 10.1038/s41593-018-0326-7

Hsiao, Y. H., Chen, Y. T., Tseng, C. M., Wu, L. A., Perng, D. W., Chen, Y. M., et al. (2017). Sleep disorders and an increased risk of parkinson's disease in individuals with non-apnea sleep disorders: a population-based cohort study. *J. Sleep Res.* 26, 623–628. doi: 10.1111/jsr.12545

Huang, M. H., Cheng, C. M., Huang, K. L., Hsu, J. W., Bai, Y. M., Su, T. P., et al. (2019). Bipolar disorder and risk of Parkinson disease: a nationwide longitudinal study. *Neurology* 92, e2735–e2742. doi: 10.1212/WNL.0000000000007649

Huang, P., Lou, Y., Xuan, M., Gu, Q., Guan, X., Xu, X., et al. (2016). Cortical abnormalities in Parkinson's disease patients and relationship to depression: a surface-based morphometry study. *Psychiatry Res. Neuroimaging* 250, 24–28. doi: 10.1016/j.pscychresns.2016.03.002

International Obsessive Compulsive Disorder Foundation Genetics Collaborative (LOCDF-GC) and OCD Collaborative Genetics Association Studies (OCGAS) (2018). Revealing the complex genetic architecture of obsessive-compulsive disorder using meta-analysis. *Mol. Psychiatry* 23, 1181–1188. doi: 10.1038/mp.2017.154

Ishihara-Paul, L., Wainwright, N. W., Khaw, K. T., Luben, R. N., Welch, A. A., Day, N. E., et al. (2008). Prospective association between emotional health and clinical evidence of Parkinson's disease. *Eur. J. Neurol.* 15, 1148–1154. doi: 10.1111/j.1468-1331.2008.02299.x

Jacob, E. L., Gatto, N. M., Thompson, A., Bordelon, Y., and Ritz, B. (2010). Occurrence of depression and anxiety prior to Parkinson's disease. *Parkinsonism Relat. Disord.* 16, 576–581. doi: 10.1016/j.parkreldis.2010.06.014

Kamat, M. A., Blackshaw, J. A., Young, R., Surendran, P., Burgess, S., Danesh, J., et al. (2019). Phenoscanner v2: an expanded tool for searching human genotype-phenotype associations. *Bioinformatics* 35, 4851–4853. doi: 10.1093/bioinformatics/btz469

Karlsen, K. H., Tandberg, E., Arsland, D., and Larsen, J. P. (2000). Health related quality of life in Parkinson's disease: a prospective longitudinal study. *J. Neurol. Neurosurg. Psychiatry* 69, 584–589. doi: 10.1136/jnnp.69.5.584

Kim, H. S., Cheon, S. M., Seo, J. W., Ryu, H. J., Park, K. W., and Kim, J. W. (2013). Nonmotor symptoms more closely related to Parkinson's disease: comparison with normal elderly. *J. Neurol. Sci.* 324, 70–73. doi: 10.1016/j.jns.2012.10.004

Krishnan, S., Sarma, G., Sarma, S., and Kishore, A. (2011). Do nonmotor symptoms in Parkinson's disease differ from normal aging? *Mov. Disord.* 26, 2110–2113. doi: 10.1002/mds.23826

Kurki, M. I., Karjalainen, J., Palta, P., Sipilä, T. P., Kristiansson, K., Donner, K., et al. (2023). Author correction: Finngen provides genetic insights from a well-phenotyped isolated population. *Nature*. doi: 10.1038/s41586-023-05837-8

Kuusimaki, T., Al-Abdulrasul, H., Kurki, S., Hietala, J., Hartikainen, S., Koponen, M., et al. (2021). Increased risk of Parkinson's disease in patients with schizophrenia spectrum disorders. *Mov. Disord.* 36, 1353–1361. doi: 10.1002/mds.28484

Lees, A. J., Hardy, J., and Revesz, T. (2009). Parkinson's disease. *Lancet* 373, 2055–2066. doi: 10.1016/S0140-6736(09)60492-X

Li, K. L., Huang, H. Y., Ren, H., and Yang, X. L. (2022). Role of exosomes in the pathogenesis of inflammation in Parkinson's disease. *Neural Regen. Res.* 17, 1898–1906. doi: 10.4103/1673-5374.335143

Lin, H. L., Lin, H. C., and Chen, Y. H. (2014). Psychiatric diseases predated the occurrence of Parkinson disease: a retrospective cohort study. *Ann. Epidemiol.* 24, 206–213. doi: 10.1016/j.annepidem.2013.12.010

Lin, C. H., Lin, J. W., Liu, Y. C., Chang, C. H., and Wu, R. M. (2015). Risk of Parkinson's disease following anxiety disorders: a nationwide population-based cohort study. *Eur. J. Neurol.* 22, 1280–1287. doi: 10.1111/ene.12740

Liou, Y. J., Bai, Y. M., Chen, M. H., Cheng, C. M., Chen, T. J., and Tsai, S. J. (2022). Obsessive-compulsive disorder and risk of Parkinson disease: a nationwide longitudinal study. *Psychosom. Med.* 84, 1096–1102. doi: 10.1097/PSY.0000000000001120

Liu, W., Jiang, X., Deng, Z., Jia, L., Sun, Q., Kong, L., et al. (2022). Altered dynamic amplitude of low-frequency fluctuation between bipolar type i and type ii in the depressive state. *Neuroimage Clin* 36:103184. doi: 10.1016/j.nicl.2022.103184

Maier, F., Merkl, J., Ellereit, A. L., Lewis, C. J., Eggers, C., Pedrosa, D. J., et al. (2014). Hypomania and mania related to dopamine replacement therapy in Parkinson's disease. *Parkinsonism Relat. Disord.* 20, 421–427. doi: 10.1016/j.parkreldis.2014.01.001

Marsden, C. D. (1990). Parkinson's disease. *Lancet* 335, 948–949. doi: 10.1016/0140-6736(90)91006-v

Minelli, C., Del, G. M. F., van der Plaat, D. A., Bowden, J., Sheehan, N. A., and Thompson, J. (2021). The use of two-sample methods for mendelian randomization analyses on single large datasets. *Int. J. Epidemiol.* 50, 1651–1659. doi: 10.1093/ije/dyab084

Mullins, N., Forstner, A. J., O'Connell, K. S., Coombes, B., Coleman, J., Qiao, Z., et al. (2021). Genome-wide association study of more than 40,000 bipolar disorder cases provides new insights into the underlying biology. *Nat. Genet.* 53, 817–829. doi: 10.1038/s41588-021-00857-4

Nagel, M., Jansen, P. R., Stringer, S., Watanabe, K., de Leeuw, C. A., Bryois, J., et al. (2018). Meta-analysis of genome-wide association studies for neuroticism in 449,484 individuals identifies novel genetic loci and pathways. *Nat. Genet.* 50, 920–927. doi: 10.1038/s41588-018-0151-7

Nalls, M. A., Blauwendraat, C., Vallerga, C. L., Heilbron, K., Bandres-Ciga, S., Chang, D., et al. (2019). Identification of novel risk loci, causal insights, and heritable risk for Parkinson's disease: a meta-analysis of genome-wide association studies. *Lancet Neurol.* 18, 1091–1102. doi: 10.1016/S1474-4422(19)30320-5

Ng, A., Chander, R. J., Tan, L. C., and Kandiah, N. (2015). Influence of depression in mild Parkinson's disease on longitudinal motor and cognitive function. *Parkinsonism Relat. Disord.* 21, 1056–1060. doi: 10.1016/j.parkreldis.2015.06.014

Perry, D. C., Sturm, V. E., Peterson, M. J., Pieper, C. F., Bullock, T., Boeve, B. F., et al. (2016). Association of traumatic brain injury with subsequent neurological and psychiatric disease: a meta-analysis. *J. Neurosurg.* 124, 511–526. doi: 10.3171/2015.2.JNS14503

Plana-Ripoll, O., Pedersen, C. B., Agerbo, E., Holtz, Y., Erlangsen, A., Canudas-Romo, V., et al. (2019). A comprehensive analysis of mortality-related health metrics associated with mental disorders: a nationwide, register-based cohort study. *Lancet* 394, 1827–1835. doi: 10.1016/S0140-6736(19)32316-5

Plotnikov, D., and Guggenheim, J. A. (2019). Mendelian randomisation and the goal of inferring causation from observational studies in the vision sciences. *Ophthalmic Physiol. Opt.* 39, 11–25. doi: 10.1111/opo.12596

Pontone, G. M., and Koch, G. (2019). An association between bipolar disorder and Parkinson disease: when mood makes you move. *Neurology* 92, 1125–1126. doi: 10.1212/WNL.0000000000007641

Purves, K. L., Coleman, J., Meier, S. M., Rayner, C., Davis, K., Cheesman, R., et al. (2020). A major role for common genetic variation in anxiety disorders. *Mol. Psychiatry* 25, 3292–3303. doi: 10.1038/s41380-019-0559-1

Roessner, V., Bleich, S., Banaschewski, T., and Rothenberger, A. (2005). Olfactory deficits in anorexia nervosa. *Eur. Arch. Psychiatry Clin. Neurosci.* 255, 6–9. doi: 10.1007/s00406-004-0525-y

Saiki, S. (2014). The association of Parkinson's disease pathogenesis with inflammation. *Rinsho Shinkeigaku* 54, 1125–1127. doi: 10.5692/clinicalneurol.54.1125

Sanyal, J., Chakraborty, D. P., Sarkar, B., Banerjee, T. K., Mukherjee, S. C., Ray, B. C., et al. (2010). Environmental and familial risk factors of Parkinsons disease: case-control study. *Can. J. Neurol. Sci.* 37, 637–642. doi: 10.1017/s0317167100010829

Schrag, A., Horsfall, L., Walters, K., Noyce, A., and Petersen, I. (2015). Prediagnostic presentations of Parkinson's disease in primary care: a case-control study. *Lancet Neurol.* 14, 57–64. doi: 10.1016/S1474-4422(14)70287-X

Schreder, T., Albrecht, J., Kleemann, A. M., Schopf, V., Kopietz, R., Anzinger, A., et al. (2008). Olfactory performance of patients with anorexia nervosa and healthy subjects in hunger and satiety. *Rhinology* 46, 175–183. PMID: 18853867

Sekar, M. K., Arcelus, J., and Palmer, R. L. (2010). Micrographia and hypophonia in anorexia nervosa. *Int. J. Eat. Disord.* 43, 762–765. doi: 10.1002/eat.20768

Stievenard, A., Mequinion, M., Andrews, Z. B., Destee, A., Chartier-Harlin, M. C., Viltart, O., et al. (2017). Is there a role for ghrelin in central dopaminergic systems? Focus on nigrostriatal and mesocorticolimbic pathways. *Neurosci. Biobehav. Rev.* 73, 255–275. doi: 10.1016/j.neubiorev.2016.11.021

Temel, Y., Kessels, A., Tan, S., Topdag, A., Boon, P., and Visser-Vandewalle, V. (2006). Behavioural changes after bilateral subthalamic stimulation in advanced Parkinson disease: a systematic review. *Parkinsonism Relat. Disord.* 12, 265–272. doi: 10.1016/j.parkreldis.2006.01.004

Terracciano, A., Aschwanden, D., Stephan, Y., Cerasa, A., Passamonti, L., Toschi, N., et al. (2021). Neuroticism and risk of Parkinson's disease: a meta-analysis. *Mov. Disord.* 36, 1863–1870. doi: 10.1002/mds.28575

Trubetskoy, V., Pardinas, A. F., Qi, T., Panagiotaropoulou, G., Awasthi, S., Bigdeli, T. B., et al. (2022). Mapping genomic loci implicates genes and synaptic biology in schizophrenia. *Nature* 604, 502–508. doi: 10.1038/s41586-022-04434-5

Vansteelandt, S., Dukes, O., and Martinussen, T. (2018). Survivor bias in mendelian randomization analysis. *Biostatistics* 19, 426–443. doi: 10.1093/biostatistics/kxx050

Verbanck, M., Chen, C. Y., Neale, B., and Do, R. (2018). Detection of widespread horizontal pleiotropy in causal relationships inferred from mendelian randomization between complex traits and diseases. *Nat. Genet.* 50, 693–698. doi: 10.1038/s41588-018-0099-7

Vieta, E., Berk, M., Schulze, T. G., Carvalho, A. F., Suppes, T., Calabrese, J. R., et al. (2018). Bipolar disorders. *Nat. Rev. Dis. Primers.* 4:18008. doi: 10.1038/nrdp.2018.8

von Campenhausen, S., Bornschein, B., Wick, R., Botzel, K., Sampaio, C., Poewe, W., et al. (2005). Prevalence and incidence of parkinson's disease in europe. *Eur. Neuropsychopharmacol.* 15, 473–490. doi: 10.1016/j.euroneuro.2005.04.007

Wang, S., Mao, S., Xiang, D., and Fang, C. (2018). Association between depression and the subsequent risk of parkinson's disease: a meta-analysis. *Prog. Neuro-Psychopharmacol. Biol. Psychiatry* 86, 186–192. doi: 10.1016/j.pnpbp.2018.05.025

Watanabe, K., Jansen, P. R., Savage, J. E., Nandakumar, P., Wang, X., Hinds, D. A., et al. (2022). Genome-wide meta-analysis of insomnia prioritizes genes associated with metabolic and psychiatric pathways. *Nat. Genet.* 54, 1125–1132. doi: 10.1038/s41588-022-01124-w

Watson, H. J., Yilmaz, Z., Thornton, L. M., Hubel, C., Coleman, J., Gaspar, H. A., et al. (2019). Genome-wide association study identifies eight risk loci and implicates metabo-psychiatric origins for anorexia nervosa. *Nat. Genet.* 51, 1207–1214. doi: 10.1038/s41588-019-0439-2

Weintraub, D., Chiang, C., Kim, H. M., Wilkinson, J., Marras, C., Stanislawski, B., et al. (2017). Antipsychotic use and physical morbidity in Parkinson disease. *Am. J. Geriatr. Psychiatry* 25, 697–705. doi: 10.1016/j.jagp.2017.01.076

Weisskopf, M. G., Chen, H., Schwarzschild, M. A., Kawachi, I., and Ascherio, A. (2003). Prospective study of phobic anxiety and risk of Parkinson's disease. *Mov. Disord.* 18, 646–651. doi: 10.1002/mds.10425

Zimmerman, M., Martinez, J. H., Morgan, T. A., Young, D., Chelminski, I., and Dalrymple, K. (2013). Distinguishing bipolar ii depression from major depressive disorder with comorbid borderline personality disorder: demographic, clinical, and family history differences. *J. Clin. Psychiatry* 74, 880–886. doi: 10.4088/JCP.13m08428

frontiers | Frontiers in Aging Neuroscience

TYPE Original Research
PUBLISHED 02 June 2023
DOI 10.3389/fnagi.2023.1152917

OPEN ACCESS

EDITED BY
Muthuraman Muthuraman,
University Hospital Würzburg, Germany

REVIEWED BY
Robert Peach,
Imperial College London, United Kingdom
Manuel Bange,
Johannes Gutenberg University Mainz, Germany

*CORRESPONDENCE
Sara Mollà-Casanova
✉ sara.molla@uv.es

RECEIVED 28 January 2023
ACCEPTED 16 May 2023
PUBLISHED 02 June 2023

CITATION
Pedrero-Sánchez JF, Belda-Lois JM, Serra-Añó P, Mollà-Casanova S and López-Pascual J (2023) Classification of Parkinson's disease stages with a two-stage deep neural network.
Front. Aging Neurosci. 15:1152917.
doi: 10.3389/fnagi.2023.1152917

Classification of Parkinson's disease stages with a two-stage deep neural network

José Francisco Pedrero-Sánchez[1], Juan Manuel Belda-Lois[1,2], Pilar Serra-Añó[3], Sara Mollà-Casanova[3]* and Juan López-Pascual[1]

[1]Instituto de Biomecánica (IBV), Universitat Politècnica de València, Valencia, Spain, [2]Department of Mechanical and Materials Engineering (DIMM), Universitat Politècnica de València, Valencia, Spain, [3]UBIC, Department of Physiotherapy, Faculty of Physiotherapy, Universitat de València, Valencia, Spain

Introduction: Parkinson's disease is one of the most prevalent neurodegenerative diseases. In the most advanced stages, PD produces motor dysfunction that impairs basic activities of daily living such as balance, gait, sitting, or standing. Early identification allows healthcare personnel to intervene more effectively in rehabilitation. Understanding the altered aspects and impact on the progression of the disease is important for improving the quality of life. This study proposes a two-stage neural network model for the classifying the initial stages of PD using data recorded with smartphone sensors during a modified Timed Up & Go test.

Methods: The proposed model consists on two stages: in the first stage, a semantic segmentation of the raw sensor signals classifies the activities included in the test and obtains biomechanical variables that are considered clinically relevant parameters for functional assessment. The second stage is a neural network with three input branches: one with the biomechanical variables, one with the spectrogram image of the sensor signals, and the third with the raw sensor signals.

Results: This stage employs convolutional layers and long short-term memory. The results show a mean accuracy of 99.64% for the stratified k-fold training/validation process and 100% success rate of participants in the test phase.

Discussion: The proposed model is capable of identifying the three initial stages of Parkinson's disease using a 2-min functional test. The test easy instrumentation requirements and short duration make it feasible for use feasible in the clinical context.

KEYWORDS

Parkinson's disease, classification severity, neural network, smartphone, functional assessment

1. Introduction

Parkinson's disease (PD) is a prevalent progressive neurodegenerative disease (Ascherio and Schwarzschild, 2016; Simon et al., 2020). In the advanced stages, PD can cause motor dysfunction that alters the performance of basic activities of daily living (ADLs). Early identification of PD through clinical evaluation and functional tests allows the healthcare personnel to intervene properly in rehabilitation plans (Ascherio and Schwarzschild, 2016). Understanding the specific functional alterations in ADL, such as balance, gait, sitting, or standing, can help clinicians develop individualized rehabilitation plans and improve the quality of life of PD patients (Ascherio and Schwarzschild, 2016).

In the recent years there has been a trend toward sensorizing and applying data processing techniques to clinical functional tests. Portable sensors such as instrumented insoles, accelerometers, or inertial sensors (Ponciano et al., 2020) have been used to obtain clinically relevant parameters for studying the functional alterations of PD patients (Serra-Añó et al., 2020; Mollà-Casanova et al., 2022). The use of instrumented functional tests have also resulted in the generation of significant amounts of data (Weiss et al., 2011; Channa et al., 2020; Fuentes-Abolafio et al., 2020), opening up the possibility of applying advanced data analysis techniques such as machine learning and deep learning (Rehman et al., 2019; Butt et al., 2020; Xia et al., 2020; Mirelman et al., 2021).

In PD, clinically relevant parameters obtained from functional tests have been used to generate mathematical models that establish disease severity classifications (Bhidayasiri and Tarsy, 2012), determine functional status categories (Wrisley and Kumar, 2010), or identify risk levels (Sun and Sosnoff, 2018; Friedrich et al., 2021). Many studies have focused on analysing signals in the space-time domain, calculating biomechanical variables such as the trajectory of the center of pressures or time distribution during gait phases (Tong et al., 2021). Various classification techniques, including support vector machine (SVM), random forest (RF), decision trees (DT), or k-nearest neighbors (KNN; Trabassi et al., 2022), have been used to classify the severity of Parkinson's disease with an accuracy around 80 and 90%.

Although discrete variables-based methods have shown good results, they have a significant disadvantage of requiring prior feature selection and signal parametrization. This process is time-consuming and may lead to the loss of valuable information. These drawbacks may be overcome using the sensor raw data as the input to an artificial neural network (ANN), letting the ANN itself to identify the relevant information and extract the features to build the model. This approach has already shown very good results in the classification of PD severity, with an accuracy between 95 and 98%, using convolutional neural networks (CNN; El Maachi et al., 2020), long short-term memory (LSTM; Zhao et al., 2018a; Butt et al., 2020), or a combination of both (Zhao et al., 2018b; Xia et al., 2020).

Some authors have explored the analysis in the frequency domain instead of the time domain (Kim et al., 2018). The processed the spectrogram image of inertial sensors recordings using CNN, hypothesizing that the frequency components of involuntary movements could aid in identifying the level of severity of the disease. Although the accuracy rate in classifying PD stages was lower with this frequency analysis approach (83–85%) compared to the time domain approach, it may provide complementary information valuable for clinical evaluation of PD.

Considering the aforementioned findings, we hypothesize that a mixed input model comprising all three types of data (biomechanical variables, time domain, and frequency domain) would be capable of extracting all the relevant clinical features, outperforming the accuracy of simpler models.

The main objective of this study is to assess the accuracy of a mixed input model for classifying the early stages of PD using an instrumented functional assessment test. To achieve this, we developed a two-stage model that employs biomechanical variables, sensor raw data, and frequency analysis as inputs. We compared the performance of the proposed model was with that of simpler models that only utilized a subset of the inputs (raw signals only, frequency analysis only, and biomechanical variables only). As a secondary objective, we tested the accuracy of a CNN in automating the process of signal semantic segmentation and biomechanical variables calculation from the sensor raw data.

2. Materials and methods

2.1. Participants

Eighty-seven participants with PD distributed according to the Hoehn and Yahr (HY) scale (21 stage I, 30 stage II, and 36 stage III) agreed to participate in this cross-sectional study. Inclusion criteria for participation in the study has been as follows: (i) PD diagnosed by a neurologist [HY I, II, and III] (Hoehn and Yahr, 1967), (ii) have optimized and stable medical therapy at least one month before enrolment; (iii) have good cognitive status, defined as a score higher than 23 on the Mini-Mental State Exam (Folstein et al., 1975), (iv) ability to perform a modified Timed up & go (TUG) independently.

Exclusion criteria has been: (i) medical contraindications to physical activity, (ii) neurological or orthopedic injuries limiting independent walking and sitting or standing up from a chair, (iii) deafness or hearing problems, (iv) vestibular impairment, (v) blindness or a visual impairment, (vi) mental illness, (vii) any surgical procedure within the past 6 months before enrolment; (viii) people with IV and V stages of PD.

Participants were prospectively classified using the HY scale by their referring neurologist. Then, a physiotherapist conducted the functional assessment proposed, and scored the participant again on the HY scale. Stages IV and V were excluded from the study due to the implied severe disability that made it difficult to perform the test independently without the use of assistive products (Giladi et al., 2001; Goetz et al., 2004; Lescano et al., 2016).

All procedures were conducted in agreement with the World Medical Association Declaration of Helsinki principles. Ethical approval for the study was granted by the Ethics Committee of Universitat de València (H1517239006520), and all volunteers that participated in the study provided written informed consent.

2.2. Functional assessment

The functional assessment test is based on a modification of the TUG test already used and validated in this type of population (Serra-Añó et al., 2020; Mollà-Casanova et al., 2022). The modification to the TUG consists on: the inclusion of a pre-balance phase, the assessment of the reaction time to an external sound stimulus (Serra-Añó et al., 2019). The assessment of sitting-up and standing-up from a chair. The test consists of the following four phases (Figure 1):

- **Phase 1:** bipodal balance for 30 s with arms alongside the body.
- **Phase 2:** walking in a straight line toward a chair 3 m away when the external sound stimulus is produced.

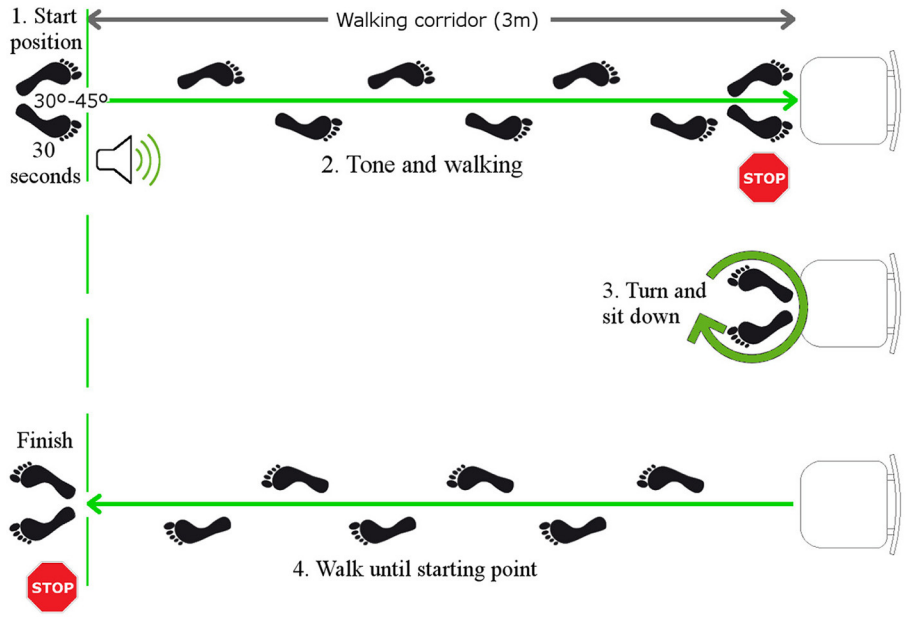

FIGURE 1
Functional assessment test execution sequence. 1. Balance standing upright for 30 s until the sound stimulus sounds; 2. Walk in a straight line toward the chair located 3 m away; 3. Turn around and sit in the chair; 4. Walk 3 m to the starting area and end the recording of the functional test.

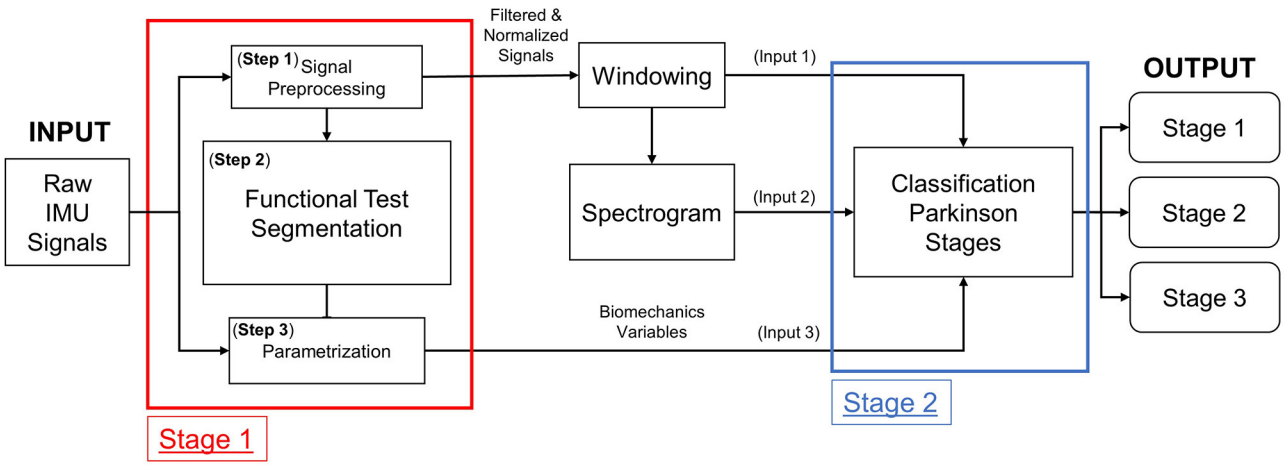

FIGURE 2
Structure of the two-stage Parkinson classifier model.

- **Phase 3:** turn around and sit on the chair, get up from the chair.
- **Phase 4:** walk 3 m back to the starting area.

The participants were asked to perform the protocol as quickly as possible while staying within their safety margins to avoid any possible harm. The test was conducted using an inertial sensor embedded in an Android smartphone (High Performance 6-Axis MEMS MotionTrackingTM composed of 3-axis gyroscope; 3-axis accelerometer at 100 Hz) attached to the back of the waist (L4-L5 vertebrae) with a strap. Throughout the study, the sensor signals were recorded using the Fallskip® system app. FallSkip® is a commercial system developed by the IBV (Instituto de Biomecánica de Valencia). This system was solely used in our study for recording the measurements and controlling the testing times. No calculations or analysis were performed by the FallSkip® application. Instead, all the calculations and analysis were performed offline on dedicated scripts for the analysis of the data.

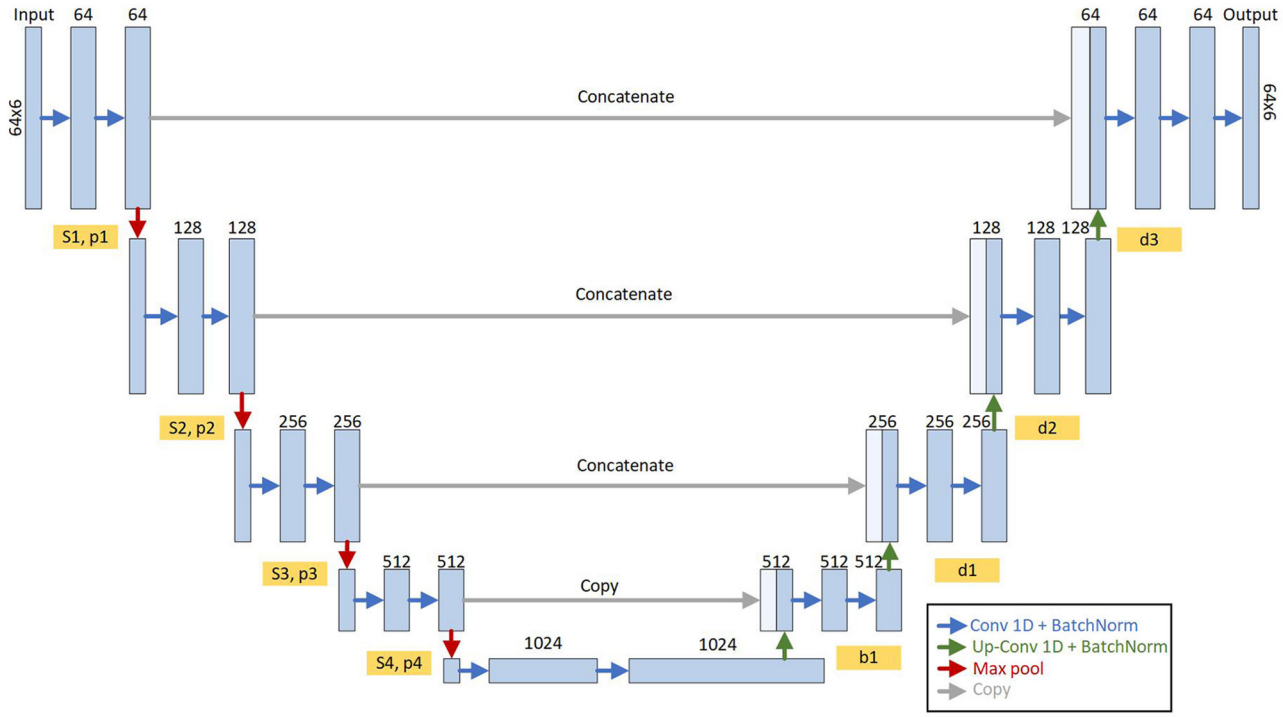

FIGURE 3
Structure of the Unet model for semantic segmentation of functional assessment. It is composed of four encoder blocks and four decoder blocks interconnected with a bridge in the central part where all the characteristics of the input signals are encoded. Each encoder/decoder block is composed of a series of 1D convolutional layers and a normalization (blue arrows). The outputs of these blocks (Sn and Pn) are interconnected with the next encoder block (red arrows) and with the analog decoder (gray arrows). The output of the model is the probability of each timestamp (64 input timestamps) of the activity of the functional test.

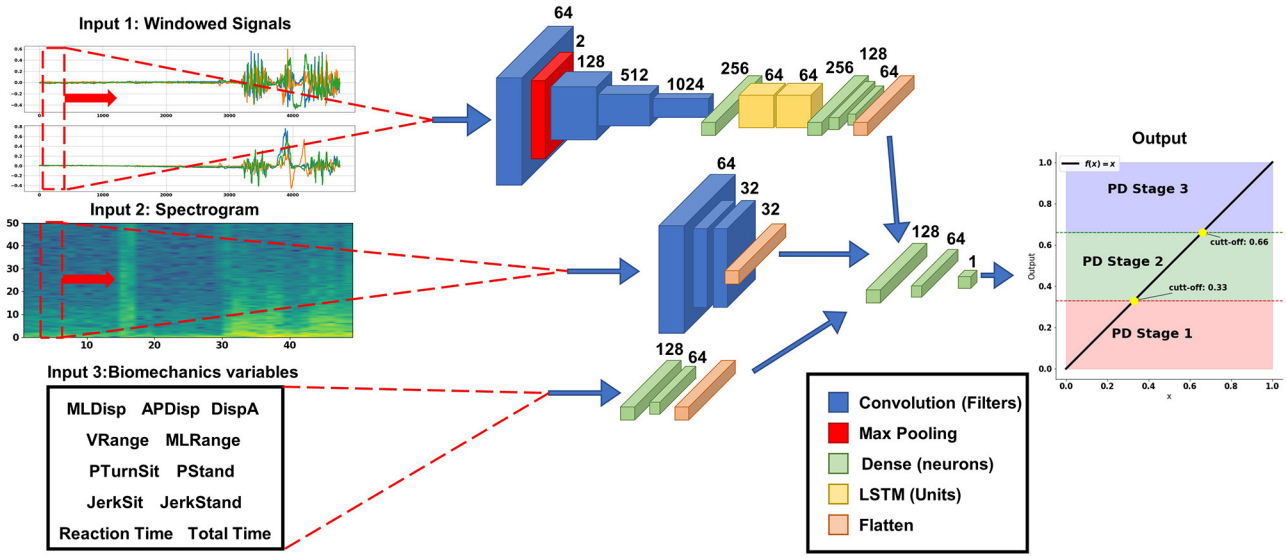

FIGURE 4
Structure of the Parkinson level classification model with mixed input data. The temporal input data (upper branch) is a moving window of 64 timestamps with the three axes of each sensor (accelerometer and gyroscope); this branch of the model is composed with a series of convolutional layers and LSTM to automatically extract the temporal characteristics of the signals. The branch with the frequency information (center branch) is the spectrogram image of the temporal signal, this branch is composed of convolutional layers to extract the information contained in the images. The branch with biomechanical variables (the lower branch) is composed of densely connected layers. All these branches are joined before the Top Model with a linear output layer between 0 and 1 with the points of 0.33 and 0.66 for the different levels.

TABLE 1 Demographic characteristics and biomechanical variables of the participants.

	All participants (n = 87)	HY-I (n = 21)	HY-II (n = 30)	HY-III (n = 36)	ANOVA (p-value)
Age (years)	69.09 (8.71)	67.14 (8.20)*	66.10 (9.40)**	72.58 (7.22)	**0.005**
Weight (*Kg*)	74.41 (15.97)	72.36 (11.88)***	85.03 (18.72)**	66.75 (9.80)	**<0.001**
Height (*cm*)	166.14 (8.31)	166.81 (6.92)	170.57 (7.34)**	162.06 (7.97)	**<0.001**
Sex (*n*, %)					
Women	30, 34.48	8, 38.10	5, 16.67	17, 47.22	–
Men	57, 65.52	13, 61.90	25, 93.33	19, 52.78	–
MLDisp (*mm*)	9.29 (7.95)	5.43 (2.65)	8.86 (8.34)	11.89 (8.81)	**0.01**
APDisp (*mm*)	22.90 (11.56)	18.44 (9.52)	21.02 (8.57)	27.07 (13.52)	**0.012**
DispA (mm^2)	773.63 (1191.73)	294.41 (258.85)	717.18 (1251.94)	1100.22 (1379.32)	**0.044**
VRange (*mm*)	24.34 (7.08)	28.34 (6.84)	25.27 (6.58)	21.22 (6.36)	**<0.001**
MLRange (*mm*)	47.71 (23.75)	49.03 (16.81)	45.12 (24.77)	49.09 (26.60)	0.766
PTurnSit (*W*)	87.41 (42.33)	111.66 (29.56)	96.93 (50.27)	65.33 (29.64)	**<0.001**
PStand (*W*)	271.03 (86.50)	252.65 (97.75)	236.76 (74.02)	179.81 (76.59)	**0.002**
JerkSit (m/s^3)	16.99 (7.40)	16.91 (4.14)	18.34 (7.96)	15.90 (8.35)	0.419
JerkStand (m/s^3)	21.66 (11.42)	21.08 (5.90)	24.66 (16.22)	19.51 (8.36)	0.184
TTime (*s*)	14.74 (3.75)	11.83 (1.52)	14.34 (2.66)	16.76 (4.24)	**<0.001**
RTime (*s*)	1.18 (0.42)	1.03 (0.41)	1.23 (0.49)	1.23 (0.34)	0.147

HY-I, participant in stage according to Hoehn & Yahr; HY-II, participant in stage according to Hoehn & Yahr; HY-III, participant in stage according to Hoehn & Yahr.
MLDisp, range of the Medial-lateral displacement of center of mass (COM); APDisp, range of the Anterior-posterior displacement of COM; DispA, Displacement Area; VRange, range of the Vertical displacement of COM; MLRange, range of the Medial-lateral displacement of COM; PTurnSit, Turn-to-sit power; PStand, Sit-to- stand power; TTime, total time; RTime, reaction time.
Data are expressed as mean (standard deviation).
*$p < 0.05$ between participants with level I and III.
**$p < 0.05$ between participants with level II and III.
***$p < 0.05$ between participants with level I and II.
Bold < 0.05 ANOVA between levels I, II, and III.
Table adapted from Mollà-Casanova et al. (2022).

2.3. Model data flow

A two-stage model has been designed (Figure 2). The raw sensor signals are the input of **Stage 1**, where are filtered and normalized in a first step (**Step 1**) before running the automatic segmentation of the test phases at step 2 (**Step 2**) which delivers the start and end times of each phase. Finally, the biomechanical variables are computed in step 3 (**Step 3**; Mollà-Casanova et al., 2022). The classification model based on neural networks of mixed input data is implemented in **Stage 2**. Each input branch of the model characterizes one aspect of the input signal: (**Input 1**) time-domain analysis, (**Input 2**) frequency-domain analysis (from the spectrogram), and (**Input 3**) biomechanical variables selected from literature (Serra-Añó et al., 2020; Mollà-Casanova et al., 2022). All this information is concatenated into a model (**Stage 2**) that classifies into the first three Parkinson's stages.

In the following sections, each of the processes that comprise the proposed two-stage model are described. All data processing were written in Python (v3.X).

2.4. Stage 1

2.4.1. Step 1—Signal preprocessing

Signal processing was carried out following the methodology proposed in Pedrero-Sánchez et al. (2022) which builds on the work of Zijlstra (2004) and Nishiguchi et al. (2012) for analyzing the data from inertial sensors. First, a linear interpolation was applied to standardize the sampling frequency of all signals to 100 Hz. Next, a 4th-order zero-lag Butterworth low-pass filter with a cutoff frequency of 20 Hz was applied. Then, we used the MinMaxScaler preprocessing function from the SciKitLearn library (Pedregosa et al., 2011) to normalize each signal between −1 and 1.

Before segmenting the functional test with the model, we employed a sliding window process because the segmentation model uses convolutional layers that require input data of uniform shape. Specifically, we applied a 64-sample moving window to the six sensor signals (three axes of accelerometer and three axes of gyroscope) to produce a matrix of shape 64 timestamps by six signals. The sliding window was then shifted through the entire signal, overlapping by 63 samples.

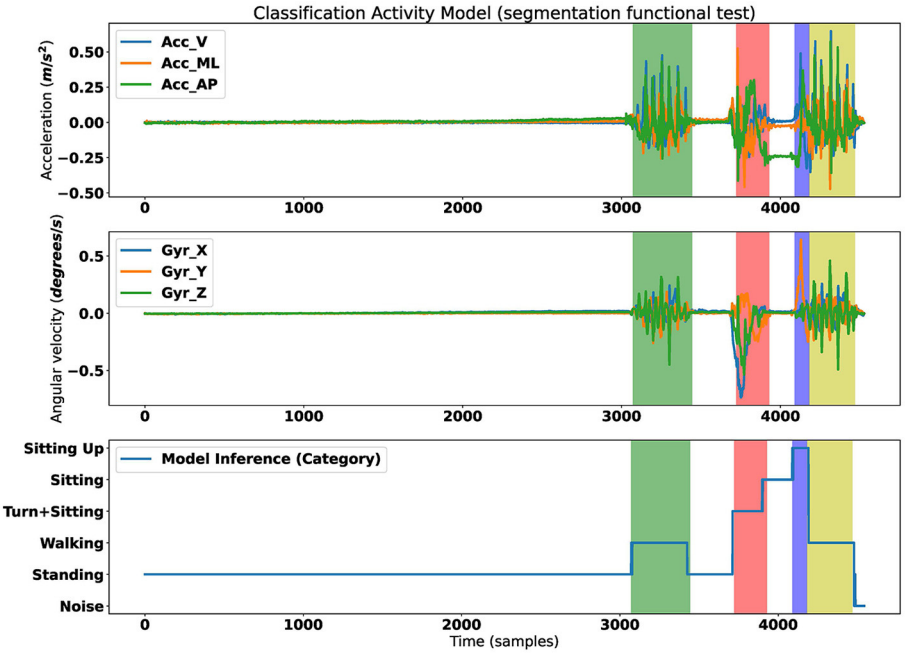

FIGURE 5
Results of segmentation assessment. **(Top)** Acceleration signal. **(Middle)** Gyroscope signal. **(Bottom)** Result of classification phases of the assessment. Shaded colors are the ground truth segmentation; Green, phase 2 gait; Red, phase 3 turn to sit; Blue, stand from the chair; Yellow, phase 4 gait.

2.4.2. Step 2—Functional test segmentation

To automatically segment the different phases of the functional test, a 1D Unet model was set up. This model is necessary to calculate the features of the sensor signals before passing them as input to the classification model. Typically, semantic segmentation RNN models have an Encoder-Decoder structure, where the input and output have the same shape. A forward feedback is performed between the layers forming a Unet structure (Ronneberger et al., 2015). The segmentation model proposed by Ronneberger was originally designed to segment images, but for this study, the internal structure of each encoding and decoding block has been modified to work with 1D vectors.

The structure of the model is depicted in Figure 3, where the input consists of the sliding windows from Step 1 (Section 2.4.1). The output has a shape 64 samples by 6 possible categories, corresponding to each of the possible phases of the test: balance, walking, turning and sitting, sitting, getting up, and a noise category.

Given that the model outputs an activity type for each sample in the window, we opted to identify the activity within the window by choosing the activity with the highest frequency as the identified activity. Then, once we identified all the activities in each sample of the complete functional test, we proceeded to detect the start and end instants of each phase of the test where the changes in activity occurred.

The model was developed from scratch, with the Adam optimizer, a learning rate of 0.001, and "categorical crossentropy" as the loss function. The Adam optimizer (Bock and Weiss, 2019) is the most widely used variation of gradient descent algorithms.

2.4.3. Step 3—Signal features

The input features calculated for the model (Step 3) have been previously validated in studies such as Ribeiro et al. (2003), Zijlstra (2004), Esser et al. (2009), and Nishiguchi et al. (2012). The features included are:

- **Phase 1, balance:** range of the Medial-Lateral Displacement (MLDisp) of the Center Of Mass (COM); range of Anterior-Posterior Displacement (APDisp) of the COM; and Swept Area (DispA).
- **Phase 2 and 4, gait:** range of the Vertical displacement (Vrange) of the COM; range of the Medial-Lateral displacement (MLRange) of the COM.
- **Phase 3, turn-to-sit-to-stand:** Turn-to-sit power (PTurnSit); Sit-to-stand power (PStand) (Lindemann et al., 2003); range of jerk to sit (JerkSit); range of jerk to stand (JerkStand; Weiss et al., 2011).
- **Complete assessment:** Reaction time (Reaction Time); Total time (Total Time).

The variables have been transformed with the MinMaxScaler from SciKitLearn library (Pedregosa et al., 2011) to the range between 0 and 1.

2.5. Stage 2

2.5.1. Windowing

This windowing differs from the previously performed for segmentation and it was intended to feed the time domain and frequency domain analysis (Section 2.4.1). The size of the window

TABLE 2 Validation and comparison of the classification models.

	Three-fold cross (%) validation	F1-score (%)	G-mean (%)
CNN+LSTM	86.46	79.00	84.00
CNN+ Biomechanical variables	92.23	81.00	84.00
Proposed two-stage model	99.64	100.00	100.00

TABLE 3 Sensibility of Stratified three-folds Cross Validation forcing one of the inputs to be all zeros then making the inference with the other two inputs.

	Mean accuracy	Difference with all inputs
Time-domain analysis	68.97	30.67
Frequency-domain analysis	65.85	33.79
Biomechanics variables	71.23	28.41

Mean accuracy is the accuracy in cross validation when the input is set to zero. **Difference with all inputs** is the difference in the mean accuracy obtained with the full input substracting the mean accuracy when the input is set to zero.

was 64 timestamps with a 50% overlap. The size and overlap were chosen based on the literature recommendations for human activities to capture the temporal dynamics of the signal while ensuring that the data had sufficient resolution for analysis (Banos et al., 2014; Dehghani et al., 2019).

2.5.2. Model inputs

2.5.2.1. Input 1—Time-domain analysis

The **Input 1** of the classificator is the time-domain analysis branch. This branch was feeded with the 64-sample moving window (Section 2.5.1) made with the six sensor signals (three accelerometer axes and three gyroscope axes).

2.5.2.2. Input 2—Frequency-domain analysis

The **Input 2** is the branch for frequency-domain analysis. The input are the windowing signals (Section 2.5.1). We applied the short-time Fourier Transform (STFT) provided by the TensorFlow 2.9.1 framework. All the signals are concatenated as if they were a single signal of 384 samples (6 signals × 64 samples). The STFT is then performed on this new signal with frame length = 20 and frame step = 2 to obtain a spectrogram. Then we applied the logarithm of the magnitude of the Fourier transform.

2.5.2.3. Input 3—Biomechanics variables

The biomechanical variables used were those described in Section 2.4.3.

2.5.3. Classification model

Keras API (Chollet et al., 2015) and Tensor Flow (Abadi et al., 2015) 2.0 in Python 3.7.x were used for classification model development (Figure 4).

For **Input 1**, the accelerometer and gyroscope signals were used with a series of 1D convolutional layer concatenations with ReLu activation functions (Rectified Linear Unit), which can extract the features automatically. ReLu is preferred over other activation functions like sigmoid or tanh because it is computationally efficient and avoids the vanishing gradient problem, which can occur when the derivative of the activation function becomes very small (Szandała, 2021). The extracted features were then passed through two Long-Short-Term Memory (LSTM) layers to obtain the signals sequential properties (Matias et al., 2021). Finally, three dense layers with ReLu activation functions were concatenated with the other two input branches.

The **Input 2** the spectrogram image of the signals was used (Ronneberger et al., 2015; Demir et al., 2019), where three 2D convolutional layers with a kernel size of 3 × 3 and ReLu activation functions were concatenated.

For **Input 3** the biomechanical variables were used, and dense layers with ReLu activation function were employed.

Finally, on top of the above networks, two dense layers are used with 128 and 64 neurons with Relu activation function and one output layer with one neuron were used for regression, with a linear activation, to produce a continuous output in the range [0, 1]. The cut-off points for each Parkinson's level were at 0.33 and 0.66.

To compile the model, mean square error was used as the loss measure for the regression problem, and the Adam optimizer.was employed. The evaluation metrics used was "mean square error" which considers the distance between the various categories and imposes a higher error penalty on the categories that are further away from the true value. An iterative design process was performed to fit the model, and the best results were obtained for a configuration with a batch size of 32 for 50 training epochs.

A grid search approach was used to systematically explore different combinations of hyperparameters, such as learning rate, batch size, and number of epochs, and evaluated the model's performance on the training and validation sets. Based on the results of each experiment, the hyperparameters were adjusted, and the process was repeated until the best performance was achieved.

2.6. Training, validation, and testing of the classification model

For training and validation the sample has been divided in different dataset:

Firstly, the sample has been divided in two separated datasets. Fifteen participants (five subjects from each group) have been reserved as **test dataset** for testing the classifier. This dataset did not intervened in the training, neither in the validation process. It was just kept apart for the final assessment of performance of the classifier.

The remaining 72 participants composed the training and validation dataset. This dataset was itself divided into three independent folds to perform a stratified three-fold cross-validation

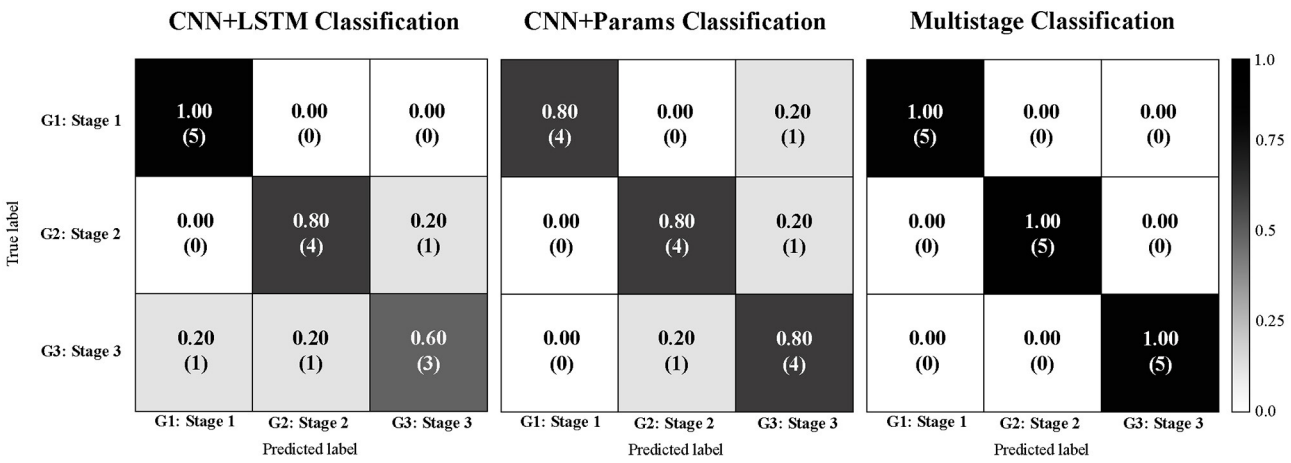

FIGURE 6
Confusion matrices comparison: Convolutional with Long short-term memory classification Parkinson disease model **(left)**; Convolutional with biomechanical parameters classification Parkinson disease model **(center)**; Proposed two-stage classification Parkinson disease model **(right)**.

(Xia et al., 2020). Two of the three-folds were combined and used in the model training, while the remaining fold was used for model validation. Each training set was resampled and resized using the SMOTE algorithm (Chawla et al., 2002) for the biomechanical variables and with data augmentation (rotating the axes of the sensors artificially 90 and 180°; Pedrero-Sánchez et al., 2022) for the signals, so that the number of instances of each class was approximately balanced. The accuracy and loss evolution plots over the training epochs were obtained.

Once the training was complete, the test dataset was used to evaluate the model performance using a confusion matrix and the geometric mean (G-mean; Kubat and Matwin, 1997).

2.7. Sensitivity analysis and comparison with simpler models

To assess the effectiveness of the model topologies identified in the literature and to perform a sensitivity analysis, it is important to evaluate the model's explainability in a clinical setting. Understanding the deep learning model's explainability aids in accurately interpreting the results it generates. To this end, we conducted a sensitivity analysis of the classifier to determine the impact of each input on the model's output.

The sensitivity analysis was performed by making alterations to the inputs and forcing one input to be all zeros when making the inference. This process was repeated for each input. Finally, we compared the outputs obtained for each input variation and analyzed their influence on the output.

Additionally, we used the same training and validation data to train two simplified models based on previous literature: (i) a simplified model that uses only input 1 (which includes convolutional layers and LSTM) called CNN+LSTM (Butt et al., 2020; Xia et al., 2020), and (ii) a simplified model that uses input 1 (including convolutional layers) and input 3 (including dense connected layers) called CNN+biomechanical variables (Pedrero-Sánchez et al., 2022). Input 2 was excluded because no models were found in the literature that used only the spectrogram image as input for Parkinson's disease classification.

We also obtained confusion matrices and mean accuracy for the training and validation folds of these models using the same test dataset.

3. Results

3.1. Participants

A description of the demographic characteristics and biomechanical variables of the participants, as well as the differences among the HY groups (Table 1).

3.2. Validation of the segmentation model

From the second epoch on, the segmentation model achieved an accuracy of 90% and a loss below 0.1. The comparison between the segmentation of the model and a manual segmentation from an expert shows a good agreement (Figure 5).

Therefore, we have used this automatic segmentation to calculate the biomechanical variables and use them as input for the classifier model.

3.3. Validation and comparison of the classification models

The accuracy evolution curve during the training of the two-stage classification stabilized at 100% after 5th epoch. The mean of the accuracy results obtained from the three-fold stratified cross-validation for each model in the training and validation phases shown in Table 2.

- CNN + LSTM: 86.42%
- CNN + biomechanical variables: 92.23%
- Proposed Two-stage: 99.64%

The two-stage classification model performed an accurate classification of all the 15 participants of the test sample (Figure 6) and the G-mean obtained was 1.00. Both, the CNN + LSTM and CNN + biomechanical variables achieved a G-mean of 0.84. For, the f1-score, was 0.79 for CNN + LSTM, 0.81 for CNN + Biomechanical variables, and 1.0 for two-stage.

The sensitivity analysis results shows that the major contributions to the model were the image of spectrogram with an accuracy decay of 33.79% (Table 3).

For a better understanding of the influence of the anthropometric data in the results, a separate analysis using a standard classifier with only the subject parameters (age, weight, height) as input variables was conducted. The results are presented as Supplementary material.

4. Discussion

This paper proposes a two-stage model to classify the early stages of PD (HY-I, HY-II, and HY-III) using a functional assessment test. The test involves the assessment of static balance, gait and lower limb power while sitting and rising from a chair, all within a 2 min timeframe using a single inertial sensor embedded in an Android smartphone (Serra-Añó et al., 2020; Mollà-Casanova et al., 2022).

As already shown in the previous study (Mollà-Casanova et al., 2022), the biomechanical variables obtained from the test are already indicators of disease progression, such as the total time (i.e., Ttime) that increases proportionally. The proposed test provides information on the state of balance MLDisp ($p < 0.05$), APDisp ($p < 0.05$), DispA ($p < 0.05$), gait Vrange ($p < 0.05$), and power in the lower limbs during sit to stand from a chair. There are significant differences ($p < 0.05$) in the biomechanical variables PTurnSit and PStand between the three groups.

The proposed model has been built on two Stages. Regarding Stage 1, the model is able to classify the activity on an instant-by-instant basis, reaching 90% of accuracy from the third epoch onwards. This has been accomplished by utilizing the signals from the inertial sensors and employing semantic segmentation models that have been validated in previous studies for pixel classification in images (Ronneberger et al., 2015) and for electrocardiogram (ECG) analysis (Matias et al., 2021). This semantic segmentation allowed to obtain the signal features that will later be used as input in the classification models. This automatic segmentation has a direct impact on the accuracy of the model. On the other hand, to ensure that all relevant characteristics of the signal in the time domain are captured, one of the input branches of the neural network includes the raw signals themselves, combined with convolutional and LSTM layers of the neural network as Zhao et al. (2018b) and El Maachi et al. (2020), respectively.

With respect to the Stage 2, the proposed model demonstrates a significant improvement in accuracy compared to variables based models in previous studies: 99.64% accuracy using the proposed model, compared to 80% accuracy using SVM, KNN, DT, and RF models (Trabassi et al., 2022). These classifiers have the limitation of using only signal-derived variables, which are clinically relevant for assessing Parkinson's grades, but still have potential for improvement.

When comparing neural network-based classifiers, such as CNN or LSTM, the results are similar, 98% accuracy with CNN (El Maachi et al., 2020) and 92.3% accuracy with LSTM (Butt et al., 2020) and 99% with the combination of CNN and LSTM (Zhao et al., 2018a). Although these results are already very good at classifying PD stages, they have the limitation of only focusing on the time domain. However, it should be noted that in more advanced stages of the disease, certain involuntary tremors may appear, which should be taken into account (Xing et al., 2022). Although some authors have found interesting results analyzing the consequences of tremors using variables in the time domain (e.g., sample entropy; di Biase et al., 2017; Su et al., 2021), the most direct approach would be to consider studying the frequency domain.

Despite the unbalanced training sample, the model responds correctly. To address this issue, training and validation have been carried out using stratified k-fold with artificially augmented data, which allowed balancing and data augmentation to fine-tune the model following the process used in Xia et al. (2020).

Another benefit presented in this paper is the combination of time domain and signal frequency information, along with clinically relevant biomechanical variables selected from the literature. It is worth noting that anthropometric variables of the subjects such as age, sex, height, and weight which have been shown to be important in determining the severity of the diseases (Joshi et al., 2010) have not been used in the classification model. This is because a comparative analysis by group was carried out and there were differences. These variables have been excluded in order to avoid bias in the classification, even though we know that they are important. In this way, the classification model only takes into account the functional test itself (Supplementary material).

The results of our study provide to the scientific community a new model to classify the early stages of PD. The model automatically processes the data recorded by a portable inertial sensor during the execution of a fast an easy functional assessment. Although we do not intend to substitute clinical assessment, we hypothesize that this model may be of interest in the future to better extract functional features in this population, beyond the instability, asymmetry or independence reported in the HY scale. This could lead to more accurate classifications and patient monitoring related to functional capability. To achieve this, further research is needed to validate this new method by comparing it to other clinical scales, such as the PD Questionnaire-8 or the Unified Parkinson's Disease Rating Scale (UPDRS). We believe that detecting different Parkinson's profiles may redefine the stages of Parkinson's and enable anticipation and prevention of its deleterious effects. Additionally, this approach provides a first step toward the development of automated, continuous, and non-invasive monitoring of functionality.

It is important to cautiously interpret the results of this study due to the limitations related to the small sample size. Although the anthropometric parameters were excluded from the model, the differences found between the HY groups could have biased the

results. It would be important in future research to consider the use of the modified HY scale, including the intermediate stages (i.e., 0.5, 1.5, and 2.5) to explore the capability of the model to classify all the early-to-moderate stages of the disease. A wider validation including multicentric data, homogeneous samples (regarding anthropometric variables) and additional diagnostic tools would be needed to confirm future clinical applications.

5. Conclusion

We show that our two-stage deep learning model can accurately classify people suffering from the first stages of PD. This CNN and LSTM-based technique is more accurate than another parametric technique of machine learning. These results demonstrated that the use of techniques managing raw data, combine with frequency analysis and biomechanical variables, prevents unexpected loss of information. Further, these classification models have been based on the information of a single sensor easily placed on the waist region of the participants in 2 min assessment test. The easy instrumentation required and the short duration of the test make its use feasible in the clinical context.

Data availability statement

The raw data supporting the conclusions of this article will be made available by the authors, without undue reservation.

Ethics statement

The studies involving human participants were reviewed and approved by Ethics Committee of Universitat de València (H1517239006520). The patients/participants provided their written informed consent to participate in this study.

Author contributions

JP-S: conceptualization, methodology, software, and formal analysis. JB-L: resources, conceptualization, supervision, and formal analysis. PS-A: conceptualization, methodology, validation, and investigation. SM-C: investigation and data curation. JL-P: conceptualization, supervision, and project administration. All authors contributed to the article and approved the submitted version.

Funding

Research Activity (IMAMCA/2022/7) supported by Instituto Valenciano de Competitividad Empresarial (IVACE) and Valencian Regional Government (GVA), and supported by the Universitat de València [INV19-01-13-07, 2019] funding and developed within the framework of the IBERUS project. Technological Network of Biomedical Engineering applied to degenerative pathologies of the neuromusculoskeletal system in clinical and outpatient settings (CER-20211003), CERVERA Network financed by the Ministry of Science and Innovation through the Center for Industrial Technological Development (CDTI), charged to the General State Budgets 2021, and the Recovery, Transformation, and Resilience Plan.

Conflict of interest

The authors declare that the research was conducted in the absence of any commercial or financial relationships that could be construed as a potential conflict of interest.

Publisher's note

All claims expressed in this article are solely those of the authors and do not necessarily represent those of their affiliated organizations, or those of the publisher, the editors and the reviewers. Any product that may be evaluated in this article, or claim that may be made by its manufacturer, is not guaranteed or endorsed by the publisher.

Supplementary material

The Supplementary Material for this article can be found online at: https://www.frontiersin.org/articles/10.3389/fnagi.2023.1152917/full#supplementary-material

References

Abadi, M., Agarwal, A., Barham, P., Brevdo, E., Chen, Z., Citro, C., et al. (2015). TensorFlow: Large-scale machine learning on heterogeneous systems. arXiv:1603.04467v2. doi: 10.48550/arXiv.1603.04467

Ascherio, A., and Schwarzschild, M. A. (2016). The epidemiology of Parkinson's disease: risk factors and prevention. *Lancet Neurol.* 15, 1257–1272. doi: 10.1016/S1474-4422(16)30230-7

Banos, O., Galvez, J.-M., Damas, M., Pomares, H., and Rojas, I. (2014). Window size impact in human activity recognition. *Sensors* 14, 6474–6499. doi: 10.3390/s140406474

Bhidayasiri, R., and Tarsy, D. (2012). "Parkinson's disease: hoehn and yahr scale," in *Movement Disorders: A Video Atlas: A Video Atlas, Current Clinical Neurology*, eds R. Bhidayasiri and D. Tarsy (Totowa, NJ: Humana Press), 4–5. doi: 10.1007/978-1-60327-426-5_2

Bock, S., and Weiss, M. (2019). "A proof of local convergence for the adam optimizer," in *2019 International Joint Conference on Neural Networks (IJCNN)* (Budapest), 1–8. doi: 10.1109/IJCNN.2019.8852239

Butt, A. H., Cavallo, F., Maremmani, C., and Rovini, E. (2020). "Biomechanical parameters assessment for the classification of Parkinson Disease using Bidirectional Long Short-Term Memory," in *2020 42nd Annual International Conference of the IEEE Engineering in Medicine & Biology Society (EMBC)* (Montreal, QC), 5761–5764. doi: 10.1109/EMBC44109.2020.9176051

Channa, A., Popescu, N., and Ciobanu, V. (2020). Wearable solutions for patients with Parkinson's disease and neurocognitive disorder: a systematic review. *Sensors* 20:E2713. doi: 10.3390/s20092713

Chawla, N. V., Bowyer, K. W., Hall, L. O., and Kegelmeyer, W. P. (2002). SMOTE: synthetic minority over-sampling technique. *J. Artif. Intell. Res.* 16, 321–357. doi: 10.1613/jair.953

Chollet, F. (2015). *keras*. GitHub. Available online at: https://github.com/fchollet/keras

Dehghani, A., Sarbishei, O., Glatard, T., and Shihab, E. (2019). A quantitative comparison of overlapping and non-overlapping sliding windows for human activity recognition using inertial sensors. *Sensors* 19:5026. doi: 10.3390/s19225026

Demir, F., Şengür, A., Bajaj, V., and Polat, K. (2019). Towards the classification of heart sounds based on convolutional deep neural network. *Health Inform. Sci. Syst.* 7:16. doi: 10.1007/s13755-019-0078-0

di Biase, L., Brittain, J.-S., Shah, S. A., Pedrosa, D. J., Cagnan, H., Mathy, A., et al. (2017). Tremor stability index: a new tool for differential diagnosis in tremor syndromes. *Brain* 140, 1977–1986. doi: 10.1093/brain/awx104

El Maachi, I., Bilodeau, G.-A., and Bouachir, W. (2020). Deep 1D-Convnet for accurate Parkinson disease detection and severity prediction from gait. *Expert Syst. Appl.* 143:113075. doi: 10.1016/j.eswa.2019.113075

Esser, P., Dawes, H., Collett, J., and Howells, K. (2009). IMU: inertial sensing of vertical CoM movement. *J. Biomech.* 42, 1578–1581. doi: 10.1016/j.jbiomech.2009.03.049

Folstein, M. F., Folstein, S. E., and McHugh, P. R. (1975). "Mini-mental state". A practical method for grading the cognitive state of patients for the clinician. *J. Psychiatr. Res.* 12, 189–198. doi: 10.1016/0022-3956(75)90026-6

Friedrich, B., Lau, S., Elgert, L., Bauer, J. M., and Hein, A. (2021). A deep learning approach for TUG and SPPB score prediction of (pre-) frail older adults on real-life IMU data. *Healthcare* 9:149. doi: 10.3390/healthcare9020149

Fuentes-Abolafio, I. J., Stubbs, B., Pérez-Belmonte, L. M., Bernal-López, M. R., Gómez-Huelgas, R., and Cuesta-Vargas, A. (2020). Functional parameters indicative of mild cognitive impairment: a systematic review using instrumented kinematic assessment. *BMC Geriatr.* 20:282. doi: 10.1186/s12877-020-01678-6

Giladi, N., Shabtai, H., Rozenberg, E., and Shabtai, E. (2001). Gait festination in Parkinson's disease. *Parkinsonism Relat. Disord.* 7, 135–138. doi: 10.1016/S1353-8020(00)00030-4

Goetz, C. G., Poewe, W., Rascol, O., Sampaio, C., Stebbins, G. T., Counsell, C., et al. (2004). Movement Disorder Society Task Force report on the Hoehn and Yahr staging scale: status and recommendations The Movement Disorder Society Task Force on rating scales for Parkinson's disease. *Mov. Disord.* 19, 1020–1028. doi: 10.1002/mds.20213

Hoehn, M. M., and Yahr, M. D. (1967). Parkinsonism: onset, progression and mortality. *Neurology* 17, 427–442. doi: 10.1212/WNL.17.5.427

Joshi, S., Shenoy, D., Simha, G. G. V., Rrashmi, P. L., Venugopal, K. R., and Patnaik, L. M. (2010). "Classification of Alzheimer's disease and parkinson's disease by using machine learning and neural network methods," in *Second International Conference on Machine Learning and Computing* (Bangalore), 218–222. doi: 10.1109/ICMLC.2010.45

Kim, H. B., Lee, W. W., Kim, A., Lee, H. J., Park, H. Y., Jeon, H. S., et al. (2018). Wrist sensor-based tremor severity quantification in Parkinson's disease using convolutional neural network. *Comput. Biol. Med.* 95, 140–146. doi: 10.1016/j.compbiomed.2018.02.007

Kubat, M., and Matwin, S. (1997). "Addressing the curse of imbalanced training sets: one-sided selection," in *Proceedings of the Fourteenth International Conference on Machine Learning* (Nashville, TN: Morgan Kaufmann), 179–186.

Lescano, C. N., Rodrigo, S. E., and Christian, D. A. (2016). A possible parameter for gait clinimetric evaluation in Parkinson's disease patients. *J. Phys.* 705:012019. doi: 10.1088/1742-6596/705/1/012019

Lindemann, U., Claus, H., Stuber, M., Augat, P., Muche, R., Nikolaus, T., and Becker, C. (2003). Measuring power during the sit-to-stand transfer. *Eur. J. Appl. Physiol.* 89, 466–470. doi: 10.1007/s00421-003-0837-z

Matias, P., Folgado, D., Gamboa, H., and Carreiro, A. (2021). Time series segmentation using neural networks with cross-domain transfer learning. *Electronics* 10:1805. doi: 10.3390/electronics10151805

Mirelman, A., Frank, M. B. O., Melamed, M., Granovsky, L., Nieuwboer, A., Rochester, L., et al. (2021). Detecting sensitive mobility features for Parkinson's disease stages via machine learning. *Mov. Disord.* doi: 10.1002/mds.28631

Mollà-Casanova, S., Pedrero-Sánchez, J., Inglés, M., López-Pascual, J., Muñoz-Gómez, E., Aguilar-Rodríguez, M., et al. (2022). Impact of Parkinson's disease on functional mobility at different stages. *Front. Aging Neurosci.* 14:935841. doi: 10.3389/fnagi.2022.935841

Nishiguchi, S., Yamada, M., Nagai, K., Mori, S., Kajiwara, Y., Sonoda, T., et al. (2012). Reliability and validity of gait analysis by android-based smartphone. *Telemed. e-Health* 18, 292–296. doi: 10.1089/tmj.2011.0132

Pedregosa, F., Varoquaux, G., Gramfort, A., Michel, V., Thirion, B., Grisel, O., et al. (2011). Scikit-learn: machine learning in Python. *J. Mach. Learn. Res.* 12, 2825–2830.

Pedrero-Sánchez, J. F., Belda-Lois, J.-M., Serra-Añó, P., Inglés, M., and López-Pascual, J. (2022). Classification of healthy, Alzheimer and Parkinson populations with a multi-branch neural network. *Biomed. Signal Process. Control* 75:103617. doi: 10.1016/j.bspc.2022.103617

Ponciano, V., Pires, I. M., Ribeiro, F. R., and Spinsante, S. (2020). Sensors are capable to help in the measurement of the results of the timed-up and go test? A systematic review. *J. Med. Syst.* 44:199. doi: 10.1007/s10916-020-01666-8

Rehman, R. Z. U., Del Din, S., Guan, Y., Yarnall, A. J., Shi, J. Q., and Rochester, L. (2019). Selecting clinically relevant gait characteristics for classification of early Parkinson's disease: a comprehensive machine learning approach. *Sci. Rep.* 9:17269. doi: 10.1038/s41598-019-53656-7

Ribeiro, J. G. T., Castro, J. T. P. D., and Freire, J. L. F. (2003). "Using the Fft-Ddi method to measure displacements with piezoelectric, resistive and Icp accelerometers," in *XXI International Modal Analysis ConferenceAt* (Orlando, FL), 189–196.

Ronneberger, O., Fischer, P., and Brox, T. (2015). "U-Net: convolutional networks for biomedical image segmentation," in *Medical Image Computing and Computer-Assisted Intervention MICCAI 2015, Lecture Notes in Computer Science*, eds N. Navab, J. Hornegger, W. M. Wells, and A. F. Frangi (Cham: Springer International Publishing), 234–241. doi: 10.1007/978-3-319-24574-4_28

Serra-Añó, P., Pedrero-Sánchez, J. F., Hurtado-Abellán, J., Inglés, M., Espí-López, G. V., and López-Pascual, J. (2019). Mobility assessment in people with Alzheimer disease using smartphone sensors. *J. NeuroEng. Rehabil.* 16:103. doi: 10.1186/s12984-019-0576-y

Serra-Añó, P., Pedrero-Sánchez, J. F., Inglés, M., Aguilar-Rodríguez, M., Vargas-Villanueva, I., and López-Pascual, J. (2020). Assessment of functional activities in individuals with Parkinson's disease using a simple and reliable smartphone-based procedure. *Int. J. Environ. Res. Public Health* 17:E4123. doi: 10.3390/ijerph17114123

Simon, D. K., Tanner, C. M., and Brundin, P. (2020). parkinson disease epidemiology, pathology, genetics, and pathophysiology. *Clin. Geriatr. Med.* 36, 1–12. doi: 10.1016/j.cger.2019.08.002

Su, D., Zhang, F., Liu, Z., Yang, S., Wang, Y., Ma, H., et al. (2021). Different effects of essential tremor and Parkinsonian tremor on multiscale dynamics of hand tremor. *Clin. Neurophysiol.* 132, 2282–2289. doi: 10.1016/j.clinph.2021.04.017

Sun, R., and Sosnoff, J. J. (2018). Novel sensing technology in fall risk assessment in older adults: a systematic review. *BMC Geriatr.* 18:14. doi: 10.1186/s12877-018-0706-6

Szandała, T. (2021). "Review and comparison of commonly used activation functions for deep neural networks," in *Bio-Inspired Neurocomputing. Studies in Computational Intelligence, Vol 903,* eds A. Bhoi, P. Mallick, C. M. Liu, and V. Balas (Singapore: Springer), 203–224. doi: 10.1007/978-981-15-5495-7_11

Tong, J., Zhang, J., Dong, E., and Du, S. (2021). Severity classification of Parkinson's disease based on permutation-variable importance and persistent entropy. *Appl. Sci.* 11:1834. doi: 10.3390/app11041834

Trabassi, D., Serrao, M., Varrecchia, T., Ranavolo, A., Coppola, G., De Icco, R., et al. (2022). Machine learning approach to support the detection of Parkinson's disease in IMU-based gait analysis. *Sensors* 22:3700. doi: 10.3390/s22103700

Weiss, A., Herman, T., Plotnik, M., Brozgol, M., Giladi, N., and Hausdorff, J. M. (2011). An instrumented timed up and go: the added value of an accelerometer for identifying fall risk in idiopathic fallers. *Physiol. Measure.* 32, 2003–2018. doi: 10.1088/0967-3334/32/12/009

Wrisley, D. M., and Kumar, N. A. (2010). Functional gait assessment: concurrent, discriminative, and predictive validity in community-dwelling older adults. *Phys. Ther.* 90, 761–773. doi: 10.2522/ptj.20090069

Xia, Y., Yao, Z., Ye, Q., and Cheng, N. (2020). A dual-modal attention-enhanced deep learning network for quantification of Parkinson's disease characteristics. *IEEE Trans. Neural Syst. Rehabil. Eng.* 28, 42–51. doi: 10.1109/TNSRE.2019.2946194

Xing, X., Luo, N., Li, S., Zhou, L., Song, C., and Liu, J. (2022). Identification and classification of Parkinsonian and essential tremors for diagnosis using machine learning algorithms. *Front. Neurosci.* 16:701632. doi: 10.3389/fnins.2022.701632

Zhao, A., Qi, L., Dong, J., and Yu, H. (2018a). Dual channel LSTM based multi-feature extraction in gait for diagnosis of Neurodegenerative diseases. *Knowl. Based Syst.* 145, 91–97. doi: 10.1016/j.knosys.2018.01.004

Zhao, A., Qi, L., Li, J., Dong, J., and Yu, H. (2018b). A hybrid spatio-temporal model for detection and severity rating of Parkinson's disease from gait data. *Neurocomputing* 315, 1–8. doi: 10.1016/j.neucom.2018.03.032

Zijlstra, W. (2004). Assessment of spatio-temporal parameters during unconstrained walking. *Eur. J. Appl. Physiol.* 92, 39–44. doi: 10.1007/s00421-004-1041-5

frontiers | Frontiers in Aging Neuroscience

TYPE Original Research
PUBLISHED 28 June 2023
DOI 10.3389/fnagi.2023.1187684

OPEN ACCESS

EDITED BY
Muthuraman Muthuraman,
University Hospital Würzburg, Germany

REVIEWED BY
Jifeng Guo,
Central South University, China
Mahmoud Iravani,
University of Hertfordshire, United Kingdom

*CORRESPONDENCE
Tao Wu
✉ wutao69@163.com
Hongjian He
✉ hhezju@zju.edu.cn

RECEIVED 16 March 2023
ACCEPTED 09 June 2023
PUBLISHED 28 June 2023

CITATION
Zhang D, Yao J, Sun J, Wang J, Chen L, He H and Wu T (2023) Iron accumulation in the ventral tegmental area in Parkinson's disease. *Front. Aging Neurosci.* 15:1187684. doi: 10.3389/fnagi.2023.1187684

Iron accumulation in the ventral tegmental area in Parkinson's disease

Dongling Zhang[1,2,3], Junye Yao[4], Junyan Sun[1,2,3], Junling Wang[1,2,3], Lili Chen[1,2,3], Hongjian He[4,5]* and Tao Wu[1,2,3]*

[1]Center for Movement Disorders, Department of Neurology, Beijing Tiantan Hospital, Capital Medical University, Beijing, China, [2]China National Clinical Research Center for Neurological Diseases, Beijing, China, [3]Parkinson's Disease Center, Beijing Institute for Brain Disorders, Capital Medical University, Beijing, China, [4]Center for Brain Imaging Science and Technology, College of Biomedical Engineering and Instrument Science, Zhejiang University, Hangzhou, Zhejiang, China, [5]School of Physics, Zhejiang University, Hangzhou, Zhejiang, China

Introduction: The ventral tegmental area (VTA) is less affected compared to substantia nigra pars compacta (SNc) in Parkinson's disease (PD). This study aimed to quantitatively evaluate iron content in the VTA across different stages of PD in order to help explain the selective loss of dopamine neurons in PD.

Methods: Quantitative susceptibility mapping (QSM) data were obtained from 101 PD patients, 35 idiopathic rapid eye movement sleep behavior disorder (RBD) patients, and 62 healthy controls (HCs). The mean QSM values in the VTA and SNc were calculated and compared among the groups.

Results: Both RBD and PD patients had increased iron values in the bilateral SNc compared with HCs. RBD and PD patients in the Hoehn–Yahr (H & Y) stage 1 did not show elevated iron values in the VTA, while PD patients with more than 1.5 H & Y staging had increased iron values in bilateral VTA compared to HCs.

Discussion: This study shows that there is no increased iron accumulation in the VTA during the prodromal and early clinical stages of PD, but iron deposition increases significantly as the disease becomes more severe.

KEYWORDS

Parkinson's disease, ventral tegmental area (VTA), idiopathic rapid eye movement sleep behavior disorder (RBD), iron deposition, quantitative susceptibility mapping

1. Introduction

The dopamine (DA) neurons in the ventral tegmental area (VTA) principally project to the nucleus accumbens in the ventral striatum, as well as the amygdala and prefrontal cortex, as part of the mesocorticolimbic pathway, whereas the DA neurons in the substantia nigra pars compacta (SNc) mainly project to the dorsal striatum, as part of the nigrostriatal pathway. The mesocorticolimbic pathway involves a variety of behaviors and psychopathological states, such as depression, anxiety, feeding, and reward-related and goal-directed behaviors (Alberico et al., 2015). In Parkinson's disease (PD), an impaired dopaminergic mesocorticolimbic system is considered the leading cause of neuropsychiatric symptoms (Castrioto et al., 2016). In PD, degeneration of the DA neurons in the SNc is the most prominent symptom; in contrast, the DA neurons in the VTA are less affected (Ropper et al., 2019). Although some theories have been suggested, such as the variety of neurons found in the VTA (Nair-Roberts et al., 2008), lower expression of the dopamine transporters (Lammel et al., 2008), differences in calcium channel expression (Mosharov et al., 2009), levels of cytosolic DA, and the presence of α-synuclein (Mosharov et al., 2009; Pan and Ryan, 2012), it remains unclear why the VTA is relatively spared in PD.

It has been demonstrated that abnormal iron deposition may contribute to the damage of DA neurons in PD (Hare and Double, 2016). Quantitative susceptibility mapping (QSM) is more sensitive and can better detect increased iron in PD than R2 and R2* mapping (Barbosa et al., 2015). Using QSM, several research studies have shown that iron accumulation was both cross-sectionally and longitudinally increased in the substantia nigra (SN) in PD patients, and iron levels were correlated with clinical manifestations, using QSM (Bergsland et al., 2019; Sun et al., 2020; Uchida et al., 2020). In contrast, our knowledge of iron accumulation in the VTA in PD remains limited. A study on chronic 1-methyl-4-phenyl-1,2,3,6-tetrahydropyridine (MPTP)-treated PD mice detected an increased iron level in the SNc, but not in the VTA, and suggested that difference in iron deposition might be a reason contributing to the selective degeneration of DA neurons (Lv et al., 2011). So far, only one imaging study has investigated iron accumulation in the VTA in PD patients and found increased iron content (Ahmadi et al., 2020). However, as the primary purpose was to use transcranial sonography and QSM to localize the SN, the previous study did not investigate the iron levels at prodromal and different clinical stages of PD or the relationship between iron levels and clinical characteristics.

Thus, it is still unclear if increased iron deposition occurs in the VTA during the prodromal and early clinical stage of PD, whether iron accumulation increases as the disease becomes more severe, and whether iron deposition in the VTA correlates with clinical manifestations. Therefore, this study aimed to quantitatively evaluate iron contents in the VTA across the prodromal and different clinical stages of PD. Idiopathic rapid eye movement sleep behavior disorder (RBD) patients were included in the current study to evaluate iron content in the prodromal stage. RBD is considered a prodromal stage of α-synucleinopathies since RBD patients have a high rate of conversion to neurodegenerative disorders, especially α-synucleinopathies, such as PD, dementia with Lewy bodies, and multiple system atrophy (Schenck et al., 2013). We hypothesized that iron content in the VTA is not elevated in the early stage of PD but gradually increased as the disease becomes more severe. This study will help to clarify the pattern of iron deposition in the VTA and may provide an explanation of the selective damage of DA neurons in PD.

2. Materials and methods

2.1. Participants

This experiment was performed in accordance with the Declaration of Helsinki and was approved by the Institutional Review Board of Xuanwu Hospital of Capital Medical University. All participants (35 RBD patients, 101 PD patients, and 62 HCs) provided written consent before the experiment and were recruited from the Movement Disorders Clinic of the Xuanwu Hospital of Capital Medical University. The RBD patients were screened by the International Classification of Sleep Disorder-Third Edition diagnostic criteria (American Academy of Sleep Medicine, 2014) and were confirmed by polysomnography. PD patients were diagnosed by the MDS Clinical Diagnostic Criteria (Andrew et al., 1992). The inclusion criteria for HCs were (1) no family history of movement disorders, (2) no neurological or psychiatric diseases, and (3) no obvious cerebral lesions on structural images in magnetic resonance imaging (MRI).

The PD patients were evaluated using the Movement Disorder Society (MDS) Unified Parkinson's Disease Rating Scale, Part III (MDS-UPDRS III) and Hoehn and Yahr (H & Y) stage while off their anti-parkinsonian medicine for 12 h. The RBD patients were assessed by the Rapid Eye Movement Sleep Behavior Disorder Questionnaire–Hong Kong (RBDQ-HK) and the MDS-UPDRS III. In addition, all participants were evaluated using the Hamilton Depression Scale (HAMD), Montreal Cognitive Assessment (Chinese version; C-MoCA), Non-Motor Symptoms Scale for Parkinson's Disease (NMSS), Brief Smell Identification Test (BSIT), Epworth Sleepiness Scale (ESS), Pittsburgh Sleep Quality Index (PSQI), and Apathy Scale (AS). Demographic information is summarized in Table 1.

2.2. MRI data collection

MRI data were collected on a 3T MAGNETOM Skyra scanner (Siemens, Erlangen, Germany) using a 20-channel head coil. The signals from different coils were combined by the sum of squares method. A single-echo 3-dimensional (3-D) gradient echo (GRE) sequence was collected with the following parameters: voxel size = 0.667 × 0.667 × 1.5 mm^3, repetition time (TR) = 25 ms, echo time (TE) = 17.5 ms, slice thickness = 1.5 mm, flip angle = 15°, field of view (FoV) = 256 × 192 mm^2, and scanning time = 5 min 6 s. A whole-brain sagittal 3-D T1 magnetization-prepared rapid gradient echo (MP-RAGE) imaging was performed with the following parameter: voxel size = 1 × 1 × 1 mm^3, TR = 2,530 ms, TE = 2.98 ms, TI = 1,100 ms; slice thickness = 1 mm, flip angle = 7°, FoV = 256 × 224 mm^2, and scanning time = 5 min 13 s.

2.3. Image analysis

The QSM reconstruction was performed using MATLAB 2017b based STI Suite.[1] The phase images were unwrapped using a Laplacian-based algorithm method (Wu et al., 2012). The unwrapped phase images were used to remove the background field using the V-SHARP method (Li et al., 2014). The magnetic susceptibility was determined using streaking artifact reduction for QSM (STAR-QSM; Wei et al., 2015).

Image registration was performed using FMRIB Software Library (FSL) v6.0.[2] Individual 3D-T1 images were first skull stripped and registered to a standard space [Montreal Neurological Institute (MNI) 152] using FSL's FLIRT and FNIRT tools. The inverted warping field from standard to native space was then obtained by inverting the warping field. Thereafter, the individual 3D-T1 image was also registered to GRE's magnitude image using

1 https://people.eecs.berkeley.edu/~chunlei.liu/software.html

2 https://fsl.fmrib.ox.ac.uk/fsl/fslwiki/

TABLE 1 Demographic and clinical data of participants and the QSM values in ROIs.

	HC (mean ± SD) $n = 62$	RBD (mean ± SD) $n = 35$	PD (mean ± SD) $n = 101$	*P*	*P (post-hoc)*		
					HC vs. RBD	RBD vs. PD	HC vs. PD
Age	64.97 ± 5.76	65.86 ± 6.31	64.21 ± 6.67	0.388[a]	1	0.550	1
Sex (M/F)	25/37	21/14	54/47	0.123[a]	0.062	0.503	0.103
RBDQ-HK	7.11 ± 5.75	34.44 ± 13.69	20.89 ± 16.36	**<0.001**[a]	**<0.001**	**<0.001**	**<0.001**
HAMD	3.20 ± 3.10	5.76 ± 4.04	5.67 ± 3.96	**<0.001**[a]	**0.024**	1	**<0.001**
C-MoCA	26.00 ± 2.28	25.11 ± 2.84	23.76 ± 3.74	**0.001**[a]	0.781	0.212	**<0.001**
NMSS	14.04 ± 13.21	21.65 ± 13.54	38.77 ± 33.79	**<0.001**[a]	0.688	**0.013**	**<0.001**
BSIT	8.86 ± 2.48	7.37 ± 2.13	7.27 ± 2.91	**0.002**[a]	0.052	1	**0.002**
ESS	4.26 ± 2.98	5.47 ± 3.03	5.72 ± 3.26	0.061[a]	0.394	1	0.061
PSQI	6.21 ± 5.26	7.09 ± 4.09	6.09 ± 3.70	0.518[a]	1	0.793	1
AS	6.49 ± 6.30	9.35 ± 7.57	12.48 ± 9.04	**<0.001**[a]	0.508	0.360	**<0.001**
UPDRS III	-	5.09 ± 3.83	32.27 ± 13.68	-	-	-	-
Duration (year)	-	3.01 ± 1.48	4.85 ± 2.68	-	-	-	-
H & Y stage	-	-	1.97 ± 0.69	-	-	-	-
VTA_L (ppm)	0.0193 ± 0.003	0.0204 ± 0.003	0.0213 ± 0.002	**<0.001**[b]	0.174	0.341	**<0.001**
VTA_R	0.0197 ± 0.003	0.0208 ± 0.002	0.0214 ± 0.002	**<0.001**[b]	0.137	0.570	**<0.001**
SNc_L	0.0280 ± 0.011	0.0393 ± 0.014	0.0508 ± 0.022	**<0.001**[b]	**0.009**	**0.004**	**<0.001**
SNc_R	0.0263 ± 0.014	0.0398 ± 0.014	0.0467 ± 0.026	**0.001**[b]	**0.008**	0.240	**<0.001**

HC, healthy control; RBD, rapid eye movement sleep behavior disorder; PD, Parkinson's disease; M, male; F, female; RBDQ-HK, Rapid Eye Movement Sleep Behavior Disorder Questionnaire–Hong Kong; HAMD, Hamilton Depression Scale; C-MoCA, Montreal Cognitive Assessment (Chinese version); NMSS, Non-Motor Symptoms Scale for Parkinson's Disease; BSIT, Brief Smell Identification Test; ESS, Epworth Sleepiness Scale; PSQI, Pittsburgh Sleep Quality Index; AS, Apathy Scale; MDS-UPDRS III, Movement Disorder Society Unified Parkinson's Disease Rating Scale, Part III; VTA, ventral tegmental area; SNc, substantia nigra pars compacta; ppm, parts per million; L, left; R, right.
[a]ANOVA, analysis of variance.
[b]ANCOVA, analysis of covariance.
-, Not applicable. Bold values: $P < 0.05$.

the FLIRT tool to get a second warping field. Both warping fields were combined to converted to obtain warping fields covert MNI152 so that it was well-coregistered with individual's susceptibility map.

The VTA and SNc were defined by the California Institute of Technology (CIT) 168 atlas of subcortical nuclei (Pauli et al., 2018), with a threshold of 0.25. The CIT168 atlas divides the VTA into the parabrachial pigmented nucleus (PBP) and VTA nucleus. Using FSL, we merged the VTA nucleus and PBP into a whole VTA for two reasons: (1) there is little evidence that the VTA component nuclei represent neural populations specialized and distinct in function (Trutti et al., 2019) and (2) as a probabilistic atlas (Pauli et al., 2018), there is some overlap between the VTA nucleus and PBP. The bilateral SNc and merged VTA were used as the ROIs in the current study (Figure 1). The ROIs in standard MNI152 space were normalized to individual magnitude space using the above-mentioned warping fields using FSL. Finally, the individual ROIs were obtained in order to calculate QSM values.

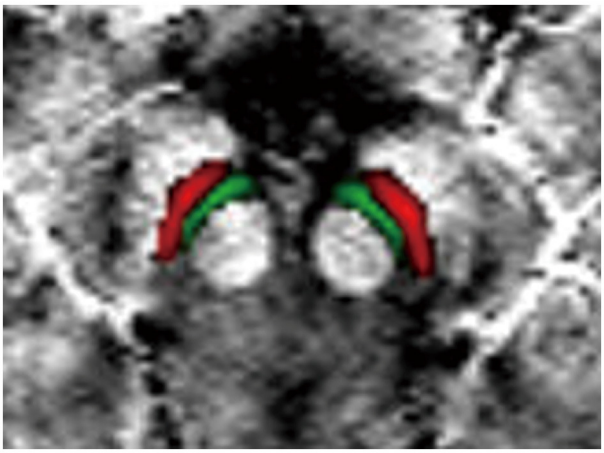

FIGURE 1
Definition of regions of interest (ROIs). The ROIs include the VTA (green) and SNc (red). VTA, ventral tegmental area; SNc, substantia nigra pars compacta.

2.4. Statistical analyses

The demographic and clinical characteristics of HC, RBD, and PD groups were compared using the analysis of variance (ANOVA). *Post-hoc* tests with Bonferroni correction were used for intergroup comparisons. The Pearson chi-square test was applied for sex frequency among the groups.

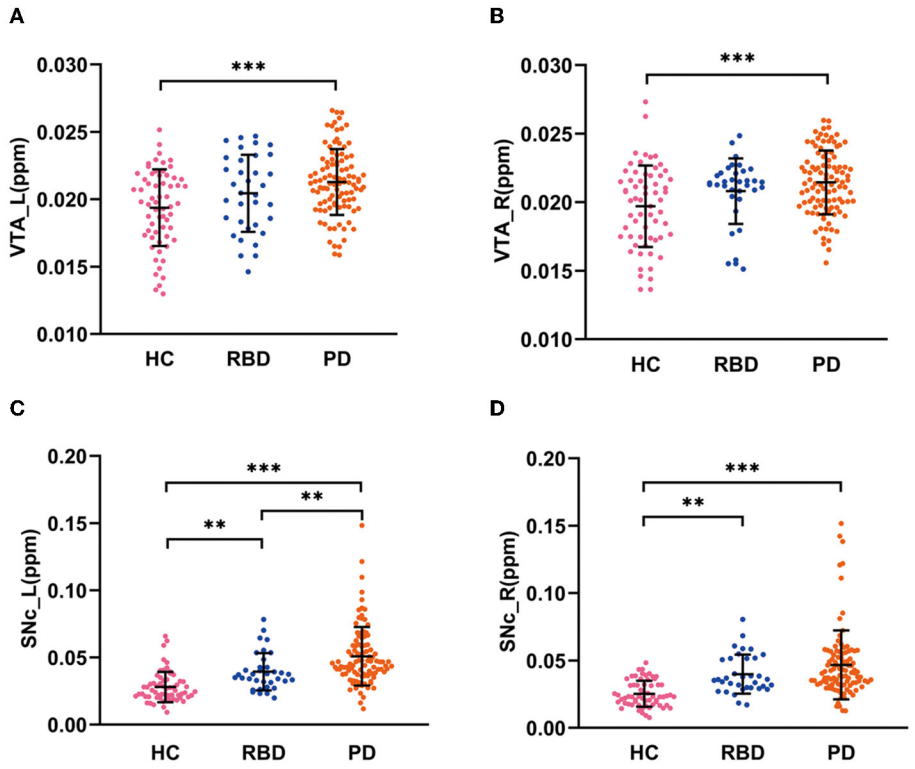

FIGURE 2
QSM values in the VTA and SNc in three groups. **(A, B)** QSM values in the VTA in HC, RBD, and PD groups. **(C, D)** QSM values in the SNc in HC, RBD, and PD groups. HC, healthy control; RBD, idiopathic rapid eye movement sleep behavior disorder; PD, Parkinson's disease. VTA, ventral tegmental area; SNc, substantia nigra pars compacta; ppm, parts per million; L, left; R, right. ***$P < 0.001$; **$P < 0.01$.

The normal distribution of QSM values was confirmed using the one-sample Kolmogorov–Smirnov test. The differences in QSM values among the three groups in each ROI were analyzed using the analysis of covariance (ANCOVA) with age and sex as covariables. *Post-hoc* tests with Bonferroni correction were used for intergroup comparisons ($P < 0.05$). In order to reveal the iron levels in different stages of PD, we further divided our PD patients into three subgroups according to the H & Y stage: 26 PD patients with H & Y stage 1 (PD-H&Y1), 43 PD patients with H & Y stage 1.5 and 2 (PD-H&Y2, including four patients with H & Y stage 1.5), and 32 PD patients with H & Y stage 2.5 and 3 (PD-H&Y3, including 14 patients with H & Y stage 2.5). The differences in QSM values among the HCs and three PD subgroups in each ROI were also analyzed using ANCOVA. *Post-hoc* tests with Bonferroni correction were used for intergroup comparisons ($P < 0.05$).

In addition, we calculated the mean QSM values of the bilateral VTA, as well as the differences in mean QSM values between the groups and the different H & Y stages.

Correlations between QSM values and clinical assessments in RBD and PD patients were performed using Pearson's correlation analysis, while Spearman's correlation analysis was used to analyze the correlation between H & Y stage and QSM values in PD patients. Statistical analyses were performed using IBM SPSS Statistics (version 20, IBM Corp, Armonk, NY, USA).

3. Results

No significant differences were observed among the three groups in age, sex, and PSQI (ANOVA, $P > 0.05$), while there were significant differences in RBDQ-HK, HAMD, C-MoCA, NMSS, BSIT, ESS, and AS scores (ANOVA, $P < 0.05$; Table 1).

There were significant differences in QSM values in the bilateral VTA and SNc among the HC, RBD, and PD groups (ANCOVA, $P < 0.001$). The RBD group did not show enhanced iron values in the bilateral VTA (*post-hoc* test, $P > 0.05$, Bonferroni corrected), but had increased iron values in the bilateral SNc (*post-hoc* test, $P < 0.01$, Bonferroni corrected) compared with HCs. PD patients had increased iron values in the bilateral VTA and SNc compared with HCs (*post-hoc* test, $P < 0.001$, Bonferroni corrected) and had enhanced iron values in the left SNc compared with RBD patients (*post-hoc* test, $P < 0.01$, Bonferroni corrected; Table 1 and Figures 2A–D).

The QSM values had significant differences among the HCs and three PD subgroups in the bilateral VTA and SNc (ANCOVA, $P < 0.001$). In the bilateral VTA, the PD-H&Y1 group did not show significantly higher iron values than the HC group (*post-hoc* test, $P > 0.05$, Bonferroni corrected), while the PD-H&Y2 and PD-H&Y3 groups showed higher values (*post-hoc* test, $P < 0.01$, Bonferroni corrected). In the left VTA, the PD-H&Y3 group had increased iron values compared with the PD-H&Y1 and PD-H&Y2 groups (*post-hoc* test, $P < 0.001$, Bonferroni corrected), while the

10.3389/fnagi.2023.1187684

TABLE 2 QSM values of HC and PD patients with different H & Y stages in ROIs.

	HC	PD-H&Y1	PD-H&Y2	PD-H&Y3	ANCOVA	*P (post-hoc)*					
	(mean ± SD)	(mean ± SD)	(mean ± SD)	(mean ± SD)	*P*	HC vs. PD-H&Y1	HC vs. PD-H&Y2	HC vs. PD-H&Y3	PD-H&Y1 vs. H&Y2	PD-H&Y2 vs. H&Y3	PD-H&Y1 vs. H&Y3
	n = 62	*n* = 26	*n* = 43	*n* = 32							
VTA_L	0.0193 ± 0.003	0.0194 ± 0.002	0.0210 ± 0.002	0.0232 ± 0.002	**<0.001**	1	**0.004**	**<0.001**	**0.037**	**0.001**	**<0.001**
VTA_R	0.0197 ± 0.003	0.0207 ± 0.002	0.0215 ± 0.002	0.0219 ± 0.002	**<0.001**	1	**0.004**	**0.001**	0.750	1	0.284
SNc_L	0.0280 ± 0.011	0.0414 ± 0.015	0.0450 ± 0.016	0.0661 ± 0.026	**<0.001**	**0.011**	**<0.001**	**<0.001**	1	**<0.001**	**<0.001**
SNc_R	0.0253 ± 0.010	0.0394 ± 0.013	0.0441 ± 0.023	0.0554 ± 0.030	**<0.001**	**0.035**	**<0.001**	**<0.001**	1	0.126	**0.019**

HC, healthy control; PD, Parkinson's disease; VTA, ventral tegmental area; SNc, substantia nigra pars compacta; L, left; R, right; ANCOVA, analysis of covariance. Bold values: $P < 0.05$.

PD-H&Y2 group also had an increase of iron values compared with the PD-H&Y1 group (*post-hoc* test, $P < 0.05$, Bonferroni corrected). In comparison to HCs, all three PD subgroups showed higher iron values in the bilateral SNc (*post-hoc* test, $P < 0.05$, Bonferroni corrected). The PD-H&Y3 group had increased iron values in the left SNc compared with the PD-H&Y1 and PD-H&Y2 groups (*post-hoc* test, $P < 0.001$, Bonferroni corrected) and had elevated iron values in the right SNc compared with the PD-H&Y1 group (*post-hoc* test, $P < 0.05$, Bonferroni corrected; Table 2 and Figures 3A, B).

We found significant differences in mean VTA QSM values between the groups and at different stages, which was similar to the results of the left and right VTA QSM values (Supplementary Tables 1, 2).

In PD patients, the QSM values in the left VTA were positively correlated with H & Y stage ($r = 0.543$, $p < 0.001$, Figure 4A), HAMD scores ($r = 0.275$, $p = 0.007$, Figure 4B), and NMSS ($r = 0.238$, $p = 0.027$, Figure 4C). In RBD patients, QSM values in the left SNc were positively correlated with disease duration ($r = 0.356$, $p = 0.045$) and RBDQ-HK scores ($r = 0.388$, $p = 0.023$), while QSM values in the right SNc were negatively correlated with BSIT scores ($r = -0.496$, $p = 0.008$). The QSM values in the bilateral SNc were positively correlated with disease duration (left: $r = 0.306$, $p = 0.002$; right: $r = 0.211$, $p = 0.034$). In addition, the QSM values in the left SNc were positively correlated with the H & Y stage ($r = 0.462$, $p < 0.001$), MDS-UPDRS III ($r = 0.250$, $p = 0.013$), and HAMD scores ($r = 0.233$, $p = 0.022$), while the QSM values in the right SNc were positively correlated with the AS scores ($r = 0.226$, $p = 0.045$) in PD patients.

4. Discussion

In the current study, we investigated iron accumulation in the VTA across different stages of PD. The novel finding is that iron contents are not increased in the RBD patients and PD patients at H & Y stage 1. The iron accumulation in the VTA becomes significant in PD patients at mid stages and advanced stages. QSM values in the left VTA positively correlate with the H & Y stage, NMSS, and HAMD scores in PD patients.

We found that both RBD and PD patients had enhanced iron contents in the bilateral SNc, which is consistent with previous reports (Guan et al., 2017; Sun et al., 2020). In contrast, there was no increased iron content in the VTA in RBD patients and PD patients at H & Y stage 1. Age-related iron accumulation might be an important factor contributing to neurodegeneration, as aging processes might compromise the iron homoeostatic system, leading to an excess of iron that is not efficiently chelated by storage proteins or other molecules (Killilea et al., 2004; Ward et al., 2014). An elevated level of iron deposition in PD may result from increased iron influx (Moos et al., 2007), loss of intracellular homeostasis (Zucca et al., 2017), or impaired iron efflux (Bonaccorsi di Patti et al., 2018). The interaction between excess iron and DA can produce neurotoxic intermediate or end-products, leading to the formation of DNA adducts, lipid peroxidation, loss of membrane integrity, and induction of apoptosis (Blum et al., 2001; Hare and Double, 2016). It has been approved that α-synuclein could form toxic

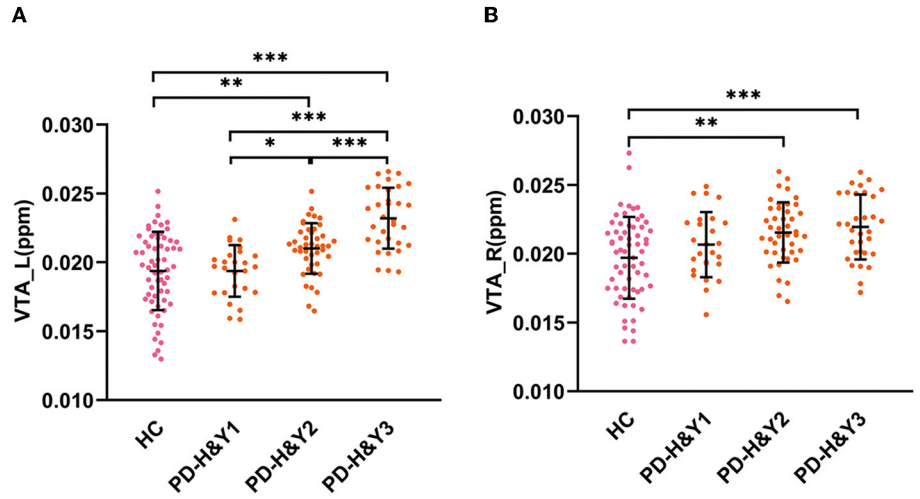

FIGURE 3
QSM values in the VTA in HCs and PD patients with different H & Y stages. **(A)** The QSM values in the left VTA; **(B)** the QSM values in the right VTA; HC, healthy control; PD, Parkinson's disease; H & Y stage, Hoehn and Yahr stage; VTA, ventral tegmental area; ppm, parts per million; L, left; R, right. ***$P < 0.001$; **$P < 0.01$; *$P < 0.05$.

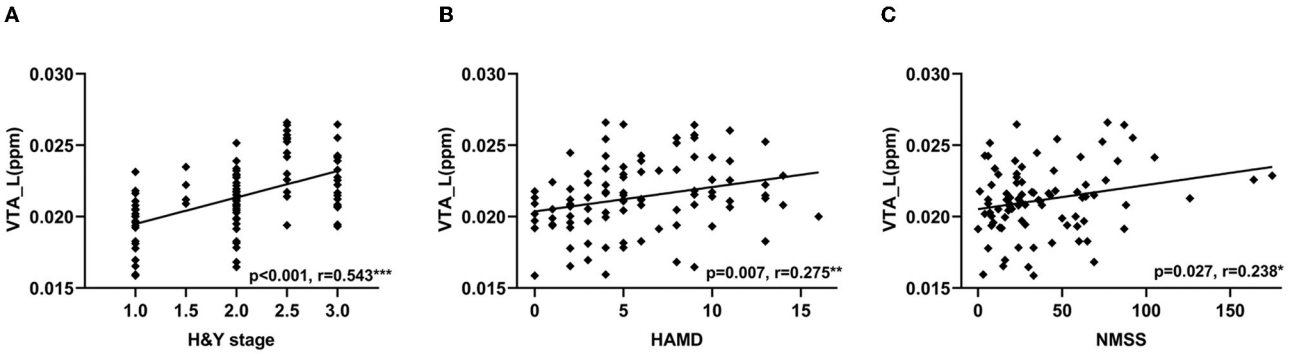

FIGURE 4
Correlations between QSM values in the VTA and clinical features in PD patients. Correlation between QSM values in the left VTA and H & Y stage **(A)**, HAMD **(B)**, and NMSS scores **(C)**. VTA, ventral tegmental area; QSM, quantitative susceptibility mapping; PD, Parkinson's disease; H & Y stage, Hoehn and Yahr stage; HAMD, Hamilton Depression Scale; NMSS, Non-Motor Symptoms Scale for Parkinson's Disease. ***$P < 0.001$; **$P < 0.01$; *$P < 0.05$.

aggregates in the presence of iron, which is considered to contribute to the formation of Lewy bodies in DA neurons via oxidative stress (Ostrerova-Golts et al., 2000). It has been proposed that the vulnerability of DA neurons requires redox load from a combination of relatively high iron and dopamine together (Hare et al., 2014). Therefore, increased iron deposition is believed to mediate the death of SNc dopaminergic neurons (Hare and Double, 2016). Previous studies have suggested that several reasons may relate to less damaged DA neurons in the VTA compared with SNc, such as the variety of neurons found in the VTA (Nair-Roberts et al., 2008), lower expression of the dopamine transporter (Lammel et al., 2008), differences in calcium channel expression and the presence of α-synuclein (Mosharov et al., 2009), differences in vesicular monoamine transporter-2 and neuromelanin (Liang et al., 2004), less degree of oxidative stress and more inducible copper-zinc superoxide dismutase activities (Hung and Lee, 1998), and more brain-derived neurotrophic factor mRNA gene expression (Hung and Lee, 1996). According to our findings, less accumulation of iron is also a likely reason contributing to the relatively spared DA neurons in the VTA during the prodromal and early clinical stages of PD.

The underlying reasons contributing to the less accumulation of iron in the VTA compared with SNc remain unclear. Previous studies on chronic MPTP-treated mice have suggested that misregulation of iron transporters, such as increased expression of divalent metal transporter 1 and decreased expression of ferroportin 1, might correlate with nigral iron accumulation. However, this pattern of misregulation of iron transporters was not detected in the VTA (Lv et al., 2011). These selective changes in iron transporters may help explain the differential iron accumulation in the SNc and VTA in PD.

Our PD patients at more than 1.5 H & Y staging had enhanced iron deposition in the VTA. This finding is consistent with a previous report (Ahmadi et al., 2020), in which PD patients with an average of 1.97 H & Y staging showed increased iron accumulation in the VTA compared with HC. In addition, the QSM values in the left VTA were positively correlated with the H & Y stage. These observations suggest that as the disease becomes more severe, iron deposition in the VTA becomes more significant, and may induce the death of DA neurons at the mid-stage and advanced stage of PD. Studies on the post-mortem brain of PD patients have proved that there was a 40–77% loss of DA neurons in the VTA (Alberico et al., 2015).

The neurons in the VTA project to extensive brain regions, including the nucleus accumbens, amygdala, prefrontal cortex, hippocampus, ventral pallidum, periaqueductal gray, bed nucleus of the stria terminalis, olfactory tubercle, and locus coeruleus, which are related to the various non-motor symptoms (Alberico et al., 2015; Morales and Margolis, 2017). However, only a small number of imaging studies have focused on the relationship between physiological changes in the VTA and clinical phenotypes of PD. The VTA showed an attenuated neural response to reward outcomes in PD patients (van der Vegt et al., 2013). Increased functional coupling between the VTA and default mode network has been reported in PD patients with freezing of gait (Steidel et al., 2021). In addition, increased functional connectivity between the VTA and anterior cingulate cortex was related to depression in PD (Wei et al., 2018). We found that the QSM values in the left VTA were positively correlated with NMSS and HAMD scores, which provides further support that damaged VTA is a reason contributing to non-motor symptoms, especially depression, in PD patients.

We found that only the iron contents of left VTA, not right VTA, were significantly correlated with clinical symptoms in PD patients. This phenomenon is likely due to the asymmetry of motor symptoms as most of our PD patients had right-side onset (65 of 101 patients). As our RBD patients did not show significant motor symptoms, we could not define the more- and less-affected sides in RBD patients. Thus, we only performed between-group comparisons of QSM values on the left and right sides.

In RBD patients, the QSM values in the SNc were positively correlated with disease duration, which is consistent with our previous report (Sun et al., 2020) and indicates that iron deposition in the SNc increases with the progression of RBD. In addition, the QSM values in the SNc correlated with RBDQ-HK and BSIT scores. Olfactory dysfunction is associated with an increased risk of developing PD, and RBD patients with hyposmia are at high risk for converting to PD (Lyu et al., 2021). These results suggest that iron accumulation in the SNc is associated with the severity of RBD and may have the potential to predict the conversion to α-synucleinopathies, which needs to be proved in future longitudinal studies.

In the bilateral SNc, PD patients had significantly enhanced iron contents, which is consistent with previous studies (He et al., 2015; Guan et al., 2017; Bergsland et al., 2019; Ahmadi et al., 2020; Sun et al., 2020; Fu et al., 2021), and the QSM values were positively correlated with disease duration and the H & Y stage (Du et al., 2016; Fu et al., 2021). The QSM values were positively correlated with the MDS-UPDRS III and HAMD scores in the left SNc (He et al., 2015; Fu et al., 2021) as well as the AS scores in the right SNc. The enhanced iron might aggravate the dysfunction of the nigrostriatal pathway with disease progression and severity (Hare and Double, 2016), which exacerbates the motor and non-motor symptoms. These findings suggest that the QSM technique has the potential to be a neuroimaging marker of disease progression, which needs to be examined in future longitudinal studies.

There are some limitations in our study. First, this is a cross-sectional study, and longitudinal studies are needed to reveal the progress of iron deposition in the VTA and its relationship with clinical progression. Second, as we only had a small number of patients at the H & Y stage 4, the iron accumulation in the VTA in more advanced PD patients was not investigated in the current study.

5. Conclusion

Using the QSM, we demonstrate that the iron content in the VTA is not enhanced in the prodromal and early clinical stage of PD but becomes significantly increased as the disorder becomes more severe. Moreover, the iron deposition in the VTA is associated with the non-motor symptoms in PD. Our findings may help to understand the iron deposition in the VTA at different stages of PD and its relationship with clinical manifestations of PD.

Data availability statement

The raw data supporting the conclusions of this article will be made available by the authors, without undue reservation.

Ethics statement

The studies involving human participants were reviewed and approved by Institutional Review Board of Xuanwu Hospital of Capital Medical University (2011-27). The patients/participants provided their written informed consent to participate in this study.

Author contributions

DZ and JY contributed to the organization and execution of the research project. DZ drafted the manuscript. DZ, JY, JS, JW, and LC contributed to the acquisition, post-processing, and analysis of the data. TW and HH revised the manuscript. All authors contributed to the article and approved the submitted version.

Funding

This research was supported by the National Natural Science Foundation of China (82071423), the Fundamental Research

Funds for the Central Universities (226-2023-00095), and the Open Research Fund of the State Key Laboratory of Cognitive Neuroscience and Learning.

Acknowledgments

The authors would like to thank the participants who have contributed to this research.

Conflict of interest

The authors declare that the research was conducted in the absence of any commercial or financial relationships that could be construed as a potential conflict of interest.

Publisher's note

All claims expressed in this article are solely those of the authors and do not necessarily represent those of their affiliated organizations, or those of the publisher, the editors and the reviewers. Any product that may be evaluated in this article, or claim that may be made by its manufacturer, is not guaranteed or endorsed by the publisher.

Supplementary material

The Supplementary Material for this article can be found online at: https://www.frontiersin.org/articles/10.3389/fnagi.2023.1187684/full#supplementary-material

References

Ahmadi, S. A., Botzel, K., Levin, J., Maiostre, J., Klein, T., Wein, W., et al. (2020). Analyzing the co-localization of substantia nigra hyper-echogenicities and iron accumulation in Parkinson's disease: a multi-modal atlas study with transcranial ultrasound and MRI. *Neuroimage Clin.* 26, 102185. doi: 10.1016/j.nicl.2020.102185

Alberico, S. L., Cassell, M. D., and Narayanan, N. S. (2015). The vulnerable ventral tegmental area in Parkinson's disease. *Basal Ganglia* 5, 51–55. doi: 10.1016/j.baga.2015.06.001

American Academy of Sleep Medicine (2014). *International Classification of Sleep Disorders, 3rd Edn.* Darien, IL: American Academy of Sleep Medicine.

Andrew, J. H., Susan, E. D., Linda, K., and Andrew, J. L. (1992). Accuracy of clinical diagnosis of idiopathic Parkinson's disease: a clinico-pathological study of 100 cases. *J. Neurol. Neurosurg. Psychiatry* 55, 181–184. doi: 10.1136/jnnp.55.3.181

Barbosa, J. H., Santos, A. C., Tumas, V., Liu, M., Zheng, W., Haacke, E. M., et al. (2015). Quantifying brain iron deposition in patients with Parkinson's disease using quantitative susceptibility mapping, R2 and R2. *Magn. Reson. Imag.* 33, 559–565. doi: 10.1016/j.mri.2015.02.021

Bergsland, N., Zivadinov, R., Schweser, F., Hagemeier, J., Lichter, D., and Guttuso, T. Jr. (2019). Ventral posterior substantia nigra iron increases over 3 years in Parkinson's disease. *Mov. Disord.* 34, 1006–1013. doi: 10.1002/mds.27730

Blum, D., Torch, S., Lambeng, N., Nissou, M.-F., Benabid, A.-L., Sadoul, R., et al. (2001). Molecular pathways involved in the neurotoxicity of 6-OHDA, dopamine and MPTP: contribution to the apoptotic theory in Parkinson's disease. *Prog. Neurobiol.* 65, 135–172. doi: 10.1016/S0301-0082(01)00003-X

Bonaccorsi di Patti, M. C., Cutone, A., Polticelli, F., Rosa, L., Lepanto, M. S., Valenti, P., et al. (2018). The ferroportin-ceruloplasmin system and the mammalian iron homeostasis machine: regulatory pathways and the role of lactoferrin. *Biometals* 31, 399–414. doi: 10.1007/s10534-018-0087-5

Castrioto, A., Thobois, S., Carnicella, S., Maillet, A., and Krack, P. (2016). Emotional manifestations of PD: neurobiological basis. *Mov. Disord.* 31, 1103–1113. doi: 10.1002/mds.26587

Du, G., Liu, T., Lewis, M. M., Kong, L., Wang, Y., Connor, J., et al. (2016). Quantitative susceptibility mapping of the midbrain in Parkinson's disease. *Mov. Disord.* 31, 317–324. doi: 10.1002/mds.26417

Fu, X., Deng, W., Cui, X., Zhou, X., Song, W., Pan, M., et al. (2021). Time-specific pattern of iron deposition in different regions in Parkinson's disease measured by quantitative susceptibility mapping. *Front. Neurol.* 12, 631210. doi: 10.3389/fneur.2021.631210

Guan, X., Xuan, M., Gu, Q., Huang, P., Liu, C., Wang, N., et al. (2017). Regionally progressive accumulation of iron in Parkinson's disease as measured by quantitative susceptibility mapping. *NMR Biomed.* 30, 3489. doi: 10.1002/nbm.3489

Hare, L. P., Ayton, S., Roberts, B. R., Grimm, R., George, J. L., Bishop, D. P., et al. (2014). An iron–dopamine index predicts risk of parkinsonian neurodegeneration in the substantia nigra pars compacta. *Chem. Sci.* 5, 2160–2169. doi: 10.1039/C3SC53461H

Hare, L. P., and Double, K. L. (2016). Iron and dopamine: a toxic couple. *Brain* 139, 1026–1035. doi: 10.1093/brain/aww022

He, N., Ling, H., Ding, B., Huang, J., Zhang, Y., Zhang, Z., et al. (2015). Region-specific disturbed iron distribution in early idiopathic Parkinson's disease measured by quantitative susceptibility mapping. *Hum. Brain Mapp.* 36, 4407–4420. doi: 10.1002/hbm.22928

Hung, H. C., and Lee, E. (1996). The mesolimbic dopaminergic pathway is more resistant than the nigrostriatal dopaminergic pathway to MPTP and MPP+ toxicity: role of BDNF gene expression. *Mol. Brain Res.* 41, 16–26. doi: 10.1016/0169-328X(96)00062-9

Hung, H. C., and Lee, E. (1998). MPTP produces differential oxidative stress and antioxidative responses in the nigrostriatal and mesolimbic dopaminergic pathways. *Free Radic. Biol. Med.* 24, 76–84. doi: 10.1016/S0891-5849(97)00206-2

Killilea, D., Wong, S., Cahaya, H., Atamna, H., and Ames, B. (2004). Iron accumulation during cellular senescence. *Ann. N. Y. Acad. Sci.* 1019, 365–367. doi: 10.1196/annals.1297.063

Lammel, S., Hetzel, A., Hackel, O., Jones, I., Liss, B., and Roeper, J. (2008). Unique properties of mesoprefrontal neurons within a dual mesocorticolimbic dopamine system. *Neuron* 57, 760–773. doi: 10.1016/j.neuron.2008.01.022

Li, W., Wu, B., Batrachenko, A., Bancroft-Wu, V., Morey, R. A., Shashi, V., et al. (2014). Differential developmental trajectories of magnetic susceptibility in human brain gray and white matter over the lifespan. *Hum. Brain Mapp.* 35, 2698–2713. doi: 10.1002/hbm.22360

Liang, C. L., Nelson, O., Yazdani, U., Pasbakhsh, P., and German, D. C. (2004). Inverse relationship between the contents of neuromelanin pigment and the vesicular monoamine transporter-2: human midbrain dopamine neurons. *J. Comp. Neurol.* 473, 97–106. doi: 10.1002/cne.20098

Lv, Z., Jiang, H., Xu, H., Song, N., and Xie, J. (2011). Increased iron levels correlate with the selective nigral dopaminergic neuron degeneration in Parkinson's disease. *J. Neural Transm.* 118, 361–369. doi: 10.1007/s00702-010-0434-3

Lyu, Z., Zheng, S., Zhang, X., Mai, Y., Pan, J., Hummel, T., et al. (2021). Olfactory impairment as an early marker of Parkinson's disease in REM sleep behaviour disorder: a systematic review and meta-analysis. *J. Neurol. Neurosurg. Psychiatry* 92, 271–281. doi: 10.1136/jnnp-2020-325361

Moos, T., Nielsen, T. R., Skjorringe, T., and Morgan, E. H. (2007). Iron trafficking inside the brain. *J. Neurochem.* 103, 1730–1740. doi: 10.1111/j.1471-4159.2007.04976.x

Morales, M., and Margolis, E. B. (2017). Ventral tegmental area: cellular heterogeneity, connectivity and behaviour. *Nat. Rev. Neurosci.* 18, 73–85. doi: 10.1038/nrn.2016.165

Mosharov, E. V., Larsen, K. E., Kanter, E., Phillips, K. A., Wilson, K., Schmitz, Y., et al. (2009). Interplay between cytosolic dopamine, calcium, and alpha-synuclein causes selective death of substantia nigra neurons. *Neuron* 62, 218–229. doi: 10.1016/j.neuron.2009.01.033

Nair-Roberts, R. G., Chatelain-Badie, S. D., Benson, E., White-Cooper, H., Bolam, J. P., and Ungless, M. A. (2008). Stereological estimates of dopaminergic, GABAergic and glutamatergic neurons in the ventral tegmental area, substantia nigra and retrorubral field in the rat. *Neuroscience* 152, 1024–1031. doi: 10.1016/j.neuroscience.2008.01.046

Ostrerova-Golts, N., Petrucelli, L., Hardy, J., Lee, J., Farer, M., and Wolozin, B. (2000). The A53T a-synuclein mutation increases iron-dependent aggregation and toxicity. *J. Neurosci.* 20, 6048–6054. doi: 10.1523/JNEUROSCI.20-16-06048.2000

Pan, P. Y., and Ryan, T. A. (2012). Calbindin controls release probability in ventral tegmental area dopamine neurons. *Nat. Neurosci.* 15, 813–815. doi: 10.1038/nn.3099

Pauli, W. M., Nili, A. N., and Tyszka, J. M. (2018). A high-resolution probabilistic *in vivo* atlas of human subcortical brain nuclei. *Sci. Data* 5, 180063. doi: 10.1038/sdata.2018.63

Ropper, A. H., Samuels, M. A., Klein, J., and Prasad, S. (2019). *Adams And Victor's Principles Of Neurology. 11th Edn*. New York, NY: McGraw-Hill Education Medical.

Schenck, C. H., Boeve, B. F., and Mahowald, M. W. (2013). Delayed emergence of a parkinsonian disorder or dementia in 81% of older men initially diagnosed with idiopathic rapid eye movement sleep behavior disorder: a 16-year update on a previously reported series. *Sleep Med.* 14, 744–748. doi: 10.1016/j.sleep.2012.10.009

Steidel, K., Ruppert, M. C., Palaghia, I., Greuel, A., Tahmasian, M., Maier, F., et al. (2021). Dopaminergic pathways and resting-state functional connectivity in Parkinson's disease with freezing of gait. *Neuroimage Clin.* 32, 102899. doi: 10.1016/j.nicl.2021.102899

Sun, J., Lai, Z., Ma, J., Gao, L., Chen, M., Chen, J., et al. (2020). Quantitative evaluation of iron content in idiopathic rapid eye movement sleep behavior disorder. *Mov. Disord.* 35, 478–485. doi: 10.1002/mds.27929

Trutti, A. C., Mulder, M. J., Hommel, B., and Forstmann, B. U. (2019). Functional neuroanatomical review of the ventral tegmental area. *Neuroimage* 191, 258–268. doi: 10.1016/j.neuroimage.2019.01.062

Uchida, Y., Kan, H., Sakurai, K., Inui, S., Kobayashi, S., Akagawa, Y., et al. (2020). Magnetic susceptibility associates with dopaminergic deficits and cognition in Parkinson's disease. *Mov. Disord.* 35, 1396–1405. doi: 10.1002/mds.28077

van der Vegt, J. P., Hulme, O. J., Zittel, S., Madsen, K. H., Weiss, M. M., Buhmann, C., et al. (2013). Attenuated neural response to gamble outcomes in drug-naive patients with Parkinson's disease. *Brain* 136, 1192–1203. doi: 10.1093/brain/awt027

Ward, R. J., Zucca, F. A., Duyn, J. H., Crichton, R. R., and Zecca, L. (2014). The role of iron in brain ageing and neurodegenerative disorders. *Lancet Neurol.* 13, 1045–1060. doi: 10.1016/S1474-4422(14)70117-6

Wei, H., Dibb, R., Zhou, Y., Sun, Y., Xu, J., Wang, N., et al. (2015). Streaking artifact reduction for quantitative susceptibility mapping of sources with large dynamic range. *NMR Biomed.* 28, 1294–1303. doi: 10.1002/nbm.3383

Wei, L., Hu, X., Yuan, Y., Liu, W., and Chen, H. (2018). Abnormal ventral tegmental area-anterior cingulate cortex connectivity in Parkinson's disease with depression. *Behav. Brain Res.* 347, 132–139. doi: 10.1016/j.bbr.2018.03.011

Wu, B., Li, W., Guidon, A., and Liu, C. (2012). Whole brain susceptibility mapping using compressed sensing. *Magn. Reson. Med.* 67, 137–147. doi: 10.1002/mrm.23000

Zucca, F. A., Segura-Aguilar, J., Ferrari, E., Munoz, P., Paris, I., Sulzer, D., et al. (2017). Interactions of iron, dopamine and neuromelanin pathways in brain aging and Parkinson's disease. *Prog. Neurobiol.* 155, 96–119. doi: 10.1016/j.pneurobio.2015.09.012

frontiers | Frontiers in Aging Neuroscience

TYPE Original Research
PUBLISHED 04 July 2023
DOI 10.3389/fnagi.2023.1156265

OPEN ACCESS

EDITED BY
Huaibin Cai,
National Institute on Aging (NIH), United States

REVIEWED BY
Zhiquan Li,
University of Copenhagen, Denmark
Xiao-Gang Zhou,
Southwest Medical University, China

*CORRESPONDENCE
Qin-Li Wan
✉ wanqinli@hotmail.com
Kwok-Fai So
✉ hrmaskf@hku.hk

†These authors have contributed equally to this work and share first authorship

RECEIVED 01 February 2023
ACCEPTED 20 June 2023
PUBLISHED 04 July 2023

CITATION
Zheng J, Luo Z, Chiu K, Li Y, Yang J, Zhou Q, So K-F and Wan Q-L (2023) *Lycium barbarum* glycopeptide prolong lifespan and alleviate Parkinson's disease in *Caenorhabditis elegans*. *Front. Aging Neurosci.* 15:1156265. doi: 10.3389/fnagi.2023.1156265

Lycium barbarum glycopetide prolong lifespan and alleviate Parkinson's disease in *Caenorhabditis elegans*

Jingming Zheng[1†], Zhenhuan Luo[1†], Kin Chiu[2†], Yimin Li[1], Jing Yang[3], Qinghua Zhou[3], Kwok-Fai So[4*] and Qin-Li Wan[1*]

[1]Department of Pathogen Biology, School of Medicine, Jinan University, Guangzhou, Guangdong, China, [2]State Key Lab of Brain and Cognitive Sciences, Department of Psychology, The University of Hong Kong, Hong Kong, Hong Kong SAR, China, [3]Faculty of Medical Science, The Biomedical Translational Research Institute, Jinan University, Guangzhou, Guangdong, China, [4]Guangdong-Hongkong-Macau Institute of Central Nervous System (CNS) Regeneration, Ministry of Education Central Nervous System (CNS) Regeneration Collaborative Joint Laboratory, Jinan University, Guangzhou, Guangdong, China

Introduction: *Lycium barbarum* glycopeptide (LbGp) is the main bioactive compound extracted from the traditional Chinese medicine. *L. barbarum* berries and has been proven to have numerous health benefits, including antioxidative, anti-inflammatory, anticancer, and cytoprotective activities. However, the antiaging effect of LbGp remains unknown.

Methods: The lifespan and body movement of *C. elegans* were used to evaluate the effect of LbGp on lifespan and health span. The thrashing assay was used to determine the role of LbGp in Parkinson's disease. To investigate the mechanisms of LbGp-induced antiaging effects, we analyzed changes in lifespan, movement, and the expression of longevity-related genes in a series of worm mutants after LbGp treatment.

Results: We found that LbGp treatment prolonged the lifespan and health span of *C. elegans*. Mechanistically, we found that LbGp could activate the transcription factors DAF-16/FOXO, SKN-1/Nrf2, and HSF-1, as well as the nuclear receptor DAF-12, thereby upregulating longevity-related genes to achieve lifespan extension. In addition, we found that the lifespan extension induced by LbGp partially depends on mitochondrial function. Intriguingly, LbGp also ameliorated neurodegenerative diseases such as Parkinson's disease in a DAF-16-, SKN-1-, and HSF-1-dependent manner.

Conclusion: Our work suggests that LbGp might be a viable candidate for the treatment and prevention of aging and age-related diseases.

KEYWORDS

***Lycium barbarum* glycopeptide, *Caenorhabditis elegans*, antiaging, Parkinson's disease, health span**

1. Introduction

Aging, an intrinsic biological process of life, is commonly characterized as a progressive loss of physiological integrity, eventually leading to organ failure (Moskalev et al., 2022). This deterioration of aging is the principal risk factor for many chronic diseases, such as cancer, neurodegenerative disorders, diabetes and cardiovascular diseases (Niccoli and Partridge, 2012). Currently, the percentage of the population over the age of 65 years old

has been increasing steadily, which has led to a global burden of age-related chronic diseases (Stegemann et al., 2010). Therefore, slowing the rate of biological aging and the progression of aging-associated diseases will considerably improve the quality of human life. For years, people have been searching for and discovering many natural substances that can prevent aging and aging-related diseases. For example, previous studies have shown that numerous plant extracts and natural bioactive products, such as usnic acid (Xiao et al., 2022), urolithin (Ryu et al., 2016), resveratrol (Park et al., 2012), saponins isolated from *Radix polygalae* (Zeng et al., 2021), and flavonoids from *Lycium barbarum* (*L. barbarum*) leaves (Niu et al., 2022), have lifespan-extending properties in different organism models.

Plant polysaccharides play increasingly important roles in human health and nutrition due to their multiple physiological activities and pharmacological functions (Wang et al., 2020). The berries of *L. barbarum* (*Goji*) (a Solanaceous defoliated shrubbery), a well-known traditional Chinese medicine and super functional food, contain a variety of health-promoting bioactive compounds with numerous nutritional and pharmacological functions (Jin et al., 2013). *L. barbarum* polysaccharides (LBPs) are the main functional constituents of *L. barbarum* and are composed of a variety of acidic heteropolysaccharides and polypeptides or proteins (Masci et al., 2018). Numerous studies have shown different biological activities of LBPs, including antioxidation (Liang et al., 2021), anticancer effects (Mao et al., 2011), antiaging effects (Tang et al., 2019; Zhang et al., 2019), immunoregulation (Ding et al., 2019), reproductive protection, and cytoprotective activity (Zhang et al., 2020). Among them, increasing attention has been given to the functions of LBPs in antioxidative stress and antiaging. Recently, researchers have deeply excavated the main antiaging active ingredients in LBPs and elucidated the underlying molecular mechanisms. For example, Huang W. et al. (2022) showed that the arabinogalactan-protein complex LBGP70 from crude LBPs were able to delay cellular senescence by activating aging-related genes. Zhang et al. (2022) revealed that the acidic heteropolysaccharide LFP-05S from LBPs could prolong the lifespan and enhance stress resistance in *Caenorhabditis elegans* (*C. elegans*) by eliminating unfavorable ROS overproduction.

Recently, researchers further separated and purified LBPs and obtained another component, *L. barbarum* glycopeptide (LbGp), which is the most promising monomeric substance (Peng et al., 2001). LbGp is a kind of glycoprotein whose monosaccharide composition includes glucose, arabinose and galactose and contains 30% protein linked to glycans by O-linkages (Tian, 1995). Accumulating evidence has shown that LbGp protects the kidney, promotes reproduction, enhances immunity, and exerts antitumor and anti-inflammatory effects (Gong et al., 2020; Zhou et al., 2022). The pharmacological functions of LbGp have many similarities with LBPs but also have many differences. For example, previous studies have shown that both LBPs and LbGp can maintain the balance of the intestinal environment by promoting the growth of probiotics, but their effects on the abundance of different types of gut microflora, such as *Akkermansia* and *Alistipes,* are distinctly different (Huang Y. et al., 2022). Therefore, it is valuable to deeply explore the pharmacological activities and underlying molecular mechanisms of LbGp. Considering that LBPs have antioxidant, antiaging and neuroprotective effects, and LbGp is the main active ingredient in LBP, we questioned whether and how LbGp plays a role in ameliorating aging and aging-related disease. Therefore, in this study, we used *C. elegans* to explore the longevity effect of LbGp and its underlying molecular mechanisms.

The nematode *C. elegans* is a robust multicellular model organism with multiple advantages, including a short life cycle, simple physiological structure and easy procedures for manipulation (Wan et al., 2021). Most aging-associated signaling pathways are evolutionarily conserved between *C. elegans* and mammals, including the insulin/insulin-like growth factor signaling (IIS) pathway, dietary restriction (DR)-related pathway, reproductive signaling pathway and mitochondrial dysfunction-related pathways (Xiao et al., 2022). Therefore, *C. elegans* has been widely used in aging research and screening of natural bioactive extracts with antiaging effects (Park et al., 2012; Ryu et al., 2016; Zeng et al., 2021; Xiao et al., 2022).

Our results showed that LbGp significantly increased the lifespan and health span and ameliorated PD-related features in *C. elegans*. Further studies revealed that several aging-related signaling pathways, including the IIS pathway, reproductive signaling pathway and mitochondrial function, were involved in the LbGp-induced longevity effect.

2. Materials and methods

2.1. Reagents, *C. elegans* strains, and maintenance

Lycium barbarum glycopeptide (LbGp) was provided by Ningxia Tianren Goji Biotechnology. LbGp was dissolved in water, and all NGM plates with LbGp were equilibrated overnight before use.

The *Caenorhabditis* Genetics Center (University of Minnesota, Minneapolis, MN, USA) provided the *C. elegans* strains used in this study: wild-type Bristol N2, GR1310 *akt-1(mg144)V,* CB1370 *daf-2(e1370)III,* CF1038 *daf-16(mu86)I,* PS3551 *hsf-1(sy441)I,* CF1903 *glp-1(e2144)III,* AA86 *daf-12(rh61rh411)X,* CB4876 *clk-1(e2519)III,* MQ887 *isp-1(qm150)IV,* RB754 *aak-2(ok524)X,* CF1553 muIs84 [(pAD76)*sod-3p*::GFP + *rol-6(su1006)*], CL2070 dvIs70 [*hsp-16.2p*::GFP + *rol-6(su1006)*], and UM0010 *dat-1p*::GFP; *aex-3p*::α-*syn*(A53T). New strains were generated by standard genetic crosses, and genotypes were confirmed by PCR or sequencing. Here, UM0010 was crossed with CF1038, PS3551, and AA86 to create the double mutants *daf-16(mu86)I; dat-1p*::GFP; *aex-3p*::α-*syn*(A53T), *hsf-1(sy441)I; dat-1p*::GFP; *aex-3p*::α-*syn*(A53T), and *daf-12(rh61rh411)X; dat-1p*::GFP; *aex-3p*::α-*syn*(A53T). All strains were grown and maintained using standard protocols (Jia et al., 2022).

2.2. Lifespan assays

All lifespan experiments, except for those with the CF1903 strains, were performed according to the standard protocols at 20°C, as previously described (Jia et al., 2022). In brief, approximately 100–150 young adult worms were picked into fresh plates containing different concentrations of LbGp and 10 μM *5-fluoro-2′-deoxyuridine* (FUDR, Sigma), which was used to prevent

progeny production. For CF1903, the synchronized L1 worms were grown at 20°C for 12 h, transferred to 25°C until the young adult stage to eliminate the germline, and finally returned to 20°C for the lifespan assays. For all lifespan assays, heat-inactivated (65°C, 30 min) *Escherichia coli* OP50 was used as food to prevent the metabolism of LbGp by bacteria. Worms were transferred to fresh plates with LbGp every other day. Death events were scored daily, and the lifespan assays were repeated three times. Statistical analyses were performed using the SPSS package, and the *P*-value was determined by the log-rank (Mantel-Cox) method. *P*-value < 0.05 was considered statistically significant. The mean, SEM, *P*-value and lifespan value are summarized in **Supplementary Table 1**.

2.3. Movement assays

The body movement assays were performed using the standard protocol as previously described (Jia et al., 2022). In brief, approximately 150 young adult worms were transferred to plates with or without LbGp at 20°C and maintained as described in the lifespan assays. Then, the movement of the worms was scored daily. When the plates were tapped, the worms moving in a continuous and coordinated sinusoidal pattern were defined to have fast movement; otherwise, they were defined as having non-fast movement.

2.4. Thrashing assays

The synchronized L1 PD model worms were grown at 20°C on NGM plates to the young adult stage, transferred to FUDR-containing plates with or without LbGp at 25°C and maintained as described in the lifespan assays. Day 5 worms were picked into a drop of M9 buffer, and the thrashing was recorded for 30 s at × 0.75 magnification with a Motic stereomicroscope as previously described (Huang et al., 2021). At least 30 worms were counted per experiment, and the thrashing assays were repeated three times.

2.5. RNA extraction and quantitative RT-PCR

The synchronized L1 worms were grown on plates with or without LbGp to the young adult stage, collected in M9 buffer and washed several times. Worm samples were resuspended using AG RNA^{ex} PRO reagent (Accurate Biology, Changsha, China), and total RNA was isolated by chloroform extraction and isopropanol precipitation. Then, 500 ng RNA was used to synthesize cDNA with a high-capacity cDNA transcription kit (RK20400, ABclonal, Wuhan, China). Quantitative RT-PCR was performed using SYBR Green Select Master Mix (RK21203, ABclonal, Wuhan, China) on a LightCycler480 real-time system (Roche, USA), and each assay was repeated three times. The mRNA expression of the genes was quantified after normalization to the reference gene *cdc-42*, and the *P*-value was computed using the two-tailed Student's *t*-test. The primers used in this study are shown in **Supplementary Table 2**.

2.6. Fluorescence microscopy and image analyses

For analysis of the fluorescence intensity of *sod-3p*::GFP and *hsp-16.2p*::GFP, the CF1553 and CL2070 strains were grown on plates with or without LbGp to the young adult stage. For CF1553, animals were picked onto 2% agar pads after anesthetizing with 10 μM levamisole, and then, the fluorescence was observed under a Nikon Ti2-U microscope with a 20 × air objective. For CL2070, young adult worms were heated at 35°C for 2 h to stimulate the expression of *hsp-16.2p*::GFP. After recovery at 20°C for 12 h, the CL2070 worms were observed using a Nikon Ti2-U fluorescence microscope with a 20 × air objective. The fluorescence intensity was quantified using ImageJ software. At least 30 animals were used in each group. The *P*-value was calculated by the two-tailed Student's *t*-test.

2.7. Measurement of reactive oxygen species (ROS)

2′7′-Dichlorofluorescein diacetate (H2DCF-DA) was used to detect the levels of intracellular ROS. The synchronized L1 worms were grown on plates with or without LbGp to the young adult stage, transferred to plates with 10 μM H2DCF-DA and incubated for 1 h. In addition, to create oxidative stress conditions, worms were treated with 5 mM paraquat for 12 h before staining with H2DCF-DA. Then, animals were picked onto 2% agar pads after anesthetizing with 10 μM levamisole, and the fluorescence was observed under a Nikon Ti2-U microscope with a 20 × air objective. The fluorescence intensity was quantified using ImageJ software. At least 30 animals were used in each group. The *P*-value was calculated by the two-tailed Student's *t*-test.

2.8. Western blot analyses

CF1553 and CL2070 worms were treated and maintained as described in the section on quantification of fluorescence intensity. Worms were collected in M9 buffer, subjected to three rounds of freezing and thawing, and then lysed in RIPA buffer. The protein samples were boiled at 95°C for 5 min after quantification using a BCA Protein Assay Kit. Next, the protein samples were separated by SDS-PAGE and transferred to PVDF membranes. The membranes were then blocked in 5% milk and incubated with primary antibodies against β-actin (1:5,000, Sigma-Aldrich, A1978) or GFP (1:5,000, Roche, 11814460001). The primary antibodies were visualized by horseradish peroxidase-conjugated anti-mouse secondary antibody and ECL Western Blotting Substrate.

2.9. Statistical analyses

The lifespan statistical analyses were performed using the SPSS package, and survival analyses were conducted using the Kaplan-Meier method. *P*-value was determined by log-rank (Mantel-Cox) test for individual experiments. Other data were analyzed

by the two-tailed Student's *t*-test. Statistical significance was defined as $P < 0.05$ and represented as stars ($^{*}P < 0.05$, $^{**}P < 0.01$, and $^{***}P < 0.001$). All experiments were repeated three times independently.

3. Results

3.1. LbGp enhances lifespan and ameliorates PD-related features in *C. elegans*

To determine whether LbGp plays a role in lifespan regulation, we treated adult worms with different doses of LbGp (200, 400, 600, and 800 μg/mL) and recorded their survival. We found that LbGp dose-dependently enhanced the lifespan of wild-type N2 worms (**Figures 1A, B**), with 600 μg/mL LbGp showing the best lifespan extension effect (**Figures 1A, B**). Therefore, 600 μg/mL was selected as the optimal concentration in all subsequent experiments. We also investigated the effect of LbGp on the health span by examining the effect of LbGp on body movement, an aging-related parameter (Huang et al., 2004). The results showed that the period of fast movement was significantly prolonged when worms were treated with LbGp compared with that of the untreated controls (**Figure 1C**). Taken together, these results demonstrated that LbGp not only prolonged lifespan but also had pronounced health span effects in *C. elegans*, with a concentration of 600 μg/mL showing the best effect.

Given that LbGp can extend lifespan and health span, we asked whether it could have benefits on aging-related diseases, such as Parkinson's disease (PD). UM0010 is a well-characterized PD model in *C. elegans* by pan-neuron overexpression of human α-synuclein (A53T), which recapitulates some distinct characteristics of PD, including the loss of dopaminergic neurons and motor deficits (Deng and Yuan, 2014). Using UM0010 transgenic worms, we found that LbGp significantly increased the rate of body bending of UM0010 worms at Day 5 (**Figure 1D**) through a thrashing assay, suggesting that LbGp could ameliorate PD features in *C. elegans*.

3.2. LbGp-induced lifespan extension requires the IIS pathway

We next determined which molecular mechanisms contribute to the lifespan extension conferred by LbGp. The transcription factor DAF-16, a homolog of human Forkhead box O (FOXO), is one of the main downstream regulators of oxidative stress resistance and the aging process (Li et al., 2019). DAF-16 is the determinant of the longevity effect induced by LBPs and *L. barbarum* berry extracts (Zhang et al., 2019; Xiong et al., 2021). Therefore, we first investigated the role of DAF-16 in the beneficial longevity induced by LbGp. Our results showed that the lifespan of *daf-16(mu86)* worms was not extended by LbGp (**Figure 2A**). In addition, we found that the transcription levels of the DAF-16 target genes (*ctl-1*, *ctl-2*, *sod-2,* and *sod-3*) were significantly increased by LbGp (**Figure 2B**). Furthermore, using the GFP fused reporter strain CF1553 (containing a *sod-3p*::GFP fusing transgene), we found that both the fluorescence intensity (**Figures 2C, D**) and GFP expression level (**Figure 2E**) were considerably increased when worms treated with LbGP, suggesting that LbGp triggered the expression of *sod-3*, a specific downstream target gene of DAF-16. Consequently, these results indicated that LbGp-induced lifespan extension depends on DAF-16. In addition, we found that LbGp was unable to increase the rate of body bending of UM0010 worms with a *daf-16-null* background (**Figure 2F**), indicating that similar to lifespan extension, amelioration of PD conferred by LbGp also depends on DAF-16.

Considering that DAF-16 is a key effector downstream of the IIS pathway, we speculated that the LbGp-induced longevity effects might depend on inhibiting the IIS signaling pathway, which is a well-known aging-related signaling pathway (Li et al., 2019). In *C. elegans*, DAF-2 is the insulin/IGF-1 transmembrane receptor homologous to mammals, which cascades to regulate the activity of the phosphoinositide 3-kinase (PI3K)/Akt kinase, eventually leading to the nuclear translocation of DAF-16/FOXO transcription factor and regulating longevity (Li et al., 2019). Using *daf-2(e1370)* and *akt-1(mg144)* mutants, we found that LbGp-induced lifespan extension was abrogated by *daf-2* and *akt-1* mutants (**Figures 2G, H**), indicating that LbGp-induced lifespan extension was associated with the IIS signaling pathway.

3.3. The transcription factors SKN-1/Nrf2 and HSF-1 mediate LbGp-induced longevity

In addition to DAF-16, the transcription factor SKN-1 is a key longevity regulator downstream of the IIS signaling pathway, which activates various downstream antioxidant and phase II detoxification genes in response to oxidative stress (Tullet et al., 2008). Previous studies have shown that *L. barbarum* extracts and LBPs could activate the antioxidant system of *C. elegans* through the transcription factor SKN-1 to enhance oxidative stress resistance (Meng et al., 2022). We first analyzed the antioxidant activity of LbGp in worms by detecting intracellular ROS accumulation levels using H2DCF-DA (a free radical sensor that can be deacetylated by intracellular esterases to emit fluorescence signals associated with ROS). We found that LbGp treatment significantly reduced the level of ROS under normal conditions (**Figure 3A**) or oxidative stress conditions (treatment with paraquat) (**Figure 3B**), suggesting that LbGp has antioxidant capacity to scavenge harmful ROS. Then, we wondered whether SKN-1 functions in lifespan extension induced by LbGp. Conducting survival analyses, we found that similar to the results of *daf-16*, the LbGp-induced survival benefit was blocked by RNAi knockdown of *skn-1* (**Figures 3C, D**). Moreover, we found that LbGp failed to improve motility in UM0010 worms under *skn-1* RNAi conditions (**Figure 3E**). Altogether, these results demonstrated that amelioration of aging and aging-related PD conferred by LbGp required the transcription factor SKN-1.

The heat-shock transcription factor HSF-1, another downstream target of the IIS pathway, plays a key role in the lifespan-extending effects of LBPs (Chiang et al., 2012). We also determined the effect of LbGp on the *hsf-1* mutant and found that LbGp-induced lifespan extension was abrogated in the *hsf-1-null* mutant (**Figure 3F**). Meanwhile, LbGp failed to prolong the lifespan in WT worms under *hsf-1* RNAi conditions

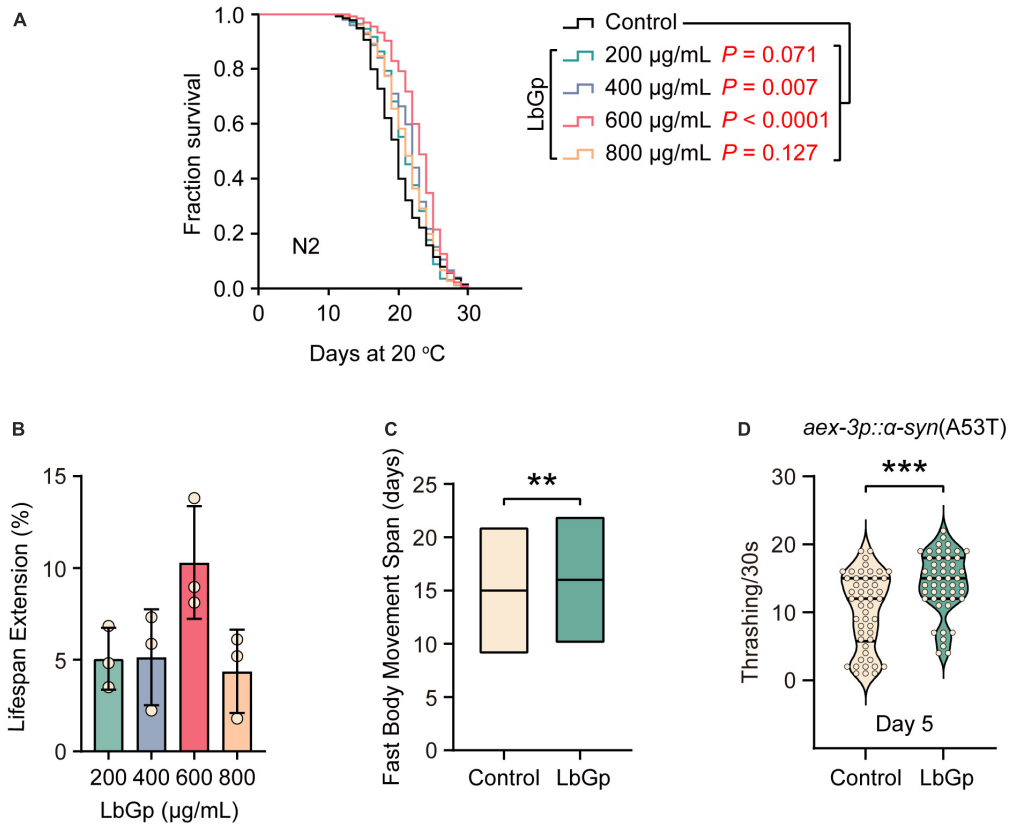

FIGURE 1
LbGp extended the lifespan and health span of *C. elegans* and improved the body motility of the nematode model of PD. **(A)** Lifespan analyses of N2 worms cultured at different doses of LbGp (200, 400, 600, and 800 μg/mL). **(B)** Statistical analyses of the effect of LbGp on N2 worms lifespan. The data are presented as the mean ± SD of three independent lifespan assays. **(C)** Movement analyses of N2 worms treated with LbGp (600 μg/mL) or vehicle (water). **(D)** Body bend analyses of the PD model strain UM0010 [*aex-3p*::α-*syn*(A53T)] treated with LbGp (600 μg/mL) or vehicle (water) at Day 5. In panels **(A,B)**, lifespan analyses were performed using Kaplan-Meier plotter, and the *P*-value was calculated by the log-rank test. In panels **(C,D)**, mean ± SD, $n \geq 30$ per group. $^{**}P < 0.01$, $^{***}P < 0.001$ (two-tailed Student's *t*-test).

(Figure 3G). Subsequently, we also confirmed that the mRNA levels of HSF-1 targets, including *hsp-12.6*, *hsp-16.1*, *hsp-16.2*, and *hsp-70*, were obviously increased by LbGp (Figure 3H). Moreover, we observed an elevated transcription level of *hsp-16.2* by detecting the fluorescence intensity and GFP protein level of the *hsp-16.2p*::GFP transgenic strains in the presence or absence of LbGp (Figures 3I, J, K). Similar to DAF-16 and SKN-1, we also found that the deletion of *hsf-1* eliminated the beneficial effect of LbGp on PD models (Figure 3L). Collectively, these results demonstrated that the LbGp-induced longevity effect was attributed to regulation of the IIS signaling pathway in a DAF-16-, HSF-1- and SKN-1-dependent manner.

3.4. LbGp-induced longevity depends on the reproductive signaling pathway

In *C. elegans*, germline depletion extends lifespan by remodeling the transcriptional landscape through activation of several aging-related transcription factors, including DAF-16 and SKN-1 (Berman and Kenyon, 2006). Based on our results above, we questioned whether the LbGp-induced longevity effect was related to the reproductive signaling pathway. Our results showed that LbGp was unable to further increase the lifespan of *glp-1(e2144)* worms, a germline-less and long-lived mutant (Figure 4A). The nuclear steroid receptor DAF-12 is activated by bile acid-like steroids to extend lifespan in germline-less worms (Motola et al., 2006). A recent study showed that DAF-12 contributed to the lifespan extension conferred by LBPs in *C. elegans* (Zhang et al., 2019). Concordantly, we also found that LbGp failed to extend the lifespan of *daf-12(rh61rh411)* (Figure 4B). Additionally, LbGp significantly enhanced the expression of DAF-12 target genes (*cdr-6* and *lips-17*) (Figure 4C). Furthermore, we found that improvement of motility of UM0010 worms was disappeared in a *daf-12-null* background (Figure 4D). Altogether, these findings illustrated that the survival benefits induced by LbGp were mediated by the reproductive signaling pathway.

3.5. LbGp-induced longevity partially depends on mitochondrial function

Attenuated mitochondrial respiratory function and mitochondrial dysfunction are major causes of aging. SKN-1 has been shown to improve mitochondrial function by regulating

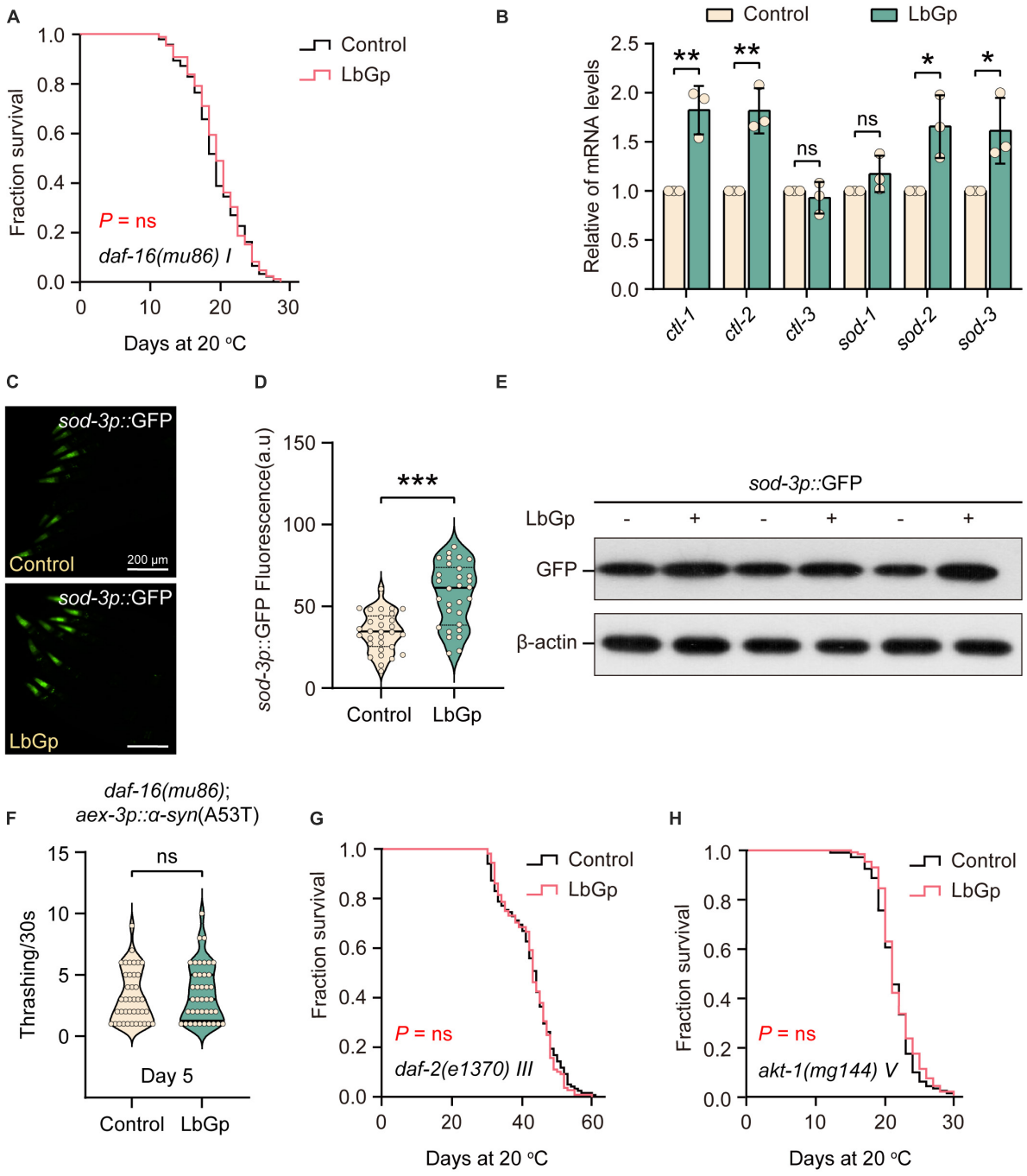

FIGURE 2
LbGp-induced lifespan extension depended on the IIS pathway. **(A)** Survival curves of *daf-16(mu86)* mutants treated with LbGp (600 μg/mL) or vehicle (water). **(B)** The relative mRNA expression of DAF-16-targeted genes (*ctl-1*, *ctl-2*, *ctl-3*, *sod-1*, *sod-2*, and *sod-3*) in N2 worms treated with LbGp (600 μg/mL) or vehicle (water). **(C,D)** Image **(C)** and quantification **(D)** of GFP fluorescence in the head region of the *sod-3*-reporter strain CF1553 (*sod-3p*::GFP) treated with LbGp (600 μg/mL) or vehicle (water). **(E)** Western blot analyses of GFP from LbGp-treated and non-LbGp-treated CF1553 (*sod-3p*::GFP) transgenic worms. The experiment was repeated three times. The corresponding uncropped western blot figure is shown in **Supplementary Figure 1A**. **(F)** Body bend analyses of the strain *daf-16(mu86); aex-3p*::α-*syn*(A53T) treated with LbGp (600 μg/mL) or vehicle (water) at Day 5. **(G,H)** Survival curves of *akt-1(mg144)* **(G)** and *daf-2(e1370)* **(H)** mutants treated with LbGp (600 μg/mL) or vehicle (water). In panels **(D,F)**, mean ± SD, $n \geq 30$ per group. In panels **(B,D,F)**, ns, not significant, $^{*}P < 0.05$, $^{**}P < 0.01$, and $^{***}P < 0.001$ (two-tailed Student's *t*-test).

mitochondrial biogenesis, ultimately extending the lifespan of *C. elegans* (Palikaras et al., 2015). Thus, we further investigated the effect of LbGp on the long-lived mitochondrial mutants *clk-1(e2519)* and *isp-1(qm150)*. *clk-1* encodes the human coenzyme Q7 hydroxylase homolog, and *isp-1* is the Rieske iron-sulfur polypeptide 1 homolog in *C. elegans*. Our results showed that the lifespan of *clk-1(e2519)* was unable to be extended by LbGp (**Figure 5A**), but that of *isp-1(qm150)* could be (**Figure 5B**), suggesting that the LbGp-induced longevity effect required mitochondrial function in a *clk-1*-specific manner.

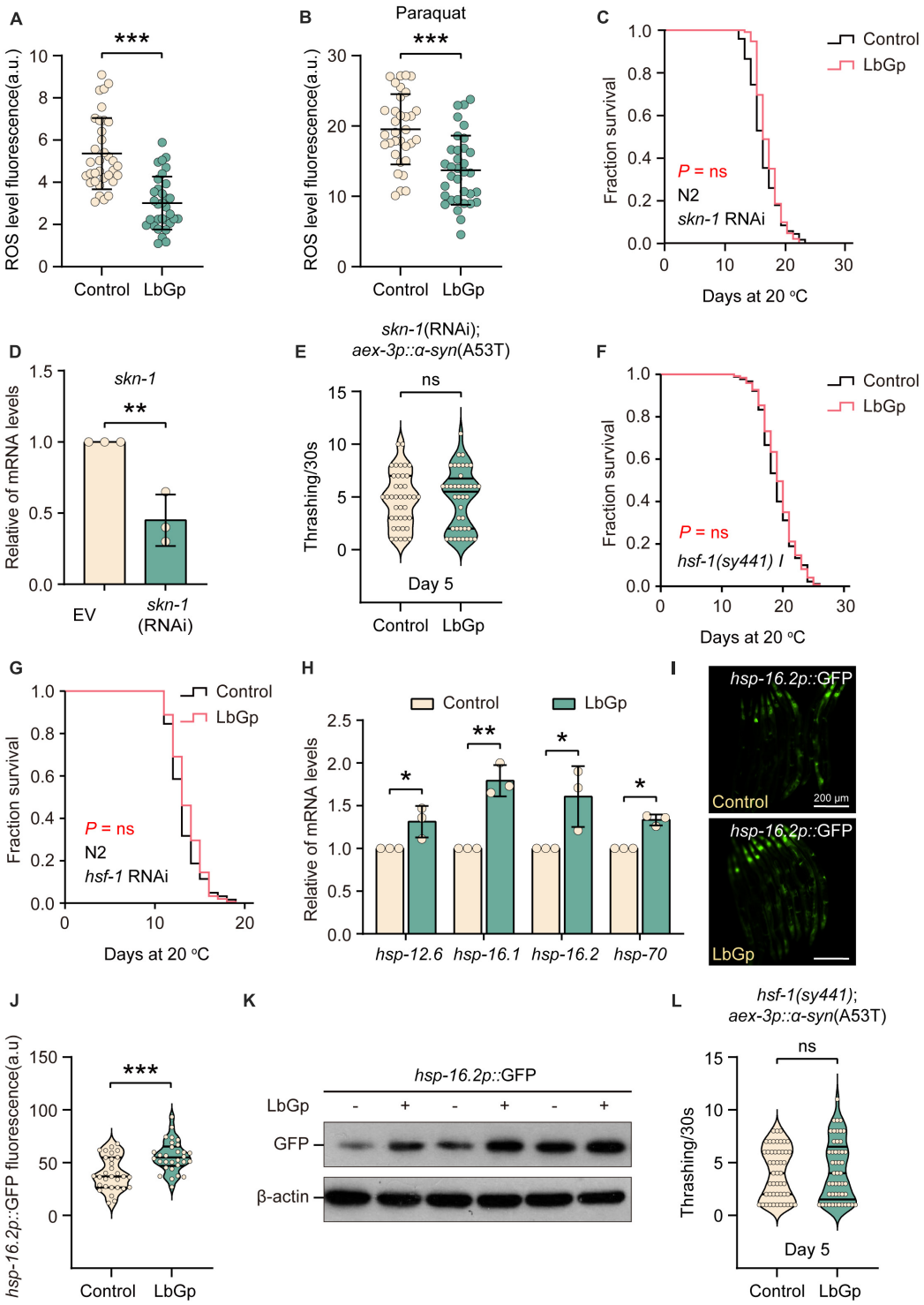

FIGURE 3
LbGp-induced lifespan extension was mediated by the transcription factors HSF-1 and SKN-1/*Nrf2*. **(A,B)** Quantitation of intracellular levels of ROS in N2 worms treated with LbGp (600 μg/mL) or vehicle (water) under normal conditions **(A)** or oxidative stress conditions (treatment with 5 mM paraquat) **(B)**. **(C)** Survival curves of N2 worms treated with LbGp (600 μg/mL) or vehicle (water) under *skn-1* RNAi conditions. **(D)** Relative *skn-1* mRNA expression in N2 worms fed HT115 bacteria carrying the *skn-1* RNAi vector or empty vector L4440. **(E)** Body bend analyses of the PD model strain UM0010 [*aex-3p*::α-*syn*(A53T)] treated with LbGp (600 μg/mL) or vehicle (water) at Day 5 under *skn-1* RNAi conditions. **(F)** Survival curves of *hsf-1(sy441)* mutants treated with LbGp (600 μg/mL) or vehicle (water). **(G)** Survival curves of N2 worms treated with LbGp (600 μg/mL) or vehicle (water) under *hsf-1* RNAi conditions. **(H)** The relative mRNA expression of *hsf-1*-targeted genes (*hsp-12.6*, *hsp-16.1*, *hsp-16.2*, and *hsp-70*) in the N2 worms treated with LbGp (600 μg/mL) or vehicle (water). **(I,J)** Image **(I)** and quantification **(J)** of GFP fluorescence in the *hsp-16.2*-reporter strain CL2070 (*hsp-16.2p*::GFP) treated with LbGp (600 μg/mL) or vehicle (water). **(K)** Western blot analyses of GFP from LbGp-treated and non-LbGp-treated CL2070 (*hsp-16.2p*::GFP) transgenic worms. The experiment was repeated three times. The corresponding uncropped western blot figure is shown in **Supplementary Figure 1B**. **(L)** Body bend analyses of the strain *hsf-1(sy441); aex-3p*::α-*syn*(A53T) treated with LbGp (600 μg/mL) or vehicle (water) at Day 5. In panels **(A,B,E,J,L)**, mean ± SD, $n > 30$ per group. In panels **(A,B,D,E,H,J,L)**, ns, not significant, $^{*}P < 0.05$, $^{**}P < 0.01$, and $^{***}P < 0.001$ (two-tailed Student's *t*-test).

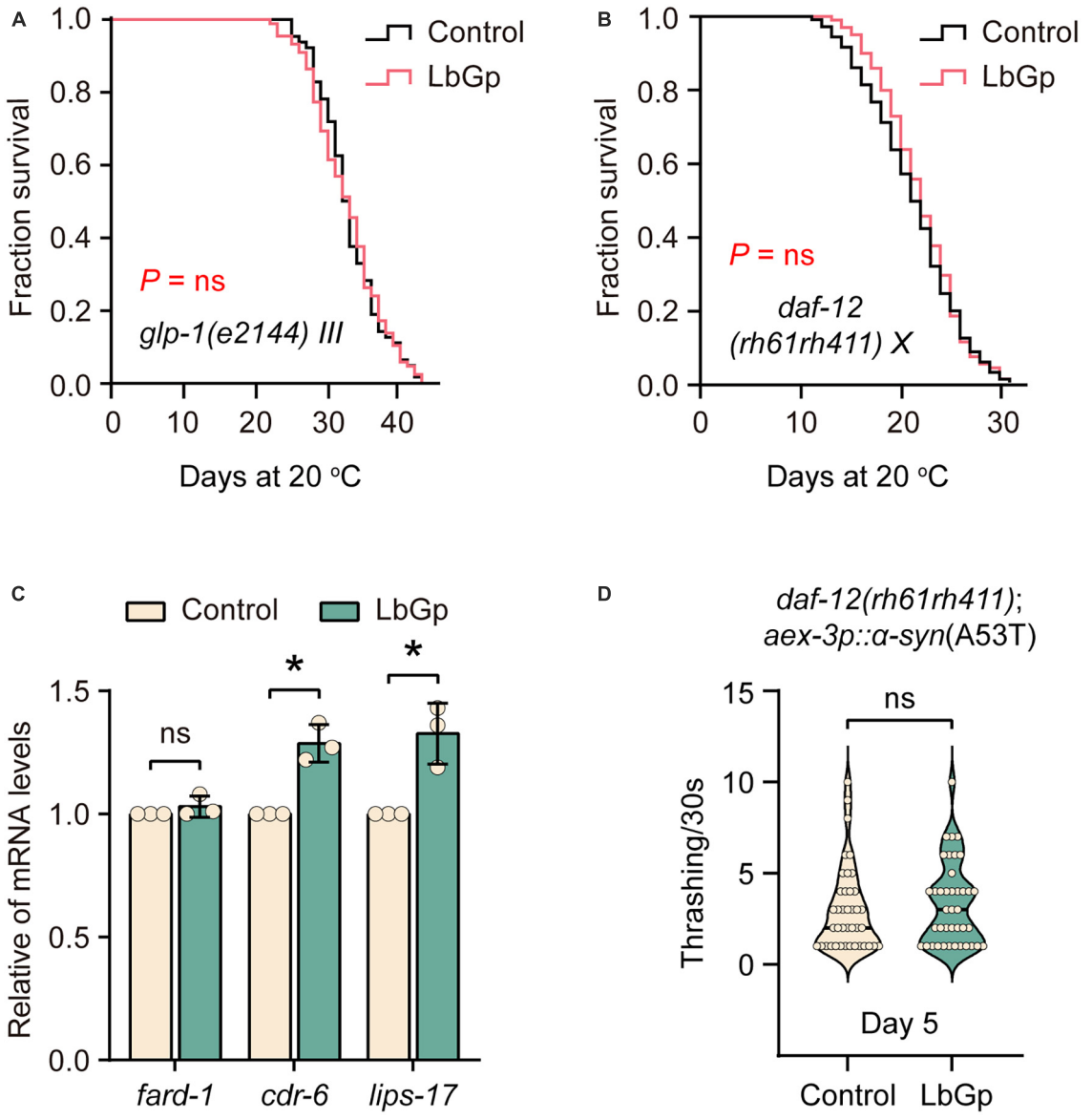

FIGURE 4
LbGp-induced lifespan extension depended on the reproductive signaling pathway. **(A,B)** Survival curves of *glp-1(e2144)* **(A)** and *daf-12(rh61rh411)* **(B)** mutants treated with LbGp (600 μg/mL) or vehicle (water). **(C)** The relative mRNA expression of the *daf-12*-targeted genes (*fard-1*, *cdr-6* and *lips-17*) in the N2 worms treated with LbGp (600 μg/mL) or vehicle (water). **(D)** Body bend analyses of the strain *daf-12(rh61rh411); aex-3p*::α-*syn*(A53T) treated with LbGp (600 μg/mL) or vehicle (water) at Day 5. In panel **(D)**, mean ± SD, $n > 30$ per group. In panels **(C,D)**, mean ± SD, ns, not significant, $^*P < 0.05$ (two-tailed Student's *t*-test).

Mitochondrial are the central organelle of energy production. The discovery of a mechanism by which LbGp regulates lifespan associated with mitochondrial function motivated us to deduce whether LbGp prolongs lifespan by influencing energy generation. In *C. elegans*, *aak-2* encodes a catalytic subunit of AMP-activated kinase (AMPK), which senses energy levels and is activated by a low ATP level to regulate lifespan (Apfeld et al., 2004). We found that LbGp could further extend the lifespan of the *aak-2* mutant (**Figure 5C**), suggesting that *aak-2* is dispensable for the survival advantage induced by LbGp. Therefore, this result indicated that LbGp-induced lifespan extension was independent of the regulation of energy production.

4. Discussion

Aging is always accompanied by a deterioration of physiological function and an increase in degenerative disease (e.g., Alzheimer's disease and Parkinson's disease) (Niccoli and Partridge, 2012). As the global population ages, the need to find substances that can treat aging-related diseases, delay the aging process, and prolong lifespan is urgent. Functional and nutraceutical foods have gradually attracted attention because of their few side effects. *L. barbarum* has been recognized and used as traditional Chinese medicine for 2,500 years, and its use is now expanding to all Western countries, where it is consumed mostly as food supplements (Amagase and Farnsworth, 2011). In this study, we found that LbGp, a potential

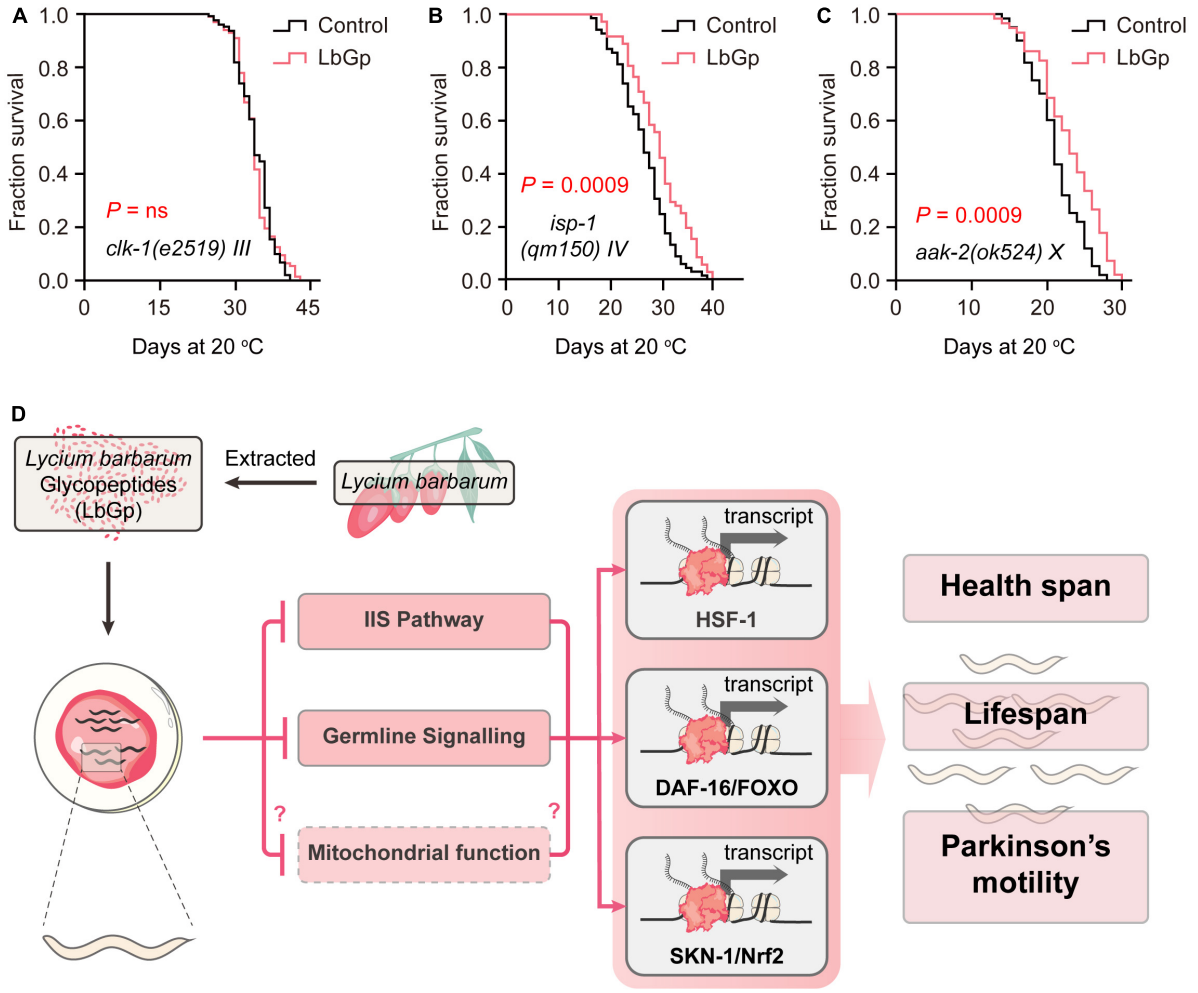

FIGURE 5
LbGp-induced lifespan extension partially depended on mitochondrial function. **(A–C)** Survival curves of *clk-1(e2519)* **(A)**, *isp-1(qm150)* **(B)** and *aak-2(ok524)* **(C)** mutants treated with LbGp (600 μg/mL) or vehicle (water). **(D)** Mechanisms of action of LbGp in *C. elegans*.

ingredient of *L. barbarum* berry, could extend lifespan and health span, as well as alleviate the progression of aging-related PD. In an in-depth study of the mechanism, we found that the amelioration of aging and aging-related disease conferred by LbGp was mediated by regulating the IIS signaling pathway and reproductive signaling pathway, subsequently activating the stress response transcription factors DAF-16, HSF-1 and SKN-1 and the nuclear receptor DAF-12, thereby triggering the expression of downstream longevity-related target genes to extend lifespan. Furthermore, mitochondrial function was involved in the survival benefits induced by LbGp (**Figure 5D**).

The imbalance between the production and elimination of free radicals is one of the major factors in aging and aging-associated disorders, and the supplementation of antioxidants can delay aging and improve oxidative stress resistance (Hekimi et al., 2011). Previous studies have shown that LBPs have antioxidant bioactivity and can reduce DNA damage by eliminating free radicals and inhibiting oxidative stress (Zhang et al., 2017). Consistently, we also found that LbGp could activate the expression of several antioxidant genes. Moreover, we confirmed that SKN-1, a major oxidative stress response factor, contributes to LbGp-induced lifespan extension. These results demonstrated that, similar to LBPs, LbGp prolonged lifespan depending on its antioxidant bioactivity, at least in part. Indeed, we also found that LbGp extended lifespan in an antioxidant-independent manner, that is, regulation of *glp-1* by LbGp. The longevity of germline-deficient mutants is associated with increased ROS in the soma (Wei and Kenyon, 2016). However, we found that LbGp, an antioxidant, did not influence the lifespan of *glp-1(e2144)* worms, which seems to contradict our observation that LbGp improves the antioxidant capacity. These findings implied that LbGp-induced lifespan extension in *C. elegans* depended not only on the antioxidant capacity but also on other biological activities.

Aging is the greatest risk factor for most age-related disorders, and delaying the rate of biological aging through the consumption of antiaging drugs or foods is able to slow the onset and progression of age-related diseases (Xiao et al., 2022). In the present study, we found that LbGp could improve motility in a PD model of *C. elegans* through mechanisms consistent with antiaging, indicating that LbGp can ameliorate the progression of PD. In support of our findings, previous studies reported that the crude extracts and polysaccharides of *L. barbarum* berry have protective effects against

many aging-associated disorders, including cardiovascular diseases and neurodegenerative diseases. For example, supplementation with LBPs protected neurons against β-amyloid-induced apoptosis and improved the learning and memory abilities of Sprague Dawley rats with scopolamine-induced brain injury; crude extracts from LB can alleviate the neurotoxicity of α-synuclein protein, β-amyloid, and Aβ peptide *in vitro* and *in vivo* (Meng et al., 2022). Those studies and our present results indicated that LbPs could improve the symptoms of neurodegenerative disorders and that LbGp may be the one of the main active ingredients in LBPs exert these protective effects.

5. Conclusion

In conclusion, the innovation of this study lies in the discovery that LbGp extracted from *L. barbarum* berries can prolong the lifespan and health span and delay the occurrence of aging-related diseases such as PD in *C. elegans*. These findings provide a new strategy for preventing aging and aging-related diseases. Mechanistically, the molecular mechanism of LbGp-induced longevity is closely related to the IIS pathway, reproductive signaling pathway and mitochondrial function-related signaling pathway. It is necessary to expand our findings on LbGp to mammalian model organisms. Therefore, in future research, we will continue to search for new protective effects against other neurodegenerative diseases and clarify the molecular mechanisms of LbGp against aging and aging-related diseases in different animal models.

Data availability statement

All data needed to evaluate the conclusions in this manuscript are present in this manuscript and/or the **Supplementary material**. Requests to access the datasets should be directed to Q-LW, wanqinli@hotmail.com.

Author contributions

JZ: investigation, methodology, software, visualization, and writing–editing. ZL: investigation, methodology, visualization, and writing–original draft. KC: investigation, methodology, and visualization. YL and JY: methodology. QZ: investigation and funding acquisition. K-FS: investigation and writing–reviewing and editing. Q-LW: investigation, writing–reviewing and editing, and funding acquisition. All authors contributed to the article and approved the submitted version.

Funding

This work was supported by the National Key R&D Program of China (2021YFA0804903), the National Natural Science Foundation of China (No. 82001465), and the Guangdong Provincial Basic Research Program, China (2020A1515111026).

Acknowledgments

We thank the *Caenorhabditis* Genetic Center (CGC) for providing the worm strains.

Conflict of interest

The authors declare that the research was conducted in the absence of any commercial or financial relationships that could be construed as a potential conflict of interest.

Publisher's note

Supplementary material

The Supplementary Material for this article can be found online at: https://www.frontiersin.org/articles/10.3389/fnagi.2023.1156265/full#supplementary-material

References

Amagase, H., and Farnsworth, N. R. (2011). A review of botanical characteristics, phytochemistry, clinical relevance in efficacy and safety of *Lycium barbarum* fruit (Goji). *Food Res. Int.* 44, 1702–1717. doi: 10.1016/j.foodres.2011.03.027

Apfeld, J., O'connor, G., Mcdonagh, T., Distefano, P. S., and Curtis, R. (2004). The AMP-activated protein kinase AAK-2 links energy levels and insulin-like signals to lifespan in *C. elegans*. *Genes Dev.* 18, 3004–3009. doi: 10.1101/gad.1255404

Berman, J. R., and Kenyon, C. (2006). Germ-cell loss extends *C. elegans* life span through regulation of DAF-16 by kri-1 and lipophilic-hormone signaling. *Cell* 124, 1055–1068. doi: 10.1016/j.cell.2006.01.039

Chiang, W. C., Ching, T. T., Lee, H. C., Mousigian, C., and Hsu, A. L. (2012). HSF-1 regulators DDL-1/2 link insulin-like signaling to heat-shock responses and modulation of longevity. *Cell* 148, 322–334. doi: 10.1016/j.cell.2011.12.019

Deng, H., and Yuan, L. (2014). Genetic variants and animal models in SNCA and Parkinson disease. *Ageing Res. Rev.* 15, 161–176. doi: 10.1016/j.arr.2014.04.002

Ding, Y., Yan, Y., Chen, D., Ran, L., Mi, J., Lu, L., et al. (2019). Modulating effects of polysaccharides from the fruits of *Lycium barbarum* on the immune response and gut microbiota in cyclophosphamide-treated mice. *Food Funct.* 10, 3671–3683. doi: 10.1039/C9FO00638A

Gong, G., Liu, Q., Deng, Y., Dang, T., Dai, W., Liu, T., et al. (2020). Arabinogalactan derived from *Lycium barbarum* fruit inhibits cancer cell growth via cell cycle arrest and apoptosis. *Int. J. Biol. Macromol.* 149, 639–650. doi: 10.1016/j.ijbiomac.2020.01.251

Hekimi, S., Lapointe, J., and Wen, Y. (2011). Taking a "good" look at free radicals in the aging process. *Trends Cell Biol.* 21, 569–576. doi: 10.1016/j.tcb.2011.06.008

Huang, C., Xiong, C., and Kornfeld, K. (2004). Measurements of age-related changes of physiological processes that predict lifespan of *Caenorhabditis elegans*. *Proc. Natl. Acad. Sci. U.S.A.* 101, 8084–8089. doi: 10.1073/pnas.0400848101

Huang, W., Zhao, M., Wang, X., Tian, Y., Wang, C., Sun, J., et al. (2022). Revisiting the structure of arabinogalactan from *Lycium barbarum* and the impact of its side chain on anti-ageing activity. *Carbohydr. Polym.* 286, 119282. doi: 10.1016/j.carbpol.2022.119282

Huang, X., Wang, C., Chen, L., Zhang, T., Leung, K. L., and Wong, G. (2021). Human amyloid beta and α-synuclein co-expression in neurons impair behavior and recapitulate features for Lewy body dementia in *Caenorhabditis elegans*. *Biochim. Biophys. Acta Mol. Basis Dis.* 1867:166203. doi: 10.1016/j.bbadis.2021.166203

Huang, Y., Zheng, Y., Yang, F., Feng, Y., Xu, K., Wu, J., et al. (2022). *Lycium barbarum* Glycopeptide prevents the development and progression of acute colitis by regulating the composition and diversity of the gut microbiota in mice. *Front. Cell. Infect. Microbiol.* 12:921075. doi: 10.3389/fcimb.2022.921075

Jia, W., Wang, C., Zheng, J., Li, Y., Yang, C., Wan, Q.-L., et al. (2022). Pioglitazone hydrochloride extends the lifespan of *Caenorhabditis elegans* by activating DAF-16/FOXO- and SKN-1/NRF2-Related signaling pathways. *Oxid. Med. Cell. Longev.* 2022:8496063. doi: 10.1155/2022/8496063

Jin, M., Huang, Q., Zhao, K., and Shang, P. (2013). Biological activities and potential health benefit effects of polysaccharides isolated from *Lycium barbarum* L. *Int. J. Biol. Macromol.* 54, 16–23. doi: 10.1016/j.ijbiomac.2012.11.023

Li, S.-T., Zhao, H.-Q., Zhang, P., Liang, C.-Y., Zhang, Y.-P., Hsu, A.-L., et al. (2019). DAF-16 stabilizes the aging transcriptome and is activated in mid-aged *Caenorhabditis elegans* to cope with internal stress. *Aging Cell* 18:e12896. doi: 10.1111/acel.12896

Liang, R., Zhao, Q., Zhu, Q., He, X., Gao, M., and Wang, Y. (2021). *Lycium barbarum* polysaccharide protects ARPE-19 cells against H2O2-induced oxidative stress via the Nrf2/HO-1 pathway. *Mol. Med. Rep.* 24:769. doi: 10.3892/mmr.2021.12409

Mao, F., Xiao, B., Jiang, Z., Zhao, J., Huang, X., and Guo, J. (2011). Anticancer effect of *Lycium barbarum* polysaccharides on colon cancer cells involves G0/G1 phase arrest. *Med. Oncol.* 28, 121–126. doi: 10.1007/s12032-009-9415-5

Masci, A., Carradori, S., Casadei, M. A., Paolicelli, P., Petralito, S., Ragno, R., et al. (2018). *Lycium barbarum* polysaccharides: Extraction, purification, structural characterisation and evidence about hypoglycaemic and hypolipidaemic effects. A review. *Food Chem.* 254, 377–389. doi: 10.1016/j.foodchem.2018.01.176

Meng, J., Lv, Z., Guo, M., Sun, C., Li, X., Jiang, Z., et al. (2022). A *Lycium barbarum* extract inhibits β-amyloid toxicity by activating the antioxidant system and mtUPR in a *Caenorhabditis elegans* model of Alzheimer's disease. *FASEB J.* 36:e22156. doi: 10.1096/fj.202101116RR

Moskalev, A., Guvatova, Z., Lopes, I. A., Beckett, C. W., Kennedy, B. K., De Magalhaes, J. P., et al. (2022). Targeting aging mechanisms: Pharmacological perspectives. *Trends Endocrinol. Metab.* 33, 266–280. doi: 10.1016/j.tem.2022.01.007

Motola, D. L., Cummins, C. L., Rottiers, V., Sharma, K. K., Li, T., Li, Y., et al. (2006). Identification of ligands for DAF-12 that govern dauer formation and reproduction in *C. elegans*. *Cell* 124, 1209–1223. doi: 10.1016/j.cell.2006.01.037

Niccoli, T., and Partridge, L. (2012). Ageing as a risk factor for disease. *Curr. Biol.* 22, R741–R752. doi: 10.1016/j.cub.2012.07.024

Niu, Y., Liao, J., Zhou, H., Wang, C. C., Wang, L., and Fan, Y. (2022). Flavonoids from *Lycium barbarum* leaves exhibit anti-aging effects through the redox-modulation. *Molecules* 27:4952. doi: 10.3390/molecules27154952

Palikaras, K., Lionaki, E., and Tavernarakis, N. (2015). Coordination of mitophagy and mitochondrial biogenesis during ageing in *C. elegans*. *Nature* 521, 525–528. doi: 10.1038/nature14300

Park, S.-J., Ahmad, F., Philp, A., Baar, K., Williams, T., Luo, H., et al. (2012). Resveratrol ameliorates aging-related metabolic phenotypes by inhibiting cAMP phosphodiesterases. *Cell* 148, 421–433. doi: 10.1016/j.cell.2012.01.017

Peng, X.-M., Huang, L.-J., Qi, C.-H., Zhang, Y.-X., and Tian, G.-Y. (2001). Studies on chemistry and immunomodulating mechanism of a glycoconjugate from *Lycium barbarum* L. *Chin. J. Chem.* 19, 1190–1197. doi: 10.1002/cjoc.20010191206

Ryu, D., Mouchiroud, L., Andreux, P. A., Katsyuba, E., Moullan, N., Nicolet-Dit-Félix, A. A., et al. (2016). Urolithin A induces mitophagy and prolongs lifespan in *C. elegans* and increases muscle function in rodents. *Nat. Med.* 22, 879–888. doi: 10.1038/nm.4132

Stegemann, S., Ecker, F., Maio, M., Kraahs, P., Wohlfart, R., Breitkreutz, J., et al. (2010). Geriatric drug therapy: Neglecting the inevitable majority. *Ageing Res. Rev.* 9, 384–398. doi: 10.1016/j.arr.2010.04.005

Tang, R., Chen, X., Dang, T., Deng, Y., Zou, Z., Liu, Q., et al. (2019). *Lycium barbarum* polysaccharides extend the mean lifespan of *Drosophila melanogaster*. *Food Funct.* 10, 4231–4241. doi: 10.1039/C8FO01751D

Tian, G. (1995). Isolation, Purification and Properties of LbGP and Characterization of Its Glycan-Peptide Bond. *Chin. Sci. Abstr. Ser. B* 4:38.

Tullet, J. M., Hertweck, M., An, J. H., Baker, J., Hwang, J. Y., Liu, S., et al. (2008). Direct inhibition of the longevity-promoting factor SKN-1 by insulin-like signaling in *C. elegans*. *Cell* 132, 1025–1038. doi: 10.1016/j.cell.2008.01.030

Wan, Q. L., Meng, X., Dai, W., Luo, Z., Wang, C., Fu, X., et al. (2021). N(6)-methyldeoxyadenine and histone methylation mediate transgenerational survival advantages induced by hormetic heat stress. *Sci. Adv.* 7:eabc3026. doi: 10.1126/sciadv.abc3026

Wang, W., Xue, C., and Mao, X. (2020). Radioprotective effects and mechanisms of animal, plant and microbial polysaccharides. *Int. J. Biol. Macromol.* 153, 373–384. doi: 10.1016/j.ijbiomac.2020.02.203

Wei, Y., and Kenyon, C. (2016). Roles for ROS and hydrogen sulfide in the longevity response to germline loss in *Caenorhabditis elegans*. *Proc. Natl. Acad. Sci. U.S.A.* 113, E2832–E2841. doi: 10.1073/pnas.1524727113

Xiao, Y., Zhang, H., Sheng, Y., Liu, F., Gao, J., Liu, G., et al. (2022). Usnic Acid extends healthspan and improves the neurodegeneration diseases via mTOR/PHA-4 signaling pathway in *Caenorhabditis elegans*. *iScience* 25:105539. doi: 10.1016/j.isci.2022.105539

Xiong, L., Deng, N., Zheng, B., Li, T., and Liu, R. H. (2021). HSF-1 and SIR-2.1 linked insulin-like signaling is involved in goji berry (*Lycium* spp.) extracts promoting lifespan extension of *Caenorhabditis elegans*. *Food Funct.* 12, 7851–7866. doi: 10.1039/D0FO03300F

Zeng, W., Wu, A. G., Zhou, X.-G., Khan, I., Zhang, R. L., Lo, H. H., et al. (2021). Saponins isolated from Radix polygalae extent lifespan by modulating complement C3 and gut microbiota. *Pharmacol. Res.* 170:105697. doi: 10.1016/j.phrs.2021.105697

Zhang, F., Zhang, X., Guo, S., Cao, F., Zhang, X., Wang, Y., et al. (2020). An acidic heteropolysaccharide from *Lycii fructus*: Purification, characterization, neurotrophic and neuroprotective activities in vitro. *Carbohydr. Polym.* 249:116894. doi: 10.1016/j.carbpol.2020.116894

Zhang, F., Zhang, X., Liang, X., Wu, K., Cao, Y., Ma, T., et al. (2022). Defensing against oxidative stress in *Caenorhabditis elegans* of a polysaccharide LFP-05S from *Lycii fructus*. *Carbohydr. Polym.* 289:119433. doi: 10.1016/j.carbpol.2022.119433

Zhang, L., Li, Q., Zheng, G., Chen, Y., Huang, M., Zhang, L., et al. (2017). Protective effect of *Lycium barbarum* polysaccharides against cadmium-induced testicular toxicity in male mice. *Food Funct* 8, 2322–2330. doi: 10.1039/c6fo01583b

Zhang, Z., Zhou, Y., Fan, H., Billy, K. J., Zhao, Y., Zhan, X., et al. (2019). Effects of *Lycium barbarum* polysaccharides on health and aging of *C. elegans* depend on daf-12/daf-16. *Oxid. Med. Cell. Longev.* 2019:6379493. doi: 10.1155/2019/6379493

Zhou, X., Zhang, Z., Shi, H., Liu, Q., Chang, Y., Feng, W., et al. (2022). Effects of *Lycium barbarum* glycopeptide on renal and testicular injury induced by di(2-ethylhexyl) phthalate. *Cell Stress Chaperones* 27, 257–271. doi: 10.1007/s12192-022-01266-0

frontiers | Frontiers in Aging Neuroscience

TYPE Original Research
PUBLISHED 18 July 2023
DOI 10.3389/fnagi.2023.1213977

OPEN ACCESS

EDITED BY
Muthuraman Muthuraman,
University Hospital Würzburg, Germany

REVIEWED BY
Wooyoung Jang,
Gangneung Asan Hospital, Republic of Korea
Steven Gunzler,
University Hospitals Cleveland Medical Center, United States

*CORRESPONDENCE
Ming-Hong Chang
✉ cmh500809@gmail.com

RECEIVED 28 April 2023
ACCEPTED 04 July 2023
PUBLISHED 18 July 2023

CITATION
Fang T-C, Tsai Y-S and Chang M-H (2023) Sequential change in olfaction and (non) motor symptoms: the difference between anosmia and non-anosmia in Parkinson's disease.
Front. Aging Neurosci. 15:1213977.
doi: 10.3389/fnagi.2023.1213977

Sequential change in olfaction and (non) motor symptoms: the difference between anosmia and non-anosmia in Parkinson's disease

Ting-Chun Fang[1], Yu-Shan Tsai[1] and Ming-Hong Chang[1,2,3]*

[1]Department of Neurology, Taichung Veterans General Hospital, Neurological Institute, Taichung, Taiwan, [2]Department of Post-Baccalaureate Medicine, College of Medicine, National Chung Hsing University, Taichung, Taiwan, [3]Brain and Neuroscience Research Center, College of Medicine, National Chung Hsing University, Taichung, Taiwan

Introduction: Hyposmia is a common prodrome in patients with Parkinson's disease (PD). This study investigates whether olfactory changes in PD differ according to the degree of olfactory dysfunction and whether there are changes in motor and non-motor symptoms.

Methods: The 129 subjects with PD were divided into two groups: anosmia and non-anosmia. All cases were reassessed within 1–3 years after the initial assessment. The assessment included the MDS-Unified PD Rating Scale (MDS-UPDRS), the University of Pennsylvania Smell Identification Test (UPSIT), Beck's Depression Inventory-II (BDI-II), Montreal Cognitive Assessment (MoCA), and equivalence dose of daily levodopa (LEDD). The generalized estimating equation (GEE) model with an exchangeable correlation structure was used to analyze the change in baseline and follow-up tracking and the disparity in change between these two groups.

Results: The anosmia group was older and had a longer disease duration than the non-anosmia group. There was a significant decrease in UPSIT after follow-up in the non-anosmia group ($\beta = -3.62$, $p < 0.001$) and a significant difference in the change between the two groups (group-by-time effect, $\beta = 4.03$, $p < 0.001$). In the third part of the UPDRS motor scores, there was a tendency to increase the score in the non-anosmia group compared to the anosmia group (group-by-time effect, $\beta = -4.2$, $p < 0.038$). There was no significant difference in the group-by-time effect for UPDRS total score, LEDD, BDI-II, and MoCA scores.

Discussion: In conclusion, this study found that olfactory sensation may still regress in PD with a shorter disease course without anosmia, but it remains stable in the anosmia group. Such a decline in olfaction may not be related to cognitive status but may be associated with motor progression.

KEYWORDS

Parkinson's disease, olfactory dysfunction, UPSIT, MDS-UPDRS, equivalence dose of daily levodopa, cognition, depression

1. Introduction

Parkinson's disease (PD) is the second most common neurodegenerative disease, with a prevalence of around 1.4–3.0 per thousand in Taiwan which increases with aging (Liu et al., 2016a,b). In addition to motor symptoms such as bradykinesia, tremor, and rigidity, non-motor symptoms contribute to poor quality of life in patients with PD (Rodríguez-Violante et al., 2015; Tibar et al., 2018; Santos Garcia et al., 2019). Some non-motor symptoms appear before motor symptoms, known as prodromal non-motor symptoms of PD (Poewe et al., 2017). Olfactory dysfunction, constipation, depression, and rapid eye movement (REM) sleep behavior disorder (RBD) can represent prodromal symptoms.

The Braak staging system explains prodromal symptoms because alpha-synuclein aggregates, a pathological hallmark of PD, are initially found in the olfactory bulb and the dorsal motor nucleus of the vagus (Braak et al., 2003). One route of propagation of alpha-synuclein inclusion in the dual-hit hypothesis starts from the enteric nervous system with the gut to brain spreading. This route is suggested to be associated with the involvement of the autonomic nervous system and premotor RBD, naming the body-first subtype. The other route of alpha-synuclein pathology starts from the olfactory bulb and anterior olfactory nucleus and spreads to adjacent areas such as the olfactory tubercle, piriform cortex, periamygdaloid cortex, and entorhinal cortex. However, the evidence of entry via the olfactory pathway is still controversial because no advanced lesions are found in non-olfactory cortical areas (Braak et al., 2003; Horsager et al., 2020). In a PD mouse model, RBD-like behavior occurred earlier than hyposmia, which correlates with the finding in humans that PD patients with RBD were more hyposmic than PD patients without RBD (Taguchi et al., 2020). These findings suggest that the ascending pathway of the brainstem may predominate in the spread of alpha-synuclein, despite the initial deposition in the olfactory bulb (Braak et al., 2003; Horsager et al., 2020).

However, hyposmia is still one of the common non-motor symptoms in PD related to Lewy body pathology in the olfactory system (Haehner et al., 2009; Rodríguez-Violante et al., 2017). As the disease progresses, Lewy body pathology increases in the olfactory system, but most studies show inconsistent results in the relationship between hyposmia and disease severity (Berendse et al., 2011; Yoo et al., 2020). Few studies discuss the association between the duration of the disease and olfactory dysfunction, and most of them did not show an obvious correlation, and even the results of some longitudinal studies are inconsistent (Ercoli et al., 2022). Due to the ambiguous relationship between olfactory dysfunction and disease duration, this study aims to investigate the longitudinal change of olfactory function in PD patients based on their degree of olfactory dysfunction. Given this uncertainty, we also conducted a comprehensive analysis of disease severity, medication usage, cognitive function, and depression during the longitudinal follow-up period to provide a more comprehensive comparison.

2. Materials and methods

2.1. Participants

Participants were recruited from the outpatient clinic at Taichung Veteran General Hospital from 2017. Subjects were selected on the basis of International Parkinson and MDS Clinical Diagnostic Criteria for Parkinson's disease. At the first visit (T0), all subjects received a complete survey that included the MDS-Unified Parkinson's Disease Rating Scale (MDS-UPDRS), the University of Pennsylvania Smell Identification Test (UPSIT), Beck's Depression Inventory-II (BDI-II), and Montreal's Cognitive Assessment (MoCA). Follow-up (T1) was conducted for these patients with PD in 1–3 years after the first visit, and a comprehensive survey was also conducted including MDS-UPDRS, UPDIT, BDI, and MoCA. The equivalent dose of daily levodopa was also calculated on the date of the first visit and the follow-up, respectively. Individuals were excluded if they did not meet the MDS clinical diagnostic criteria for Parkinson's disease during follow-up or could not complete the questionnaire. Those who had upper respiratory tract infection and sinonasal disease which might affect olfaction were also excluded. Written informed consent was obtained from all participants. This study was approved by Taichung Veterans General Hospital Institutional Review Board/Ethics Committee (No. CE22189B). All methods were performed in accordance with the Declaration of Helsinki guidelines and hospital regulations.

2.2. Variables

The olfactory function was evaluated with the validated Taiwanese version of UPSIT, an odor identification (Jiang et al., 2010). The total score was 40 in this test and the cutoff value of total anosmia was less than 19. Considering that the mean UPSIT score is 17–20 in PD patients which is close to the cutoff value 19 of anomia in UPSIT, we divided subjects into two groups, anosmia and non-anosmia based on the UPSIT score at the first visit to represent the characteristics of profound olfactory deficit or milder symptom in PD, respectively (Doty, 2001, 2012; Picillo et al., 2014; Lawton et al., 2016). Non-motor symptoms of PD were also assessed. For cognition, we used MoCA due to its validation for assessing global cognitive abilities in PD (Litvan et al., 2012). BDI-II was used for mood investigation (Beck et al., 1996). Regarding the severity of motor symptoms in PD, the part 3 score of MDS-UPDRS (UPDRS 3) and the equivalent dose of daily levodopa (LEDD) were used to determine the severity of motor symptoms (Goetz et al., 2008). The total score of MDS-UPDRS (UPDRS T) was used to represent the disease burden of PD. Scores of MDS-UPDRS Part 1 and Part 2 were used to represent the non-motor and motor experiences of daily living, and Part 4 was used for motor complication. To determine the motor subtypes, we utilized 11 items (2.10, 3.15–3.18) for tremor and five items (2.12, 2.13, 3.10–3.12) for postural instability/gait difficulty (PIGD) from the MDS-UPDRS. The ratio of mean tremor scores to the mean PIGD scores was

employed to define the following subtypes: (1) tremor subtype with a ratio ≥ 1.15 and (2) PIGD subtype with a ratio ≤ 0.90 (Stebbins et al., 2013).

2.3. Statistical analysis

Baseline clinical characteristics between the anosmia and non-anosmia groups were compared by using chi-square test for binary variables. UPSIT, MoCA, BDI-II, MDS UPDRS scores, and LEDD scores were analyzed as continuous variables. For continuous variables that follow a normal distribution, Student *t*-tests were used for analysis. For variables that do not follow a normal distribution, non-parametric Mann–Whitney U tests were used for analysis. Multiple linear regression adjusted for age, gender and disease was carried out to analyze the relationship between UPSIT and each variable including MoCA, BDI-II, UPDRS 3, UPDRS T, and LEDD scores at baseline. Generalized estimating equation (GEE) model with an exchangeable correlation structure, was used to assess the change of longitudinal data, including MoCA, BDI-II, UPDRS 3, UPDRS T, and LEDD, between the anosmia and non-anosmia groups at T1 compared with T0.

All tests were with a statistical significance level of $p < 0.05$ and were reported with 95% confidence intervals (CIs). Data analysis was performed with SPSS software (IBM Corporation, Armonk, New York, NY, USA).

3. Results

3.1. Demographic data

A total of 129 participants were enrolled in this study. Table 1 shows that the anosmia and non-anosmia groups comprised 73 and 56 subjects, respectively. At baseline, the anosmia group was older than the non-anosmia group (66.65 vs. 63.21, $p = 0.032$) and had a longer disease duration (4.89 years vs. 3.27, $p = 0.033$). The group with anosmia also demonstrated higher scores on UPDRST and UPDRS3, but exhibited lower scores on the MoCA. However, no significant differences were found between the two groups regarding gender, follow-up interval, motor subtypes, scores of UPDRS1, 2, and 4, LEDD and BDI scores. After the follow-up for UPSIT re-evaluation, it was observed that 20 patients from the non-anosmia group at the first visit had developed anosmia, accounting for 35.7% of the non-anosmia group. Conversely, seven patients from the anosmia group had transitioned to non-anosmia. Eventually, the anosmia and non-anosmia groups comprised 86 and 43 subjects, respectively.

TABLE 1 Characteristics of the participants at baseline.

Characteristic	Anosmia (n = 73)	Non-anosmia (n = 56)	P-value
Age, mean (SD), y	66.65 (8.63)	63.21 (9.33)	0.032*
Gender (%)			
Male	39 (53.5)	37 (66.1)	0.148
Female	34 (46.5)	19 (33.9)	
Disease duration, mean (SD), y	4.89 (5.07)	3.27 (3.46)	0.033*
Follow-up interval, mean (SD), y	1.52 (0.63)	1.65 (0.73)	0.288
UPDRST†	51.0 (37.0, 66.0)	43.0 (28.2, 53.0)	0.007*
UPDRS1†	9.0 (5.0, 14.0)	8.0 (5.0, 11.0)	0.378
UPDRS2†	8.0 (3.0, 13.5)	7.0 (3.2, 10.7)	0.211
UPDRS3†	32.0 (23.0, 41.0)	25.5 (17.0, 34.7)	0.002*
UPDRS4†	0 (0, 1.0)	0 (0, 0.7)	0.843
Motor subtype (%)			0.907
PIGD	34 (46.6)	24 (42.9)	
Tremor	25 (34.2)	21 (37.5)	
Indeterminate	14 (19.2)	11 (19.6)	
LEDD†	474.0 (201.8, 787.5)	377.5 (140.6, 637.5)	0.090
MoCA†	26.0 (21.5, 28.0)	27.0 (25.0, 29.0)	0.016*
BDI†	10.0 (4.0, 17.0)	8.5 (4.0, 14.5)	0.447

y, years; SD, standard deviation; UPDRS, MDS-UPDRS; LEDD, equivalent dose of daily levodopa; MoCA, Montreal's Cognitive Assessment; BDI-II, Beck's Depression Inventory-II; PIGD, postural instability/gait difficulty. †Analyzed by non-parametric Mann–Whitney U-tests, and presented with median (1st and 3rd quartile). *Significance, $p < 0.05$.

3.2. Correlations between UPSIT and clinical features at baseline

The UPSIT scores of all participants at baseline were significantly correlated with MoCA (β = 0.14, $p = 0.015$), UPDRS 3 (β = −0.67, $p = 0.001$), and UPDRS T (β = −0.84, $p = 0.007$), after adjusting for age, gender, and disease duration. However, no significant correlations were found between UPSIT and BDI or LEDD.

3.3. Change in olfactory identification in anosmia/non-anosmia groups

In the GEE analysis (Table 2), a significant group effect revealed a lower UPSIT score in the anosmia group (β = −10.58, $p < 0.001$). The time effect was significant in the non-anosmia group (β = −3.62, $p < 0.001$) but not in the anosmia group. The group-by-time effect was also significant (β = 4.03, $p < 0.001$), indicating that the UPSIT score remained stable in the anosmia group but decreased significantly in the non-anosmia group (Figure 1A). These results remained significant after adjusting for age, gender, and disease duration (Table 3).

3.4. Change in motor symptoms in anosmia/non-anosmia groups

Significant group effects were found for UPDRS 3 and UPDRS T (Table 3), indicating higher scores in the anosmia group at

TABLE 2 Generalized estimating equation analysis for the comparison of outcomes.

	Mean (SD)		Group effect (anosmia vs. non-anosmia)		Time effect, anosmia (T1 vs. T0)		Time effect, non-anosmia (T1 vs. T0)		Group x time effect	
Outcome	Anosmia	Non-anosmia	*B*	*P*-value	*B*	*P*-value	*B*	*P*-value	*B*	*P*-value
UPSIT										
T0	12.57 (4.45)	23.16 (3.46)	−10.58	<0.001*	NA	NA	NA	NA	NA	NA
T1	12.98 (4.75)	19.53 (6.29)			0.41	0.55	−3.62	<0.001*	4.03	<0.001*
LEDD										
T0	545.39 (389.33)	429.43 (325.62)	115.95	0.064	NA	NA	NA	NA	NA	NA
T1	697.40 (443.47)	588.23 (360.69)			152.01	<0.001*	158.79	<0.001*	−6.78	0.879
MoCA										
T0	24.19 (5.36)	26.32 (3.57)	−2.13	0.007*	NA	NA	NA	NA	NA	NA
T1	24.00 (5.22)	25.85 (3.88)			−0.19	0.684	−0.46	0.183	0.27	0.642
BDI-II										
T0	11.20 (8.63)	10.00 (8.23)	1.2	0.416	NA	NA	NA	NA	NA	NA
T1	10.73 (7.89)	10.90 (9.82)			−0.46	0.682	0.83	0.462	−1.29	0.418
UPDRS3										
T0	34.10 (14.82)	25.87 (12.23)	8.23	<0.001*	NA	NA	NA	NA	NA	NA
T1	32.86 (13.64)	28.91 (9.54)			−1.24	0.425	3.03	0.022*	−4.28	0.037*
UPDRST										
T0	55.21 (25.71)	42.75 (18.66)	12.46	0.001*	NA	NA	NA	NA	NA	NA
T1	54.06 (24.00)	49.12 (21.29)			−1.15	0.683	6.37	0.014*	−7.52	0.049*

T0, first visit; T1, follow-up visit; SD, standard deviation; B, beta coefficient; UPSIT, University of Pennsylvania Smell Identification Test; LEDD, equivalent dose of daily levodopa; MoCA, Montreal's Cognitive Assessment; BDI-II, Beck's Depression Inventory-II; UPDRS3, part 3 score of MDS-UPDRS; UPDRST, total score of MDS-UPDRS. *Significance, $p < 0.05$.

10.3389/fnagi.2023.1213977

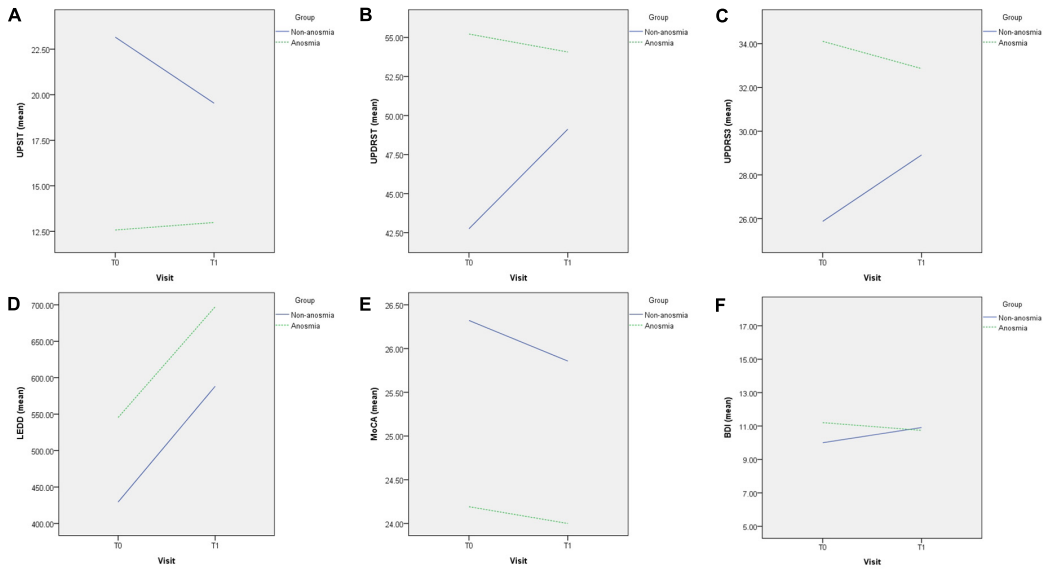

FIGURE 1
Difference in changes between non-anosmia and anosmia group in UPSIT **(A)**, UPDRST **(B)**, UPDRS3 **(C)**, LEDD **(D)**, MoCA **(E)**, and BDI-II **(F)** during the follow-up. T0, first visit; T1, follow-up visit; UPSIT, University of Pennsylvania Smell Identification Test; UPDRST, total score of MDS-UPDRS; UPDRS3, part 3 score of MDS-UPDRS; LEDD, equivalent dose of daily levodopa; MoCA, Montreal's Cognitive Assessment; BDI-II, Beck's Depression Inventory-II.

baseline. Although there were trends of increasing UPDRS T and UPDRS 3 scores in the non-anosmia group at follow-up (**Figures 1B, C** and **Table 2**), the time effect lost its significance after adjustment (**Table 3**). However, the group-by-time effect for UPDRS 3 remained significant ($\beta = -4.2$, $p < 0.038$) after adjusting for age, gender, and disease duration (**Table 3**). The increase in UPDRS 3 score was much more pronounced in the non-anosmia group (**Figure 1C**).

Regarding LEDD, the time effects for both the anosmia group ($\beta = 116.90$, $p = 0.001$) and the non-anosmia group ($\beta = 122.28$, $p = 0.001$) were significant, but there was no significance in either group effect or group-by-time effect (**Figure 1D** and **Table 3**).

3.5. Change in cognition and mood in anosmia/non-anosmia groups

The MoCA score was lower in the anosmia group with a significant group effect ($\beta = -2.13$, $p = 0.007$) (**Table 2**), but the significance disappeared after adjusting for age, gender, and disease duration (**Table 3**). No significant effects for MoCA were found for time or group-by-time effects (**Figure 1E** and **Table 3**). Likewise, no significant effects were found for BDI in terms of group effect, time effect, or group-by-time effect (**Figure 1F** and **Table 3**).

4. Discussion

The present study demonstrated that the UPSIT score regressed in the non-anosmia group while remaining stable in the anosmia group. Notably, the non-anosmia group had a relatively short course of the disease in this study. Our findings are consistent with those of other longitudinal studies. For instance, Lewis et al. (2020) analyzed PD patients annually and found that UPSIT significantly decreased in early and middle-stage PD but not in later-stage PD with disease duration exceeding 5 years. Domellof et al. (2017) explored the UPSIT outcome with the interaction effect between the group (hyposmic/normosmic) and time, revealing that UPSIT deteriorated over time in the normosmic group while remaining stable in the hyposmic group. Meusel et al. (2010) showed a larger olfactory decline in the subgroup of patients with no severe initial olfactory deficit over 5 years of tracking. The patients with marked olfactory regression had an average disease duration of 2.3 years at the beginning of the visit.

Our results support these findings by indicating that the rate of olfactory decline with disease progression is more pronounced in patients without severe initial olfactory deficits, whereas the olfactory deficit remains relatively stable in patients with profound olfactory deficits. While olfactory impairment is considered a premotor feature of Parkinson's disease (PD), it is important to note that the olfactory impairment may continue to progress even after motor symptoms have emerged until it reaches a point known as the "floor effect" in the current olfactory test (Fullard et al., 2017). This corresponds to the hypothesis proposed by Huisman et al. (2004) suggesting that dopaminergic neurons in the olfactory bulb, which act as possible suppressors in olfactory transmission, increase as a compensatory mechanism to the dopamine deficit in the basal ganglia. With disease progression, the decrease in olfactory bulb volume and the deposition of Lewy bodies in the olfactory bulb may neutralize such inhibitory changes, resulting in less significant olfactory degeneration (Herting et al., 2008). However, olfactory loss in PD may not be simply explained by imbalance of dopamine projection because the olfactory function involves several neurotransmitters such as acetylcholine, norepinephrine, serotonin and GABA (Doty, 2017). As olfactory

TABLE 3 Generalized estimating equation analysis for the comparison of outcomes, adjusted for age, gender, and disease duration.

	Mean (SD)		Group effect (anosmia vs. non-anosmia)		Time effect, anosmia (T1 vs. T0)		Time effect, non-anosmia (T1 vs. T0)		Group × time effect	
Outcome	Anosmia	Non-anosmia	*B*	*P*-value	*B*	*P*-value	*B*	*P*-value	*B*	*P*-value
UPSIT										
T0	12.57 (4.45)	23.16 (3.46)	−10.39	<0.001*	NA	NA	NA	NA	NA	NA
T1	12.98 (4.75)	19.53 (6.29)			0.55	0.435	−3.48	<0.001*	4.03	<0.001*
LEDD										
T0	545.39 (389.33)	429.43 (325.62)	84.79	0.112	NA	NA	NA	NA	NA	NA
T1	697.40 (443.47)	588.23 (360.69)			116.9	0.001*	122.28	0.001*	−5.37	0.904
MoCA										
T0	24.19 (5.36)	26.32 (3.57)	−1.26	0.061	NA	NA	NA	NA	NA	NA
T1	24.00 (5.22)	25.85 (3.88)			−0.01	0.978	−0.23	0.53	0.21	0.711
BDI-II										
T0	11.20 (8.63)	10.00 (8.23)	0.47	0.751	NA	NA	NA	NA	NA	NA
T1	10.73 (7.89)	10.90 (9.82)			−0.8	0.491	0.42	0.712	0	0.447
UPDRS3										
T0	34.10 (14.82)	25.87 (12.23)	6.9	0.002*	NA	NA	NA	NA	NA	NA
T1	32.86 (13.64)	28.91 (9.54)			−1.9	0.239	2.32	0.095	−4.2	0.038*
UPDRST										
T0	55.21 (25.71)	42.75 (18.66)	8.52	0.015*	NA	NA	NA	NA	NA	NA
T1	54.06 (24.00)	49.12 (21.29)			−3.31	0.265	4.01	0.138	−7.33	0.054

T0, first visit; T1, follow-up visit; SD, standard deviation; B, beta coefficient; UPSIT, University of Pennsylvania Smell Identification Test; LEDD, equivalent dose of daily levodopa; MoCA, Montreal's Cognitive Assessment; BDI-II, Beck's Depression Inventory-II; UPDRS3, part 3 score of MDS-UPDRS; UPDRST, total score of MDS-UPDRS. *Significance, $p < 0.05$.

10.3389/fnagi.2023.1213977

dysfunction appears to be more closely associated with the body-first type of alpha-synuclein propagation, the pathology primarily affecting the dorsal motor nucleus of the vagus or brainstem may impact olfactory function through the development of alpha-synucleinopathy in the bilateral olfactory bulbs or other brainstem nuclei that project to the olfactory system (Borghammer, 2021). Some cross-sectional studies have shown that olfactory degeneration is unrelated to the disease's course (Cavaco et al., 2015; Masala et al., 2018). Other longitudinal studies have also shown no significant change in olfaction over time in patients with PD (Doty et al., 1988; Muller et al., 2002; Herting et al., 2008; Campabadal et al., 2017; Fujio et al., 2020). Such different results may be related to different study designs, such as the number of patients enrolled, the characteristics of different patient groups, and so on. In our study, patients were divided into two groups, anosmia and non-anosmia, and the course of the disease differed between the two groups. Therefore, grouping patients according to the degree or duration of olfactory abnormalities may explain the discrepancies between the results of these studies.

Olfactory deterioration in patients with PD is thought to be associated with cognitive decline, and in particular, the accuracy of olfactory identification tests is often affected by cognitive decline (Laing and Doty, 2003). However, the results of this study showed that although the UPSIT scores of the non-anosmia group decreased after follow-up, there was no significant difference in the MoCA scores for the cognitive function component. This may suggest that while there is a significant association between hyposmia in PD patients and cognitive decline, the initial regression in olfactory identification is not solely attributed to cognitive decline. Other factors, such as Lewy body-related pathology in the peripheral and central olfactory organs or change in the balance of neurotransmitters, may play a role.

Regarding disease severity, although the association with olfactory abnormalities remains inconclusive, our study found a significant association between UPSIT and UPDRS T score and UPDRS 3 scores, in line with the results of other studies (Roos et al., 2019). Unlike the longitudinal study by He et al. (2020) which showed that olfactory abnormalities were predictive of disease progression, our study found no change in UPDRS T and UPDRS 3 score in the anosmia group during short-term follow-up, but there was a tendency for symptoms to progress in the non-anosmia group. These different results may be due to differences in the length of follow-up, patient subgroups, and analysis methods.

In addition, the worsening of Parkinson's symptoms and olfaction in the non-anosmia group during the follow-up period may indirectly support the theory of Lewy body pathology between the brainstem and olfactory organs, as well as the influence of neurotransmitters such as dopamine. In the Braak staging system, Lewy body pathology was initially found in the olfactory bulb, but this lesion did not progress further, suggesting that a cascade of pathological changes from the brainstem upward is the main pathway (Braak et al., 2003). Horsager et al. (2020) proposed a body-first and brain-first model for the progression of PD pathology based on the presence or absence of RBD and the results of 123I-metaiodobenzylguanidine (MIBG) scintigraphy. The body-first model corresponds to the spreading pathway of the Braak staging system. In addition to autonomic-related prodrome and RBD, the body-first model has a faster progression of motor symptoms and earlier olfactory abnormalities than the brain-first model (Borghammer et al., 2021). These features of the body-first model may reflect the association between olfactory Lewy pathology and the caudo-rostral progression of Lewy pathology. However, olfactory Lewy pathology is not only related to caudo-rostral progression. Kok et al. (2021) found two features of olfactory Lewy pathology in the Vantaa85 + cohort: caudo-rostral progression and amygdala-based progression, corresponding to the body-first and brain-first models, respectively. This may also explain why not all patients in the non-anosmia group in our study turned to anosmia during follow-up and indicates that the severity and pathological changes of olfaction in PD are not a single pattern of progression. Further research with larger, more definitive patient classification, longer follow-up studies, and the inclusion of pathology and imaging is required to elucidate the relationship between olfaction and PD.

This study has some limitations. First, the follow-up period of 1–3 years and the single follow-up session may not have been sufficient to detect changes in clinical data over a longer period. However, changes in olfaction in patients with shorter disease duration and non-anosmia progressed within 3 years, while the severity of significant motor symptoms and cognitive function may require a longer follow-up period to observe a difference. Second, although we tried to exclude the possibility that olfactory tests were affected by diseases such as sinonasal disease or upper respiratory tract infection, which commonly affect the sense of smell, there are many other causes of olfactory abnormalities, including idiopathic causes (which may account for 18% of patients with olfactory abnormalities), that may affect test results (Temmel et al., 2002). Thirdly, for safety and the subjects' preference, we used the On status UPDRS score for the assessment of motor symptoms and disease severity, and therefore, the assessment may be influenced by medication. Nevertheless, these patients are regularly followed up in the outpatient clinic, and the physician ensures that the patient's medication dosage is adequate. We also analyzed LEDD, which showed that the non-anosmia group had a lower LEDD than the anosmia group, but there was no significant difference between the two. This indirectly implies that the non-anosmia group was not using fewer medications despite having a lower UPDRS score. Therefore, the effect of insufficient dosage of medication on the increasing UPDRS score in the non-anosmia group in this study may be subtle.

5. Conclusion

In conclusion, this study shows that olfactory sensation may still regress in Parkinson's patients with a shorter course of the disease without anosmia, while it remains stable in the anosmia group. Such a decline in olfaction may not be related to cognitive status but may be associated with disease progression. Larger, long-term follow-up studies incorporating pathology and imaging analysis are needed to elucidate the underlying mechanisms.

Data availability statement

The raw data supporting the conclusions of this article will be made available by the authors, without undue reservation.

Ethics statement

The studies involving human participants were reviewed and approved by the Taichung Veterans General Hospital Institutional Review Board/Ethics Committee (No. CE22189B). The patients/participants provided their written informed consent to participate in this study.

Author contributions

T-CF and M-HC conceptualized the project. T-CF and Y-ST performed the data acquisition and analysis. T-CF wrote the first draft of the manuscript. M-HC critically reviewed the manuscript. All authors contributed to writing and revising the manuscript.

Funding

This study was funded by the Taichung Veterans General Hospital TCVGH 1123402C and 1123401C.

Acknowledgments

We thank the staffs at the Department of Neurology in Taichung Veteran General Hospital for participant recruitment.

Conflict of interest

The authors declare that the research was conducted in the absence of any commercial or financial relationships that could be construed as a potential conflict of interest.

Publisher's note

All claims expressed in this article are solely those of the authors and do not necessarily represent those of their affiliated organizations, or those of the publisher, the editors and the reviewers. Any product that may be evaluated in this article, or claim that may be made by its manufacturer, is not guaranteed or endorsed by the publisher.

References

Beck, A., Steer, R., and Brown, G. (1996). *BDI-II: Beck Depression Inventory Manual*, 2nd Edn. San Antonio: Psychological Corporation.

Berendse, H. W., Roos, D. S., Raijmakers, P., and Doty, R. L. (2011). Motor and non-motor correlates of olfactory dysfunction in Parkinson's disease. *J. Neurol. Sci.* 310, 21–24. doi: 10.1016/j.jns.2011.06.020

Borghammer, P. (2021). The alpha-Synuclein Origin and Connectome Model (SOC Model) of Parkinson's Disease: Explaining motor asymmetry, non-motor phenotypes, and cognitive decline. *J. Parkinsons Dis.* 11, 455–474. doi: 10.3233/JPD-202481

Borghammer, P., Horsager, J., Andersen, K., Van Den Berge, N., Raunio, A., Murayama, S., et al. (2021). Neuropathological evidence of body-first vs. brain-first Lewy body disease. *Neurobiol. Dis.* 161:105557. doi: 10.1016/j.nbd.2021.105557

Braak, H., Del Tredici, K., Rub, U., de Vos, R. A., Jansen Steur, E. N., and Braak, E. (2003). Staging of brain pathology related to sporadic Parkinson's disease. *Neurobiol. Aging* 24, 197–211. doi: 10.1016/s0197-4580(02)00065-9

Campabadal, A., Uribe, C., Segura, B., Baggio, H. C., Abos, A., Garcia-Diaz, A. I., et al. (2017). Brain correlates of progressive olfactory loss in Parkinson's disease. *Parkinsonism Relat. Disord.* 41, 44–50. doi: 10.1016/j.parkreldis.2017.05.005

Cavaco, S., Goncalves, A., Mendes, A., Vila-Cha, N., Moreira, I., Fernandes, J., et al. (2015). Abnormal Olfaction in Parkinson's Disease Is Related to Faster Disease Progression. *Behav. Neurol.* 2015:976589. doi: 10.1155/2015/976589

Domellof, M. E., Lundin, K. F., Edstrom, M., and Forsgren, L. (2017). Olfactory dysfunction and dementia in newly diagnosed patients with Parkinson's disease. *Parkinsonism Relat. Disord.* 38, 41–47. doi: 10.1016/j.parkreldis.2017.02.017

Doty, R. L. (2001). *The Smell Identification Test Administration Manual*. Philadelphia, PA: Sensonics, Inc.

Doty, R. L. (2012). Olfactory dysfunction in Parkinson disease. *Nat. Rev. Neurol.* 8, 329–339. doi: 10.1038/nrneurol.2012.80

Doty, R. L. (2017). Olfactory dysfunction in neurodegenerative diseases: is there a common pathological substrate? *Lancet Neurol.* 16, 478–488. doi: 10.1016/S1474-4422(17)30123-0

Doty, R. L., Deems, D. A., and Stellar, S. (1988). Olfactory dysfunction in parkinsonism: a general deficit unrelated to neurologic signs, disease stage, or disease duration. *Neurology* 38, 1237–1244. doi: 10.1212/wnl.38.8.1237

Ercoli, T., Masala, C., Cadeddu, G., Mascia, M. M., Orofino, G., Gigante, A. F., et al. (2022). Does Olfactory Dysfunction Correlate with Disease Progression in Parkinson's Disease? A Systematic Review of the Current Literature. *Brain Sci.* 12, 513. doi: 10.3390/brainsci12050513

Fujio, H., Inokuchi, G., Kuroki, S., Tatehara, S., Katsunuma, S., Kowa, H., et al. (2020). Three-year prospective study on olfaction of patients with Parkinson's disease. *Auris. Nasus Larynx* 47, 899–904. doi: 10.1016/j.anl.2019.08.008

Fullard, M. E., Morley, J. F., and Duda, J. E. (2017). Olfactory Dysfunction as an Early Biomarker in Parkinson's Disease. *Neurosci. Bull.* 33, 515–525. doi: 10.1007/s12264-017-0170-x

Goetz, C. G., Tilley, B. C., Shaftman, S. R., Stebbins, G. T., Fahn, S., Martinez-Martin, P., et al. (2008). Movement Disorder Society-sponsored revision of the Unified Parkinson's Disease Rating Scale (MDS-UPDRS): scale presentation and clinimetric testing results. *Mov. Disord.* 23, 2129–2170. doi: 10.1002/mds.22340

Haehner, A., Boesveldt, S., Berendse, H. W., Mackay-Sim, A., Fleischmann, J., Silburn, P. A., et al. (2009). Prevalence of smell loss in Parkinson's disease–a multicenter study. *Parkinsonism Relat. Disord.* 15, 490–494. doi: 10.1016/j.parkreldis.2008.12.005

He, R., Zhao, Y., He, Y., Zhou, Y., Yang, J., Zhou, X., et al. (2020). Olfactory dysfunction predicts disease progression in Parkinson's Disease: A longitudinal study. *Front. Neurosci.* 14:569777. doi: 10.3389/fnins.2020.569777

Herting, B., Schulze, S., Reichmann, H., Haehner, A., and Hummel, T. (2008). A longitudinal study of olfactory function in patients with idiopathic Parkinson's disease. *J. Neurol.* 255, 367–370. doi: 10.1007/s00415-008-0665-5

Horsager, J., Andersen, K. B., Knudsen, K., Skjaerbaek, C., Fedorova, T. D., Okkels, N., et al. (2020). Brain-first versus body-first Parkinson's disease: a multimodal imaging case-control study. *Brain* 143, 3077–3088. doi: 10.1093/brain/awaa238

Huisman, E., Uylings, H. B., and Hoogland, P. V. (2004). A 100% increase of dopaminergic cells in the olfactory bulb may explain hyposmia in Parkinson's disease. *Mov. Disord.* 19, 687–692. doi: 10.1002/mds.10713

Jiang, R. S., Su, M. C., Liang, K. L., Shiao, J. Y., Wu, S. H., and Hsin, C. H. (2010). A pilot study of a traditional Chinese version of the University of Pennsylvania Smell Identification Test for application in Taiwan. *Am. J. Rhinol. Allergy* 24, 45–50. doi: 10.2500/ajra.2010.24.3388

Kok, E. H., Savola, S., Raunio, A., Oinas, M., Tuimala, J., Polvikoski, T., et al. (2021). Alpha-synuclein pathology of olfactory bulbs/peduncles in the Vantaa85+ cohort exhibit two divergent patterns: a population-based study. *Acta Neuropathol.* 142, 777–780. doi: 10.1007/s00401-021-02364-6

Laing, D. G. D. G., and Doty, R. L. (2003). *Psychophysical measurement of human olfactory function, including odorant mixture assessment*. New York City, NY: Marcel Dekker.

Lawton, M., Hu, M. T., Baig, F., Ruffmann, C., Barron, E., Swallow, D. M., et al. (2016). Equating scores of the University of Pennsylvania smell identification test and sniffin' sticks test in patients with Parkinson's disease. *Parkinsonism Relat. Disord.* 33, 96–101. doi: 10.1016/j.parkreldis.2016.09.023

Lewis, M. M., Harkins, E., Lee, E. Y., Stetter, C., Snyder, B., Corson, T., et al. (2020). Clinical Progression of Parkinson's Disease: Insights from the NINDS Common Data Elements. *J. Parkinsons Dis.* 10, 1075–1085. doi: 10.3233/JPD-201932

Litvan, I., Goldman, J. G., Troster, A. I., Schmand, B. A., Weintraub, D., Petersen, R. C., et al. (2012). Diagnostic criteria for mild cognitive impairment in Parkinson's disease: Movement Disorder Society Task Force guidelines. *Mov. Disord.* 27, 349–356. doi: 10.1002/mds.24893

Liu, C. C., Li, C. Y., Lee, P. C., and Sun, Y. (2016a). Variations in incidence and prevalence of parkinson's disease in Taiwan: A population-based nationwide study. *Parkinsons. Dis.* 2016:8756359. doi: 10.1155/2016/8756359

Liu, W. M., Wu, R. M., Lin, J. W., Liu, Y. C., Chang, C. H., and Lin, C. H. (2016b). Time trends in the prevalence and incidence of Parkinson's disease in Taiwan: A nationwide, population-based study. *J. Formos Med. Assoc.* 115, 531–538. doi: 10.1016/j.jfma.2015.05.014

Masala, C., Solla, P., Liscia, A., Defazio, G., Saba, L., Cannas, A., et al. (2018). Correlation among olfactory function, motors' symptoms, cognitive impairment, apathy, and fatigue in patients with Parkinson's disease. *J. Neurol.* 265, 1764–1771. doi: 10.1007/s00415-018-8913-9

Meusel, T., Westermann, B., Fuhr, P., Hummel, T., and Welge-Lussen, A. (2010). The course of olfactory deficits in patients with Parkinson's disease–a study based on psychophysical and electrophysiological measures. *Neurosci. Lett.* 486, 166–170. doi: 10.1016/j.neulet.2010.09.044

Muller, A., Reichmann, H., Livermore, A., and Hummel, T. (2002). Olfactory function in idiopathic Parkinson's disease (IPD): results from cross-sectional studies in IPD patients and long-term follow-up of de-novo IPD patients. *J. Neural Transm.* 109, 805–811. doi: 10.1007/s007020200067

Picillo, M., Pellecchia, M. T., Erro, R., Amboni, M., Vitale, C., Iavarone, A., et al. (2014). The use of University of Pennsylvania smell identification test in the diagnosis of Parkinson's disease in Italy. *Neurol. Sci.* 35, 379–383. doi: 10.1007/s10072-013-1522-6

Poewe, W., Seppi, K., Tanner, C. M., Halliday, G. M., Brundin, P., Volkmann, J., et al. (2017). Parkinson disease. *Nat. Rev. Dis. Primers* 3:17013. doi: 10.1038/nrdp.2017.13

Rodríguez-Violante, M., Camacho-Ordoñez, A., Cervantes-Arriaga, A., González-Latapí, P., and Velázquez-Osuna, S. (2015). Factors associated with the quality of life of subjects with Parkinson's disease and burden on their caregivers. *Neurología* 30, 257–263. doi: 10.1016/j.nrleng.2014.01.002

Rodríguez-Violante, M., Ospina-García, N., Pérez-Lohman, C., and Cervantes-Arriaga, A. (2017). Spotlight on olfactory dysfunction in Parkinson's disease. *J. Parkinson. Restless Legs Syndr.* 7, 33–41. doi: 10.2147/jprls.S125390

Roos, D. S., Twisk, J. W. R., Raijmakers, P., Doty, R. L., and Berendse, H. W. (2019). Hyposmia as a marker of (non-)motor disease severity in Parkinson's disease. *J. Neural Transm.* 126, 1471–1478. doi: 10.1007/s00702-019-02074-0

Santos Garcia, D., de Deus Fonticoba, T., Suarez Castro, E., Borrue, C., Mata, M., Solano Vila, B., et al. (2019). Non-motor symptoms burden, mood, and gait problems are the most significant factors contributing to a poor quality of life in non-demented Parkinson's disease patients: Results from the COPPADIS Study Cohort. *Parkinsonism Relat. Disord.* 66, 151–157. doi: 10.1016/j.parkreldis.2019.07.031

Stebbins, G. T., Goetz, C. G., Burn, D. J., Jankovic, J., Khoo, T. K., and Tilley, B. C. (2013). How to identify tremor dominant and postural instability/gait difficulty groups with the movement disorder society unified Parkinson's disease rating scale: comparison with the unified Parkinson's disease rating scale. *Mov. Disord.* 28, 668–670. doi: 10.1002/mds.25383

Taguchi, T., Ikuno, M., Hondo, M., Parajuli, L. K., Taguchi, K., Ueda, J., et al. (2020). alpha-Synuclein BAC transgenic mice exhibit RBD-like behaviour and hyposmia: a prodromal Parkinson's disease model. *Brain* 143, 249–265. doi: 10.1093/brain/awz380

Temmel, A. F., Quint, C., Schickinger-Fischer, B., Klimek, L., Stoller, E., and Hummel, T. (2002). Characteristics of olfactory disorders in relation to major causes of olfactory loss. *Arch. Otolaryngol. Head Neck Surg.* 128, 635–641. doi: 10.1001/archotol.128.6.635

Tibar, H., El Bayad, K., Bouhouche, A., Ait Ben Haddou, E. H., Benomar, A., Yahyaoui, M., et al. (2018). Non-motor symptoms of Parkinson's disease and their impact on quality of life in a cohort of moroccan patients. *Front. Neurol.* 9:170. doi: 10.3389/fneur.2018.00170

Yoo, H. S., Chung, S. J., Lee, Y. H., Ye, B. S., Sohn, Y. H., and Lee, P. H. (2020). Association between olfactory deficit and motor and cognitive function in Parkinson's Disease. *J. Mov. Disord.* 13, 133–141. doi: 10.14802/jmd.19082

frontiers | Frontiers in Aging Neuroscience

TYPE Review
PUBLISHED 19 July 2023
DOI 10.3389/fnagi.2023.1216163

OPEN ACCESS

EDITED BY
Robert Petersen,
Central Michigan University, United States

REVIEWED BY
Diego Castillo-Barnes,
University of Malaga, Spain
Carmen Jiménez-Mesa,
University of Granada, Spain

*CORRESPONDENCE
Beatriz Garcia Santa Cruz
garciasantacruz.beatriz@chl.lu

RECEIVED 03 May 2023
ACCEPTED 28 June 2023
PUBLISHED 19 July 2023

CITATION
Garcia Santa Cruz B, Husch A and Hertel F (2023) Machine learning models for diagnosis and prognosis of Parkinson's disease using brain imaging: general overview, main challenges, and future directions. *Front. Aging Neurosci.* 15:1216163. doi: 10.3389/fnagi.2023.1216163

Machine learning models for diagnosis and prognosis of Parkinson's disease using brain imaging: general overview, main challenges, and future directions

Beatriz Garcia Santa Cruz[1]*, Andreas Husch[2] and Frank Hertel[1]

[1]National Department of Neurosurgery, Centre Hospitalier de Luxembourg, Luxembourg, Luxembourg, [2]Imaging AI Group, Luxembourg Centre for Systems Biomedicine, University of Luxembourg, Esch-sur-Alzette, Luxembourg

Parkinson's disease (PD) is a progressive and complex neurodegenerative disorder associated with age that affects motor and cognitive functions. As there is currently no cure, early diagnosis and accurate prognosis are essential to increase the effectiveness of treatment and control its symptoms. Medical imaging, specifically magnetic resonance imaging (MRI), has emerged as a valuable tool for developing support systems to assist in diagnosis and prognosis. The current literature aims to improve understanding of the disease's structural and functional manifestations in the brain. By applying artificial intelligence to neuroimaging, such as deep learning (DL) and other machine learning (ML) techniques, previously unknown relationships and patterns can be revealed in this high-dimensional data. However, several issues must be addressed before these solutions can be safely integrated into clinical practice. This review provides a comprehensive overview of recent ML techniques analyzed for the automatic diagnosis and prognosis of PD in brain MRI. The main challenges in applying ML to medical diagnosis and its implications for PD are also addressed, including current limitations for safe translation into hospitals. These challenges are analyzed at three levels: disease-specific, task-specific, and technology-specific. Finally, potential future directions for each challenge and future perspectives are discussed.

KEYWORDS

Parkinson's disease, translational ML, neuroimaging, machine learning, deep learning, computer-aided diagnosis, digital health

Introduction

Computer-aided diagnosis (CAD) systems based on medical imaging has the potential to assist clinical practice in the diagnosis of Parkinson's disease (PD). However, the suitability of CAD systems for this application is still being evaluated, and several key aspects must be taken into consideration.

The primary objective of CAD systems is not to replace radiologists and clinicians, but to support them in improving the quality and efficiency of their diagnoses (Chen et al., 2013). Although CAD systems have been in use for several decades, with successful applications in detecting pulmonary nodules (Xu et al., 1997) and breast cancer (Mangasarian et al., 1995), they were previously reliant on manual feature extraction based on domain knowledge. However, with the recent emergence of Machine Learning (ML) techniques, such as Deep Learning (DL), the automatic extraction of features from imaging data has become possible

(Doi, 2007). Furthermore, the availability of large datasets and more powerful computational infrastructure has facilitated the development of advanced ML algorithms, which have the potential to significantly improve the accuracy of CAD systems (Neri et al., 2019).

Although CAD systems based on Artificial Intelligence (AI) have the potential to greatly enhance the effectiveness of clinical diagnosis and prognosis workflows, it is essential to carefully consider several key factors to ensure their safe and effective implementation in clinical practice. In fact, there is often a gap between the research literature on ML models and their final deployment in clinical applications. Closing this gap requires careful consideration and addressing several crucial aspects such as model robustness, data quality and bias, regulatory compliance, integration with existing clinical workflows, and ongoing validation in real-world settings.

A good example of a clinical deployment of an AI system that exemplified this gap is the AI-based tool by Google, Automated Retinal Disease Assessment (ARDA) system. Although this DL system was successfully developed and internally validated at the research level in 2016 (Gulshan et al., 2016), it faced several challenges in transitioning from the theoretical expectations to the reality of deploying the AI model tool in India and Thailand, as discussed in a recent paper highlighting the necessity of considering this gap (Widner et al., 2023).

While previous review papers have thoroughly covered the topic of using ML as a proof-of-concept for CAD systems (Sakai and Yamada, 2019; Mei et al., 2021), there has not been a previous review that specifically addresses the changes and potential solutions associated with the translation of these models into clinical practice for PD imaging using ML.

This review is organized as follows: first, a comprehensive background on PD, including related conditions and proposed clinical subtypes is presented. Second, the diagnosis and prognosis of PD is introduced, with a specific focus on the employment of magnetic resonance imaging (MRI). Lastly, a comprehensive analysis of the present status of computer-aided diagnosis, will be discussed, emphasizing the main limitations and future directions at three different levels. These considerations will take into account the unique features of PD, as well as the limitations of clinical brain imaging datasets, and the challenges associated with ML and DL approaches. By considering these factors, this review aims to provide insights into the potential of CAD in assisting clinical practice in the diagnosis of PD, while also highlighting the challenges that need to be addressed to ensure its safe and effective translation into clinical practice.

Parkinson's disease and related disorders

It has been more than 200 years since the first description of the symptoms of PD by James Parkinson in his essay "The Shaking Palsy" (Parkinson, 2002). This first description refers to some of the most prominent physical landmarks of the disease, such as tremors and flexed posture. Nowadays, we have a more holistic understanding of this complex neurodegenerative disease, but currently, there is no cure, and no established biomarker for differential diagnosis of the disease (Tolosa et al., 2021).

PD is the second most common neurodegenerative disorder after Alzheimer's disease (AD), with more than 10 million people affected worldwide (Marras et al., 2018). One of the main risk factor associated with PD is advanced age. Considering that the elderly population is expected to double by 2050, the number of PD patients is expected to increase accordingly (Nerius et al., 2017). It is characterized by visible motor symptoms such as slowness of movement, muscle rigidity, and tremors at rest (Sveinbjornsdottir, 2016). However, non-motor symptoms such as depression, anxiety, cognitive deficits, sleep disturbance, hyposmia, cardiovascular problems, and bladder dysfunction can also be debilitating and may present before the motor problems (Chaudhuri et al., 2006). Notably, there is growing evidence that PD is associated with gastrointestinal dysfunction and changes to the microbiome, which may have potential as a biomarker (Elfil et al., 2020). By the time the main physical symptoms of PD appear and the patient receives a diagnosis, 30%–50% of the dopamine neurons vulnerable to PD are already lost. Hence, a key goal is to detect and quantify PD biology before their symptoms appear, during the prodromal phase (Pellicano et al., 2007). Clinical markers of this phase are non-motor and motor symptoms. Non-motor symptoms include hyposmia, constipation, REM sleep behavior disorder (RBD), excessive daytime somnolence, depression and/or anxiety, global cognitive deficit, and orthostatic hypotension. Motor symptoms include voice and face akinesia (Hustad and Aasly, 2020).

PD affects various regions of the nervous system and different types of neurons. However, much attention has been given to neurons in brain regions associated with motor symptoms, particularly the *substantia nigra pars compacta* in the midbrain. This region is involved in a critical brain pathway that facilitates movements, known as the nigrostriatal pathway (Eriksen et al., 2009). One of the most widely accepted frameworks to describe the spread of sporadic PD is Braak's hypothesis, which suggests that PD progresses through six different stages, gradually evolving from the lower brain stem to the neocortex (Rietdijk et al., 2017). The gradual degeneration of dopaminergic neurons in the substantia nigra leads to the malfunction of this pathway and the characteristic motor problems. It has been proposed that not all patients follow this progression, and two subtypes have been suggested for the disease evolution: peripheral nervous system first (PNS-first) and central nervous system first (CNS-first) (Borghammer and Van Den Berge, 2019). The existence of these subtypes is supported by *in vivo* imaging studies of RBD-positive and RBD-negative patient groups (Borghammer and Van Den Berge, 2019), as well as for genetic makers (Blauwendraat et al., 2020).

Current treatments for deficits in dopamine often involve the use of drugs that either replace or mimic dopamine in the brain (Cools, 2006). However, over time, the effectiveness of these drugs tends to diminish. In addition to medication, physical therapy can be employed as a complementary approach to enhance cognitive function in individuals with dopamine deficits (da Silva et al., 2018). Physical therapy focuses on improving mobility, balance, and coordination, which can positively impact cognitive abilities. Furthermore, alternative therapeutic avenues are being explored. Probiotics have shown potential in reducing

constipation associated with Parkinson's disease (Tan et al., 2021). Additionally, anaerobic exercise has been investigated as a current approach for managing dopamine deficits (Schootemeijer et al., 2020). Moreover, emerging treatment options include drug repurposing, regenerative therapies, gene therapies, and cell-based treatments (Stoker and Barker, 2020). These innovative approaches offer promising prospects in the management of dopamine-related deficits.

Deep brain stimulation (DBS) is an effective treatment option for PD by targeting the subthalamic nucleus, globus pallidus (Lee et al., 2019), ventral intermedius nucleus (Fasano et al., 2012), and pedunculopontine nucleus (Thevathasan et al., 2018). Next-generation noninvasive DBS technologies, such as noninvasive or minimally invasive DBS (Lozano, 2017), transcranial direct current stimulation (tDCS) (Broeder et al., 2015), and transcranial magnetic stimulation (TMS) (Cantello et al., 2002), have also shown positive effects in reducing non-motor symptoms of PD when appropriate controls for side effects are in place. However, there is currently no cure for neurodegeneration, and current efforts focus on reducing symptoms to improve the quality of life.

Related conditions

Several neurological movement disorders are closely associated with PD, and differentiating it from other diseases can be challenging, especially during the initial stages of the disease (Poewe and Wenning, 2002). Related disorders that share similar clinical features with PD can be classified into two broad categories: degenerative disorders and non-degenerative disorders (Politis, 2014). Degenerative disorders, such as Multiple System Atrophy (MSA), Progressive Supranuclear Palsy (PSP), Corticobasal Degeneration (CBD), Dementia with Lewy Bodies (DLB), and AD, can present with clinical features that overlap with PD. On the other hand, non-degenerative disorders such as Essential Tremor (ET), dystonic tremor, exaggerated physiological tremor, tremor related to hyperthyroidism, vascular parkinsonism, normal pressure hydrocephalus (NPH) (Stolze et al., 2001) and drug-induced parkinsonism can also mimic some of the clinical features of PD.

Parkinson's disease clinical subtypes

The clinical and neuropathological heterogeneity of PD patients is well known, and consequently there have been many attempts to identify different subtypes. Initial approaches consisted of empirical classifications using *a priori* hypotheses (Zetusky et al., 1985; Jankovic et al., 1990). In recent years, research works have progressively employed data-driven cluster analysis that includes longitudinal assessment of motor and non-motor symptoms (De Pablo-Fernández et al., 2019; Zhang et al., 2019; Dadu et al., 2022). This classification method looks promising for informing patients about the future progression of the disease and for personalizing treatment. However, these criteria are not yet applied in clinics since more research is needed to unify and validate the criteria using well-curated longitudinal cohorts. Among the multiple attempts to separate the disease, several criteria have been applied, including early-onset vs. late-onset (Riboldi et al., 2022) slow vs. fast progression, with or without dementia or tremor-dominant vs. gait-dominant (Dadu et al., 2022).

Machine learning, deep learning and computer vision

In recent years, ML and DL have gained significant attention in healthcare and medical research. These computational tools enable the analysis of large and complex datasets to learn patterns and relationships, with DL algorithms utilizing multiple layers of artificial neural networks to extract abstract data representations such as images. Furthermore, Computer Vision (CV) seeks to enable computers to interpret and understand visual information from the surrounding environment. Supervised learning is a common type of ML employed in PD research, where labeled datasets are used to train the algorithm to make predictions on unseen data. Convolutional neural networks (CNNs) are the most frequently used type of neural network for image recognition to conduct tasks such as classification in medical imaging. In Figure 1, a graphical representation of the training and development of a ml-based system for clinical use is depicted.

The quality of data and labels are crucial factors that can significantly impact the performance of ML models. In current ML models, data is the most important component as the models learn from the data presented to them. Therefore, the quality of the data used in the training process is crucial. Other factors that can influence the quality of models include the choice of ML algorithms, feature engineering, hyperparameter tuning, and model selection. In addition to data quality, the quality of labels is also critical. Poor quality labels can result in biased models, incorrect predictions, and suboptimal performance. Moreover, data representation is equally important for a good model performance. A training set should be a representation of the event that we want to model, and a good validation strategy is essential for assessing the generability of the model.

Parkinson's disease diagnosis and prognosis

Accurate diagnosis of PD is essential, and achieving enough specificity to distinguish between similar conditions during the clinical phase is crucial. Developing monitoring tools to track disease progression and evaluate individual patient response, including the presence and magnitude of treatment side effects, is also necessary. Furthermore, quantifying the different systems, such as motor, memory, and limbic system, could help stratify patients. In terms of prognosis, ongoing efforts are focused on establishing clear criteria for patient stratification into different subtypes, which would aid in the development of targeted

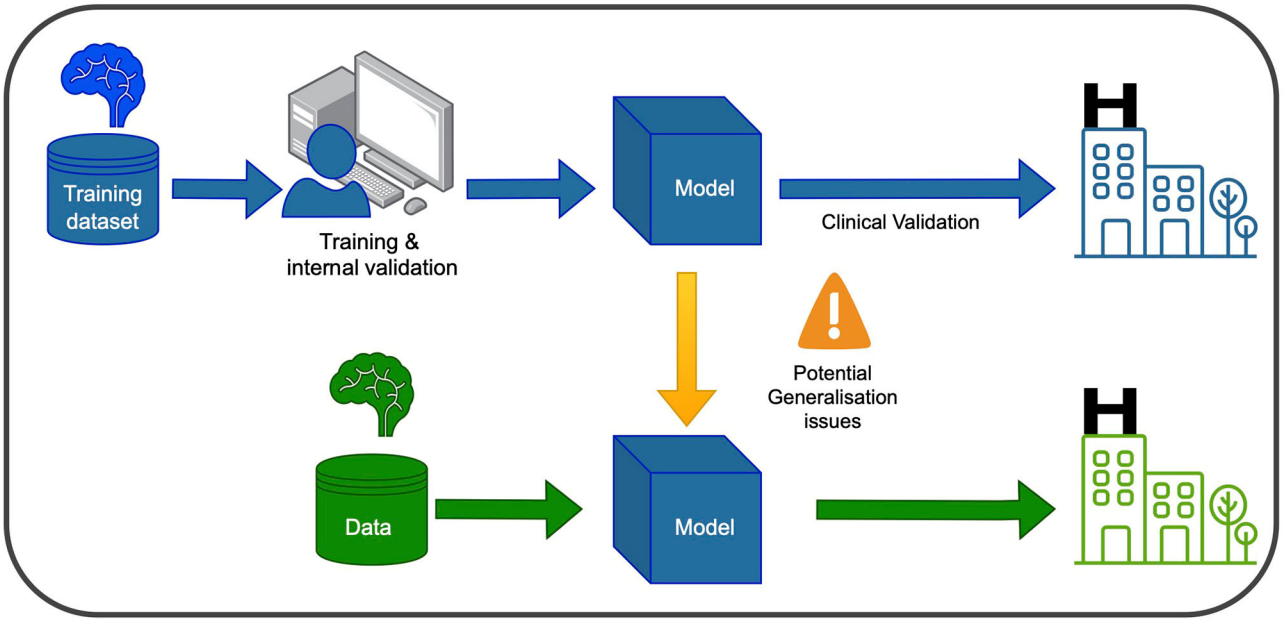

FIGURE 1
Training and using an ML model in the clinic involves two main phases. In the blue phase, the model is trained and validated using data from the same hospital. This ensures it learns from the hospital's specific context and performs well within that setting. After this, the model undergoes clinical validation to ensure its reliability and safety before deployment. In the green phase, the model can be used in new hospitals, but caution is needed to address potential generalization issues. Variations in healthcare systems and patient populations may affect its performance. Thorough testing and evaluation are necessary to ensure accurate and safe application in different healthcare settings.

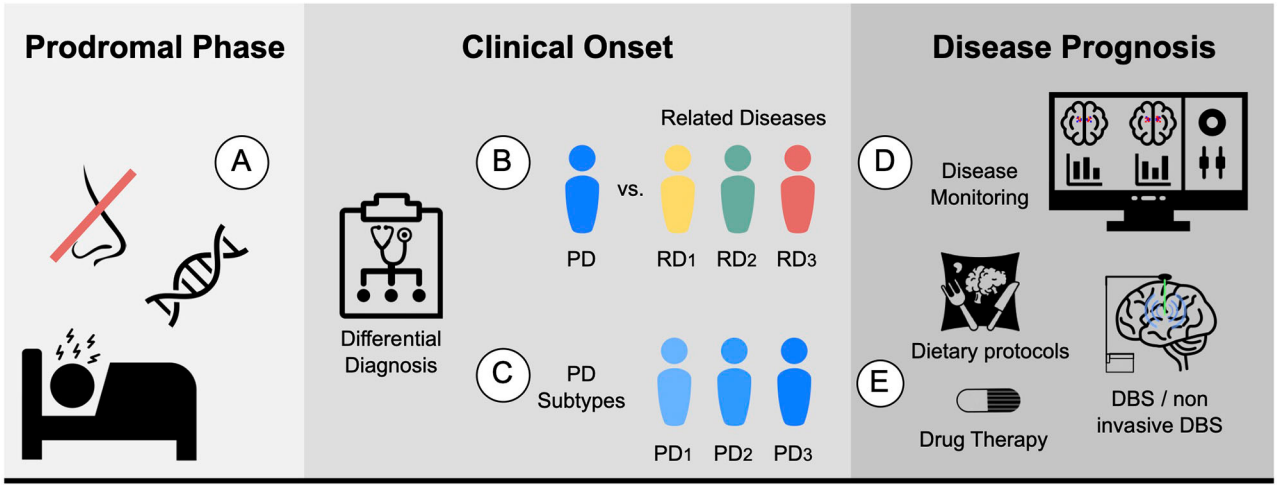

FIGURE 2
Proposed biomarkers for PD using MRI: **(A)** Prodromal biomarker: identifying brain changes during the prodromal phase. **(B)** Differential diagnosis biomarker: assisting in distinguishing PD from related diseases. For instance, ET or MSA. **(C)** Subtype biomarker: classifying PD patients into their corresponding subtypes. **(D)** Progression biomarker: aiding in predicting the progression of the disease and treatment response with disease monitoring. **(E)** Therapy response biomarker: facilitating personalized medicine by finding the best drug, dietary protocols, physical or cognitive therapies, and predicting the potential response to other therapies such as DBS and non-invasive DBS.

treatment approaches. Figure 2 proposes five different biomarkers that are relevant in the context of PD.

The current diagnostic criteria for PD is biased on a comprehensive evaluation of a patient's clinical presentation and medical history. Given the lack of a definitive diagnostic test for PD, clinicians rely on a variety of subjective and objective measures to make an accurate diagnosis. Clinical evaluation, involving detailed inquiry into the patient's symptoms, medical history, and family history, represents a fundamental component of the diagnostic process. Alongside this, a thorough physical examination aimed at assessing motor function, including muscle strength, reflexes, and coordination, as well as cognitive function and mood, is also

typically conducted. To support a clinical diagnosis, objective tests may be employed. Imaging modalities such as MRI or computed tomography (CT) scans are typically employed to rule out other conditions that may present similarly to PD. Furthermore, nuclear imaging techniques such as Single Photon Emission Computed Tomography (SPECT) and Positron Emission Tomography (PET) can serve to buttress the diagnosis of PD.

Nowadays, there is a significant effort to find biomarkers for PD. In the preclinical phase, it highlights biomedical markers, such as those that measure the activity of mitochondria dysfunction and oxidative stress (He et al., 2018). Others focus on measuring abnormal protein aggregation and accumulation, such as alpha-synuclein (Foulds et al., 2011) or tau protein (Constantinescu and Mondello, 2013). Some try to measure established clinical features such as olfactory dysfunction, RBD, or constipation. During the prodromal phase, genetic biomarkers have been explored, such as mutations in Parkin (Pickrell and Youle, 2015), Leucine-rich repeat kinase 2 (LRRK2) (Tolosa et al., 2020), or Alpha-synuclein (SNCA) (Mata et al., 2010). Finally, neuroimaging techniques are also promising.

In the context of brain imaging, a biomarker is an objective characteristic derived from an *in vivo* image that measures a normal biological process, pathological process, or response to a therapeutic intervention (Mohammadi, 2013). It must fulfill the following criteria: be quantitative, repeatable, reproducible, precise, reliable, sensitive, and specific, and be measured on a ratio or interval scale (Smith et al., 2003).

Medical imaging in Parkinson's disease

The main advantage of brain imaging is that it allows for the visualization of the functional and structural brain changes that result from underlying pathophysiological abnormalities (Saeed et al., 2017). There are several imaging techniques that can be used to aid in the diagnosis and prognosis of PD.

On the one hand, there is a set of non-invasive techniques for investigating PD, such as **structural magnetic resonance imaging** (MRI) with T1, T2, and susceptibility-weighted sequences, which allow for volumetric and voxel-based morphometric analyses, as well as MRI-derived visual signatures (Saeed et al., 2017; Chougar et al., 2021). For instance, Schwarz et al. (2014) proposed that the appearance of the dorsolateral substantia nigra as a "swallow tail" shape on high-resolution, iron-sensitive, MRI at 3T, where healthy nigrosome-1 appears as a characteristic feature that could be employed as a marker of degeneration in that area. Further, a promising structural MRI sequence for PD diagnosis is neuromelanin-sensitive MRI (NM MRI), which can detect neuromelanin, a pigment synthesized by the substantia nigra dopamine neurons that is lost when neurons die in PD patients. NM's avid binding of iron enables its detection via magnetic resonance imaging (Sulzer et al., 2018). The use of NM MRI to define regions of interest (ROIs) in the substantia nigra pars compacta (SNpc) has shown promising results compared to using T2*-weighted contrasts. This approach has yielded consistent results, and studies have found that the mean R2* in the SNpc, as defined by neuromelanin-sensitive MRI, was significantly increased in PD patients (Langley et al., 2019).

Diffusion tensor MRI (DT-MRI) is another technique used to study the structural connectivity of the brain in PD. DT-MRI investigates the integrity of white matter tracts connecting different brain regions, and studies have shown that it can detect changes in white matter connectivity in PD patients. Specifically, Yoshikawa et al. (2004) demonstrated that DT-MRI can detect the loss of fractional anisotropy (FA) in the nigrostriatal projection, indicating that more than half of the dopaminergic neurons in this projection may be lost before the onset of PD.

Furthermore, **functional magnetic resonance imaging** (fMRI) can detect changes in blood flow in response to neural activity, which enables researchers to study brain function. In PD, fMRI has been used to investigate changes in brain activity related to both motor and non-motor symptoms. For instance, Tahmasian et al. (2015) employed resting-state (rs-fMRI) to assess the effect of dopamine replacement therapies, such as levodopa and dopamine agonists, on PD patients. Additionally, researchers have used fMRI techniques to investigate the effect of DBS therapy in the modulation of specific brain regions. An example of this is a study by Boutet et al. (2021), in which fMRI brain response patterns were used to predict the optimal parameters for DBS by identifying patterns associated with clinically effective stimulation that preferentially engages the motor circuit.

Additionally, **Transcranial sonography** (TCS) is an ultrasound-based neuroimaging technique that utilizes low frequency sound waves to generate images of the brain. In the context of PD diagnosis, TCS has been employed to investigate the structure and function of the SN, among other brain regions. Mahlknecht et al. (2013) demonstrated that TCS exhibits favorable diagnostic accuracy in detecting PD subjects based on the presence of hyperechogenicity in the SN Furthermore, TCS has been investigated as a potential tool to establish disease progression biomarkers that could provide real-time feedback on the rate of dopaminergic neuronal death in animal models (Zhang et al., 2020).

On the other hand, invasive **molecular imaging** techniques such as PET and SPECT can detect reduced density of dopaminergic nerve terminals in the basal ganglia. PET is an *in vivo* functional neuroimaging technique that utilizes a variety of radionuclides to assess the integrity of the dopaminergic system, cerebral metabolism, pathological protein accumulation, and inflammation in the brain (Saeed et al., 2017). Radiotracers, such as 18F-dopa (Morrish et al., 1996) and 11C-raclopride (Politis et al., 2008), can image the integrity of presynaptic and postsynaptic nigrostriatal and hypothalamus projections, respectively. Using SPECT, dopamine transporter SPECT (DAT SPECT) imaging is an objective tool for assessing dopaminergic function of presynaptic terminals, differentiating parkinsonian disorders related to striatal dopaminergic deficiency from those not related. DAT SPECT imaging can confirm or exclude a diagnosis of dopamine-deficient parkinsonism and detect dopaminergic dysfunction in presymptomatic subjects at risk for PD. Normal DAT SPECT findings exclude presynaptic striatal dopaminergic insufficiency, while abnormal findings indicate a variety of diseases with this insufficiency as a common pathophysiological process (Akdemir et al., 2021). For instance, DaT SPECT imaging with (123I)ioflupane is a useful tool to distinguish between PD-tremor and non-PD tremor, such as ET (Bajaj et al., 2013). Besides,

other non-dopaminergic imaging techniques such as glucose metabolism and PDE10A expression have been proposed to study PD (Pagano et al., 2016). Additionally, extrastriatal ^{123}I-FP-CIT SPECT impairment has been proposed to detect early cases of PD (Nicastro et al., 2020).

While imaging techniques are currently used for research purposes and can assist in challenging cases, they are not commonly used for diagnosing PD. However, it is worth noting that most PD diagnoses do not involve imaging. In the future, brain imaging could be integrated into the diagnostic process as advancements in techniques like ML and CV hold promise for improving the analysis of imaging data. These developments may enable more accurate and reliable diagnostic applications of imaging in PD.

Computer-aided diagnosis using brain imaging: main limitations and future directions

The main limitations of CAD systems in the context of PD can be grouped into three categories. The first set of limitations represented in Figure 3 pertains to the particularities of PD, its diagnosis, and prognosis. The second set of limitations is associated with the characteristics of datasets consisting of brain imaging. These limitations include factors such as the heterogeneity of the imaging modalities used, variability in image acquisition protocols, challenges in image preprocessing and feature extraction, and issues related to sample size and data quality. The third set of limitations is associated with the use of ML/DL-based algorithms for CAD systems. These limitations include challenges such as overfitting, lack of interpretability, bias and generalization issues, and difficulties in integrating multiple data sources. A summary of the main limitations can be found in Table 1, which will serve as a reference point throughout the discussion of potential solutions to address these limitations.

CAD systems have the potential to improve the accuracy and efficiency of diagnosing various diseases. By analyzing medical imaging data, genetic data, and clinical data, these systems can identify patterns and biomarkers associated with the disease that may be difficult to detect otherwise, which can accelerate the diagnostic and treatment workflows in clinical pathways. Moreover, CAD systems can be employed to evaluate disease progression, measure therapeutic responses to drugs in clinical trials, and speed up the development of new treatments.

Other benefits of CAD systems include the objectification of diagnosis, as the current diagnosis relies on subjective evaluation of motor and non-motor symptoms, making CAD systems promising tools for the objective evaluation of symptoms. In the context of MRI for PD, CAD systems can provide quantitative measures of the changes associated with the disease at physical, functional, and metabolic levels. Furthermore, the employment of CAD systems could aid in the unification of clinical diagnosis criteria. Additionally, CV solutions, including those that employ DL as an optimisation technique, have been shown to excel at detecting subtle changes and complex patterns in comparison with human vision. Therefore, CAD systems have the potential to serve as a valuable second or supporting opinion, as they do not experience a reduction in productivity over time, as can happen with human experts.

There are many research-level papers proposing proof-of-concept approaches for CAD systems in PD, emphasizing the importance of robust models. For instance, Castillo-Barnes et al. (2018) utilized the PPMI dataset and proposed an Ensemble Classification model to classify PD patients. Similarly, Augimeri et al. (2016) demonstrated the potential of support vector machines in combination with careful feature extraction to analyze DaTSCAN scans for PD applications. In line with these studies, Martínez-Murcia et al. (2014) also proposed a PD classification method using DaTSCAN scans.

Similarly, machine learning (ML) has been employed to distinguish between PD and related disorders. For instance, Talai et al. (2021) propose a multimedia approach using T1-weighted, T2-weighted, and diffusion tensor imaging (DTI) to aid in the differential diagnosis of progressive supranuclear palsy Richardson's syndrome (PSP-RS). In the same vein, Martins et al. (2021) reported on the use of PET uptake and MRI for distinguishing Parkinsonian syndromes. Similarly, Castillo-Barnes et al. (2020) conducted a study that employed SPECT scans from the PPMI database and compared different ML methods.

More recently, CNN has been successfully proposed for the classification of brain imaging in PD. For instance, Chakraborty et al. (2020) proposed a classification using T1 weighted MRI scans using CNNs. Similarly, Martinez-Murcia et al. (2019) demonstrated the use of autoencoders to classify complex neurological diseases such as Alzheimer's. Finally, Shinde et al. (2019) also demonstrated the potential of CNNs in the modality of neuromelanin-sensitive MRI with great performance (Biondetti et al., 2020).

The mentioned research-level papers and alike ones, provide a valuable insights into the potential of CAD systems for PD. However, it is crucial to acknowledge that these studies primarily focus on demonstrating the effectiveness of specific methodologies or models in isolated aspects of PD diagnosis or classification. While their findings are promising and essential to the progress in the area, they represent only a fraction of what is required for the development of comprehensive and practical clinical systems.

To build end-to-end clinically useful CAD systems for PD, various aspects need to be considered beyond the individual proof-of-concept models. These aspects may include data acquisition and quality assurance, integration with existing clinical workflows, interpretability of the models, regulatory compliance, ethical considerations, scalability, and validation in diverse patient populations. The following sections of the paper will delve into these critical considerations and discuss potential solutions to ensure the successful implementation and utilization of CAD systems in real-world clinical settings.

Limitations associated with Parkinson's disease

Disease heterogeneity: intra-class variance and inter-class similarity

Medical conditions may have several etiologies. Moreover, one etiology may lead to more than one disease (Coleman and Tsongalis, 2009). Consequently, medical conditions are commonly

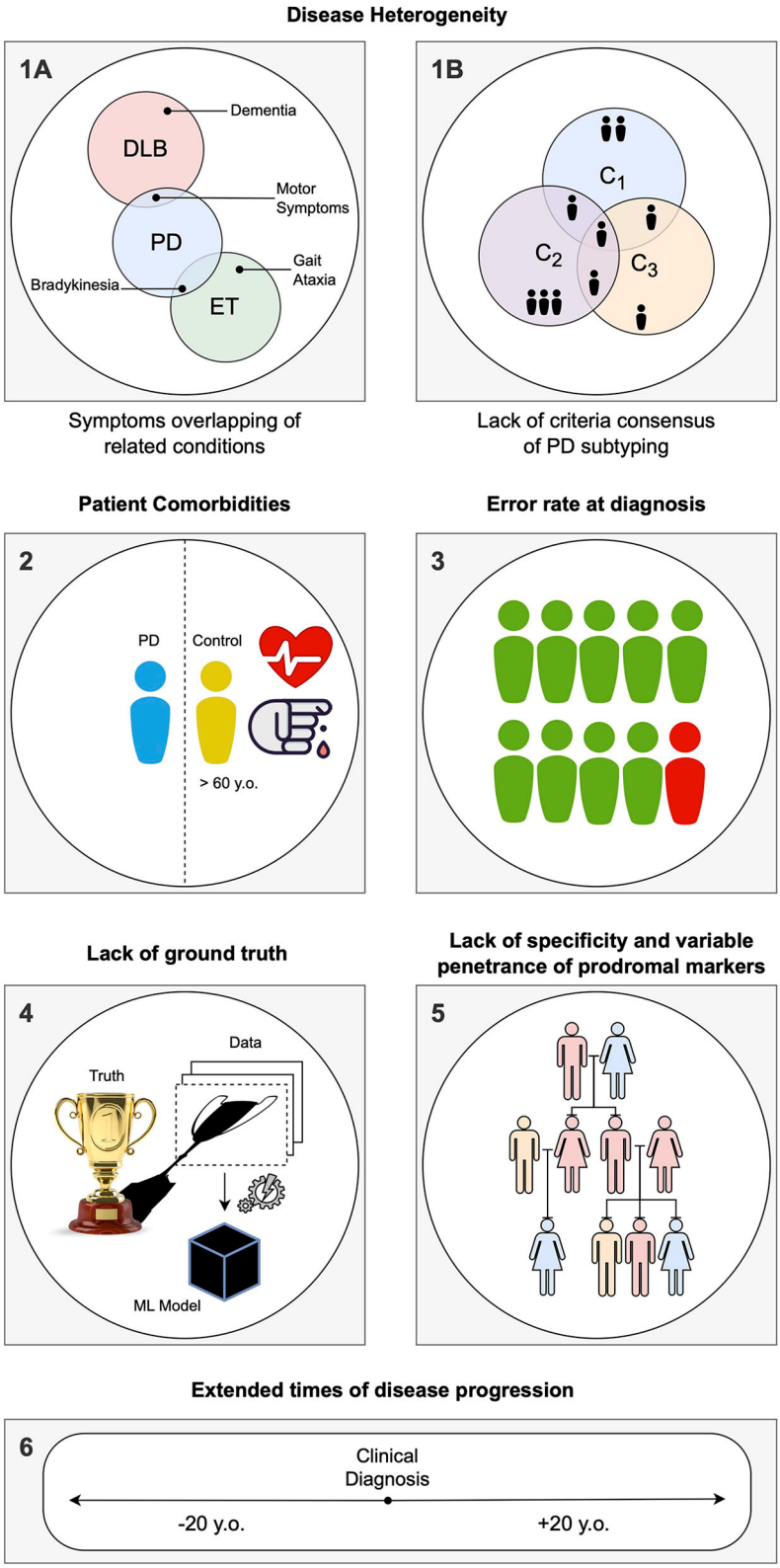

FIGURE 3
Summary of the specific limitations in computer-aided diagnosis (CAD) for Parkinson's disease (PD) associated with idiosyncrasies of the disease, as addressed in Section Limitations associated with Parkinson's disease: **(1)** During the labeling of datasets for supervised learning, several problems can be encountered. **(1A)** Building a solution for differential diagnosis can be challenging due to the overlapping symptoms of PD and related disorders. This challenge is especially significant during the initial phases of clinical diagnosis, where such solutions would be most useful. **(1B)** PD is known to have several subtypes with implications for clinical treatment, but there is a lack of clear global consensus, adding another layer of complexity. **(2)** PD being an age-related disorder, the control subjects used in age-pairing may have additional health conditions or factors that can affect their

(Continued)

FIGURE 3 (Continued)
representatives as healthy individuals. **(3)** Due to the complexity of PD, there is a notable rate of misdiagnosis, even in specialized centers, particularly during the early phases of clinical diagnosis. This hampers the accuracy of labels used in supervised learning solutions. **(4)** When acquiring data and building a model, a simplification of the disease within the context of human biology is necessary, as it is the case with any other data-driven solution. Consequently, any developed solution will have errors, particularly if the model is used in different conditions than those it was designed for. **(5)** Detecting PD in the prodromal phase is particularly challenging. A common approach is to employ known markers that increase the probability of developing the disease, such as genetic mutations. However, the specificity of these markers to PD is variable. **(6)** Conducting long-term longitudinal studies that are consistent in terms of acquisition protocol while maintaining low levels of drop-out rates is extremely difficult for PD, given its nature as a complex, long-term neurodegenerative disease.

TABLE 1 Overview of limitations and future directions at the three levels: disease-specific, task-specific, and technology-specific.

Limitations	Directions
Parkinson's disease	
Disease heterogeneity	Considering subgroups of PD and careful assessment of controls
Patients' comorbidities	Large and Long studies and control of unwanted correlations
Error rate at diagnosis	Acknowledging errors and employing noise-labeled techniques
Extended times of disease progression	Institutional incentives, importance of consistency in protocols
High variability of prodromal markers	Multimodal prodromal markers, epigenetics changes
Lack of ground truth	Objective measures, holistic multidisciplinary approach
Clinical brain imaging datasets	
Complexity of brain imaging	Multimodal approach, combination with clinical measures
Lack of standardization in acquisition	Standardization of acquisition, sharing study assumptions
Lack of standardization in preprocessing	Sharing raw data and reproducible code ability
Lack of standardization in annotation	Assisted annotation with guidelines and unsupervised learning
Machine learning/deep learning	
Generalization issues	Avoid overfitting, control for spurious correlations
Algorithmic Bias	Acknowledge algorithm bias and prioritize fairness strategies
Need for better interpretability	Prioritize transparency and ethics, GDPR compliance
Model explainability	Use explainable ML algorithms, employ interpretability methods
Model uncertainty	Documentation of uncertainty sources, calibration methods
Costly systems to develop and maintain	Pre-train models, cloud computing, decentralized ML
Security and privacy challenges	Proactive security and privacy strategies

defined clinically or pathologically (instead of etiologically). PD presents high variability at both prodromal and clinical phases (He et al., 2018). We can refer to this variability as an intra-class variance. However, another level of complexity exists due to the overlap of PD symptoms with those from other diseases, which calls for thorough differential diagnosis (Kalia and Lang, 2015). For instance, patients with arterial hypertension may exhibit distinct neuroimaging abnormalities detectable by brain MRI (van Veluw et al., 2014), which may complicate the diagnosis of PD using medical imaging techniques in these individuals. Thus, we can find a high inter-class similarity. Finally, diseases are described based on a definable deviation from a normal phenotype made evident through symptoms, and pathological markers, to then become grouped into categories. However, studies and taxonomies struggle to find a consensus for PD subtypes (Albrecht et al., 2022). Hence, studies may employ different subtypes to refer to the same biological mechanism and therapy response.

Patients' comorbidities

In addition to the aforementioned complexity, the onset age of PD in patients is typically around 60 years, making it difficult to differentiate symptoms caused by aging and other comorbidities from those of PD (Deeb et al., 2019). For instance, common comorbidities in PD patients, such as hypertension and diabetes, have an unknown effect on the pathogenesis and progression of PD (Santiago et al., 2017). This presents a twofold challenge: first, it complicates the identification of a reliable set of control and diseased subjects, making it difficult to distinguish between groups. Second, due to the lack of knowledge regarding the effects of comorbidities on PD onset and development, controlling for these characteristics is challenging. As a result, researchers may face a "lose–lose" situation, as ML models may make assumptions that cannot be refuted or confirmed by the researcher. This situation is also referred to as butterfly bias, in which a variable or feature may

be considered both a confounder and a source of M-bias (Ding and Miratrix, 2015).

To mitigate the effects of comorbidities and the heterogeneity of PD, researchers often employ large sample sizes to account for the variability in the population and the disease. For example, datasets like the Parkinson's Progression Markers Initiative (PPMI) (Marek et al., 2011) and the Oxford Parkinson's Disease Centre discovery cohort (OPDC) (Lawton et al., 2015) acknowledge the presence of subtypes and follow patients over extended periods, presenting clinical data in addition to imaging data. Moreover, studies frequently use statistical techniques such as propensity score matching (Huang et al., 2013), stratification (Virreira Winter et al., 2021), and multivariable regression (Pechevis et al., 2005) to control for confounding variables. Another approach is to utilize ML algorithms that can handle multiple confounders and nonlinear relationships between variables, such as random forest (Oprescu et al., 2019) or support vector machine models (Westreich et al., 2010).

Error rate at diagnosis

The aforementioned challenges are further compounded by the difficulty of accurately diagnosing PD. According to Hess and Okun (2016), the misdiagnosis rate of PD can range from 10 to 20% or greater, depending on clinician experience. Other studies have reported misdiagnosis rates of 20%–30% in the early stages, with the main causes being the failure to recognize atypical parkinsonian disorders such as dementia with Lewy bodies or multiple system atrophy (Poewe and Wenning, 2002). Consequently, researchers must address the challenges of training models with noisy labeled data (Karthik et al., 2021), where label noise can potentially degrade model performance.

To address noisy labeled data several approaches have been proposed, including semi-supervised learning, where a small set of labeled data is combined with a large set of unlabeled data to improve the model's accuracy (Adeli et al., 2018). Another approach is active learning, where the model is iterative trained on a small set of labeled data, and the most informative samples are selected for annotation by a human expert, reducing labeling costs while maintaining or even improving the model's accuracy (Settles, 2009; Garcia Santa Cruz et al., 2022a). Recent developments in DL have led to the emergence of new techniques that can handle label noise more robustly, such as the label Smoothing technique (Müller et al., 2019) that reduces the impact of noisy labels on the loss function by smoothing the label distribution. Ensemble techniques also help mitigate the impact of label noise on model performance by combining the predictions of multiple models, each trained on a slightly different subset of the data (Adeli et al., 2018).

Extended times of disease progression

PD is characterized by a slow progression, with a period of up to 20 years before the clinical phase (Kalia and Lang, 2015), and can survive up to 20 years in the clinical phase (Hassan et al., 2015), with a mean survival onset of 12 years (Rajput, 1992). This slow progression impacts longitudinal follow-up of study participants, which becomes difficult and prone to high dropout rates and protocol changes. It also brings another important dimension into play, as data subjects may showcase both different ages and distinct PD stages. Moreover, assumed control subjects may reveal PD symptoms in the long term, increasing the risk of ascertainment bias.

The extended duration of longitudinal studies can lead to higher rates of dropout and protocol changes. To mitigate these issues, researchers can employ remote monitoring technologies that allow patients to be monitored from their homes, reducing the need for in-person visits. Wearable sensors can also provide continuous, objective measurements of symptoms and mobility (Kubota et al., 2016; Arroyo-Gallego et al., 2018). Additionally, providing incentives to patients and institutions can help improve retention rates (Smith et al., 2019). For brain imaging studies, it is important to maintain consistent imaging protocols and analysis methods to reduce the risk of acquisition bias (Castro et al., 2020).

Lack of specificity and variable penetrance of prodromal markers

Finding markers for the prodromal phase of PD is complex in many aspects. One of the key factors hindering the discovery of such markers is the low frequency of the disease, which is estimated to be under 2% (Muangpaisan et al., 2011). This low frequency makes it challenging to find participants in the prodromal phase of the disease, as large sample sizes are required for such studies. To overcome this challenge, researchers often employ non-specific markers to identify individuals who may be in the prodromal phase of PD. These non-specific markers include rapid eye movement sleep behavior disorder (RBD), hyposmia (reduced ability to smell), depression, gastrointestinal symptoms, and mild motor symptoms. However, the use of non-specific markers has limitations, as they are not specific to PD and may be present in individuals who do not develop the disease (Durcan et al., 2019). Although specific markers such as genetic markers have been identified, their use is limited by their variable penetrance, which is often incomplete and dependent on the population. Some of the most commonly associated genes with PD are LRRK2, Glucocerebrosidase (GBA), and SNCA (Niotis et al., 2022). This means that even if an individual has a genetic marker associated with an increased risk of developing PD, there is still a significant chance that they may never develop the disease.

Finding markers for the prodromal phase of PD is complex, but one potential solution to overcome the challenge of low disease frequency and the need for large sample sizes is to collaborate with multiple research centers and establish consortium. Another approach to identifying specific markers for the prodromal phase of PD is to consider multiple sources of data, such as the hyposmia test (Siderowf et al., 2012). Finally, to address the limitations of genetic markers with incomplete penetrance, researchers can focus on identifying epigenetic modifications associated with the prodromal phase of PD, which may provide more accurate and specific markers for early detection of the disease (Chen and Ritz, 2018).

Lack of ground truth

In addition to the challenges of finding markers for the prodromal phase, there are also challenges related to generating accurate ground truth data for supervised learning. PD is not fully understood yet, which can lead to errors in the models. Deliberate idealisations are inherent in any model, but inaccurate assumptions based on insufficient knowledge can lead to biased and inaccurate representations. An example of this is the lack of understanding about comorbidity effects. Disparities in these regards can affect coherence between studies, as causal assumptions may vary across research teams and over time. Conducting further research on the disease could be a potential solution to enhance the understanding of the disease. This research can include a better understanding of the various aspects that contribute to the disease, such as adopting a complex systems approach (Cohen et al., 2022). Another solution is to develop more objective and quantitative measures of motor symptoms using wearable sensors and digital technologies.

Current diagnosis relies on assessments by physicians, often employing the current gold standard, the Unified Parkinson's Disease Rating Scale (UPDRS) (Movement Disorder Society Task Force on Rating Scales for Parkinson's Disease, 2003). Furthermore efforts are underway to develop more objective and continuous measures of motor symptoms using wearable sensors and digital technologies (Parisi et al., 2015; Lu et al., 2021). These emerging technologies can provide more accurate and reliable data for the diagnosis and monitoring of PD (Kubota et al., 2016). By replacing subjective evaluations with objective measurements, the accuracy of diagnoses may be improved, leading to earlier identification and treatment of PD. Further research on the missing link between genetic and environmental causes of the disease can also contribute to a better understanding of PD (Hill-Burns et al., 2017). Additionally, standardizing diagnostic criteria and protocols across research teams and clinical settings can increase coherence between studies and improve the accuracy of the diagnosis. One such criterion is the UK Brain Bank criteria (Postuma et al., 2018). Enhanced collaboration and communication between researchers and clinicians may serve as a valuable means to reinforce the aforementioned efforts.

Limitations associated with clinical brain imaging datasets

Diversity and complexity of *in vivo* imaging brain markers

The pathology underlying PD motor symptoms such as tremors and bradykinesia is mainly associated with the loss of dopaminergic neurons in the *substantia nigra* and other gray matter alterations visible through brain imaging. However, non-motor symptoms of PD such as hyposmia, sleep disturbances, and depression do not present a clear *in vivo* imaging brain marker, even though some NMS-related brain alterations have been described. In particular, Prell (2018) state that imaging NMS characteristics may require different modalities, e.g., rs-fMRI for fatigue, fMRI and FDG-PET for mild cognitive impairment. In addition, studies have shown that quantitative iron imaging techniques such as R2*, SWI, and QSM are reliable markers of iron content in PD. These measurements have also been found to correlate with the severity of motor symptoms. Among these techniques, QSM has been identified as more robust and reproducible than R2* and is more adequate for use in multicenter studies (Pyatigorskaya et al., 2020). Finally, some authors have even discouraged the routine use of neuroimaging techniques in clinical practice for PD (Pagano et al., 2016). As stated by Pagano et al. (2016), "despite significant evidence for the utility of neuroimaging in assessing parkinsonian patients, none of the neuroimaging techniques is specifically recommended for routine use in clinical practice."

Therefore, the impact of this variety is threefold. First, the symptoms may not associate with structural or functional brain patterns. Second, when existing, such patterns require particular brain imaging modalities. Finally, such patterns may not be specific to PD. On top of these three circumstances, the temporal evolution of the disease adds another layer of complexity. Each stage calls for different symptoms, which in turn require dedicated imaging modalities with different diagnosis specificity. In this light, accurate PD subtyping becomes challenging, as obtaining a complete view of the brain manifestations of PD symptoms requires image acquisition of several modalities or the employment of multimodal approaches (Saeed et al., 2017; Chougar et al., 2020; Albrecht et al., 2022).

One potential solution to address this issue is to use a combination of multiple imaging techniques. Multimodal approaches can provide a more complete and accurate picture of the disease by capturing different aspects of brain function and structure, as well as the density of neurotransmitter receptors such as dopamine receptors. Additionally, clinical assessments can be supplemented by specific neuropsychological questionnaires or physiological tests, with subsequent confirmation by imaging or a biochemical marker, as different modalities are suitable at different stages of disease progression (Michell et al., 2004). Moreover, the use of multi-modal data, combining clinical, motor, cognitive, and neuroimaging data, can aid in subtyping PD and potentially identifying correlations between the pathology manifested in the brain and the motor and non-motor symptoms of the patient (Albrecht et al., 2022). However, it is important to note that using multiple imaging modalities can also pose some challenges, such as the need for specialized expertise, the complexity of data integration (Behrad and Abadeh, 2022), and the increased cost and time required for imaging and analysis.

Lack of standardization in acquisition, preprocessing, and annotation pipelines

After image acquisition, another set of problems may compromise research. First, variations in the acquisition parameters may alter the observed changes in longitudinal studies. Chua et al. (2015) showed how variability in MRI acquisition parameters between scans can confound observations. Then, the diversity of preprocessing pipelines across studies presents another dimension for potential unwanted interactions and errors. For instance, the exclusion criteria for head motion may vary across studies without common criteria. Strother (2006) highlighted how

the preprocessing steps interact with every decision taken during the design and execution of fMRI experiments. The authors argue that "applying a new processing pipeline to a raw dataset may result in significantly modified spatial activation patterns as a result of changing/optimizing preprocessing techniques and/or the data analysis approach." Similarly, Power et al. (2017) identified several contributors to global fMRI signals such as hardware artifacts and head motion that were not removed from scans through denoising techniques, affecting the observed covariances. Bhagwat et al. (2021) underscored the variability introduced by preprocessing in neuroimaging pipelines. Hence, the lack of standardization in acquisition, preprocessing, and annotation pipelines can lead to unwanted interactions and errors, which has significant implications for the reliability and reproducibility of neuroimaging research (Brauneck et al., 2023).

To address this issue, it is crucial to develop and validate standardized protocols and criteria for data acquisition, preprocessing, and analysis. This can be achieved through a variety of approaches, such as establishing international consortia, promoting open data sharing, and providing training and resources for researchers. For example, the International Society for Magnetic Resonance in Medicine (ISMRM) has developed several standards for MRI data acquisition and analysis, including quantitative MR (Weingärtner et al., 2022). In addition, promoting open data sharing and encouraging researchers to openly share their raw data and analysis pipelines can help to identify potential sources of variability and errors in data processing and analysis. This can facilitate the development of more robust and reliable methods for data preprocessing and analysis. Several initiatives have already been developed to promote open data sharing in neuroimaging, such as the OpenfMRI (Poldrack et al., 2013) and NeuroVault (Gorgolewski et al., 2015) repositories. Furthermore, educating researchers about the importance of standardization in neuroimaging research (Laird et al., 2011) and providing them with the necessary tools and resources to implement standardized protocols and criteria in their research is crucial, including standardization of the metadata as a way to reflect the causal and anti-causal assumptions made during the data collection and annotation (Garcia Santa Cruz et al., 2022b). Further, standardization of the annotation pipeline is important to improve the consistency and quality of annotations. To tackle this issue, it is important to have standardized guidelines and procedures. This can reduce misinterpretation, which may result in inconsistency, making the subsequent training of the machine learning solution difficult (Miceli et al., 2020). Additionally, it's crucial to have a good way to integrate annotations from multiple annotators, carefully considering how to deal with labeling merging in unmatched results when and the seniority of the experts. Furthermore, as labeling is an expensive task, unsupervised or semi-supervised techniques could be employed to generate cheaper but potentially more consistent labels (dos Santos Ferreira et al., 2019).

To fully exploit the potential for personalized healthcare, collecting metadata may be necessary. However, current General Data Protection Regulation (GDPR) regulations impose limitations to ensure both data privacy and security. To address this challenge, several approaches have been proposed, including federated machine learning, multi-party computation, and differential privacy. These methods provide a win-win solution by enabling the collection of necessary data while preserving the privacy and security of sensitive information (Brauneck et al., 2023).

This can be achieved through training programs, workshops, and online resources that provide guidance on best practices for data acquisition, preprocessing, and analysis in neuroimaging (Borghi and Van Gulick, 2018). The development of established protocols in standardization and analysis, such as those proposed for other neurodegenerative diseases like the Alzheimer's Disease Neuroimaging Initiative (ADNI) database (Wyman et al., 2013), can also serve as important models for promoting consistency and reliability in neuroimaging research.

Limitations associated with machine learning/deep learning

Generalization issues that hinder transferability

Neural networks (NNs) have been shown to be highly effective in approximating complex functions and achieving accurate predictions by leveraging large and high-quality datasets. However, despite demonstrating good performance on the training data, there is no guarantee that the model will continue to perform well on new and unseen data. This phenomenon, known as overfitting, occurs when the model is too closely tailored to the training data, and thus, is not generalizable to new data. Out-of-distribution and out-of-domain examples can cause neural networks to learn incorrect correlations and make inaccurate predictions. Common causes of overfitting include domain shift (Kondrateva et al., 2021), task mismatch (Castro et al., 2020), and catastrophic forgetting (Gupta et al., 2021). Poor generalization can lead to unreliable and incorrect predictions on real-world tasks where the data distribution may differ significantly from the training data (Yagis et al., 2019; Ge et al., 2023). In the context of CAD for PD, this may result in incorrect predictions that could lead to misdiagnosis or failure to detect the disease, ultimately resulting in incorrect treatment or delayed diagnosis.

To reduce overfitting, techniques such as regularization (Kukačka et al., 2017) and early stopping (Prechelt, 1998) can be employed. Data augmentation techniques can also expand the dataset size and improve internal generalization (Chlap et al., 2021). However, data augmentation alone cannot address demographic representativeness issues. Thorough internal and external validation is essential to ensure reliable and accurate model performance, especially for new and unseen data (Garcia Santa Cruz et al., 2021). Cross-validation techniques such as stratified cross-validation (Zeng and Martinez, 2000) and leave-one-out cross-validation (Hastie et al., 2009) can be used for internal validation, while external validation can be achieved through external datasets. These techniques can enhance model transferability and promote generalizability.

Additionally, when dealing with a small sample size, as is often the case in biomedical datasets, splitting the dataset for cross-validation may lead to a loss of the algorithm's generalization capacity. This limitation arises from the fact that when the sample size is small, dividing it into training and validation sets further reduces the amount of data available for training, potentially hindering the algorithm's ability to generalize well. Despite the

conventional wisdom that attributes this small generalization error to properties of the model family or regularization techniques used during training (Zhang et al., 2021), it has been demonstrated that even with explicit regularization, state-of-the-art convolutional networks can fit random labeling of the training data, suggesting that these models have enough capacity to memorize the training data. A potential solution is to employ distribution-free performance bounds (Jakubovitz et al., 2019), which have been successfully implemented in neuroimaging (Górriz et al., 2019; Jimenez-Mesa et al., 2023).

To address data drift, various techniques can be employed. Calibration techniques (Wald et al., 2021) and appropriate metrics for evaluating model generalization (Jiang et al., 2019) can be used. Additionally, selecting the appropriate model architecture and hyperparameters can significantly enhance the model's generalization ability. Techniques such as grid search or Bayesian optimization (Kandasamy et al., 2018) can be employed to optimize hyperparameters. Furthermore, transfer learning has been demonstrated as an effective approach for improving model generalization, particularly when working with limited data (Yosinski et al., 2014).

Another big issue that can hinder the generalization of models is when they fail to learn the desirable patterns that characterize the phenomena we are trying to model, and instead learn spurious correlations. This can result in the model learning potential confounders, colliders, and other unwanted biases.

To address these issues, it is important to carefully evaluate the data used to train the model, identify potential confounders and colliders biases, and use appropriate statistical methods to account for them (Wang et al., 2018). Additionally, confounding removal strategies such as domain adaptation techniques can be employed during the harmonization phase (Dinsdale et al., 2021) and during the training process (Qin et al., 2020). Finally, it is crucial to regularly monitor the performance of the model and validate its results against independent and temporally updated data sets to identify and correct potential unwanted biases (Tamburri, 2020).

Algorithmic bias

This can be considered an extension of a generalization issue. Algorithmic bias is another significant challenge in ML, particularly in medical diagnosis and other decision-making applications. Societal biases and data acquisition biases can result in systematic and repeatable errors that lead to unfair outcomes and lower accuracy for certain groups (Ricci Lara et al., 2022). It is essential to address these biases in the design, training, and evaluation of NNs to ensure fairness and avoid perpetuating existing inequalities. These biases can result in systematic and repeatable errors, leading to unfair outcomes that favor certain groups over others, ultimately lowering the accuracy of the recommendation for some patient groups, particularly when there are racial biases. These biases can originate from existing inequality (Ricci Lara et al., 2022) or can also stem from selection bias introduced during the acquisition process (Garcia Santa Cruz et al., 2022b).

For example, Obermeyer et al. (2019) identified some systemic conditional disparities in risk scores based on the medical history of Black patients. In such cases, bias-correcting techniques can be employed (Wiens et al., 2020). Bias can also be introduced during the data acquisition process, resulting in technical debt and downstream effects known as data cascades (Sambasivan et al., 2021). Moreover, it is essential to address the issue of unwanted biases in the data used for current AI systems, as these systems not only have the risk of making incorrect predictions, but also of perpetuating and amplifying biases present in the data (Zhao et al., 2017).

The ML community has made interdisciplinary efforts to address the aforementioned issues, leading to the development of a range of solutions that fall under the umbrella of fairness (Mehrabi et al., 2021). By implementing such strategies in algorithm design, training, and evaluation, performance across groups can be improved, thereby mitigating the risk of unfairness in the final solution. These solutions typically target characteristics that have traditionally been the source of unfair discrepancies, such as gender and ethnicity. However, it is also crucial to ensure that algorithms perform well in cases where diseases have subgroups, such PD subtypes (Thenganatt and Jankovic, 2014) and varying degrees of disease penetrance (Espay et al., 2017). In such cases, similar metrics can be used, with the subgroups or disease penetrance considered as protected attributes.

Need for better interpretability

Another significant issue with NNs is their inability to accurately represent uncertainty in their predictions (Abdar et al., 2021). Since NNs are deterministic, they cannot capture the notion of what they know and what they do not know, or the confidence level of their predictions. Furthermore, current NNs are limited to accessing the knowledge contained in the dataset. This lack of uncertainty estimation can lead to overconfidence in their predictions, which can be problematic in critical applications such as medical diagnosis or self-driving cars.

Before implementing CAD systems for PD as decision-making tools in clinical practice, it is essential to establish an interpretability strategy (Chan et al., 2020). CAD systems with low interpretability can have severe consequences, such as decreased trust and acceptance among clinicians and patients, misdiagnoses, and ineffective treatment strategies. A transparent and understandable model can help clinicians validate the system's predictions and ensure that the model is not making decisions based on spurious correlations or biases. Additionally, interpretability can help researchers gain new insights into PD and refine the diagnostic criteria.

The lack of uncertainty estimation can lead to overconfidence in their predictions, which can have severe consequences such as misdiagnoses and ineffective treatment strategies. Therefore, it is essential to establish an interpretability strategy before implementing CAD systems in clinical practice. Furthermore, the limitations of current explainability methods used in ML decision-making systems suggest that unless there are significant advances in explainable ML, we must treat these systems as black boxes, justified by their reliable and experimentally confirmed performance. Finally, it is recommended that healthcare workers exercise caution when using explanations from ML systems and regulators be judicious in listing explanations among the requirements needed for clinical deployment of ML (Ghassemi et al., 2021).

Recent regulations, such as the GDPR in the European Union (EU), emphasize the right to be informed and the right to contest an automated decision. In such cases, interpretability of AI becomes crucial for auditing the decision-making of automated agents such as ML models. In particular, Article 22 of the GDPR deals with the rights related to automated individual decision-making since data subjects cannot be subject to a decision based solely on automated processing (Council of European Union, 2016). Additionally, Articles 12 and 13 specify the right to be informed about the use of their data in an easily understandable and accessible manner. The most common use cases for participant data fall into two main scenarios: (1) data subjects provide their data to train AI models, and (2) data subjects receive a result from an AI model after providing some data. The first scenario requires informing the participants about the purpose and usage of their data. However, the second scenario requires additional clarification, as the participants should understand how a decision was made and, in particular, which input data was relevant for obtaining a specific result.

To meet the above requirements, ML solutions must be designed with transparency in mind. Some ML approaches produce models that are inherently easier to inspect. Decision tree predictive models are popular due to their intelligibility and simplicity. However, this approach does not suit all tasks. Essentially, models optimize a function that draws the boundary to separate the given classes (e.g., healthy vs. diseased) by grouping nearby instances. However, the definition of proximity differs across ML learners and interpretability measures become complex. For instance, random forest methods constitute an evolution of decision trees but at the cost of intrinsic interpretability since their internal model consists of a collection of decision trees, obfuscating the "reasoning" of the trained model (Nair et al., 2013). Another approach includes tracking the decision-making process on CNNs. For instance, Magesh et al. (2020) employ Local Interpretable Model-Agnostic Explainer (LIME) to increase the explainability of CNN-based models for PD diagnosis. Two key elements to improve interpretability are solutions to improve model *explainability* and model *uncertainty*.

Model explainability

Model explainability refers to the ability to understand how a ML model makes its predictions. It is important because in critical applications, such as healthcare or finance, it is necessary to understand why the model makes certain decisions, especially when human lives or significant resources are at stake. For example, if a model is predicting whether a patient has PD or make a recomendation about the treatment, it is important to know which factors the model is considering in its decision-making process.

Explainability and interpretability terms are is frequently used interchangeably and for this work, we do not distinguish between them. Of course, interpretability tools vary across ML methods, but there are some important methods worth mentioning that can facilitate the interpretability of the results. Molnar (2020) provides an overview of the available techniques for ML interpretability. The author distinguishes between intrinsic and *post hoc* methods. The first group concerns models whose simple structure permits human interpretation, e.g., short decision trees. The second group of methods are used after model training. Additionally, the author divides interpretability methods into model-specific and model-agnostic. The author provides yet another criterion to separate the methods into two groups, i.e., local (for methods that explain a particular result) and global (for methods that explain the whole model behavior) interpretability.

Aside from the above, solution design can impact model interpretability as well. Often models are designed in an end-to-end way that attempts to map input data with the final result with a single model. For instance, a medical imaging CAD system can be designed as a chain of several models, with the first dedicated to finding pathologies and the subsequent models mapping pathologies to diseases or conditions (e.g., through several one class classifiers) (Vega, 2021). This approach eases solution maintainance and increases interpretability, allowing inspection of the intermediate results.

To address this challenge, researchers have proposed various methods for interpreting and explaining the decisions of ML models, including model-agnostic techniques such as LIME (Visani et al., 2022) and SHapley Additive exPlanations (SHAP) (Kaur et al., 2020), as well as model-specific approaches such as attention mechanisms (Vaswani et al., 2017) and gradient-based attribution methods (Ancona et al., 2019).

Model uncertainty

In the context of medical diagnosis, the concept of model uncertainty plays a crucial role in determining the degree of confidence or uncertainty that a model has in its predictions. This consideration is particularly pertinent given the high stakes involved in clinical decision-making. The degree of certainty or uncertainty in a model's output is a crucial factor in determining appropriate actions to be taken based on the model's predictions. As such, accounting for model uncertainty can enhance the transparency and reliability of medical diagnosis, leading to more effective treatment strategies and improved patient outcomes.

Uncertainty in ML can stem from multiple sources. Some of them include data variance, lack of representativity in the data sample, label noise, and the intrinsic imperfections of any ML model developed from such data. The literature also refers to these types of uncertainty as systematic, aleatoric and epistemic, (Hüllermeier and Waegeman, 2021; Gal et al., 2022). Most of these issues cannot be fixed *a posteriori* and must be avoided through careful data acquisition design. However, documenting uncertainty sources and quantifying its magnitude in data, labels and model is of uttermost importance, in the same way we should document other aspects such as the representativity of the sample. This information is key to assess the generalization power of the solutions to new settings. For instance, reporting probability estimates together with the model prediction can indicate the model prediction confidence. However, these estimates may not accurately reflect model uncertainity calling for calibration methods (Lemay et al., 2022).

Costly systems to develop and maintain

ML solutions are also expensive in terms of data and computation. Developing and training ML models requires a

substantial amount of data, computing power, and specialized expertise. Acquiring large and diverse datasets can be challenging, and data collection, cleaning, and preprocessing can be time-consuming and labor-intensive (Ngiam and Khor, 2019). Moreover, the development and training of ML models often require specialized hardware, such as Graphics Processing Units (GPUs), which can increase energy consumption and carbon footprint (Patterson et al., 2021). It is important to consider the environmental impact of ML and take steps to reduce it, such as using energy-efficient hardware or exploring alternative training methods that require fewer computing resources (Wang et al., 2020).

In addition, ML models require ongoing monitoring, updating, and maintenance to ensure their continued accuracy. As data changes over time, the models may need to be retrained or updated to account for new patterns or trends. In the case of PD, this can be particularly challenging due to the variability in disease progression across patients, making it difficult to develop models that accurately capture the underlying patterns of the disease. Furthermore, implementing ML systems in clinical practice requires careful consideration of regulatory and ethical concerns to ensure patient safety and privacy. ML models used in clinical practice must undergo rigorous testing and validation to ensure their safety, efficacy, and reliability. The validation process involves evaluating the model's performance on independent datasets and comparing it to other established diagnostic methods (Liu et al., 2019). Additionally, models must be regularly audited to identify and mitigate biases and errors that may affect their performance (Reddy et al., 2020).

To address the challenges of cost and development associated with ML, there has been a concerted effort to develop open-source platforms and tools that make ML more accessible to researchers and clinicians. For instance, several open-source libraries, including TensorFlow (Abadi et al., 2016a), PyTorch (Paszke et al., 2019) and MONAI (Cardoso et al., 2022) provide pre-built ML models and algorithms that can be readily adapted and customized for specific applications. In addition, cloud computing platforms, such as Amazon Web Services and Google Cloud, offer scalable and cost-effective solutions for training and deploying ML models. Moreover, there is a growing trend toward collaborative and decentralized approaches to ML development (Castiglioni et al., 2021). One such approach is federated learning, which allows multiple parties to train a shared ML model without sharing their data, thus preserving data privacy and security (Tedeschini et al., 2022). Another approach is to use blockchain technology to create decentralized ML models that are transparent, auditable, and resistant to tampering (Neelakandan et al., 2022). These developments are expected to enhance the accessibility and affordability of ML solutions, thereby facilitating their wider adoption and implementation in clinical practice.

Security and privacy challenges

Healthcare institutions are frequent targets of malicious hackers, resulting in data breaches and ransomware attacks (Branch et al., 2019; Devi, 2023). In March 2023, the Hospital Clinic de Barcelona, which serves half a million people, suffered a ransomware attack by the RansomHouse group, resulting in the theft of 4.4 TB of data (Toulas, 2023). Healthcare ML models often deal with very sensitive patient data, making them attractive targets for malicious attacks.

Adversarial training is a technique used to improve the robustness of ML models against adversarial attacks (Madry et al., 2017). It involves training the model on adversarial examples generated by an adversary system to make the model more resilient to similar attacks. However, these techniques can also be used maliciously. Adversarial attacks can cause the model to make incorrect predictions, which could potentially expose personal information from healthcare ML models. In membership inference attacks, an adversary attempts to determine whether a particular individual's data was used to train a machine learning model (Hu et al., 2022). In model inversion attacks, the aim is to reconstruct an individual's data from the outputs of a machine learning model. This can be achieved by generating adversarial examples that maximize the likelihood of the individual's data, given the model outputs (Fredrikson et al., 2015). These attacks highlight the need for robust security measures to be in place to protect healthcare ML models from malicious attacks.

The most effective safety measure for healthcare ML models is to restrict access to the trained models to authorized personnel. Additionally, privacy-preserving machine learning techniques such as differential privacy and homomorphic encryption can help prevent these attacks (Abadi et al., 2016b; Aono et al., 2017). It is advisable to take a proactive approach to healthcare privacy and security during the solution design instead of a reactive approach (Song et al., 2019; Bhuyan et al., 2020).

Concluding remarks and perspectives

During recent years, both the ML and the medical community have begun to consider data quality as the most crucial factor impacting the performance of the solutions and their robustness, (Sambasivan et al., 2021). However, acquiring high-quality data, building a suitable model for the task, and determining the appropriate use for such models, remain challenging objectives toward clinically relevant models. In particular, Sambasivan et al. (2021) insist on building incentive structures across all stakeholders, stating that "many practitioners described data work as time-consuming, invisible to track, and often done under pressures to move fast due to margins–investment, constraints, and deadlines often came in the way of focusing on improving data quality." Data bootstrapping is yet another source of issues in high-stakes AI domains, as many researchers begin the AI/ML work employing existing data or data collected for non-AI purposes that leads to poor generalization. It is essential to ensure that ML models are rigorously validated and tested before they can be used in clinical practice. The employment of datasets from multiple independent studies can boost the statistical power and lead to more accurate, reliable and reproducible research. In ML, a common practice to this end is to mix several datasets. However, if the mixed datasets do not share certain degree of methodological similarity, biases may be introduced due to differences in acquisition, preprocessing or annotation.

The circumstances previously described hinder the availability of large datasets containing multiple imaging modalities as large datasets often consist of multi-center cohorts employing different acquisition devices, protocols and pipelines. Overall, developing and maintaining ML systems for clinical practice can be a costly and time-consuming process that requires significant expertise and resources. However, the potential benefits, such as improved diagnosis and treatment outcomes for patients with PD, make it a worthwhile investment. The use of CAD tools to interpreted brain images is the context of PD is very promising. However, as previously mentioned, these solutions will be used as assisting tools in a very specific context and under specialized supervision and must pass a series of verification before they can be used, as is the case with other medical products or treatments. To achieve this, the models must be accompanied by interpretability methods to ensure that clinicians can understand how the model makes its predictions.

While this review focuses primarily on brain imaging, it has become increasingly clear that a single measure is unlikely to be sufficient for diagnosing PD in the foreseeable future. Instead, a combination of measures will likely be necessary. The most critical aspect of a biomarker is not its ability to diagnose PD in its early stages, but rather its ability to reflect the disease's pathogenesis and progression. By using a multimodal approach that combines various imaging biomarkers, clinicians can make early, accurate, and objective diagnostic decisions, identify neuroanatomical and pathophysiological mechanisms, and evaluate disease progression and therapeutic responses to drugs in clinical trials.

A common approach in developing multimodal CAD systems involves combining multiple imaging modalities as well as leveraging ensemble learning to integrate data from various sources for obtaining the final result. A concrete example of a multimodal approach in PD is the employment of multiple modalities to characterize a specific pathological process in certain regions of the brain. For instance, multimodal approaches employing hybrid images created through the integration of different MRI parameters offer a valuable tool. By combining T1-, T2*-, and diffusion-weighted MRI, Barbagallo et al. (2016) proposed to enable the detection and analysis of macro- and micro-structural abnormalities in the nigrostriatal pathway. The key benefit of integrating hybrid images enhances the accuracy and reliability of CAD systems by capturing diverse aspects of neurodegeneration.

Another example of a multimodal approach consists in combining MRI techniques, particularly those visualizing pathological changes in the substantia nigra using diffusion, iron-sensitive susceptibility, and neuromelanin-sensitive sequences, which offer a more accessible imaging tool. However, these techniques may be insufficient for phenotyping or prognostication due to the heterogeneous nature of PD resulting from extranigral pathologies. In Siderowf et al. (2023) highlight the emerging role of retinal optical coherence tomography as a non-invasive technique to visualize structural changes in the retina, which can serve as potential biomarkers for early diagnosis and prognostication in PD. Ensemble learning, a popular technique employed in multimodal CAD systems, plays a crucial role in fusing information from diverse data sources. Through ensemble learning, multiple models are trained independently on different subsets of data or using distinct feature representations. Ensemble learning had been successfully applied in PD classification using multimodal voice and speech data (Ali et al., 2021).

Recent promising markers that use the biochemistry of alpha-synuclein seed amplification assays have shown potential (Siderowf et al., 2023). For instance when recommending DBS as a therapy option for PD, it is important to consider genetic information, specifically whether the patient is a carrier of mutations in the glucocerebrosidase (GBA) gene. PD patients with GBA mutations are at particularly high risk for cognitive impairment with DBS due to dysfunction of the glucocerebrosidase (GCase) enzyme, resulting in more rapid accumulation and spread of Lewy bodies. Recent research has shown that PD patients experience cognitive impairment after DBS, and this risk is even greater for those with GBA mutations. Therefore, models that assist with therapy recommendations for PD patients should carefully evaluate whether patients are carriers of GBA mutations before recommending DBS as a treatment option (Pal et al., 2022).

Furthermore, there is an extended literature of ML models that have the potential to become CAD systems in the future from diagnosis and monitoring of PD, by providing more accurate and objective measurements of motor symptoms and disease progression. However, until this model are properly validated there are far to be ready for its used in clinical settings to ensure their safety and effectiveness in clinical practice.

Ultimately, our review emphasizes the critical importance of taking a multidisciplinary approach and putting in extensive effort during the data preparation and clinical validation phases of developing ML models. It is crucial to recognize that proper design and clinical validation may be undervalued in comparison to the training of ML models, but they are indispensable for data-driven CAD solutions that are safe for a clinical use. We hope that this review will inspire both future users and developers of these systems in the context of MRI for PD.

Author contributions

BG conceived, structured, and wrote the manuscript. AH and FH supervised the manuscript. All authors contributed to the article and approved the submitted version.

Funding

BG was supported by the FNR within the PARK-QC DTU (PRIDE17/12244779/PARK-QC) and Pelican award from the Fondation du Pelican de Mie et Pierre Hippert-Faber, under the aegis of the Fondation de Luxembourg.

Conflict of interest

The authors declare that the research was conducted in the absence of any commercial or financial relationships that could be construed as a potential conflict of interest.

Publisher's note

References

Abadi, M., Chu, A., Goodfellow, I., McMahan, H. B., Mironov, I., Talwar, K., et al. (2016b). "Deep learning with differential privacy," in *Proceedings of the 2016 ACM SIGSAC Conference on Computer and Communications Security* (Savannah, GA), 308–318. doi: 10.1145/2976749.2978318

Abadi, M., Barham, P., Chen, J., Chen, Z., Davis, A., Dean, J., et al. (2016a). "Tensorflow: a system for large-scale machine learning," in *OSDI*, Volume 16 (Savannah, GA), 265–283.

Abdar, M., Pourpanah, F., Hussain, S., Rezazadegan, D., Liu, L., Ghavamzadeh, M., et al. (2021). A review of uncertainty quantification in deep learning: techniques, applications and challenges. *Inf. Fusion* 76, 243–297. doi: 10.1016/j.inffus.2021.05.008

Adeli, E., Thung, K.-H., An, L., Wu, G., Shi, F., Wang, T., et al. (2018). Semi-supervised discriminative classification robust to sample-outliers and feature-noises. *IEEE Trans. Pattern Anal. Mach. Intell.* 41, 515–522. doi: 10.1109/TPAMI.2018.2794470

Akdemir, Ü. Ö., Bora, H. A. T., and Atay, L. Ö. (2021). Dopamine transporter spect imaging in Parkinson's disease and parkinsoniandisorders. *Turk. J. Med. Sci.* 51, 400–410. doi: 10.3906/sag-2008-253

Albrecht, F., Poulakis, K., Freidle, M., Johansson, H., Ekman, U., Volpe, G., et al. (2022). Unraveling Parkinson's disease heterogeneity using subtypes based on multimodal data. *Parkinsonism Relat. Disord.* 102, 19–29. doi: 10.1016/j.parkreldis.2022.07.014

Ali, L., He, Z., Cao, W., Rauf, H. T., Imrana, Y., Bin Heyat, M. B., et al. (2021). MMDD-ensemble: a multimodal data-driven ensemble approach for Parkinson's disease detection. *Front. Neurosci.* 15, 754058. doi: 10.3389/fnins.2021.754058

Ancona, M., Ceolini, E., Öztireli, C., and Gross, M. (2019). "Gradient-based attribution methods," in *Explainable AI: Interpreting, Explaining and Visualizing Deep Learning*, eds W. Samek, G. Montavon, A. Vedaldi, L. Hansen, and K. R. Müller (Cham: Springer), 169–191. doi: 10.1007/978-3-030-28954-6_9

Aono, Y., Hayashi, T., Wang, L., Moriai, S., et al. (2017). Privacy-preserving deep learning via additively homomorphic encryption. *IEEE Trans. Inf. Forensics Secur.* 13, 1333–1345. doi: 10.1109/TIFS.2017.2787987

Arroyo-Gallego, T., Ledesma-Carbayo, M. J., Butterworth, I., Matarazzo, M., Montero-Escribano, P., Puertas-Martín, V., et al. (2018). Detecting motor impairment in early Parkinson's disease via natural typing interaction with keyboards: validation of the neuroqwerty approach in an uncontrolled at-home setting. *J. Med. Internet Res.* 20, e89. doi: 10.2196/jmir.9462

Augimeri, A., Cherubini, A., Cascini, G. L., Galea, D., Caligiuri, M. E., Barbagallo, G., et al. (2016). Coflupane in diagnosi–computer-aided datscan analysis. *EJNMMI Phys.* 3, 1–13. doi: 10.1186/s40658-016-0140-9

Bajaj, N., Hauser, R. A., and Grachev, I. D. (2013). Clinical utility of dopamine transporter single photon emission CT (DAT-SPECT) with (123I) ioflupane in diagnosis of parkinsonian syndromes. *J. Neurol. Neurosurg. Psychiatry* 84, 1288–1295. doi: 10.1136/jnnp-2012-304436

Barbagallo, G., Sierra-Peña, M., Nemmi, F., Traon, A. P.-L., Meissner, W. G., Rascol, O., et al. (2016). Multimodal MRI assessment of nigro-striatal pathway in multiple system atrophy and Parkinson disease. *Mov. Disord.* 31, 325–334. doi: 10.1002/mds.26471

Behrad, F., and Abadeh, M. S. (2022). An overview of deep learning methods for multimodal medical data mining. *Expert Syst. Appl.* 200, 117006. doi: 10.1016/j.eswa.2022.117006

Bhagwat, N., Barry, A., Dickie, E. W., Brown, S. T., Devenyi, G. A., Hatano, K., et al. (2021). Understanding the impact of preprocessing pipelines on neuroimaging cortical surface analyses. *GigaScience* 10, giaa155. doi: 10.1093/gigascience/giaa155

Bhuyan, S. S., Kabir, U. Y., Escareno, J. M., Ector, K., Palakodeti, S., Wyant, D., et al. (2020). Transforming healthcare cybersecurity from reactive to proactive: current status and future recommendations. *J. Med. Syst.* 44, 1–9. doi: 10.1007/s10916-019-1507-y

Biondetti, E., Gaurav, R., Yahia-Cherif, L., Mangone, G., Pyatigorskaya, N., Valabrègue, R., et al. (2020). Spatiotemporal changes in substantia nigra neuromelanin content in Parkinson's disease. *Brain* 143, 2757–2770. doi: 10.1093/brain/awaa216

Blauwendraat, C., Nalls, M. A., and Singleton, A. B. (2020). The genetic architecture of Parkinson's disease. *Lancet Neurol.* 19, 170–178. doi: 10.1016/S1474-4422(19)30287-X

Borghammer, P., and Van Den Berge, N. (2019). Brain-first versus gut-first Parkinson's disease: a hypothesis. *J. Parkinsons Dis.* 9, S281–S295. doi: 10.3233/JPD-191721

Borghi, J. A., and Van Gulick, A. E. (2018). Data management and sharing in neuroimaging: practices and perceptions of MRI researchers. *PLoS ONE* 13, e0200562. doi: 10.1371/journal.pone.0200562

Boutet, A., Madhavan, R., Elias, G. J., Joel, S. E., Gramer, R., Ranjan, M., et al. (2021). Predicting optimal deep brain stimulation parameters for Parkinson's disease using functional MRI and machine learning. *Nat. Commun.* 12, 3043. doi: 10.1038/s41467-021-23311-9

Branch, L., Eller, W., Bias, T., McCawley, M., Myers, D., Gerber, B., et al. (2019). Trends in malware attacks against united states healthcare organizations, 2016-2017. *Glob. Biosecur.* 1, 15–24. doi: 10.31646/gbio.7

Brauneck, A., Schmalhorst, L., Kazemi Majdabadi, M. M., Bakhtiari, M., Völker, U., Baumbach, J., et al. (2023). Federated machine learning, privacy-enhancing technologies, and data protection laws in medical research: scoping review. *J. Med. Internet Res.* 25, e41588. doi: 10.2196/41588

Broeder, S., Nackaerts, E., Heremans, E., Vervoort, G., Meesen, R., Verheyden, G., et al. (2015). Transcranial direct current stimulation in Parkinson's disease: neurophysiological mechanisms and behavioral effects. *Neurosci. Biobehav. Rev.* 57, 105–117. doi: 10.1016/j.neubiorev.2015.08.010

Cantello, R., Tarletti, R., and Civardi, C. (2002). Transcranial magnetic stimulation and Parkinson's disease. *Brain Res. Rev.* 38, 309–327. doi: 10.1016/S0165-0173(01)00158-8

Cardoso, M. J., Li, W., Brown, R., Ma, N., Kerfoot, E., Wang, Y., et al. (2022). MONAI: an open-source framework for deep learning in healthcare. *arXiv*. [preprint]. doi: 10.48550/arXiv.2211.0270

Castiglioni, I., Rundo, L., Codari, M., Di Leo, G., Salvatore, C., Interlenghi, F., et al. (2021). AI applications to medical images: from machine learning to deep learning. *Phys. Med.* 83, 9–24. doi: 10.1016/j.ejmp.2021.02.006

Castillo-Barnes, D., Martinez-Murcia, F. J., Ortiz, A., Salas-Gonzalez, D., RamÍrez, J., and Górriz, J. M. (2020). Morphological characterization of functional brain imaging by isosurface analysis in Parkinson's disease. *Int. J. Neural Syst.* 30, 2050044. doi: 10.1142/S0129065720500446

Castillo-Barnes, D., Ramírez, J., Segovia, F., Martínez-Murcia, F. J., Salas-Gonzalez, D., and Górriz, J. M. (2018). Robust ensemble classification methodology for I123-ioflupane spect images and multiple heterogeneous biomarkers in the diagnosis of Parkinson's disease. *Front. Neuroinform.* 12, 53. doi: 10.3389/fninf.2018.00053

Castro, D. C., Walker, I., and Glocker, B. (2020). Causality matters in medical imaging. *Nat. Commun.* 11, 3673. doi: 10.1038/s41467-020-17478-w

Chakraborty, S., Aich, S., and Kim, H.-C. (2020). Detection of Parkinson's disease from 3t t1 weighted MRI scans using 3D convolutional neural network. *Diagnostics* 10, 402. doi: 10.3390/diagnostics10060402

Chan, H.-P., Hadjiiski, L. M., and Samala, R. K. (2020). Computer-aided diagnosis in the era of deep learning. *Med. Phys.* 47, e218–e227. doi: 10.1002/mp.13764

Chaudhuri, K. R., Healy, D. G., and Schapira, A. H. (2006). Non-motor symptoms of Parkinson's disease: diagnosis and management. *Lancet Neurol.* 5, 235–245. doi: 10.1016/S1474-4422(06)70373-8

Chen, C.-M., Chou, Y.-H., Tagawa, N., and Do, Y. (2013). Computer-aided detection and diagnosis in medical imaging. *Comput. Math. Methods Med.* 2013, 790608. doi: 10.1155/2013/790608

Chen, H., and Ritz, B. (2018). The search for environmental causes of Parkinson's disease: moving forward. *J. Parkinsons Dis.* 8, S9–S17. doi: 10.3233/JPD-181493

Chlap, P., Min, H., Vandenberg, N., Dowling, J., Holloway, L., Haworth, A., et al. (2021). A review of medical image data augmentation techniques for deep learning applications. *J. Med. Imaging Radiat. Oncol.* 65, 545–563. doi: 10.1111/1754-9485.13261

Chougar, L., Faouzi, J., Pyatigorskaya, N., Yahia-Cherif, L., Gaurav, R., Biondetti, E., et al. (2021). Automated categorization of parkinsonian syndromes using magnetic resonance imaging in a clinical setting. *Mov. Disord.* 36, 460–470. doi: 10.1002/mds.28348

Chougar, L., Pyatigorskaya, N., Degos, B., Grabli, D., and Lehéricy, S. (2020). The role of magnetic resonance imaging for the diagnosis of atypical parkinsonism. *Front. Neurol.* 11, 665. doi: 10.3389/fneur.2020.00665

Chua, A. S., Egorova, S., Anderson, M. C., Polgar-Turcsanyi, M., Chitnis, T., Weiner, H. L., et al. (2015). Handling changes in MRI acquisition parameters in modeling whole brain lesion volume and atrophy data in multiple sclerosis subjects: comparison of linear mixed-effect models. *Neuroimage Clin.* 8, 606–610. doi: 10.1016/j.nicl.2015.06.009

Cohen, A. A., Ferrucci, L., Fülöp, T., Gravel, D., Hao, N., Kriete, A., et al. (2022). A complex systems approach to aging biology. *Nat. Aging* 2, 580–591. doi: 10.1038/s43587-022-00252-6

Coleman, W. B., and Tsongalis, G. J. (2009). *Molecular Pathology: The Molecular Basis of Human Disease*. Cambridge, MA: Academic Press.

Constantinescu, R., and Mondello, S. (2013). Cerebrospinal fluid biomarker candidates for parkinsonian disorders. *Front. Neurol.* 3, 187. doi: 10.3389/fneur.2012.00187

Cools, R. (2006). Dopaminergic modulation of cognitive function-implications for l-dopa treatment in Parkinson's disease. *Neurosci. Biobehav. Rev.* 30, 1–23. doi: 10.1016/j.neubiorev.2005.03.024

Council of European Union (2016). *General Data Protection Regulation*. Avaialble online at: http://eur-lex.europa.eu/legal-content/EN/TXT/?qid=1416170084502anduri=CELEX:32014R0269 (accessed July 1, 2023).

da Silva, F. C., Iop, R. R., de Oliveira, L. C., Boll, A. M., de Alvarenga, J. G. S., Gutierres Filho, P. J. B., et al. (2018). Effects of physical exercise programs on cognitive function in Parkinson's disease patients: a systematic review of randomized controlled trials of the last 10 years. *PLoS ONE* 13, e0193113. doi: 10.1371/journal.pone.0193113

Dadu, A., Satone, V., Kaur, R., Hashemi, S. H., Leonard, H., Iwaki, H., et al. (2022). Identification and prediction of Parkinson's disease subtypes and progression using machine learning in two cohorts. *NPJ Parkinsons Dis.* 8, 172. doi: 10.1038/s41531-022-00439-z

De Pablo-Fernández, E., Lees, A. J., Holton, J. L., and Warner, T. T. (2019). Prognosis and neuropathologic correlation of clinical subtypes of Parkinson disease. *JAMA Neurol.* 76, 470–479. doi: 10.1001/jamaneurol.2018.4377

Deeb, W., Nozile-Firth, K., and Okun, M. S. (2019). Parkinson's disease: diagnosis and appreciation of comorbidities. *Handb. Clin. Neurol.* 167, 257–277. doi: 10.1016/B978-0-12-804766-8.00014-5

Devi, S. (2023). Cyber-attacks on health-care systems. *Lancet Oncol.* 24, e148. doi: 10.1016/S1470-2045(23)00119-5

Ding, P., and Miratrix, L. W. (2015). To adjust or not to adjust? Sensitivity analysis of m-bias and butterfly-bias. *J. Causal Inference* 3, 41–57. doi: 10.1515/jci-2013-0021

Dinsdale, N. K., Jenkinson, M., and Namburete, A. I. (2021). Deep learning-based unlearning of dataset bias for MRI harmonisation and confound removal. *Neuroimage* 228, 117689. doi: 10.1016/j.neuroimage.2020.117689

Doi, K. (2007). Computer-aided diagnosis in medical imaging: historical review, current status and future potential. *Comput. Med. Imaging Graph.* 31, 198–211. doi: 10.1016/j.compmedimag.2007.02.002

dos Santos Ferreira, A., Freitas, D. M., da Silva, G. G., Pistori, H., and Folhes, M. T. (2019). Unsupervised deep learning and semi-automatic data labeling in weed discrimination. *Comput. Electron. Agric.* 165, 104963. doi: 10.1016/j.compag.2019.104963

Durcan, R., Wiblin, L., Lawson, R. A., Khoo, T. K., Yarnall, A., Duncan, G. W., et al. (2019). Prevalence and duration of non-motor symptoms in prodromal Parkinson's disease. *Eur. J. Neurol.* 26, 979–985. doi: 10.1111/ene.13919

Elfil, M., Kamel, S., Kandil, M., Koo, B. B., and Schaefer, S. M. (2020). Implications of the gut microbiome in Parkinson's disease. *Mov. Disord.* 35, 921–933. doi: 10.1002/mds.28004

Eriksen, N., Stark, A. K., and Pakkenberg, B. (2009). "Age and Parkinson's disease-related neuronal death in the substantia nigra pars compacta," in *Birth, Life and Death of Dopaminergic Neurons in the Substantia Nigra*, eds G. Giovanni, V. Di Matteo, and E. Esposito (Vienna: Springer), 203–213. doi: 10.1007/978-3-211-92660-4_16

Espay, A. J., Brundin, P., and Lang, A. E. (2017). Precision medicine for disease modification in parkinson disease. *Nat. Rev. Neurol.* 13, 119–126. doi: 10.1038/nrneurol.2016.196

Fasano, A., Daniele, A., and Albanese, A. (2012). Treatment of motor and non-motor features of Parkinson's disease with deep brain stimulation. *Lancet Neurol.* 11, 429–442. doi: 10.1016/S1474-4422(12)70049-2

Foulds, P. G., Mitchell, J. D., Parker, A., Turner, R., Green, G., Diggle, P., et al. (2011). Phosphorylated α-synuclein can be detected in blood plasma and is potentially a useful biomarker for Parkinson's disease. *FASEB J.* 25, 4127–4137. doi: 10.1096/fj.10-179192

Fredrikson, M., Jha, S., and Ristenpart, T. (2015). "Model inversion attacks that exploit confidence information and basic countermeasures," in *Proceedings of the 22nd ACM SIGSAC Conference on Computer and Communications Security* (New York, NY), 1322–1333. doi: 10.1145/2810103.2813677

Gal, Y., Koumoutsakos, P., Lanusse, F., Louppe, G., and Papadimitriou, C. (2022). Bayesian uncertainty quantification for machine-learned models in physics. *Nat. Rev. Phys.* 4, 573–577. doi: 10.1038/s42254-022-00498-4

Garcia Santa Cruz, B., Bossa, M. N., Sölter, J., and Husch, A. D. (2021). Public covid-19 x-ray datasets and their impact on model bias-a systematic review of a significant problem. *Med. Image Anal.* 74, 102225. doi: 10.1016/j.media.2021.102225

Garcia Santa Cruz, B., Slter, J., Gomez-Giro, G., Saraiva, C., Sabate-Soler, S., Modamio, J., et al. (2022a). Generalising from conventional pipelines using deep learning in high-throughput screening workflows. *Sci. Rep.* 12, 11465. doi: 10.1038/s41598-022-15623-7

Garcia Santa Cruz, B., Vega, C., and Hertel, F. (2022b). "The need of standardised metadata to encode causal relationships: towards safer data-driven machine learning biological solutions," in *Computational Intelligence Methods for Bioinformatics and Biostatistics: 17th International Meeting, CIBB 2021, Virtual Event, November 15-17, 2021*. Revised Selected Papers (Cham: Springer), 200–216. doi: 10.1007/978-3-031-20837-9_16

Ge, W., Lueck, C., Suominen, H., and Apthorp, D. (2023). Has machine learning over-promised in healthcare? A critical analysis and a proposal for improved evaluation, with evidence from Parkinson's disease. *Artif. Intell. Med.* 139, 102524. doi: 10.1016/j.artmed.2023.102524

Ghassemi, M., Oakden-Rayner, L., and Beam, A. L. (2021). The false hope of current approaches to explainable artificial intelligence in health care. *Lancet Digit. Health* 3, e745–e750. doi: 10.1016/S2589-7500(21)00208-9

Gorgolewski, K. J., Varoquaux, G., Rivera, G., Schwarz, Y., Ghosh, S. S., Maumet, C., et al. (2015). NeuroVault.org: a web-based repository for collecting and sharing unthresholded statistical maps of the human brain. *Front. Neuroinform.* 9, 8. doi: 10.3389/fninf.2015.00008

Górriz, J. M., Ramirez, J., Suckling, J., Consortium, M. A., et al. (2019). On the computation of distribution-free performance bounds: application to small sample sizes in neuroimaging. *Pattern Recognit.* 93, 1–13. doi: 10.1016/j.patcog.2019.03.032

Gulshan, V., Peng, L., Coram, M., Stumpe, M. C., Wu, D., Narayanaswamy, A., et al. (2016). Development and validation of a deep learning algorithm for detection of diabetic retinopathy in retinal fundus photographs. *JAMA* 316, 2402–2410. doi: 10.1001/jama.2016.17216

Gupta, S., Singh, P., Chang, K., Qu, L., Aggarwal, M., Arun, N., et al. (2021). Addressing catastrophic forgetting for medical domain expansion. *arXiv*. [preprint]. doi: 10.48550/arXiv.2103.13511

Hassan, A., Wu, S. S., Schmidt, P., Simuni, T., Giladi, N., Miyasaki, J. M., et al. (2015). The profile of long-term Parkinson's disease survivors with 20 years of disease duration and beyond. *J. Parkinsons Dis.* 5, 313–319. doi: 10.3233/JPD-140515

Hastie, T., Tibshirani, R., Friedman, J. H., and Friedman, J. H. (2009). *The Elements of Statistical Learning: Data Mining, Inference, and Prediction, Volume 2*. Cham: Springer. doi: 10.1007/978-0-387-84858-7

He, R., Yan, X., Guo, J., Xu, Q., Tang, B., Sun, Q., et al. (2018). Recent advances in biomarkers for Parkinson's disease. *Front. Aging Neurosci.* 10, 305. doi: 10.3389/fnagi.2018.00305

Hess, C. W., and Okun, M. S. (2016). Diagnosing parkinson disease. *Contin. Lifelong Learn. Neurol.* 22, 1047–1063. doi: 10.1212/CON.0000000000000345

Hill-Burns, E. M., Debelius, J. W., Morton, J. T., Wissemann, W. T., Lewis, M. R., Wallen, Z. D., et al. (2017). Parkinson's disease and Parkinson's disease medications have distinct signatures of the gut microbiome. *Mov. Disord.* 32, 739–749. doi: 10.1002/mds.26942

Hu, H., Salcic, Z., Sun, L., Dobbie, G., Yu, P. S., Zhang, X., et al. (2022). Membership inference attacks on machine learning: a survey. *ACM Comput. Surv.* 54(11s), 1–37. doi: 10.1145/3523273

Huang, Y.-P., Chen, L.-S., Yen, M.-F., Fann, C.-Y., Chiu, Y.-H., Chen, H.-H., et al. (2013). Parkinson's disease is related to an increased risk of ischemic stroke–a population-based propensity score-matched follow-up study. *PLoS ONE* 8, e68314. doi: 10.1371/journal.pone.0068314

Hüllermeier, E., and Waegeman, W. (2021). Aleatoric and epistemic uncertainty in machine learning: an introduction to concepts and methods. *Mach. Learn.* 110, 457–506. doi: 10.1007/s10994-021-05946-3

Hustad, E., and Aasly, J. O. (2020). Clinical and imaging markers of prodromal Parkinson's disease. *Front. Neurol.* 11, 395. doi: 10.3389/fneur.2020.00395

Jakubovitz, D., Giryes, R., and Rodrigues, M. R. (2019). "Generalization error in deep learning," in *Compressed Sensing and Its Applications: Third International MATHEON Conference 2017*, eds H. Boche, G. Caire, R. Calderbank, G. Kutyniok, R. Mathar, and P. Petersen (Cham: Springer), 153–193. doi: 10.1007/978-3-319-73074-5_5

Jankovic, J., McDermott, M., Carter, J., Gauthier, S., Goetz, C., Golbe, L., et al. (1990). Variable expression of Parkinson's disease: a base-line analysis of the dat atop cohort. *Neurology* 40, 1529–1529. doi: 10.1212/WNL.40.10.1529

Jiang, Y., Neyshabur, B., Mobahi, H., Krishnan, D., and Bengio, S. (2019). Fantastic generalization measures and where to find them. *arXiv*. [preprint]. doi: 10.48550/arXiv.1912.02178

Jimenez-Mesa, C., Ramirez, J., Suckling, J. Vöglein, J., Levin, J., Gorriz, J. M., Initiative, A. D. N., et al. (2023). A non-parametric statistical inference framework for deep learning in current neuroimaging. *Inf. Fusion* 91, 598–611. doi: 10.1016/j.inffus.2022.11.007

Kalia, L. V., and Lang, A. E. (2015). Parkinson's disease. *Lancet* 386, 896–912. doi: 10.1016/S0140-6736(14)61393-3

Kandasamy, K., Neiswanger, W., Schneider, J., Poczos, B., and Xing, E. P. (2018). Neural architecture search with bayesian optimisation and optimal transport. *Adv. Neural Inf. Process. Syst*. 31, 2016–2026. doi: 10.5555/3326943.3327130

Karthik, S., Revaud, J., and Chidlovskii, B. (2021). Learning from long-tailed data with noisy labels. *arXiv*. [preprint]. doi: 10.48550/arXiv.2108.11096

Kaur, H., Nori, H., Jenkins, S., Caruana, R., Wallach, H., Wortman Vaughan, J., et al. (2020). "Interpreting interpretability: understanding data scientists' use of interpretability tools for machine learning," in *Proceedings of the 2020 CHI Conference on Human Factors in Computing Systems* (New York, NY), 1–14. doi: 10.1145/3313831.3376219

Kondrateva, E., Pominova, M., Popova, E., Sharaev, M., Bernstein, A., Burnaev, E., et al. (2021). "Domain shift in computer vision models for MRI data analysis: an overview," in *Thirteenth International Conference on Machine Vision*, Volume 11605 (Bellingham, WA: SPIE), 126–133. doi: 10.1117/12.2587872

Kubota, K. J., Chen, J. A., and Little, M. A. (2016). Machine learning for large-scale wearable sensor data in Parkinson's disease: concepts, promises, pitfalls, and futures. *Mov. Disord*. 31, 1314–1326. doi: 10.1002/mds.26693

Kukačka, J., Golkov, V., and Cremers, D. (2017). Regularization for deep learning: a taxonomy. *arXiv*. [preprint]. doi: 10.48550/arXiv.1710.10686

Laird, A. R., Eickhoff, S. B., Fox, P. M., Uecker, A. M., Ray, K. L., Saenz, J. J., et al. (2011). The brainmap strategy for standardization, sharing, and meta-analysis of neuroimaging data. *BMC Res. Notes* 4, 1–9. doi: 10.1186/1756-0500-4-349

Langley, J., He, N., Huddleston, D. E., Chen, S., Yan, F., Crosson, B., et al. (2019). Reproducible detection of nigral iron deposition in 2 Parkinson's disease cohorts. *Mov. Disord*. 34, 416–419. doi: 10.1002/mds.27608

Lawton, M., Baig, F., Rolinski, M., Ruffman, C., Nithi, K., May, M. T., et al. (2015). Parkinson's disease subtypes in the oxford parkinson disease centre (OPDC) discovery cohort. *J. Parkinsons Dis*. 5, 269–279. doi: 10.3233/JPD-140523

Lee, D. J., Lozano, C. S., Dallapiazza, R. F., and Lozano, A. M. (2019). Current and future directions of deep brain stimulation for neurological and psychiatric disorders: JNSPG 75th anniversary invited review article. *J. Neurosurg*. 131, 333–342. doi: 10.3171/2019.4.JNS181761

Lemay, A., Hoebel, K., Bridge, C. P., Befano, B., De Sanjosé, S., Egemen, D., et al. (2022). Improving the repeatability of deep learning models with Monte Carlo dropout. *Npj Digit. Med*. 5, 174. doi: 10.1038/s41746-022-00709-3

Liu, X. CONSORT-AI, T., and Group, S.-A. S. (2019). Reporting guidelines for clinical trials evaluating artificial intelligence interventions are needed. *Nat. Med*. 25, 1467–1468. doi: 10.1038/s41591-019-0603-3

Lozano, A. M. (2017). Waving hello to noninvasive deep-brain stimulation. *N. Engl. J. Med*. 377, 1096–1098. doi: 10.1056/NEJMcibr1707165

Lu, M., Zhao, Q., Poston, K. L., Sullivan, E. V., Pfefferbaum, A., Shahid, M., et al. (2021). Quantifying Parkinson's disease motor severity under uncertainty using mds-updrs videos. *Med. Image Anal*. 73, 102179. doi: 10.1016/j.media.2021.102179

Madry, A., Makelov, A., Schmidt, L., Tsipras, D., and Vladu, A. (2017). Towards deep learning models resistant to adversarial attacks. *arXiv*. [preprint]. doi: 10.48550/arXiv.1706.06083

Magesh, P. R., Myloth, R. D., and Tom, R. J. (2020). An explainable machine learning model for early detection of Parkinson's disease using lime on datscan imagery. *Comput. Biol. Med*. 126, 104041. doi: 10.1016/j.compbiomed.2020.104041

Mahlknecht, P., Seppi, K., Stockner, H., Nocker, M., Scherfler, C., Kiechl, S., et al. (2013). Substantia nigra hyperechogenicity as a marker for Parkinson's disease: a population-based study. *Neurodegener. Dis*. 12, 212–218. doi: 10.1159/000348595

Mangasarian, O. L., Street, W. N., and Wolberg, W. H. (1995). Breast cancer diagnosis and prognosis via linear programming. *Oper. Res*. 43, 570–577. doi: 10.1287/opre.43.4.570

Marek, K., Jennings, D., Lasch, S., Siderowf, A., Tanner, C., Simuni, T., et al. (2011). The parkinson progression marker initiative (PPMI). *Prog. Neurobiol*. 95, 629–635. doi: 10.1016/j.pneurobio.2011.09.005

Marras, C., Beck, J., Bower, J., Roberts, E., Ritz, B., Ross, G., et al. (2018). Prevalence of Parkinson's disease across north america. *NPJ Parkinsons Dis*. 4, 1–7. doi: 10.1038/s41531-018-0058-0

Martínez-Murcia, F. J., Górriz, J. M., Ramírez, J., Illán, I., Ortiz, A., Initiative, P. P. M., et al. (2014). Automatic detection of parkinsonism using significance measures and component analysis in datscan imaging. *Neurocomputing* 126, 58–70. doi: 10.1016/j.neucom.2013.01.054

Martinez-Murcia, F. J., Ortiz, A., Gorriz, J.-M., Ramirez, J., and Castillo-Barnes, D. (2019). Studying the manifold structure of alzheimer's disease: a deep learning approach using convolutional autoencoders. *IEEE J. Biomed. Health Inform*. 24, 17–26. doi: 10.1109/JBHI.2019.2914970

Martins, R., Oliveira, F., Moreira, F., Moreira, A. P., Abrunhosa, A., Januário, C., et al. (2021). Automatic classification of idiopathic Parkinson's disease and atypical parkinsonian syndromes combining [11C] raclopride pet uptake and MRI grey matter morphometry. *J. Neural. Eng*. 18, 046037. doi: 10.1088/1741-2552/abf772

Mata, I. F., Shi, M., Agarwal, P., Chung, K. A., Edwards, K. L., Factor, S. A., et al. (2010). SNCA variant associated with parkinson disease and plasma α-synuclein level. *Arch. Neurol*. 67, 1350–1356. doi: 10.1001/archneurol.2010.279

Mehrabi, N., Morstatter, F., Saxena, N., Lerman, K., and Galstyan, A. (2021). A survey on bias and fairness in machine learning. *ACM Comput. Surv*. 54, 1–35. doi: 10.1145/3457607

Mei, J., Desrosiers, C., and Frasnelli, J. (2021). Machine learning for the diagnosis of Parkinson's disease: a review of literature. *Front. Aging Neurosci*. 13, 633752. doi: 10.3389/fnagi.2021.633752

Miceli, M., Schuessler, M., and Yang, T. (2020). Between subjectivity and imposition: power dynamics in data annotation for computer vision. *Proc. ACM Hum.-Comput. Interact*. 4(CSCW2), 1–25. doi: 10.1145/3415186

Michell, A., Lewis, S., Foltynie, T., and Barker, R. (2004). Biomarkers and Parkinson's disease. *Brain* 127, 1693–1705. doi: 10.1093/brain/awh198

Mohammadi, D. (2013). The harvard biomarker study's big plan. *Lancet Neurol*. 12, 739–740. doi: 10.1016/S1474-4422(13)70155-8

Molnar, C. (2020). *Interpretable machine learning*. Available online at: https://christophm.github.io/interpretableml-book/ (accessed July 1, 2023).

Morrish, P., Sawle, G., and Brooks, D. (1996). An [18F] dopa-pet and clinical study of the rate of progression in Parkinson's disease. *Brain* 119, 585–591. doi: 10.1093/brain/119.2.585

Movement Disorder Society Task Force on Rating Scales for Parkinson's Disease (2003). The unified Parkinson's disease rating scale (UPDRS): status and recommendations. *Mov. Disord*. 18, 738–750. doi: 10.1002/mds.10473

Muangpaisan, W., Mathews, A., Hori, H., and Seidel, D. (2011). A systematic review of the worldwide prevalence and incidence of Parkinson's disease. *J. Med. Assoc. Thailand* 94, 749.

Müller, R., Kornblith, S., and Hinton, G. E. (2019). When does label smoothing help? *Adv. Neural Inf. Process. Syst*. 32, 4671–4681. Available online at: https://dl.acm.org/doi/10.5555/3454287.3454709

Nair, S. R., Tan, L. K., Mohd Ramli, N., Lim, S. Y., Rahmat, K., Mohd Nor, H., et al. (2013). A decision tree for differentiating multiple system atrophy from Parkinson's disease using 3-T MR imaging. *Eur. Radiol*. 23, 1459–1466. doi: 10.1007/s00330-012-2759-9

Neelakandan, S., Beulah, J. R., Prathiba, L., Murthy, G., Irudaya Raj, E. F., Arulkumar, N., et al. (2022). Blockchain with deep learning-enabled secure healthcare data transmission and diagnostic model. *Int. J. Model. Simul. Sci. Comput*. 13, 2241006. doi: 10.1142/S1793962322410069

Neri, E., de Souza, N., Brady, A., Bayarri, A. A., Becker, C. D., Coppola, F., et al. (2019). What the radiologist should know about artificial intelligence-an ESR white paper. *Insights Imaging* 10, 44. doi: 10.1186/s13244-019-0738-2

Nerius, M., Fink, A., and Doblhammer, G. (2017). Parkinson's disease in germany: prevalence and incidence based on health claims data. *Acta Neurol. Scand*. 136, 386–392. doi: 10.1111/ane.12694

Ngiam, K. Y., and Khor, W. (2019). Big data and machine learning algorithms for health-care delivery. *Lancet Oncol*. 20, e262–e273. doi: 10.1016/S1470-2045(19)30149-4

Nicastro, N., Garibotto, V., and Burkhard, P. R. (2020). Extrastriatal 123 I-FP-CIT spect impairment in Parkinson's disease-the PPMI cohort. *BMC Neurol*. 20, 1–9. doi: 10.1186/s12883-020-01777-2

Niotis, K., West, A. B., and Saunders-Pullman, R. (2022). Who to enroll in parkinson disease prevention trials?: the case for genetically at-risk cohorts. *Neurology* 99(7 Supplement 1), 10–18. doi: 10.1212/WNL.0000000000200812

Obermeyer, Z., Powers, B., Vogeli, C., and Mullainathan, S. (2019). Dissecting racial bias in an algorithm used to manage the health of populations. *Science* 366, 447–453. doi: 10.1126/science.aax2342

Oprescu, M., Syrgkanis, V., and Wu, Z. S. (2019). "Orthogonal random forest for causal inference," in *International Conference on Machine Learning* (New York, NY: PMLR), 4932–4941.

Pagano, G., Niccolini, F., and Politis, M. (2016). Imaging in Parkinson's disease. *Clin. Med*. 16, 371. doi: 10.7861/clinmedicine.16-4-371

Pal, G., Mangone, G., Hill, E. J., Ouyang, B., Liu, Y., Lythe, V., et al. (2022). Parkinson disease and subthalamic nucleus deep brain stimulation: cognitive effects in GBA mutation carriers. *Ann. Neurol*. 91, 424–435. doi: 10.1002/ana.26302

Parisi, F., Ferrari, G., Giuberti, M., Contin, L., Cimolin, V., Azzaro, C., et al. (2015). Body-sensor-network-based kinematic characterization and comparative outlook of UPDRS scoring in leg agility, sit-to-stand, and gait tasks in Parkinson's disease. *IEEE J. Biomed. Health Inf.* 19, 1777–1793. doi: 10.1109/JBHI.2015.2472640

Parkinson, J. (2002). An essay on the shaking palsy. *J. Neuropsychiatry Clin. Neurosci*. 14, 223–236. doi: 10.1176/jnp.14.2.223

Paszke, A., Gross, S., Massa, F., Lerer, A., Bradbury, J., Chanan, G., et al. (2019). Pytorch: an imperative style, high-performance deep learning library. *Adv. Neural Inf. Process. Syst*. 32, 7994–8006. Available online at: https://dl.acm.org/doi/10.5555/3454287.3455008

Patterson, D., Gonzalez, J., Le, Q., Liang, C., Munguia, L.-M., Rothchild, D., et al. (2021). Carbon emissions and large neural network training. *arXiv*. [preprint]. doi: 10.48550/arXiv.2104.10350

Pechevis, M., Clarke, C., Vieregge, P., Khoshnood, B., Deschaseaux-Voinet, C., Berdeaux, G., et al. (2005). Effects of dyskinesias in Parkinson's disease on quality of life and health-related costs: a prospective european study. *Eur. J. Neurol*. 12, 956–963. doi: 10.1111/j.1468-1331.2005.01096.x

Pellicano, C., Benincasa, D., Pisani, V., Buttarelli, F. R., Giovannelli, M., Pontieri, F. E., et al. (2007). Prodromal non-motor symptoms of Parkinson's disease. *Neuropsychiatr. Dis. Treat*. 3, 145. doi: 10.2147/nedt.2007.3.1.145

Pickrell, A. M., and Youle, R. J. (2015). The roles of pink1, parkin, and mitochondrial fidelity in Parkinson's disease. *Neuron* 85, 257–273. doi: 10.1016/j.neuron.2014.12.007

Poewe, W., and Wenning, G. (2002). The differential diagnosis of Parkinson's disease. *Eur. J. Neurol*. 9, 23–30. doi: 10.1046/j.1468-1331.9.s3.3.x

Poldrack, R. A., Barch, D. M., Mitchell, J. P., Wager, T. D., Wagner, A. D., Devlin, J. T., et al. (2013). Toward open sharing of task-based fmri data: the openfmri project. *Front. Neuroinform*. 7, 12. doi: 10.3389/fninf.2013.00012

Politis, M. (2014). Neuroimaging in parkinson disease: from research setting to clinical practice. *Nat. Rev. Neurol*. 10, 708–722. doi: 10.1038/nrneurol.2014.205

Politis, M., Piccini, P., Pavese, N., Koh, S.-B., and Brooks, D. J. (2008). Evidence of dopamine dysfunction in the hypothalamus of patients with Parkinson's disease: an in vivo 11c-raclopride pet study. *Exp. Neurol*. 214, 112–116. doi: 10.1016/j.expneurol.2008.07.021

Postuma, R. B., Poewe, W., Litvan, I., Lewis, S., Lang, A. E., Halliday, G., et al. (2018). Validation of the mds clinical diagnostic criteria for Parkinson's disease. *Mov. Disord*. 33, 1601–1608. doi: 10.1002/mds.27362

Power, J. D., Plitt, M., Laumann, T. O., and Martin, A. (2017). Sources and implications of whole-brain fmri signals in humans. *Neuroimage* 146, 609–625. doi: 10.1016/j.neuroimage.2016.09.038

Prechelt, L. (1998). "Early stopping-but when?" in *Neural Networks: Tricks of the Trade*, eds G. B. Orr, and K. R. Müller (Berlin: Springer), 55–69. doi: 10.1007/3-540-49430-8_3

Prell, T. (2018). Structural and functional brain patterns of non-motor syndromes in Parkinson's disease. *Front. Neurol*. 9, 138. doi: 10.3389/fneur.2018.00138

Pyatigorskaya, N., Sanz-Morère, C. B., Gaurav, R., Biondetti, E., Valabregue, R., Santin, M., et al. (2020). Iron imaging as a diagnostic tool for Parkinson's disease: a systematic review and meta-analysis. *Front. Neurol*. 11, 366. doi: 10.3389/fneur.2020.00366

Qin, R., Zhang, H., Jiang, L., Qiao, K., Hai, J., Chen, J., et al. (2020). Multicenter computer-aided diagnosis for lymph nodes using unsupervised domain-adaptation networks based on cross-domain confounding representations. *Comput. Math. Methods Med*. 2020, 3709873. doi: 10.1155/2020/3709873

Rajput, A. (1992). Frequency and cause of Parkinson's disease. *Can. J. Neurol. Sci*. 19, 103–107. doi: 10.1017/S0317167100041457

Reddy, S., Allan, S., Coghlan, S., and Cooper, P. (2020). A governance model for the application of ai in health care. *J. Am. Med. Inform. Assoc*. 27, 491–497. doi: 10.1093/jamia/ocz192

Riboldi, G. M., Frattini, E., Monfrini, E., Frucht, S. J., and Di Fonzo, A. (2022). A practical approach to early-onset parkinsonism. *J. Parkinsons Dis*. 12, 1–26. doi: 10.3233/JPD-212815

Ricci Lara, M. A., Echeveste, R., and Ferrante, E. (2022). Addressing fairness in artificial intelligence for medical imaging. *Nat. Commun*. 13, 4581. doi: 10.1038/s41467-022-32186-3

Rietdijk, C. D., Perez-Pardo, P., Garssen, J., Van Wezel, R. J., and Kraneveld, A. D. (2017). Exploring Braak's hypothesis of Parkinson's disease. *Front. Neurol*. 8, 37. doi: 10.3389/fneur.2017.00037

Saeed, U., Compagnone, J., Aviv, R. I., Strafella, A. P., Black, S. E., Lang, A. E., et al. (2017). Imaging biomarkers in Parkinson's disease and parkinsonian syndromes: current and emerging concepts. *Transl. Neurodegener*. 6, 1–25. doi: 10.1186/s40035-017-0076-6

Sakai, K., and Yamada, K. (2019). Machine learning studies on major brain diseases: 5-year trends of 2014-2018. *Jpn. J. Radiol*. 37, 34–72. doi: 10.1007/s11604-018-0794-4

Sambasivan, N., Kapania, S., Highfill, H., Akrong, D., Paritosh, P. K., Aroyo, L. M., et al. (2021). "Everyone wants to do the model work, not the data work," *in Data Cascades in High-stakes AI* (New York, NY), 1–15. doi: 10.1145/3411764.3445518

Santiago, J. A., Bottero, V., and Potashkin, J. A. (2017). Biological and clinical implications of comorbidities in Parkinson's disease. *Front. Aging Neurosci*. 9, 394. doi: 10.3389/fnagi.2017.00394

Schootemeijer, S., van der Kolk, N. M., Bloem, B. R., and de Vries, N. M. (2020). Current perspectives on aerobic exercise in people with Parkinson's disease. *Neurotherapeutics* 17, 1418–1433. doi: 10.1007/s13311-020-00904-8

Schwarz, S. T., Afzal, M., Morgan, P. S., Bajaj, N., Gowland, P. A., Auer, D. P., et al. (2014). The 'swallow tail' appearance of the healthy nigrosome-a new accurate test of Parkinson's disease: a case-control and retrospective cross-sectional MRI study at 3T. *PLoS ONE* 9, e93814. doi: 10.1371/journal.pone.0093814

Settles, B. (2009). *Active Learning Literature Survey*. Madison, WI: University of Wisconsin–Madison.

Shinde, S., Prasad, S., Saboo, Y., Kaushick, R., Saini, J., Pal, P. K., et al. (2019). Predictive markers for Parkinson's disease using deep neural nets on neuromelanin sensitive MRI. *Neuroimage Clin*. 22, 101748. doi: 10.1016/j.nicl.2019.101748

Siderowf, A., Concha-Marambio, L., Lafontant, D.-E., Farris, C. M., Ma, Y., Urenia, P. A., et al. (2023). Assessment of heterogeneity among participants in the Parkinson's progression markers initiative cohort using α-synuclein seed amplification: a cross-sectional study. *Lancet Neurol*. 22, 407–417. doi: 10.1016/S1474-4422(23)00109-6

Siderowf, A., Jennings, D., Eberly, S., Oakes, D., Hawkins, K. A., Ascherio, A., et al. (2012). Impaired olfaction and other prodromal features in the parkinson at-risk syndrome study. *Mov. Disord*. 27, 406–412. doi: 10.1002/mds.24892

Smith, J. J., Sorensen, A. G., and Thrall, J. H. (2003). Biomarkers in imaging: realizing radiology's future. *Radiology* 227, 633–638. doi: 10.1148/radiol.2273020518

Smith, M. G., Witte, M., Rocha, S., and Basner, M. (2019). Effectiveness of incentives and follow-up on increasing survey response rates and participation in field studies. *BMC Med. Res. Methodol*. 19, 1–13. doi: 10.1186/s12874-019-0868-8

Song, L., Shokri, R., and Mittal, P. (2019). "Privacy risks of securing machine learning models against adversarial examples," in *Proceedings of the 2019 ACM SIGSAC Conference on Computer and Communications Security* (New York, NY), 241–257. doi: 10.1145/3319535.3354211

Stoker, T. B., and Barker, R. A. (2020). Recent developments in the treatment of Parkinson's disease. *F1000Res*. 9, 11. doi: 10.12688/f1000research.25634.1

Stolze, H., Kuhtz-Buschbeck, J. P., Drücke, H., Jöhnk, K., Illert, M., and Deuschl, G. (2001). Comparative analysis of the gait disorder of normal pressure hydrocephalus and Parkinson's disease. *J. Neurol. Neurosurg. Psychiatry* 70, 289–297. doi: 10.1136/jnnp.70.3.289

Strother, S. C. (2006). Evaluating fmri preprocessing pipelines. *IEEE Eng. Med. Biol Mag*. 25, 27–41. doi: 10.1109/MEMB.2006.1607667

Sulzer, D., Cassidy, C., Horga, G., Kang, U. J., Fahn, S., Casella, L., et al. (2018). Neuromelanin detection by magnetic resonance imaging (MRI) and its promise as a biomarker for Parkinson's disease. *NPJ Parkinsons Dis*. 4, 11. doi: 10.1038/s41531-018-0047-3

Sveinbjornsdottir, S. (2016). The clinical symptoms of Parkinson's disease. *J. Neurochem*. 139, 318–324. doi: 10.1111/jnc.13691

Tahmasian, M., Bettray, L. M., van Eimeren, T., Drzezga, A., Timmermann, L., Eickhoff, C. R., et al. (2015). A systematic review on the applications of resting-state fmri in Parkinson's disease: does dopamine replacement therapy play a role? *Cortex* 73, 80–105. doi: 10.1016/j.cortex.2015.08.005

Talai, A. S., Sedlacik, J., Boelmans, K., and Forkert, N. D. (2021). Utility of multi-modal MRI for differentiating of Parkinson's disease and progressive supranuclear palsy using machine learning. *Front. Neurol*. 12, 648548. doi: 10.3389/fneur.2021.648548

Tamburri, D. A. (2020). "Sustainable mlops: trends and challenges," in *2020 22nd International Symposium on Symbolic and Numeric Algorithms for Scientific Computing (SYNASC)* (Timisoara: IEEE), 17–23. doi: 10.1109/SYNASC51798.2020.00015

Tan, A. H., Lim, S.-Y., Chong, K. K., Manap, M. A. A. A., Hor, J. W., Lim, J. L., et al. (2021). Probiotics for constipation in parkinson disease: a randomized placebo-controlled study. *Neurology* 96, e772–e782. doi: 10.1212/WNL.0000000000010998

Tedeschini, B. C., Savazzi, S., Stoklasa, R., Barbieri, L., Stathopoulos, I., Nicoli, M., et al. (2022). Decentralized federated learning for healthcare networks: a case study on tumor segmentation. *IEEE Access* 10, 8693–8708. doi: 10.1109/ACCESS.2022.3141913

Thenganatt, M. A., and Jankovic, J. (2014). Parkinson disease subtypes. *JAMA Neurol*. 71, 499–504. doi: 10.1001/jamaneurol.2013.6233

Thevathasan, W., Debu, B., Aziz, T., Bloem, B. R., Blahak, C., Butson, C., et al. (2018). Pedunculopontine nucleus deep brain stimulation in Parkinson's disease: a clinical review. *Mov. Disord*. 33, 10–20. doi: 10.1002/mds.27098

Tolosa, E., Garrido, A., Scholz, S. W., and Poewe, W. (2021). Challenges in the diagnosis of Parkinson's disease. *Lancet Neurol*. 20, 385–397. doi: 10.1016/S1474-4422(21)00030-2

Tolosa, E., Vila, M., Klein, C., and Rascol, O. (2020). Lrrk2 in parkinson disease: challenges of clinical trials. *Nat. Rev. Neurol.* 16, 97–107. doi: 10.1038/s41582-019-0301-2

Toulas, B. (2023). *Hospital Clínic de Barcelona Severely Impacted by Ransomware Attack*. Available online at: https://www.bleepingcomputer.com/news/security/hospital-cl-nic-de-barcelona-severely-impacted-by-ransomware-attack/ (accessed July 1, 2023).

van Veluw, S. J., Zwanenburg, J. J., Hendrikse, J., van der Kolk, A. G., Luijten, P. R., Biessels, G. J., et al. (2014). "High resolution imaging of cerebral small vessel disease with 7 T MRI," in *Trends Neurovascular Interventions*, eds T. Tsukahara, G. Esposito, H. J. Steiger., G. Rinkel, and L. Regli (Cham: Springer), 125–130. doi: 10.1007/978-3-319-02411-0_21

Vaswani, A., Shazeer, N., Parmar, N., Uszkoreit, J., Jones, L., Gomez, A. N., et al. (2017). Attention is all you need. *Adv. Neural Inf. Process. Syst.* 30, 5999–6010. Available online at: https://dl.acm.org/doi/10.5555/3295222.3295349

Vega, C. (2021). From hume to Wuhan: an epistemological journey on the problem of induction in covid-19 machine learning models and its impact upon medical research. *IEEE Access* 9, 97243–97250. doi: 10.1109/ACCESS.2021.3095222

Virreira Winter, S., Karayel, O., Strauss, M. T., Padmanabhan, S., Surface, M., Merchant, K., et al. (2021). Urinary proteome profiling for stratifying patients with familial Parkinson's disease. *EMBO Mol. Med.* 13, e13257. doi: 10.15252/emmm.202013257

Visani, G., Bagli, E., Chesani, F., Poluzzi, A., and Capuzzo, D. (2022). Statistical stability indices for lime: obtaining reliable explanations for machine learning models. *J. Oper. Res. Soc.* 73, 91–101. doi: 10.1080/01605682.2020.1865846

Wald, Y., Feder, A., Greenfeld, D., and Shalit, U. (2021). On calibration and out-of-domain generalization. *Adv. Neural Inf. Process. Syst.* 34, 2215–2227. doi: 10.48550/arXiv.2102.10395

Wang, H., Wu, Z., Liu, Z., Cai, H., Zhu, L., Gan, C., et al. (2020). HAT: hardware-aware transformers for efficient natural language processing. *arXiv*. [preprint]. doi: 10.48550/arXiv.2005.14187

Wang, H., Wu, Z., and Xing, E. P. (2018). "Removing confounding factors associated weights in deep neural networks improves the prediction accuracy for healthcare applications," in *BIOCOMPUTING 2019: Proceedings of the Pacific Symposium* (Singapore: World Scientific), 54–65. doi: 10.1142/9789813279827_0006

Weingärtner, S., Desmond, K. L., Obuchowski, N. A., Baessler, B., Zhang, Y., Biondetti, E., et al. (2022). Development, validation, qualification, and dissemination of quantitative MR methods: overview and recommendations by the ISMRM quantitative MR study group. *Magn. Reson. Med.* 87, 1184–1206. doi: 10.1002/mrm.29084

Westreich, D., Lessler, J., and Funk, M. J. (2010). Propensity score estimation: neural networks, support vector machines, decision trees (CART), and meta-classifiers as alternatives to logistic regression. *J. Clin. Epidemiol.* 63, 826–833. doi: 10.1016/j.jclinepi.2009.11.020

Widner, K., Virmani, S., Krause, J., Nayar, J., Tiwari, R., Pedersen, E. R., et al. (2023). Lessons learned from translating ai from development to deployment in healthcare. *Nat. Med.* 29, 1304–1306. doi: 10.1038/s41591-023-02293-9

Wiens, J., Price, W. N., and Sjoding, M. W. (2020). Diagnosing bias in data-driven algorithms for healthcare. *Nat. Med.* 26, 25–26. doi: 10.1038/s41591-019-0726-6

Wyman, B. T., Harvey, D. J., Crawford, K., Bernstein, M. A., Carmichael, O., Cole, P. E., et al. (2013). Standardization of analysis sets for reporting results from adni MRI data. *Alzheimers Dement.* 9, 332–337. doi: 10.1016/j.jalz.2012.06.004

Xu, X.-W., Doi, K., Kobayashi, T., MacMahon, H., and Giger, M. L. (1997). Development of an improved CAD scheme for automated detection of lung nodules in digital chest images. *Med. Phys.* 24, 1395–1403. doi: 10.1118/1.598028

Yagis, E., DE Herrera, A. G. S., and Citi, L. (2019). "Generalization performance of deep learning models in neurodegenerative disease classification," in *2019 IEEE International Conference on Bioinformatics and Biomedicine (BIBM)* (San Diego, CA: IEEE), 1692–1698. doi: 10.1109/BIBM47256.2019.8983088

Yoshikawa, K., Nakata, Y., Yamada, K., and Nakagawa, M. (2004). Early pathological changes in the parkinsonian brain demonstrated by diffusion tensor MRI. *J. Neurol. Neurosurg. Psychiatry* 75, 481–484. doi: 10.1136/jnnp.2003.021873

Yosinski,J., Clune, J., Bengio, Y., and Lipson, H. (2014). How transferable are features in deep neural networks? *Adv. Neural Inf. Process. Syst.* 27, 3320–3329. Available online at: https://dl.acm.org/doi/10.5555/2969033.2969197

Zeng, X., and Martinez, T. R. (2000). Distribution-balanced stratified cross-validation for accuracy estimation. *J. Exp. Theor. Artif. Intell.* 12, 1–12. doi: 10.1080/095281300146272

Zetusky, W. J., Jankovic, J., and Pirozzolo, F. J. (1985). The heterogeneity of Parkinson's disease: clinical and prognostic implications. *Neurology* 35, 522–522. doi: 10.1212/WNL.35.4.522

Zhang, C., Bengio, S., Hardt, M., Recht, B., and Vinyals, O. (2021). Understanding deep learning (still) requires rethinking generalization. *Commun. ACM* 64, 107–115. doi: 10.1145/3446776

Zhang, S., Tao, K., Wang, J., Duan, Y., Wang, B., Liu, X., et al. (2020). Substantia nigra hyperechogenicity reflects the progression of dopaminergic neurodegeneration in 6-ohda rat model of Parkinson's disease. *Front. Cell. Neurosci.* 14, 216. doi: 10.3389/fncel.2020.00216

Zhang, X., Chou, J., Liang, J., Xiao, C., Zhao, Y., Sarva, H., et al. (2019). Data-driven subtyping of Parkinson's disease using longitudinal clinical records: a cohort study. *Sci. Rep.* 9, 797. doi: 10.1038/s41598-018-37545-z

Zhao, J., Wang, T., Yatskar, M., Ordonez, V., and Chang, K.-W. (2017). Men also like shopping: reducing gender bias amplification using corpus-level constraints. *arXiv*. [preprint]. doi: 10.48550/arXiv.1707.09457

frontiers | Frontiers in Aging Neuroscience

TYPE Original Research
PUBLISHED 21 July 2023
DOI 10.3389/fnagi.2023.1187167

OPEN ACCESS

EDITED BY
Robert Petersen,
Central Michigan University, United States

REVIEWED BY
Stephen Tisch,
St Vincent's Hospital Sydney, Australia
Atsushi Nambu,
National Institute for Physiological Sciences (NIPS), Japan

*CORRESPONDENCE
Feng Yin
✉ ying897@126.com

RECEIVED 15 March 2023
ACCEPTED 27 June 2023
PUBLISHED 21 July 2023

CITATION
Zhao M, Chen H, Yan X, Li J, Lu C, Cui B, Huo W, Cao S, Guo H, Liu S, Yang C, Liu Y and Yin F (2023) Subthalamic deep brain stimulation for primary dystonia: defining an optimal location using the medial subthalamic nucleus border as anatomical reference. *Front. Aging Neurosci.* 15:1187167. doi: 10.3389/fnagi.2023.1187167

Subthalamic deep brain stimulation for primary dystonia: defining an optimal location using the medial subthalamic nucleus border as anatomical reference

Mingming Zhao[1], Hui Chen[1], Xin Yan[1], Jianguang Li[1], Chao Lu[1], Bin Cui[2], Wenjun Huo[1], Shouming Cao[1], Hui Guo[1], Shuang Liu[1], Chunjuan Yang[1], Ying Liu[1] and Feng Yin[1]*

[1]Department of Neurosurgery, Aerospace Center Hospital, Beijing, China, [2]Department of Radiology, Aerospace Center Hospital, Beijing, China

Introduction: Although the subthalamic nucleus (STN) has proven to be a safe and effective target for deep brain stimulation (DBS) in the treatment of primary dystonia, the rates of individual improvement vary considerably. On the premise of selecting appropriate patients, the location of the stimulation contacts in the dorsolateral sensorimotor area of the STN may be an important factor affecting therapeutic effects, but the optimal location remains unclear. This study aimed to define an optimal location using the medial subthalamic nucleus border as an anatomical reference and to explore the influence of the location of active contacts on outcomes and programming strategies in a series of patients with primary dystonia.

Methods: Data from 18 patients who underwent bilateral STN-DBS were retrospectively acquired and analyzed. Patients were assessed preoperatively and postoperatively (1 month, 3 months, 6 months, 1 year, 2 years, and last follow-up after neurostimulator initiation) using the Toronto Western Spasmodic Torticollis Rating Scale (for cervical dystonia) and the Burke–Fahn–Marsden Dystonia Rating Scale (for other types). Optimal parameters and active contact locations were determined during clinical follow-up. The position of the active contacts relative to the medial STN border was determined using postoperative stereotactic MRI.

Results: The clinical improvement showed a significant negative correlation with the y-axis position (anterior–posterior; A+, P–). The more posterior the electrode contacts were positioned in the dorsolateral sensorimotor area of the STN, the better the therapeutic effects. Cluster analysis of the improvement rates delineated optimal and sub-optimal groups. The optimal contact coordinates from the optimal group were 2.56 mm lateral, 0.15 mm anterior, and 1.34 mm superior relative to the medial STN border.

Conclusion: STN-DBS was effective for primary dystonia, but outcomes were dependent on the active contact location. Bilateral stimulation contacts

located behind or adjacent to Bejjani's line were most likely to produce ideal therapeutic effects. These findings may help guide STN-DBS preoperative planning, stimulation programming, and prognosis for optimal therapeutic efficacy in primary dystonia.

KEYWORDS

dystonia, deep brain stimulation, subthalamic nucleus, movement disorders, neurological function

1. Introduction

Dystonia is a movement disorder characterized by sustained or intermittent muscle contractions that result in abnormal movements and/or posture (Balint and Bhatia, 2014). Treatment is challenging because of dystonia's highly complex etiology and pathogenesis (Batla et al., 2012; Balint et al., 2018; Albanese et al., 2019). Deep brain stimulation (DBS) has been widely used in the treatment of various types of drug-resistant dystonia, and the globus pallidus internus (GPi) is the most commonly used stimulation target (Kupsch et al., 2006; Volkmann et al., 2014; Meoni et al., 2017; Sobstyl et al., 2017; Tsuboi et al., 2020). Although its safety and efficacy have been proven, stimulation-induced side effects are frequent and insurmountable (Balint et al., 2018; Kosutzka et al., 2020). The high energy consumption of DBS is another drawback (Lin et al., 2019).

Increasing evidence has shown that the subthalamic nucleus (STN) is an effective target for the treatment of primary dystonia (Yao et al., 2019; Wang and Yu, 2021; Li et al., 2022; Yin et al., 2022). However, the benefits of stimulation and the required stimulation complexity vary greatly between patients, highlighting the necessity of exploring outcome and treatment predictors. The main factors affecting the success of STN-DBS include patient selection, the correct positioning of the electrodes in the target, and the optimization of stimulation programming. Choosing the optimal DBS site is a prerequisite for obtaining good therapeutic effects.

The midcommissural point (MCP) is a common anatomical reference point used in stereotactic neurosurgery. However, using this for STN-DBS localization is not ideal, as the exact location of the MCP varies among individuals (Bot et al., 2018). The red nucleus (RN) is a useful internal reference for targeting the anteroposterior coordinates of the STN (Chang et al., 2008). Bejjani's line (Bejjani et al., 2000) and the medial STN border, based on the anatomic relationship between the RN and STN, have also been used with good results in STN-DBS treatment of Parkinson's disease (PD), and a theoretical stimulation "hotspot" has been defined (Bot et al., 2018). However, the usefulness of this location in dystonia remains unclear. Therefore, we used the medial border of the STN as a reference to determine the optimal electrode location and to evaluate the relationship between active contact locations, clinical outcomes, and programming in the STN-DBS treatment of primary dystonia.

2. Materials and methods

2.1. Patients

We retrospectively analyzed data collected from 18 patients with primary dystonia who received STN-DBS in the Department of Neurosurgery at the Aerospace Center Hospital from September 2014 to January 2020. The inclusion criteria were as follows: a diagnosis of idiopathic isolated dystonia; severe dysfunction that did not respond to oral medication, botulinum toxin, or selective peripheral denervation; no other secondary cause, including the use of antipsychotic medications, was present before the onset of dystonia; normal neurological examination and brain MRI except for dystonia; and the patient was willing to receive regular counseling visits and a long-term follow up. The exclusion criteria were medical contraindications to surgery; MRI evidence of another neurological disorder, extensive brain atrophy, or anatomic abnormalities in the basal ganglia region; and severe cognitive impairment, depression, or severe mental illness. This study received ethical approval from the Aerospace Center Hospital (approval number: 20190301-YN-03), and all protocols were implemented in accordance with the Declaration of Helsinki. All patients provided written informed consent.

2.2. Surgical procedures and stimulation programming

The dorsolateral regions of the bilateral STN were selected as the targets for electrode implantation in all enrolled patients. DBS surgery was performed by the same two experienced neurosurgeons following a previously published procedure (Yin et al., 2022). All patients underwent post-operative brain CT to rule out hemorrhage. Programming was initiated 3 weeks after DBS surgery. The lead locations were confirmed by fusing post-operative high-resolution CT images with pre-operative MRI before programming. The programming method has also been described previously (Yin et al., 2022).

2.3. Clinical evaluation

Symptoms of dystonia were assessed by an independent neurologist specializing in movement disorders, who was neither aware of the stimulation status nor responsible for programming,

before (baseline) and after surgery (1 month, 3 months, 6 months, 1 year, 2 years, and at the last follow-up after neurostimulator initiation). The Toronto Western Spasmodic Torticollis Rating Scale was used to assess cervical dystonia (CD), and the Burke–Fahn–Marsden Dystonia Rating Scale (BFMDRS) was used to assess generalized dystonia, cranial dystonia, and myoclonus–dystonia. The results were normalized by calculating the percentage changes of both rating scale scores.

2.4. Electrode contact placement relative to medial STN border

The methods of Bot et al. (2018) were followed for electrode contact positioning relative to the medial STN border. In brief, 1.5-T T2-weighted MRI was performed, and measurements were performed using SurgiPlan. The medial STN border was identified in the axial plane containing the maximum diameter of the RN, which was determined using both axial- and coronal-orientated images. A line was drawn perpendicular to the anterior commissure–posterior commissure line coinciding with the anterior border of the RN, which is Bejjani's line. The point of intersection with the medial boundary of the STN was determined, defined as the medial STN border, and the stereotactic coordinates with respect to the MCP were recorded. Post-operative CT images were coregistered with stereotactic T1-weighted MRI images, and the stereotactic x- (lateral), y- (anterior–posterior), and z- (dorsal–ventral) coordinates of the contact point of active stimulation relative to the medial STN border were determined. This was done separately for the left and right hemispheres. The x-coordinates of both bilateral contacts were defined as the location of the positive contact, and the y- and z-coordinates were used to define the anterior and dorsal directions of Bejjani's line as positive and the reverse as negative.

2.5. Statistical analysis

Statistical analysis was performed using SPSS (v19.0; IBM Corp., Armonk, NY, USA). The Shapiro–Wilk test was used to analyze the distribution of the grouped data. Cluster analysis (K-means clustering) was used to identify subgroups using improvement rates. The Mann–Whitney U test was used to compare differences between clusters, between dystonia subtypes, and between coordinate values. Correlations were performed using Spearman's correlation analysis. Two-tailed p-values < 0.05 were considered statistically significant. The results are presented as mean ± SD.

3. Results

3.1. Participants

Table 1 summarizes the clinical characteristics, percentages of improvement at different follow-up times, and stimulation parameters at the last follow-up of the 18 included patients (9 male, 9 female). Nine patients had CD, five had generalized dystonia, three had cranial dystonia (one with cervical symptoms and two without), and one had myoclonus–dystonia. The mean age of onset was 39.3 ± 15.1 (range, 7–62) years. The duration of disease was 4.4 ± 2.2 (range, 1–9) years. The average age at surgery was 43.7 ± 14.9 (range, 14–69) years. The mean follow-up time was 5.5 ± 1.8 (range, 2–8) years. Two patients received routine battery replacements.

TABLE 1 Summary of patient characteristics, percent improvement at different follow-up times, and stimulation parameters at last follow-up.

Sex	
Male	9
Female	9
Age at onset (year)	39.3 ± 15.1
Childhood	1
Adolescence	1
Early adulthood	7
Late adulthood	9
Disease duration (year)	4.4 ± 2.2
Disease subtype	
Generalized	5
Cervical	9
Cranial	3
Myoclonus	1
Age at surgery (year)	43.7 ± 14.9
Duration of follow-up (year)	5.5 ± 1.8
Percentage of improvement	
1 month	23.8 ± 10.9
3 months	52.3 ± 17.2
6 months	69.4 ± 25.6
1 year	83.0 ± 22.8
2 years	85.7 ± 23.6
Last follow-up	90.6 ± 13.0
DBS parameters	
Amplitude (V)	2.4 ± 0.5
Pulse width (μs)	60.6 ± 2.3
Frequency (Hz)	134.0 ± 6.7

Data on age at onset, disease duration, age at surgery, duration of follow-up, percentage of improvement, and DBS parameters expressed as mean ± SD, and other data expressed as numbers; DBS, deep brain stimulation.

3.2. Clinical outcomes

A total of 36 DBS electrodes were placed in 18 patients, and all used the monopolar stimulation mode. For the entire cohort, the mean improvement was 23.8% at 1 month, 52.3% at 3 months, 69.4% at 6 months, 83.0% at 1 year, 85.7% at 2 years, and 90.6% at the last follow-up. The mean improvement rates of five patients with generalized dystonia at 1, 3, and 6 months and 1 year, 2 years,

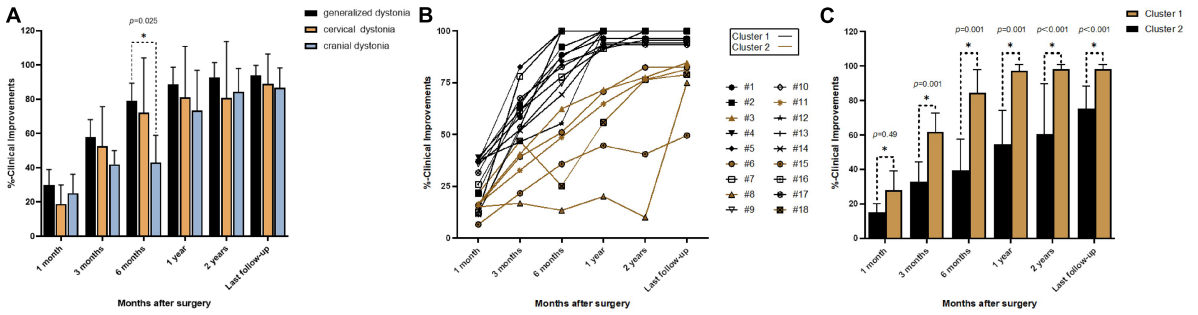

FIGURE 1
Improvement rates at different follow-up times: **(A)** mean percent improvement at different follow-up times after surgery in three types of dystonia; **(B)** line graphs showing individual percent improvement at different follow-up times after surgery; **(C)** mean percent improvement at different follow-up times after surgery in Clusters 1 and 2; *$p < 0.05$.

and the last follow-up were 29.9, 57.9, 79.2, 88.8, 92.6, and 94.0%, respectively. Correspondingly, in the nine patients with CD, these were 18.7, 52.6, 72.1, 81.0, 80.8, and 89.0%, respectively. In the three patients with cranial dystonia, these were 25.1, 41.9, 43.0, 73.5, 84.3, and 86.8%, respectively. There was no significant difference among the three types of dystonia during follow-up except for a slight difference between generalized and cranial dystonia at 6 months (Figure 1A). The patient with myoclonus–dystonia showed improvement rates at 1 month, 3 months, 6 months, 1 year, 2 years, and the last follow-up of 35.7, 52.4, 74.7, 100.0, 100.0, and 100.0%, respectively.

At the last follow-up visit, all the patients received a monopolar stimulus mode. The mean pulse width was 60.6 ± 2.3 μs, the mean frequency was 134.0 ± 6.7 Hz, and 17 patients were using constant-voltage stimulation (mean amplitude, 2.4 ± 0.5 V) and 1 patient was using constant-current stimulation (bilateral, 2.4 mA).

Cluster analysis of the improvement rates identified two different groups (Figures 1B, C). Cluster 1 included 12 patients (6 CD, 4 generalized dystonia, 1 cranial dystonia, and 1 myoclonus–dystonia), and the mean improvement rates at 1 month, 3 months, 6 months, 1 year, 2 years, and the last follow-up were 28.1, 61.9, 84.4, 97.2, 98.3, and 98.3%, respectively. Cluster 2 included six patients (3 CD, 1 generalized dystonia, and 2 cranial dystonia), and the improvement rates were 15.3, 32.9, 39.4, 54.6, 60.6, and 75.3%, respectively. The mean improvement was statistically different between these two groups at each follow-up time. Cluster 1 represents the optimal response group, and Cluster 2 represents the suboptimal response group. The two groups had no significant differences in sex (p = 0.331), age at disease onset (p = 0.174), duration of disease (p = 0.479), age at surgery (p = 0.189), duration of stimulation (p = 0.743), and stimulation parameters (left amplitude, p = 0.850; right amplitude, p = 0.395; left pulse width, p = 1.000; right pulse width, p = 0.606; frequency, p = 0.538).

3.3. Location of active electrode contacts

The mean stereotactic distances of the left and right active electrode contacts of Cluster 1 and Cluster 2 relative to the medial STN border are shown in Table 2. The active contacts in Cluster 2 were more anterior than those in Cluster 1 on both the left and right sides, but there was no significant difference in the x- or z- coordinates. In both clusters, there was no significant difference between the right and left sides for the x-, y-, or z-coordinates. For Cluster 1, the average x-, y-, and z-coordinates were 2.56 mm, 0.15 mm, and 1.34 mm, respectively. The optimal contact coordinates were obtained according to these. For Cluster 2, the average x-, y-, and z-coordinates were 2.66 mm, 1.48 mm, and 1.08 mm, respectively. Cluster 1 and Cluster 2 were statistically different in their average y-coordinates but not in their average x- or z-coordinates (Table 2).

The bilateral active contacts in all the patients are shown in Figure 2. In Cluster 2, both bilateral active contacts were more anterior in three patients, and the active contacts on one side were more anterior than the other side in three patients. The former group showed less improvement at the last follow-up than the latter group (69.7 vs. 80.9%), and the small number of cases limited statistical analysis.

3.4. Correlation between active contacts locations and outcomes

Correlations between the improvement rate at the last follow-up and the x-, y-, and z-coordinates relative to the medial STN border are shown in Figure 3. For the entire cohort, there was a significant inverse correlation between the right y-coordinate and the improvement rate at the last follow-up (p = 0.006). The improvement rate at the last follow-up showed no correlation with the left y-, bilateral x-, or bilateral z- coordinates. The average y-coordinate of the bilateral contacts was negatively correlated with the improvement rate at the last follow-up (p = 0.011), while the average x- and z- coordinates were not significantly correlated with the improvement rate at the last follow-up.

3.5. Long-term motor outcome predictors and associated factors

None of the tested factors were found to be an independent predictor of long-term movement improvement (sex, p = 0.281; age at disease onset, p = 0.061; duration of disease, p = 0.793; age at

10.3389/fnagi.2023.1187167

TABLE 2 Mean stereotactic coordinates of left and right active electrode contacts in Cluster 1 and Cluster 2 relative to the medial STN border and average coordinates on both sides.

	n	Left contact location			Right contact location			Average coordinates of bilateral contact location		
		x	*y*	*z*	*x*	*y*	*z*	*x*	*y*	*z*
Cluster 1	12	2.65 ± 0.33	−0.05 ± 0.65	1.28 ± 1.33	2.47 ± 0.3	0.36 ± 0.59	1.87 ± 1.04	2.56 ± 0.22	0.15 ± 0.60	1.34 ± 1.24
Cluster 2	6	2.55 ± 0.44	1.02 ± 0.67	0.3 ± 1.61	2.77 ± 0.3	1.93 ± 0.6	1.4 ± 1.26	2.66 ± 0.36	1.48 ± 0.57	1.08 ± 0.86
P-values		$p = 0.741$	$\mathbf{p = 0.017}$	$p = 0.280$	$p = 0.066$	$\mathbf{p = 0.001}$	$p = 0.606$	$p = 0.280$	$\mathbf{p = 0.001}$	$p = 0.398$

Significant differences between clusters indicated in bold.

surgery, $p = 0.057$; duration of stimulation, $p = 0.163$). However, the improvement rates at 1 month ($p = 0.022$) and 3 months ($p = 0.001$) were positively correlated with the improvement rate at the last follow-up.

3.6. Adverse events

No surgery-related complications (e.g., intracranial and extracranial hematoma or epileptic seizures) or hardware-related infections were found during the entire follow-up. Six patients experienced uncomfortable sensations due to the extension wire, but none required additional surgery. One patient sometimes experienced mild pain at the site of the neurostimulator, but it had no practical effect on activities of daily living. Stimulus-related adverse events included mild balance disorder (one patient), manic symptoms (one patient), mild hand weakness (two patients), and movement disorders (10 patients), all of which were alleviated through programming alterations.

4. Discussion

This study has once again confirmed the long-term safety and sustained effectiveness of STN-DBS for the treatment of different subtypes of dystonia (up to 8 years). We determined the optimal contact coordinates, which were relative to the medial STN border, for STN-DBS in the treatment of dystonia and found that the improvement of symptoms was closely related to the y-axis position of the electrode contact. The more posterior the electrode contacts were in the dorsolateral sensorimotor area of the STN, the better the therapeutic effects. This study demonstrated significant effects of STN-DBS in the treatment of myoclonus–dystonia.

Treatment with STN-DBS is more likely to induce stimulus-related dyskinesia than GPi-DBS, and this most often occurs in the early stages after the stimulator is first activated (Zheng et al., 2010; Lin et al., 2019; Liu et al., 2019). We reduced the voltage within 1 month after neurostimulator initiation to prevent discomfort and lower the risk of adverse events. If the treatment threshold was not reached, the improvement rate at the 1-month follow-up was lower. Then, by gradually increasing the stimulation voltage, the dyskinesia was overcome, and the treatment effect gradually became significant. The same strategy was used by our group for the treatment of all types of dystonia.

Cervical dystonia is the most common form of focal dystonia, and there are more reports on STN-DBS treatment of CD than other subtypes (Pahapill and O'Connell, 2010; Ostrem et al., 2011, 2017; Wagle Shukla et al., 2018; Gupta, 2020). In the present study, long-term improvement was higher than in a previous study (Ostrem et al., 2017). Our current study included five patients with generalized dystonia, who showed no significant difference in their mean motor symptom improvement rate compared with patients with CD during follow-up; this was in line with a previous study (Deng et al., 2018). A recent study showed that STN-DBS provided relatively steady improvement in the severity of generalized isolated dystonia, with increases of 66.8 and 72.6% at 1-year and last long-term follow-up, respectively (Li et al., 2022). In the three patients in the present study with cranial dystonia, the mean improvement

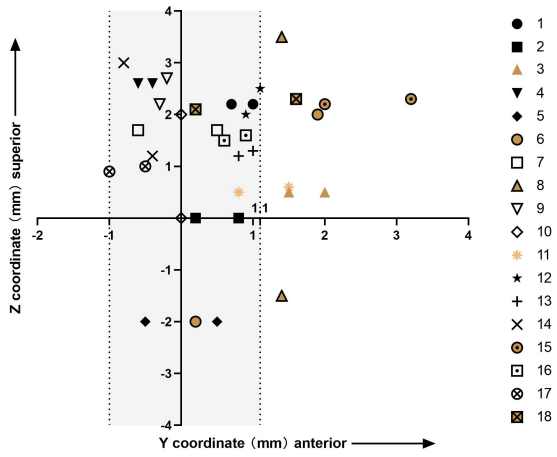

FIGURE 2
Plot of the y- and z-coordinates of the bilateral stimulation contacts for all 18 patients; the origin of the plot is the medial STN border; Clusters 1 and 2 are represented in different colors; the shaded area includes all bilateral active contacts of patients in Cluster 1 and unilateral active contacts of patients in Cluster 2.

rate was not significantly different from that in the patients with CD and generalized dystonia. A recent study showed that 32 patients with Meige syndrome had a mean improvement of 79.0% at the last follow-up (mean, 16.3 months; Wang et al., 2021), which is similar to that reported here. Another study showed that 14 patients with Meige syndrome had a mean improvement of 70.9% at the last follow-up (mean, 14.8 months; Yao et al., 2019).

Myoclonus–dystonia is a relatively rare movement disorder typically characterized by childhood-onset myoclonic jerks in the upper limbs and various extents of dystonia (Roze et al., 2018). Most studies have selected GPi as the stimulation target, and few have chosen the ventral intermediate nucleus of the thalamus. Both targets have been effective, but GPi stimulation may be preferred due to fewer stimulation-induced events (Wang and Yu, 2021). In the present study, we included one patient with myoclonus–dystonia who achieved complete improvement 1 year after STN-DBS. Similar reports have not been found.

Studies of STN-DBS for the treatment of PD, when the MCP was selected as the reference, have shown no correlation between the DBS location and motor improvement (McClelland et al., 2005, 2009; Kasasbeh et al., 2013; Weise et al., 2013; Nestor et al., 2014). Bot et al. (2018) proposed the medial STN border, which was defined as the intersection of Bejjani's line with the medial border of the STN (Bejjani et al., 2000), as a new, individualized reference point that is well delineated on standard MRI (Bot et al., 2018). They found that the medial STN border was superior compared to the MCP as an anatomical reference for correlation between the DBS location and motor improvement and defined a theoretic stimulation "hotspot." A study with a larger patient cohort study refined the "hotspot" within the STN at 2.6 mm lateral, 0.7 mm anterior, and 1.9 mm superior to the medial STN border using T2-weighted imaging (Bolier et al., 2021). Inspired by this, in the present study, we found that the "hotspot" for STN-DBS in the treatment of primary dystonia was at 2.56 mm lateral, 0.15 mm anterior, and 1.34 mm superior to the medium STN border using T2-weighted imaging. The "hotspots" for the treatment of dystonia and PD are, thus, similar. The subsequent findings of an exclusive correlation between the y-coordinate and clinical outcome suggested that the y-axis placement was an important predictor of electrode contact efficacy.

The explanation for these findings may relate to the anatomy of the STN. The STN is composed of a dorsolateral motor area, a central associative region, and a ventromedial limbic component (Haynes and Haber, 2013). The more forward the electrode contact deviates from Bejjani's line, the closer it is to the associative region, and it can thus can easily cause stimulation side effects. The dorsolateral motor area neurons are then less stimulated, resulting in a poor therapeutic effect.

In the present study, Cluster 1 represented the optimal response group, and Cluster 2 represented the suboptimal response group. During the entire follow-up period, the improvement rate of Cluster 1 was significantly better than that of Cluster 2. Interestingly, the improvement of three patients from Cluster 2, with active contacts on one side more anterior to those on the other, was superior to the three patients for whom both bilateral active contacts were more anterior, although the number of cases limited statistical analysis. This may mean that the optimal therapeutic effect requires bilateral stimulation contacts to be in an ideal location. Even if one of the stimulation contacts deviates from this position, the long-term outcome may be affected. The present study also confirmed that axial symptoms of dystonia are regulated bilaterally in the brain. The electrode deviation may have been related to brain drift caused by the loss of cerebrospinal fluid (CSF) during implantation, and the second electrode is especially more vulnerable to this. Direct puncture of the dura over the planned cortical entry point during surgery can significantly reduce the loss of CSF compared to standard incision of the dura (Piacentino et al., 2021).

The "up–top–down" rule is the programming strategy we apply, as described in our previous article, which minimizes stimulus-related side effects and reduces the energy consumption of the stimulator while maintaining efficacy (Yin et al., 2022). No significant difference was detected between Cluster 1 and Cluster 2 in the incidence of stimulation-induced dyskinesia in the present study, but Cluster 1 was less severe and easier to adapt than Cluster 2. This may be related to the better contact positions in Cluster 1.

In the present cohort, the optimal selection of active contacts was determined within 3 months for Cluster 1, and with the increase of the stimulation voltage, motor symptoms continued to improve until becoming stable. However, for Cluster 2, the mean improvement rate at 3 months was less than that in Cluster 1 (32.9 vs. 62.9%). In order to obtain better therapeutic effects, it is necessary to alter the active contacts and/or stimulation mode after 3 months of stimulation. In the present study, one patient's paroxysmal dystonia disappeared immediately after switching from constant-voltage to constant-current stimulation. The improvement rate at 3 months could predict the effects of long-term stimulation, and using the 3-month rate for prediction was superior to the 1-month rate. Thus, when the improvement rate is not ideal after 3 months, an adjustment of the stimulation strategy should be considered.

One patient in the present study became hypomanic after the stimulator was turned on, indicating that the stimulation contact was located in the ventral limbic region (Mallet et al., 2007; Prange et al., 2022). When the dorsal contacts were selected as the active

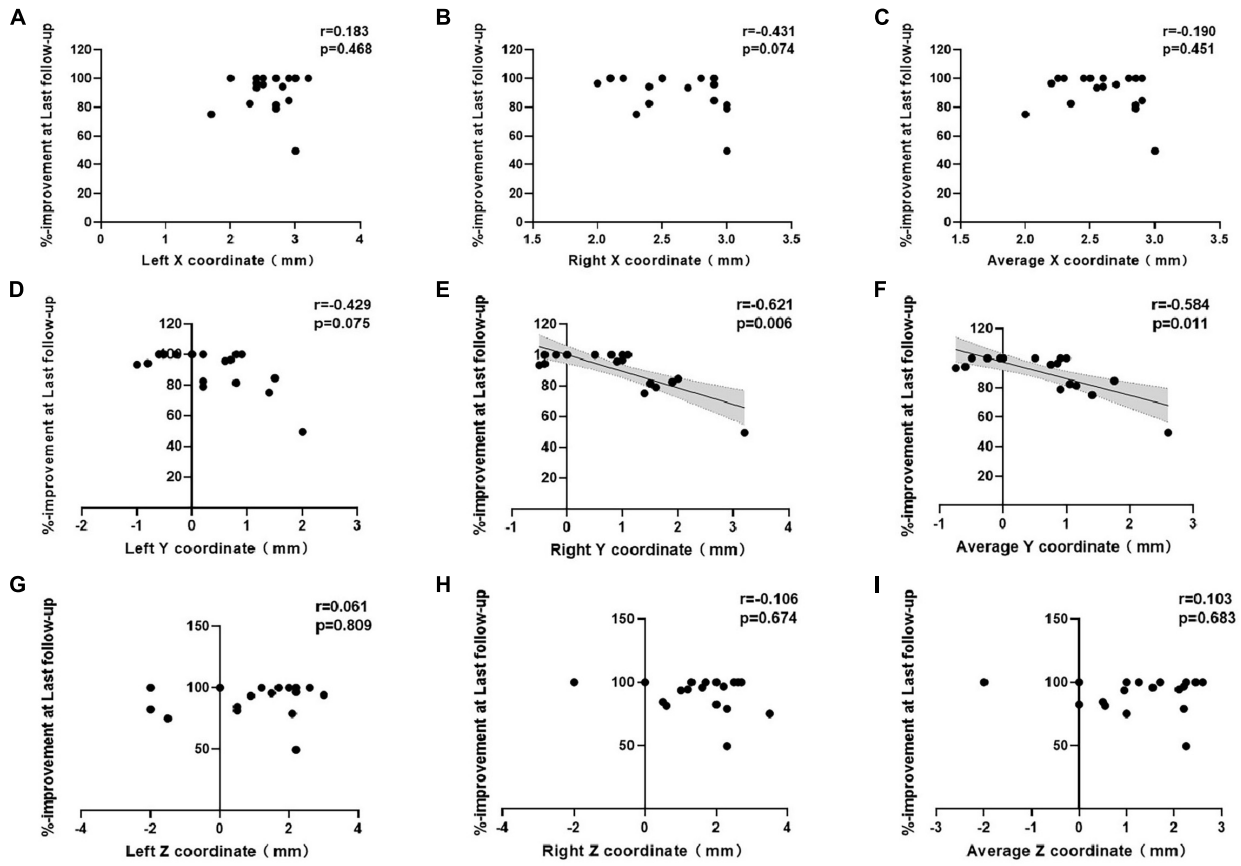

FIGURE 3
Correlations between percent improvement at last follow-up and the **(A–C)** x-, **(D–F)** y-, and **(G–I)** z-coordinates of the active contacts in all patients.

contacts, the hypomania disappeared, but the stimulation effect was poor because the stimulation contacts deviated from Bejjani's line on both sides.

This study has some limitations. First, it was not randomized or fully blinded, which may have introduced bias. Future studies are warranted that group patients randomly, by differentiation using the stimulation electrode y-coordinates, or using blind clinical assessment, which will help confirm our findings. Second, the analysis of the predictors may not be robust enough due to a lack of sufficient case numbers. Therefore, more cases and more rigorously designed studies are needed for further confirmation. Genetic testing data were not available for most of the patients in the present cohort. A growing number of studies have found that genetic signatures are some of the most promising predictors (Jinnah et al., 2017; Tisch and Kumar, 2020).

5. Conclusion

Subthalamic nucleus-deep brain stimulation can provide significant, sustained, and stable effects in the treatment of patients with various subtypes of primary dystonia. In addition, stimulation at posterior contacts in the STN on the y-axis was found to be more advantageous than at anterior contacts for improving dystonia. Special attention should be paid to electrode positioning along the anterior–posterior axis to ensure that the electrodes are positioned as close to Bejjani's line as possible.

Data availability statement

The raw data supporting the conclusions of this article will be made available by the authors, without undue reservation.

Ethics statement

This study was approved by the Ethics Committee of the Aerospace Center Hospital (Approval Number: 20190301-YN-03). Written informed consent to participate in this study was provided by the participants' legal guardian/next of kin.

Author contributions

MZ, FY, HC, and CL conceptualized the study. MZ, JL, CY, and YL conducted the study, including data collection and data analysis. XY and SC contributed to the assessment of pre- and post-operative symptoms. BC, HG, and WH contributed to the acquisition and

processing of image data. MZ and SL drafted the manuscript, which was critically reviewed by all the other authors. All the authors approved the final version of the manuscript.

Funding

This work was supported by the National Natural Science Foundation of China (No. 62171003).

Acknowledgments

We thank all the subjects who participated in this study and the nurses and anesthesiologists who participated in the surgery.

Conflict of interest

The authors declare that the research was conducted in the absence of any commercial or financial relationships that could be construed as a potential conflict of interest.

Publisher's note

References

Albanese, A., Di Giovanni, M., and Lalli, S. (2019). Dystonia: Diagnosis and management. *Eur. J. Neurol.* 26, 5–17.

Balint, B., and Bhatia, K. P. (2014). Dystonia: An update on phenomenology, classification, pathogenesis and treatment. *Curr. Opin. Neurol.* 27, 468–476.

Balint, B., Mencacci, N. E., Valente, E. M., Pisani, A., Rothwell, J., Jankovic, J., et al. (2018). Dystonia. *Nat. Rev. Dis. Primers* 4:25.

Batla, A., Stamelou, M., and Bhatia, K. P. (2012). Treatment of focal dystonia. *Curr. Treat. Options Neurol.* 14, 213–229.

Bejjani, B. P., Dormont, D., Pidoux, B., Yelnik, J., Damier, P., Arnulf, I., et al. (2000). Bilateral subthalamic stimulation for Parkinson's disease by using three-dimensional stereotactic magnetic resonance imaging and electrophysiological guidance. *J. Neurosurg.* 92, 615–625. doi: 10.3171/jns.2000.92.4.0615

Bolier, E., Bot, M., van den Munckhof, P., Pal, G., Sani, S., and Verhagen Metman, L. (2021). The medial subthalamic nucleus border as a new anatomical reference in stereotactic neurosurgery for Parkinson's disease. *Stereotact. Funct. Neurosurg.* 99, 187–195. doi: 10.1159/000510802

Bot, M., Schuurman, P. R., Odekerken, V. J. J., Verhagen, R., Contarino, F. M., De Bie, R. M. A., et al. (2018). Deep brain stimulation for Parkinson's disease: Defining the optimal location within the subthalamic nucleus. *J. Neurol. Neurosurg. Psychiatry* 89, 493–498.

Chang, J., Thakur, S. B., Huang, W., and Narayana, A. (2008). Magnetic resonance spectroscopy imaging (MRSI) and brain functional magnetic resonance imaging (fMRI) for radiotherapy treatment planning of glioma. *Technol. Cancer Res. Treat.* 7, 349–362.

Deng, Z., Pan, Y., Zhang, C., Zhang, J., Qiu, X., Zhan, S., et al. (2018). Subthalamic deep brain stimulation in patients with primary dystonia: A ten-year follow-up study. *Parkinsonism Relat. Disord.* 55, 103–110. doi: 10.1016/j.parkreldis.2018.05.024

Gupta, A. (2020). Subthalamic stimulation for cervical dystonia. *Acta Neurochir. (Wien)* 162, 1879–1881.

Haynes, W. I., and Haber, S. N. (2013). The organization of prefrontal-subthalamic inputs in primates provides an anatomical substrate for both functional specificity and integration: Implications for Basal Ganglia models and deep brain stimulation. *J. Neurosci.* 33, 4804–4814. doi: 10.1523/JNEUROSCI.4674-12.2013

Jinnah, H. A., Alterman, R., Klein, C., Krauss, J. K., Moro, E., Vidailhet, M., et al. (2017). Deep brain stimulation for dystonia: A novel perspective on the value of genetic testing. *J. Neural Transm. (Vienna)* 124, 417–430. doi: 10.1007/s00702-016-1656-9

Kasasbeh, A., Abulseoud, O. A., Matsumoto, J. Y., Stead, S. M., Goerss, S. J., Klassen, B. T., et al. (2013). Lack of differential motor outcome with subthalamic nucleus region stimulation in Parkinson's disease. *J. Clin. Neurosci.* 20, 1520–1526. doi: 10.1016/j.jocn.2013.02.006

Kosutzka, Z., Rivaud-Pechoux, S., Pouget, P., Bonnet, C., Tisch, S., Roze, E., et al. (2020). Pathophysiology of gait disorders induced by bilateral globus pallidus interna stimulation in dystonia. *Brain* 143:e3.

Kupsch, A., Benecke, R., Müller, J., Trottenberg, T., Schneider, G. H., Poewe, W., et al. (2006). Pallidal deep-brain stimulation in primary generalized or segmental dystonia. *N. Engl. J. Med.* 355, 1978–1990.

Li, J., Li, N., Wang, X., Wang, J., Wang, X., and Wang, W. (2022). Long-term outcome of subthalamic deep brain stimulation for generalized isolated dystonia. *Neuromodulation* S1094-7159(22)00757-7. doi: 10.1016/j.neurom.2022.07.003

Lin, S., Wu, Y., Li, H., Zhang, C., Wang, T., Pan, Y., et al. (2019). Deep brain stimulation of the globus pallidus internus versus the subthalamic nucleus in isolated dystonia. *J. Neurosurg.* 132, 721–732.

Liu, Y., Zhu, G., Jiang, Y., Wang, X., Chen, Y., Meng, F., et al. (2019). Comparison of short-term stimulation of the Globus pallidus interna and subthalamic nucleus for treatment of primary dystonia. *World Neurosurg.* 123, e211–e217. doi: 10.1016/j.wneu.2018.11.137

Mallet, L., Schupbach, M., N'Diaye, K., Remy, P., Bardinet, E., Czernecki, V., et al. (2007). Stimulation of subterritories of the subthalamic nucleus reveals its role in the integration of the emotional and motor aspects of behavior. *Proc. Natl. Acad. Sci. U.S.A.* 104, 10661–10666. doi: 10.1073/pnas.0610849104

McClelland, S. III, Ford, B., Senatus, P. B., Frucht, S. J., Winfield, L. M., Yu, Q., et al. (2009). Typical variations of subthalamic electrode location do not predict limb motor function improvement in Parkinson's disease. *J. Clin. Neurosci.* 16, 771–778; discussion 779. doi: 10.1016/j.jocn.2008.10.011

McClelland, S. III, Ford, B., Senatus, P. B., Winfield, L. M., Du, Y. E., Pullman, S. L., et al. (2005). Subthalamic stimulation for Parkinson disease: Determination of electrode location necessary for clinical efficacy. *Neurosurg. Focus* 19:E12.

Meoni, S., Fraix, V., Castrioto, A., Benabid, A. L., Seigneuret, E., Vercueil, L., et al. (2017). Pallidal deep brain stimulation for dystonia: A long term study. *J. Neurol. Neurosurg. Psychiatry* 88, 960–967.

Nestor, K. A., Jones, J. D., Butson, C. R., Morishita, T., Jacobson, C. E. IV, Peace, D. A., et al. (2014). Coordinate-based lead location does not predict Parkinson's disease deep brain stimulation outcome. *PLoS One* 9:e93524. doi: 10.1371/journal.pone.0093524

Ostrem, J. L., Racine, C. A., Glass, G. A., Grace, J. K., Volz, M. M., Heath, S. L., et al. (2011). Subthalamic nucleus deep brain stimulation in primary cervical dystonia. *Neurology* 76, 870–878.

Ostrem, J. L., San Luciano, M., Dodenhoff, K. A., Ziman, N., Markun, L. C., Racine, C. A., et al. (2017). Subthalamic nucleus deep brain stimulation in isolated dystonia: A 3-year follow-up study. *Neurology* 88, 25–35.

Pahapill, P. A., and O'Connell, B. (2010). Long-term follow-up study of chronic deep brain stimulation of the subthalamic nucleus for cervical dystonia. *Neuromodulation* 13, 26–30. doi: 10.1111/j.1525-1403.2009.00231.x

Piacentino, M., Beggio, G., Rustemi, O., Zambon, G., Pilleri, M., and Raneri, F. (2021). Pneumocephalus in subthalamic deep brain stimulation for Parkinson's disease: A comparison of two different surgical techniques considering factors conditioning brain shift and target precision. *Acta Neurochir. (Wien)* 163, 169–175. doi: 10.1007/s00701-020-04635-9

Prange, S., Lin, Z., Nourredine, M., Danaila, T., Laurencin, C., Lagha-Boukbiza, O., et al. (2022). Limbic stimulation drives mania in STN-DBS in Parkinson disease: A prospective study. *Ann. Neurol.* 92, 411–417. doi: 10.1002/ana.26434

Roze, E., Lang, A. E., and Vidailhet, M. (2018). Myoclonus-dystonia: Classification, phenomenology, pathogenesis, and treatment. *Curr. Opin. Neurol.* 31, 484–490.

Sobstyl, M., Brzuszkiewicz-Kuzmicka, G., Zaczynski, A., Pasterski, T., Aleksandrowicz, M., and Zabek, M. (2017). Long-term clinical outcome of bilateral pallidal stimulation for intractable craniocervical dystonia (Meige syndrome). Report of 6 patients. *J. Neurol. Sci.* 383, 153–157. doi: 10.1016/j.jns.2017.10.017

Tisch, S., and Kumar, K. R. (2020). Pallidal deep brain stimulation for monogenic dystonia: The effect of gene on outcome. *Front. Neurol.* 11:630391. doi: 10.3389/fneur.2020.630391

Tsuboi, T., Cauraugh, J. H., Wong, J. K., Okun, M. S., and Ramirez-Zamora, A. (2020). Quality of life outcomes after globus pallidus internus deep brain stimulation in idiopathic or inherited isolated dystonia: A meta-analysis. *J. Neurol. Neurosurg. Psychiatry* 91, 938–944.

Volkmann, J., Mueller, J., Deuschl, G., Kühn, A. A., Krauss, J. K., Poewe, W., et al. (2014). Pallidal neurostimulation in patients with medication-refractory cervical dystonia: A randomised, sham-controlled trial. *Lancet Neurol.* 13, 875–884. doi: 10.1016/S1474-4422(14)70143-7

Wagle Shukla, A., Ostrem, J. L., Vaillancourt, D. E., Chen, R., Foote, K. D., and Okun, M. S. (2018). Physiological effects of subthalamic nucleus deep brain stimulation surgery in cervical dystonia. *J. Neurol. Neurosurg. Psychiatry* 89, 1296–1300. doi: 10.1136/jnnp-2017-317098

Wang, N., Wang, K., Wang, Q., Fan, S., Fu, Z., Zhang, F., et al. (2021). Stimulation-induced dyskinesia after subthalamic nucleus deep brain stimulation in patients with meige syndrome. *Neuromodulation* 24, 286–292. doi: 10.1111/ner.13284

Wang, X., and Yu, X. (2021). Deep brain stimulation for myoclonus dystonia syndrome: A meta-analysis with individual patient data. *Neurosurg. Rev.* 44, 451–462. doi: 10.1007/s10143-019-01233-x

Weise, L. M., Seifried, C., Eibach, S., Gasser, T., Roeper, J., Seifert, V., et al. (2013). Correlation of active contact positions with the electrophysiological and anatomical subdivisions of the subthalamic nucleus in deep brain stimulation. *Stereotact. Funct. Neurosurg.* 91, 298–305. doi: 10.1159/000345259

Yao, C., Horn, A., Li, N., Lu, Y., Fu, Z., Wang, N., et al. (2019). Post-operative electrode location and clinical efficacy of subthalamic nucleus deep brain stimulation in Meige syndrome. *Parkinsonism Relat. Disord.* 58, 40–45. doi: 10.1016/j.parkreldis.2018.05.014

Yin, F., Zhao, M., Yan, X., Li, T., Chen, H., Li, J., et al. (2022). Bilateral subthalamic nucleus deep brain stimulation for refractory isolated cervical dystonia. *Sci. Rep.* 12:7678. doi: 10.1038/s41598-022-11841-1

Zheng, Z., Li, Y., Li, J., Zhang, Y., Zhang, X., and Zhuang, P. (2010). Stimulation-induced dyskinesia in the early stage after subthalamic deep brain stimulation. *Stereotact. Funct. Neurosurg.* 88, 29–34. doi: 10.1159/000260077

Frontiers in
Aging Neuroscience

Explores the mechanisms of central nervous system aging and age-related neural disease

The third most-cited journal in the field of geriatrics and gerontology, with a focus on understanding the mechanistic processes associated with central nervous system aging.

Discover the latest Research Topics

See more →

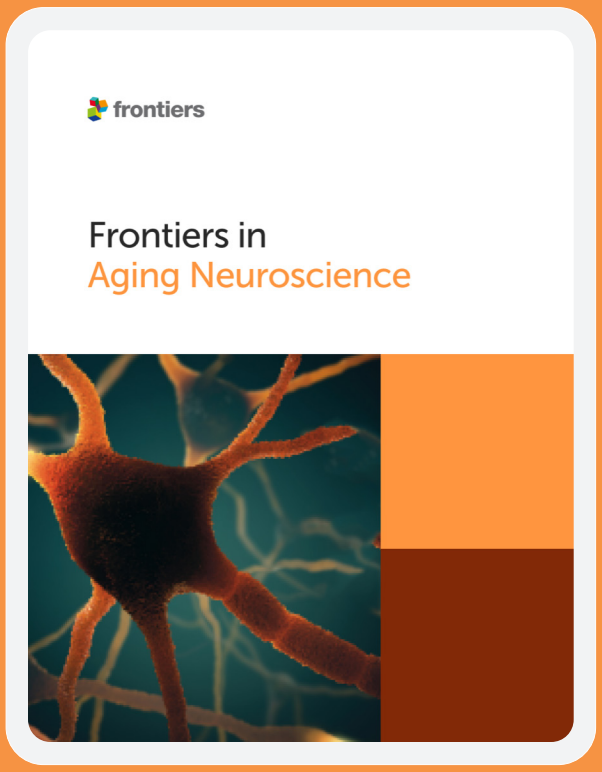

Frontiers

Avenue du Tribunal-Fédéral 34
1005 Lausanne, Switzerland
frontiersin.org

Contact us

+41 (0)21 510 17 00
frontiersin.org/about/contact